IMPERIAL COLLEGE LONDON
DEPARTMENT OF BIOENGINEERING

Thesis submitted for the degree of Doctor of Philosophy

Mouse models of intra-ocular pressure, with applications to glaucoma

Alexandra Boussommier-Calleja

Supervisor: Dr. D. R. Overby
Co-supervisor: Prof. C. R. Ethier

Abstract

Glaucoma is the second most common cause of blindness worldwide and is often associated with an increased intraocular pressure (IOP). IOP is determined by the dynamics of aqueous humour, the liquid filling the anterior segment of the eye. In primary-open angle glaucoma, the elevated IOP is caused by a decreased outflow facility of aqueous humour through the conventional pathway (decreased conventional facility, *C*). Existing glaucoma therapies aim to lower IOP, but remain inefficient because they fail to target *C*. As a result, there is growing interest in using the mouse to unravel the mechanisms controlling *C*. The mouse is a particularly powerful model because it can be routinely manipulated genetically, thereby giving insight into molecules and genes involved in determining *C*. However, it is still not clear whether mice are suitable surrogates for studying human *C*.

To fill this gap, we aim to demonstrate that the mouse is a suitable model for human IOP regulation, and to then use this model to investigate key processes in IOP regulation.

To achieve this aim we used an existing perfusion system to measure *C* in enucleated mouse eyes. First, we improved the perfusion system by including hydration and temperature control to better mimic in vivo perfusions. Secondly, selected receptor-mediated drugs were found to have similar effects on *C* in mice as they did in past human studies. Finally, we show, amongst other studies, anti-metabolic agents decreased *C*, suggesting aqueous humour outflow is metabolic dependent.

We conclude that the mouse is a valid model for studying human conventional facility, yielding novel insight into the mechanisms controlling conventional facility. Importantly, this will help the design of novel efficient anti-glaucoma treatments. Notably, this project will have brought fundamental insight into mouse eye perfusions, thereby consolidating the technique for future studies.

To my brother and parents,

To my grandmothers,
who were not given the same opportunity as me to pursue studies.

Acknowledgements

I want to thank my supervisor Dr. D. R. Overby for his help and support which were essential to the completion of these studies. I am particularly grateful for his constant willingness to dedicate time to my project and his enthusiasm about this work.

I am also very grateful to my co-supervisor Prof. Ethier for his continual availability and invaluable input, and for allowing me to form part of several studies related to my project early in my PhD.

I greatly appreciate the help from our collaborator Prof. Stamer, who has always provided us with enthusiastic advice and helped with his expertise. I am thankful to Dr. Yuan who has kindly trained me in the early stages of my project. I am also very grateful to Dr. Sharpe for welcoming me in his laboratory for a short stay and allowing me to use his equipment. I thank several members of his laboratory (Jim Swoger, Alexandre Robert Moreno), especially Laura Quintana Rio, for the time they spent helping me with my project.

I want to thank particularly Dr. Pedrigi but also Dr. Girard, Dr. Brady, Sietse Braakman and Jason Chang for their moral support. I greatly appreciate the contribution of the following persons who directly participated in the work described in this thesis: Jacques Bertrand, Kristin Perkumas, Dr. A. Thomas Read and Lawrence Lorraine. In particular, Ms. Tali Ziskind performed many experiments described in Chapter 6, along with Miss Oana Elena who pursued a related project, both of whom I have mentored during their MSc project. I thank Mr Woodward, part of Allergan Inc. for providing us with a dithia-PGE_4, a compound used in one of our studies. I also want to acknowledge the constant help of the staff at Imperial, amongst other Ken Keating, Allan Nyunt, Edith Toth, Kate Hobson, Reva Vaze and Amanda Wilson.

Last but not least, I thank my brother, first for drawing several figures shown in this thesis, but most importantly for always being so positive. Similarly, I thank my close friends for always reminding me that there is more than science. Above all, I thank my parents who have made this project possible and who have supported me during these many years of study. All in all, I thank them and my brother for always having faith in me.

Copyright and financial disclosure

I certify the studies described in this report are my own work, pursued in Dr. Overby's laboratory from March 2010 to May 2013. All studies and data from third party works have been duly referenced. I attest that this thesis does not contain any instance of plagiarism nor infringes on copyright laws. I was granted permission to reproduce my own published work by IOVS (Chapter 3) and a figure from a paper I was a co-author on (Fig. 43). I have obtained permission to reproduce figures from other publications (Fig. 2, 3, 4, 5) via the Copyright Clearance Center, when required.

I have received funding from a grant of the Bright Focus Foundation obtained by Dr. Overby and have been awarded the Entente Cordiale scholarship by the British Council in 2011. I was given the opportunity to visit Dr. Sharpe's laboratory in Spain via the "Euro-bioImaging proof of concept studies", via the European Molecular Biology Laboratory. I also received the Santander Mobility award to return in Dr. Sharpe's laboratory in 2013.

I have used a compound provided by Mr. David Woodward for one of my studies (3,7-dithia-PGE_1, Chapter 3), from the company Allergan Inc, who is a co-author on one of my publications.

Associated publications and presentations

Refereed journal publications:

- **Boussommier-Calleja A**, Ethier CR, Stamer WD, Overby DR. The metabolic dependence of conventional outflow facility in mice. *In preparation*, to be submitted to IOVS. 2013.

- **Boussommier-Calleja A**, Overby DR. The influence of genetic background on conventional outflow facility in mice. *In preparation*, to be submitted to IOVS. 2013.

- **Boussommier-Calleja A**, Bertrand J, Woodward FD, Ethier CR, Stamer WD and Overby DR. Pharmacological manipulation of conventional outflow facility in ex vivo mouse eyes. IOVS 2012 Aug 24;53(9):5838-45 (PMID: 22807298)

- Stamer WD, Lei Y, **Boussommier-Calleja** A, Overby DR, Ethier CR. eNOS, a pressure-dependent regulator of intraocular pressure. IOVS 2011 Dec 9;52(13):9438-44.(PMID:22039240)

- Lei Y, Overby DR, **Boussommier-Calleja A**, Stamer WD and Ethier CR. Outflow physiology of the mouse eye: pressure dependence and washout. IOVS 2011 Mar 29; 52(3):1865-71. (PMID:21169533)

Conference presentations:

▪ May 2013	**Boussommier-Calleja A**, Read T, Ethier CR, Stamer WD and Darryl R. Overby. Metabolic dependence of outflow facility in mice.	ARVO
▪ Oct 2012	**Boussommier-Calleja A**, Bertrand J, Ethier CR, Stamer WD and Darryl R. Overby. Temperature and hydration dependence of outflow facility in enucleated mouse eyes, with application to glaucoma research .	BMES
▪ July 2012	**Boussommier-Calleja A**, Bertrand J, Ethier CR, Stamer WD and Darryl R. Overby. The ex vivo mouse eye as a model for conventional and unconventional outflow: effects of temperature and hydration. – Podium presentation	ISER
▪ May 2012	**Boussommier-Calleja A**, Bertrand J, Woodward CF, Ethier CR, Stamer WD and Darryl R. Overby. Pharmacological manipulation of conventional outflow facility in mouse eyes.	ARVO
▪ May 2011	**Boussommier-Calleja A**, Bertrand J, Woodward CF, Ethier CR, Stamer WD and Darryl R. Overby. Sphingosine-1-phosphate decreases conventional outflow facility in mouse eyes.	ARVO

Table of Contents

List of figures

List of supplementary figures

List of tables

Glossary

Symbol/Abbreviation	Meaning
IOP	Intraocular pressure
C	Conventional facility
F_u	Unconventional outflow
EVP	Episcleral venous pressure
F_p	Aqueous humour inflow
F_c	Conventional outflow
R_c	Conventional resistance
R_t	Total outflow resistance
C_t	Total outflow facility
SC	Schlemm's canal
TM	Trabecular meshwork
JCT	Juxtacanalicular tissue
AH	Aqueous humour
CC	Collector channel
POAG	Primary-open angle glaucoma
DBG	PBS with 5.5 mM glucose
PFA	Paraformaldehyde
BSA	Bovine serum albumin
ECM	Extracellular matrix
stdev	Standard deviation

Chapter 1: Introduction

1. Problem

Glaucoma is a major ocular neuropathy that impairs vision and which can lead to blindness. In 2010, it affected approximately 60 million people, of which 8.4 were bilaterally blind[1]. Importantly, loss of vision caused by glaucoma is irreversible. Thus, the sole strategy to tackle the disease is to slow its progression in its early stages. This, however, is made difficult by the poor understanding of the disease which hampers the design of efficient diagnostic tools and therapies. Thus, there is a pressing need for deeper knowledge of the condition so as to develop targeted drugs and treatment approaches.

Notably, the diagnosis of glaucoma is challenging because it is mostly asymptomatic until its later stages. Still, an increased intraocular pressure (IOP) is known to be a primary risk factor for the disease[1]. In most cases of glaucoma, elevated intraocular pressure is a causal risk factor that progressively leads to blindness by damaging the retinal ganglion cell axons that form the optic nerve and which are responsible for transmitting visual information from the retina to the brain. Lowering IOP has been shown to be beneficial to glaucomatous patients, as well as persons suspected of being at risk of developing the condition[1]. Strikingly, in spite of being the only strategy to slow down glaucoma, treatments that lower IOP remain inefficient because the precise mechanisms underlying IOP regulation are not known.

In the majority of cases, the increased IOP associated with glaucoma is caused by an increased resistance to outflow of *aqueous humour* from the eye [2]. Aqueous humour (AH) is a liquid produced in the eye which exits either via the conventional or unconventional pathways. In glaucoma, AH outflow through the conventional pathway is impaired, although the exact underlying reasons remain unclear. Yet, current glaucoma therapies decrease IOP by increasing outflow through the unconventional pathway or by suppressing AH inflow, thus not directly addressing the root problem lying in the conventional pathway. Thus, drugs would be more efficient if they corrected the fault in the conventional pathway responsible for impairing outflow, so as to eventually reinstate the normal homeostatic functions of outflow tissues[3]. In order to help the design of such drugs, this project aims

to better understand the mechanisms of AH outflow in the conventional pathway by using the mouse as *a model for aqueous humour outflow in humans*.

Mice are incredibly powerful models because they are routinely manipulated genetically, thus providing insight into the genetic and molecular factors involved in a disease or phenotype[4]. In addition, they are inexpensive and possess a thoroughly characterized genome. As a result they have been used in a wide range of medical research fields, although they have not been used extensively for studying IOP regulation and aqueous humour outflow. This "under-use" was a consequence of the experimental challenges posed by the small size of mouse eyes, making measurement of aqueous humour outflow difficult. Also, it has not been well understood whether the mouse is a suitable surrogate for studying aqueous humour outflow in humans. In the last decade, many technical challenges have been overcome, resulting in a growing community studying murine aqueous humour outflow dynamics [5–17].

Despite this increasing interest, it is still not clear whether aqueous humour outflow dynamics in mice are similar to those in humans. This issue needs to be addressed to be able to confidently extrapolate findings observed in mice to humans. For instance, mice need to respond to drugs affecting aqueous humour outflow (and thus IOP) in a manner that is similar to humans to be suitable pharmacological models.

This study therefore aims to determine whether the mouse is a good model for human aqueous humour outflow dynamics. Further, we wish to use the mouse model to investigate fundamental mechanisms underlying outflow resistance regulation. The potential advantages of this approach are two-fold. First, it can validate the mouse as a suitable model for testing anti-glaucoma drugs. Second, it can provide invaluable insight into fundamental mechanisms underlying outflow resistance generation. In the long term, we expect that this work will motivate further research to screen novel drugs capable of specifically targeting mechanisms to lower IOP, and eventually benefit glaucoma patients.

2. Specific aims

This project has two goals. First, we wish to determine whether the mouse is a good model for studying human IOP regulation and aqueous humour outflow. Second, we wish to use the mouse as a model to investigate fundamental mechanisms of aqueous humour outflow regulation in humans. In order to investigate aqueous humour outflow, our laboratory has developed a perfusion system for measuring outflow facility in enucleated mouse eyes[12]. This technique is described in further details in Ch. 2, and will be core to most of our studies.

This thesis comprises several studies, described in separate chapters (Ch. 2-7), each with a specific aim and hypothesis as outlined below.

In Chapter 2, we hypothesise *physical factors such as hydration, temperature and post mortem times have significant effects on outflow facility measurements* in enucleated mouse eyes. We tested our hypothesis by including both temperature and hydration control in our previously developed perfusion system. More specifically, outflow facility was measured in eyes submerged (or not) in isotonic saline, and in eyes maintained at room or physiological temperature. Finally, eyes were perfused at different post mortem times. This study allowed us to characterise our improved system for measuring outflow facility of enucleated mouse eyes in a more physiologically relevant manner.

In Chapter 3, we hypothesise that the *mouse responds to the receptor mediated drugs sphingosine-1-phosphate (S1P) and the prostanoid EP4 agonist 3,7-dithia PGE1 similarly to humans*. This was tested by measuring outflow facility in mouse eyes treated with the drugs, or left untreated. Furthermore, drugs were tested 24 hrs following death, to assess whether post mortem times changed their effects on outflow facility. This study aimed to demonstrate that the mouse is a good model for studying the pharmacology of human IOP regulation as occurs in the conventional drainage pathway.

In Chapter 4, we hypothesise that *strain-specific differences in IOP are attributable to strain-specific differences in outflow facility*. To test this hypothesis, IOP was measured in vivo in BALB/cJ, C57BL/6J and CBA/J mice and outflow facility was measured in the same eyes ex vivo, using our improved perfusion system for enucleated mouse eyes. The goal of this study was to show outflow

facility is the primary determinant of IOP in mice, and to motivate further research into the molecular or genetic differences underlying differences in outflow facility between mouse strains.

In Chapter 5, we postulate *outflow facility is dependent on metabolic activity in the mouse eye*. This was tested by perfusing mouse eyes with or without anti-metabolic agents (2-Dideoxy-D-glucose and Sodium azide). The morphology of treated and untreated eyes was also investigated to analyse the effects of anti-metabolic agents the conventional outflow pathway.

In Chapter 6, we study the *effects of pressure on conventional facility, Schlemm's Canal morphology and outflow patterns*. Our governing hypotheses were the following: we postulated changes in outflow resistance occurred at higher pressures, and could be related to changes in the SC morphology. Furthermore, we hypothesised that outflow patterns would change with changes in outflow facility at high pressures. We present preliminary data on two techniques to image outflow patterns and Schlemm's Canal morphology in 3D in whole mouse eyes; these data validate the novel protocols, and form the basis of on-going studies. The long term goal of this study is to develop a technique to image both outflow patterns and morphology of the outflow pathways in 3D in whole mouse eyes, thereby relating outflow patterns to outflow facility.

In Chapter 7, we introduced *modifications to the original Goldmann's equation to account for volume and pressure effects on outflow facility*. We hypothesised this modified equation might better explain our flow rate vs. pressure data acquired in cohorts of mice used in this thesis. The fit of our modified equation against our data was then tested. The goal of this study was to investigate whether outflow facility is dependent on pressure or volume in mice, which would require the use of a novel equation to extrapolate outflow facility from our data. Importantly, this novel equation could also be used for perfusion studies in other species.

Altogether, these studies aim at consolidating the mouse as a model for investigating IOP regulation as occurs in the human conventional pathway. Before describing specific studies, the reader will be provided with the background required to appreciate their relevance and impact.

3. Background

3.1. Intraocular Pressure generation in humans

3.1.1. Intraocular Pressure

The unique purpose of the eye is to enable vision. This vital task requires the ability to focus light and convey the resulting visual information to the brain. Consequently, the mammalian eye has developed into a complex organ composed of different structures which transmit, refract or convert light.

In particular, vision requires transparent tissues that let light pass; as a result, tissues such as the cornea or lens cannot be vascularised. Instead, **aqueous humour (AH)**, a clear liquid that fills the anterior part of the eye and contacts both the cornea and the lens, is responsible for nourishing these anterior tissues. Importantly, it needs to be constantly turned over in order to provide fresh nutrients, and is also involved in clearing the anterior chamber of inflammation products. AH facilitates light transmission by being transparent and having a low protein content which minimizes light refraction or scattering[18].

In addition, the presence of AH generates a pressure within the eyeball, the so-called **intraocular pressure (IOP).** IOP is crucial for ensuring proper functioning of the eye. In particular, it dictates the shape of the eyeball which has a major influence on light refraction[18]. In addition, IOP provides support to inner tissues such as the choroid, which can otherwise detach[19]. Thus, the eye must rely on homeostatic mechanisms to tightly control IOP within its physiological range. In humans, IOP approaches 16 mmHg but oscillates by 2.7 mmHg due to choroidal blood pulsations[20]. IOP also experiences diurnal fluctuations[21,22], as well as spontaneous changes caused by environmental factors and eye movements.

The eye adapts to such perturbations because IOP generation is a dynamic process. IOP is the result of the balance between the production and drainage of aqueous humour. Thus, tissues involved in aqueous humour turnover can directly participate in controlling IOP. In fact, IOP is

principally determined by the resistance to AH *outflow through the conventional pathway*. More specifically, the increased IOP often associated with glaucoma occurs following the abnormal *increase of outflow resistance in the conventional pathway*[2], although the underlying mechanisms are unknown. In this project, we propose to improve the understanding of glaucoma by investigating AH outflow in the murine conventional pathway.

3.1.2. Eye anatomy

This section reviews the basic structures of the human eye as depicted in Fig. 1, namely the cornea, the sclera, the lens, the retina and the optic nerve. Briefly, light penetrates the cornea and is focused by the lens onto the retina. The retina contains photoreceptors responsible for converting light into electrical signals, which are transmitted to the brain via the optic nerve.

The eye can be divided into the anterior segment which comprises the structures anterior to (and including) the lens, and the posterior segment which consists of the tissues posterior to the lens. The anterior segment is filled with *aqueous humour*, whereas the posterior segment contains *vitreous humour*. A more detailed description of the anterior segment, which is most relevant to this project, is found in the following section.

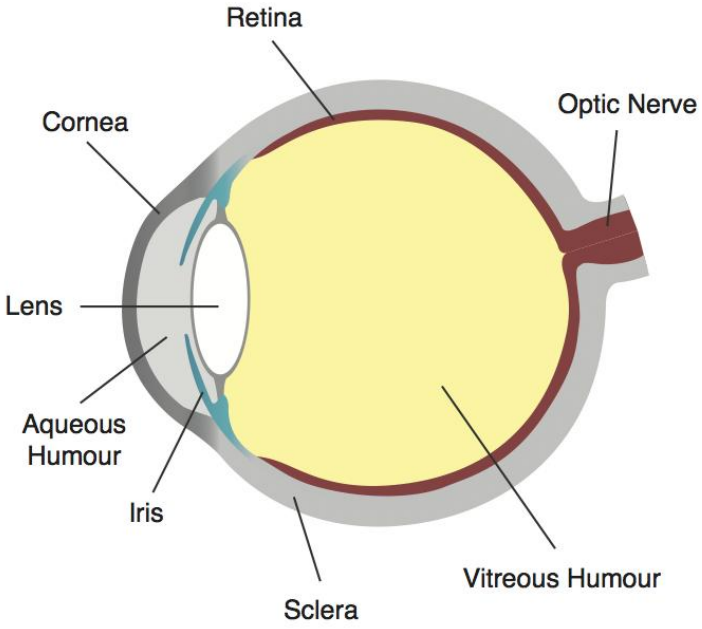

Figure 1: Simplified anatomy of the eye, drawn by M. Boussommier-Calleja

95% of the human eye is covered by the *sclera*; the remaining 5% of the outer coat of the human eye is made up of the *cornea*[23]. The sclera is opaque and provides a structural scaffold for the eye, while the cornea is transparent so as to transmit light, and serves as a protective barrier to the environment[24]. The transition between the sclera and the cornea, called the *limbus*, contains the key structures for aqueous humour drainage. Importantly, the cornea generates up to two-thirds of the refractive power of the eye[25,26], while the remainder is attributable to the lens.

The *lens* is a biconvex transparent structure whose curvature allows for light to be focused onto the retina[27]. In addition, its shape can be changed so as to focus light coming from far or near objects, a process called accommodation. This is performed by the *ciliary muscle* which transmits its tension to the lens via ligaments called *zonules*.

The *iris* extends into the anterior chamber but leaves a central aperture called the *pupil*, which participates in regulating the amount of light entering the lens[28]. Furthermore, the pupil divides the anterior segment into the anterior and posterior chambers. The iris is contiguous with the *ciliary body*, which is the attachment site of the zonules. Notably, the ciliary body contains the *ciliary muscle*, which possesses longitudinal, radial and circular fibres responsible for altering the shape of the lens [29,30].

The posterior segment is filled with a static and colourless gel called the *vitreous humour* which occupies 80% of the volume of the eye[31]. Consequently, it provides support to the eye globe but also to the *retina*, which consists of several layers of neural cells responsible for capturing and converting light into electrical signals. The neural signals are conveyed via the axons of the *retinal ganglion cells*, which converge into the *optic nerve* forming a depression, or optic disc cup. Finally, the optic nerve relays the information to the visual cortex. Glaucoma is characterized by the loss of retinal ganglion cells axons, which leads to an excavation of the optic disc cup, and is accompanied by the thinning of the nerve fibre layer surrounding the cup[1].

3.1.3. Ocular circulation

Blood is supplied to the ocular structures through the *retinal and uveal (or ciliary) vessels*, which originate from three branches of the ophthalmic artery[32]. Retinal vessels branch from the central

retinal artery, while uveal vessels are supplied by the posterior and anterior ciliary arteries. Branches of the posterior ciliary arteries form most of the choroid which lies beneath the retina and serves its outer layer. Posterior and anterior ciliary arteries anastomose to form the anterior uveal circulation in the iris which vascularises the ciliary body and ciliary muscle.

The ciliary muscle's blood flow discharges into the *anterior ciliary veins*, whereas the rest of the uveal drainage from the iris, choroid and ciliary body occurs through the four *vortex veins*. The vortex veins eventually fuse with either the superior or inferior ophthalmic veins, although most of the venous flow uses the superior ophthalmic vein. Finally, the eye also has to recycle aqueous humour, most of which joins the venous system via a complex limbal vasculature, which leads to the episcleral veins and ultimately to the superior ophthalmic vein[33]. Some aqueous humour is thought to join the vortex veins via the uveal capillaries, although this point remains unclear[34], as discussed in the next section.

3.2. Aqueous Humour turnover

This section details the turnover of AH in the anterior segment, which is responsible for generating IOP. AH is produced in the posterior chamber at the *ciliary processes*, flows into the anterior chamber through the pupil and drains either via the *trabecular or uveoscleral* pathways, which are described below.

3.2.1. Aqueous Humour production

AH is produced at the non-pigmented epithelium of the ciliary processes[18], which consist of invaginations of the ciliary body. AH is derived from the plasma in the ciliary body capillaries, mostly via active secretion and less markedly by ultrafiltration and diffusion. This results in a unique composition of aqueous humour, characterized by a low concentration of proteins to minimize light refraction[18].

3.2.2. Aqueous humour outflow

AH can exit the anterior chamber at the limbus, found at the transition between the cornea and the sclera, either via the trabecular or uveoscleral pathway. It is important to note trabecular and uveoscleral routes are *anatomical* definitions. Alternatively, AH drainage can be divided into functional components, namely conventional and unconventional outflow, according to their

dependence on IOP. Specifically, conventional outflow is defined as the portion of aqueous outflow which is dependent on IOP, while unconventional outflow is associated with the IOP-independent portion of outflow. Importantly, such anatomical and functional definitions cannot necessarily be equated. Trabecular and conventional outflow are typically equated because it is known trabecular outflow is driven by the pressure drop between the anterior chamber and the episcleral veins. However, it is not clear whether the uveoscleral outflow is strictly independent of IOP and thus whether it can be entirely considered as unconventional outflow. Since this section focuses on the anatomical features of AH drainage, the terms trabecular and uveoscleral outflow will be used.

This section reviews the morphology of both pathways, with particular attention to the trabecular pathway because it accommodates up to 90% of AH outflow in humans, and is the site of impaired outflow which causes the increased IOP often associated with glaucoma[2,35].

3.2.2.1. Trabecular pathway

AH is driven through the trabecular pathway because of the pressure drop between the anterior chamber and the episcleral veins, which is approximately 6.9 mmHg in humans[36]. As AH enters the trabecular pathway, it flows through the trabecular meshwork (TM) and Schlemm's Canal (SC) prior to entering the post-trabecular pathway which eventually fuses with the venous system[33,37–39] (Fig. 2). The morphology of each of these tissues is discussed below since it influences their resistance to AH outflow. The characteristics of the SC inner wall are described in further detail as it is thought to be an important site of AH outflow resistance.

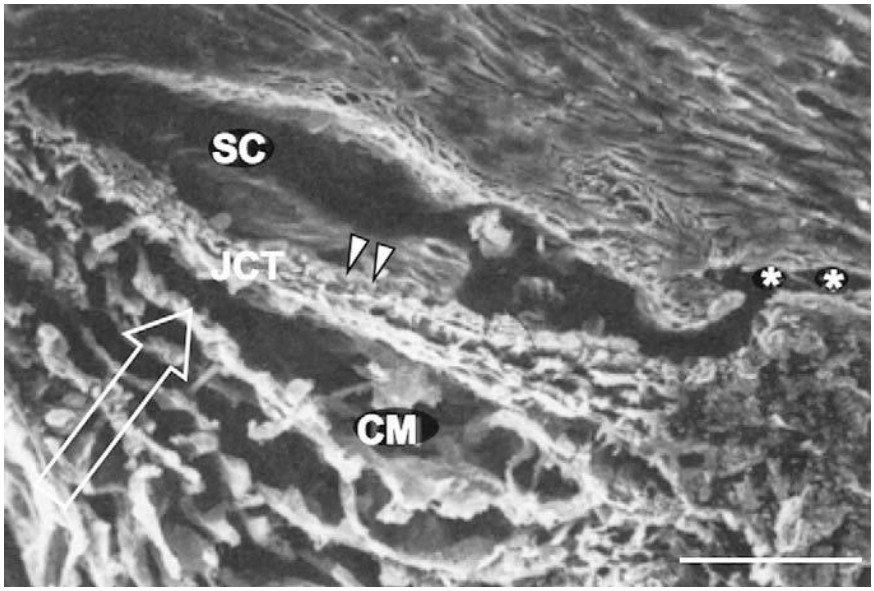

Figure 2: Scanning electron micrograph of the human conventional pathway.CM: corneoscleral meshwork, SC: Schlemm's canal, JCT: juxtacanalicular connective tissue. Asterisks show a collector channel. Arrowheads point to the inner wall of SC. White arrow represents the direction of aqueous humour flow from the anterior chamber towards the episcleral veins. Scale bar is 50 µm. Reproduced from Overby et al. 2009, *Exp Eye Res*. Reprinted with permission of Elsevier through the Copyright Clearance Centre (see Appendix 2).

a- Trabecular meshwork

The TM is triangular-shaped and is attached to Schwalbe's line at the cornea anteriorly and to the scleral spur posteriorly. The scleral spur is a protrusion of the sclera into the TM, and provides an anchoring point for some of the longitudinal fibres of the ciliary muscle[40] .

The TM consists of three different regions, namely the uveal meshwork, the corneoscleral meshwork and the juxtacanalicular tissue (JCT; Fig. 3A).The uveal and corneoscleral meshworks are porous structures made of collagen- and elastin-containing sheets or beams covered with endothelial cells (Fig. 3B) [40–42]. The spaces between lamellae decrease from 25-75 µm in the uveal meshwork to 2-15 µm in the corneoscleral meshwork[43]. In contrast, the JCT is a more irregular tissue made of cells embedded in extracellular matrix, characterized by the presence of collagen IV, laminin, fibronectin, proteoglycans and glycosaminoglycans (GAGs)[39].

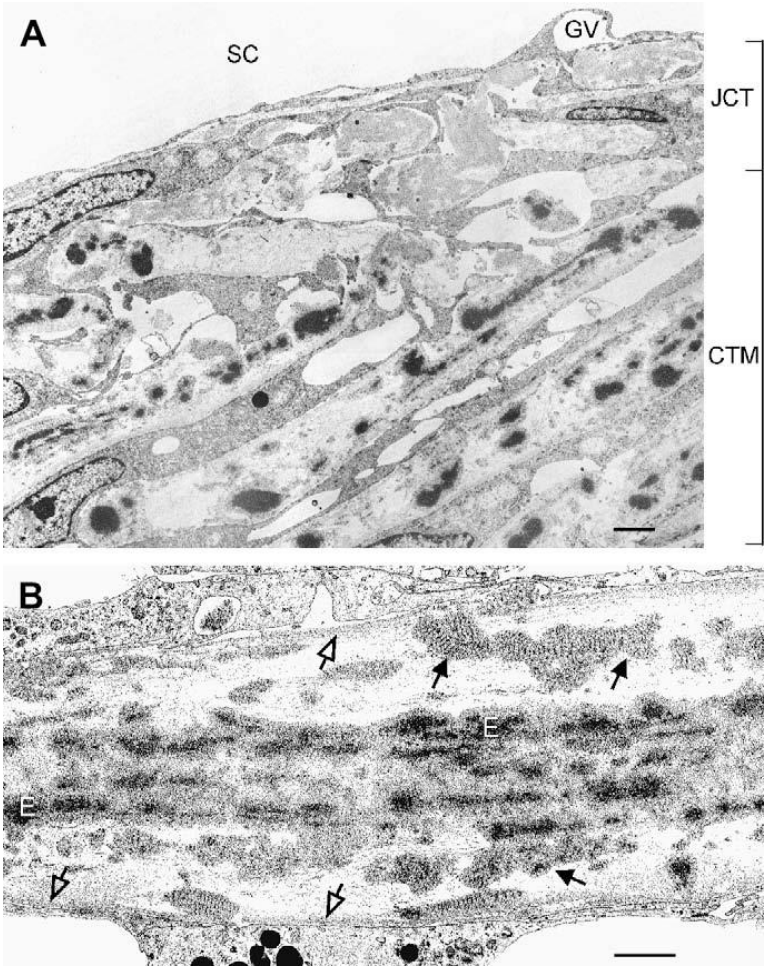

Figure 3:Electron micrograph of the trabecular meshwork (A) and of a single trabecular beam in the corneoscleral meshwork(B). The core of the beam contains an elastic fibre (E). Open arrows point to the basal lamina of the trabecular meshwork cells which cover the beam, while solid arrows point to aggregates of long-spacing collagen in the cortical region of the beam. GV=Giant Vacuole, SC=Schlemm's Canal. Image from Tamm 2009, *Exp Eye Res*. Reprinted with permission of Elsevier through the Copyright Clearance Centre (see Appendix 2).

The TM is also a contractile tissue, affected by three different groups of elastic tendons arising from the ciliary muscle: (i) the first group attaches to the cribriform plexus in the JCT (ii) a second group traverses the TM to connect with the cornea and (iii) the third group connects with the scleral spur[44]. Moreover, elastic fibres from the scleral spur are continuous with the TM elastic fibres, thereby transmitting any force exerted on the scleral spur to the TM[42]. In addition, α-smooth muscle actin has been found in TM cells, suggesting they are contractile in their own right[45,46]. This was further supported by studies showing different agents caused either contraction or relaxation of isolated TM strips[47]. On the other hand, nerve terminals have been found in the TM[48,49], which could potentially trigger contractions of TM cells. In addition, contractile cells in the sclera spur were

identified [50–52]. Thus, the TM is likely affected by the antagonistic contractility actions of the ciliary muscle, the scleral spur and TM cells[47].

Finally, TM cells are capable of phagocytosis; some TM cells contain pigment, most likely originating from the iris. Thus it is thought this process is important for the self-cleaning of the TM, which could otherwise become clogged with products such as pigment granules[42,53,54].

In essence, the filter-like structure of the TM permits AH to percolate through its trabecular spaces, which become progressively less ordered and narrower as they approach SC. In addition, its morphology can be affected by contractile action at different levels, thereby affecting AH drainage and thus IOP.

b- Schlemm's Canal

SC is a channel lined with endothelial cells which runs circumferentially in the eye, adjacent to the TM. It is 33-35 mm long [55]. Its inner wall is in contact with the JCT in the TM (Fig. 3), and is 264 µm long in its anterior-posterior diameter in normal human eyes[56]; its opposite side is called the outer wall, which contains openings to CC found irregularly around the SC circumference. SC is infiltrated perpendicularly by AH via its inner wall as the humour flows from the TM towards the episcleral veins (Fig. 2). Once AH has entered the SC, it flows circumferentially inside the canal until it reaches the opening of an aqueous vein or a collector channel on the SC outer wall[38,39]. Thus, SC inner wall cells experience both a *pressure drop* as they are traversed by AH, and *shear stress* as AH flows in SC.

Even though SC has a vascular-like endothelium linked via tight junctions, its endothelial cells at the inner wall present several unusual characteristics. First, they experience a pressure drop from their basal to apical side as opposed to most endothelial cells in the human body[37–39]. Thus they are constantly being pushed away from their basement membrane. As a result, they balloon into the SC lumen, forming giant vacuoles[39] (Fig. 4). In fact, SC cells are connected to the underlying JCT by cellular processes[57], which were shown to distend at higher pressures[58]. In addition SC cells are connected to the cribriform plexus in the JCT by connecting fibrils[44], thereby directly linking SC to the TM and the ciliary muscle.

In addition, SC cells exhibit either trans-cellular or intracellular pores[59–61] which are thought to accommodate aqueous humour outflow as it progresses from the TM towards the venous system (Fig. 4). In particular, intracellular pores form where the apical and basal membrane of SC cells fuse in giant vacuoles. However, studies have suggested pores might be an artefact from fixation[59,62]. Finally, SC cells lie on a discontinuous basement membrane[39,40]. Altogether, these characteristics make the SC endothelium a unique barrier which can significantly affect outflow resistance as discussed in section 3.4.

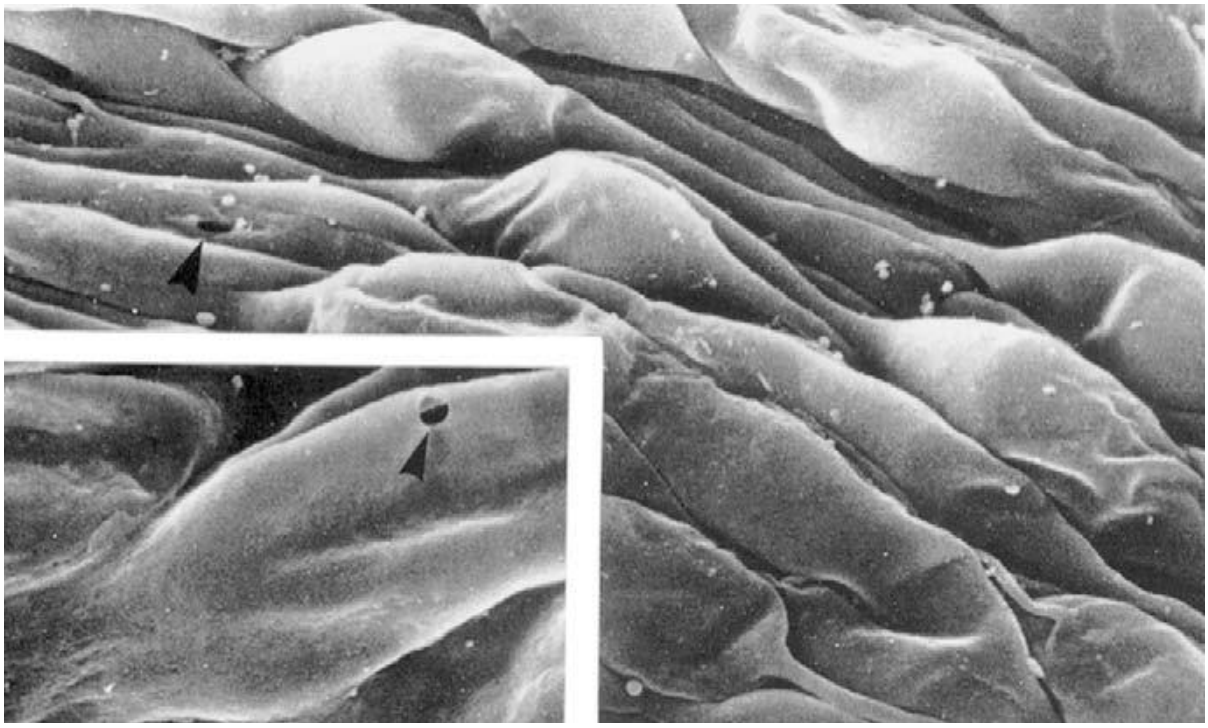

Figure 4: Scanning Electron micrograph of the inner wall of Schlemm's Canal. Cells form giant vacuoles as they are pushed away from their basement membrane. Arrowheads point to pores which are thought to accommodate aqueous humour as it traverses the SC inner wall. Reproduced from Overby et al. 2009, *Exp Eye Res*. Reprinted with permission of Elsevier through the Copyright Clearance Centre (see Appendix 2).

c- Post-trabecular pathway

After AH has penetrated SC, it continues its progression towards the venous system either via collector channels (CC) or aqueous veins, which depart directly from the outer wall of SC[33]. There are 20-30 CC or aqueous veins in humans[55], which leave irregularly from around the SC. Their openings in the SC outer wall are of variable size, ranging from 28 to 40 µm[55]. Both CC and aqueous veins eventually fuse with the venous system but differ in their trajectory, as discussed below.

CCs are shorter channels which first join the deep intrascleral venous plexus[33]. From the deep intrascleral venous plexus, aqueous humour can either directly join the venous circulation, or progress via other CC to deeper venous plexi (mid and deep venous plexus) to eventually flow into the episcleral veins. In contrast, aqueous veins link directly SC to the episcleral veins[33,63]. Once the aqueous humour has reached the episcleral veins it is transported via the ophthalmic vein to the systemic circulation[32].

3.2.2.2. Uveoscleral pathway

The uveoscleral pathway is much less well understood than the trabecular pathway. It is however a major target of current anti-glaucoma therapies. It was first detected by Bill in 1965[64], and further documented in other tracer studies[65–67] as an outflow entering the iris root, traversing the ciliary muscle, and finally discharging into the suprachoroidal space. It was shown this was bulk flow rather than diffusion-based, caused by a pressure drop between the suprachoroidal space and the AC of approximately 3.5 mmHg.[68]

Thus unconventional outflow is dependent on IOP and will shut down at pressures lower than 4 mmHg, as the pressure drop between anterior chamber and suprachoroidal space disappears. Yet Bill showed uveoscleral outflow was much less sensitive to IOP than the trabecular pathway, which explains why this route is often considered pressure-independent, and therefore typically equated to unconventional outflow. Indeed, when IOP was doubled from 11 to 22 mmHg, uveoscleral outflow increase was shown to change by only one-fold compared to five-fold for the trabecular outflow [65].

The fate of AH once it has crossed the ciliary muscle and entered the ciliary body becomes less clear: tracer studies have either suggested it diffuses through the sclera[69] or is reabsorbed by uveal circulation in the ciliary body[34]. However, it has been proposed the tracers detected in the sclera might have diffused separately from aqueous humour. The model based on uveal reabsorption of AH supposes aqueous humour is drawn into the capillaries due to both hydrostatic and osmotic pressure differences, according to Starling's hypothesis. Interestingly, such a mechanism might exclude large molecules such as albumin from passively entering the capillaries, which would therefore progress alternatively through the sclera, as observed by Bill.

Finally, it was recently suggested that lymphatics identified in the ciliary body might play a role in AH drainage[70]. This, however, remains controversial since it has long been thought that lymphatics did not exist in the eye, and that aqueous humour serves the typical functions of lymphatics (i.e. to provide egress for fluid and macromolecules to the veins, and to serve as a medium for the transport of immune cells)[71]. Thus, the trajectory of uveoscleral outflow remains poorly understood since it is experimentally challenging to visualize. However, in light of the pressure-insensitivity reported by Bill, the uveal reabsorption hypothesis could prevail, as it relies on osmotic pressure and would be therefore much less affected by changes in IOP than trans-scleral bulk flow. Alternatively, uveoscleral outflow might be only weakly pressure sensitive because increasing IOP might cause the compression of the suprachoroidal space thereby suppressing uveoscleral outflow[69].

Regardless, it is accepted that uveoscleral outflow begins at the ciliary muscle, which seems to represent the rate-limiting step to outflow[69]. Indeed, structural changes of the ciliary muscle can appreciably affect uveoscleral outflow as demonstrated by the use of prostaglandins as a means to increase uveoscleral outflow. Prostaglandins are known to pharmacologically facilitate AH progression by digesting the ECM in the ciliary muscle or by relaxing the muscle, resulting in larger spaces between muscle bundles[69,72]. Similarly, extracellular debris found in the ciliary muscle of old human patients are thought to prevent AH flow and thus explain the corresponding low uveoscleral outflow measurements[69,73].

Thus, despite being a major target of glaucoma drugs, the mechanisms underlying uveoscleral outflow still elude the scientific community. It is therefore urgent to develop protocols to visualize and measure uveoscleral dynamics directly to confirm its importance in normal and glaucomatous AH dynamics.

3.3. IOP generation: Goldmann's equation

IOP is a result of the balance between the rate of production (F_p) and drainage (F_d) of AH from the anterior segment of the eye, which at steady state are equal (Eq. 1).

$$F_p = F_d$$

Equation 1

More specifically, the rate of production of AH (F_p) matches both the pressure-dependent, or conventional outflow (F_c) and the pressure-independent, or unconventional outflow (F_u; Eq. 2).

$$F_p = F_c + F_u$$

Equation 2

In particular, outflow in the conventional pathway is driven by the difference between the pressure in the anterior chamber (i.e. IOP), and in the episcleral veins (i.e. episcleral venous pressure, or EVP), and is limited by the resistance offered by the conventional pathway (or R_c). It therefore emerges that IOP is governed by Eq. 3, called Goldmann's equation, which will be central to this thesis.

$$F_p = \frac{(IOP - EVP)}{R_c} + F_u$$

Equation 3

Equation 3 can also be expressed as a function of outflow facility of the conventional pathway (C), defined as the inverse of conventional outflow resistance, as shown in Eq. 4.

$$\mathbf{F_p = C \times (IOP - EVP) + F_u}$$

Equation 4

Equation 4 can be re-arranged as a function of IOP, as shown in Eq. 5.

$$IOP = \frac{F_p - F_u}{C} + EVP$$

Equation 5

In humans, F_p is typically 2.5[18] µL/min, IOP-EVP is 6.9 [36] mmHg, C=0.22 µL/min.mmHg^2 and F_u=0.28-1.52 µL/min[72,73]. Importantly, R_c and C refer to properties of the conventional pathway. In contrast, total resistance R_t (or total facility, C_t) refer to the total amount of AH which can be drained at a given pressure (both through the conventional and unconventional pathway), as described in Eq. 6:

$$R_t = \frac{(IOP - EVP)}{F_p}$$

Equation 6

Although Goldmann's equation is routinely used for analysis of aqueous dynamics, it is important to appreciate it is limited by important assumptions which postulate F_p, EVP, F_u and C are independent of IOP. Indeed, experimental studies suggest these quantities all change with IOP, albeit minimally[65,74–76]. Note some of these studies were conducted in primates[65,74,75] and do therefore not necessarily apply to all species. In summary, Goldmann's equation simply divides outflow into pressure-dependent vs. -independent outflow, which is a division based on functional, rather than anatomical, routes.

3.4. IOP regulation: Outflow resistance

Although Goldmann's equation shows several parameters can affect IOP, it has long been known that an increase in outflow resistance is responsible for the typical raised pressure in glaucoma[2,37,38]. In particular, Grant showed the increase in IOP is solely attributable to an increase in conventional outflow resistance, i.e. a decrease in conventional outflow facility[2]. More specifically, he showed C decreased from 0.22 µL/min/mmHg in normal eyes to lower values in glaucoma, ranging from 0 to 0.11 µL/min/mmHg. He also showed AH production was not higher in glaucomatous eyes (2.4 vs.1.5 µL/min in normal vs. glaucomatous eyes) and could therefore not explain their increased IOP. Importantly, pioneering studies have described outflow resistance as metabolic-independent[77,78]. Thus, outflow resistance is typically considered as being passively generated by the trabecular pathway's filter-like morphology. Such studies consisted of showing several poisonous substances had no effect on outflow resistance[78], or that there were no temperature-related changes of outflow facility except for those attributable to changes in the viscosity of aqueous humour[77]. Surprisingly, this has not deterred many studies from investigating the role of enzymes or signal transduction [79–87] in outflow resistance generation, which should have been silenced by anti-metabolic agents. Thus, after more than a century of research, the mechanisms underlying outflow resistance generation remain unclear, thereby preventing the

design of efficient treatments for elevated IOP. This section reviews the current knowledge of outflow resistance generation and its pharmacology.

3.4.1. Outflow resistance generation

The anatomy of the conventional pathway was previously described (cf. Section 3.2.2) as composed of the trabecular meshwork, Schlemm's Canal and the post-trabecular pathway. The TM's first two layers, the uveal and corneoscleral meshworks, comprise openings too large to account for any significant resistance to outflow. In fact, this was demonstrated both theoretically using Poiseuille's law[88] and experimentally by showing that their removal did not affect outflow resistance in enucleated human eyes[89]. On the other hand, Bill and Mäepea showed that more than 50% of outflow resistance lies in the vicinity of the inner wall of the Schlemm's Canal, within the JCT[75]. The JCT was shown to have large pores apparently capable of generating only few percent of total outflow resistance, unless these pores were filled with a gel of GAGs[90]. However, the evidence for the presence of GAGs is debatable: in separate studies, GAG-degrading enzymes were shown to either decrease outflow resistance[78] or leave it unaffected[91]. Moreover, GAGs were not detected either with transmission electron microscopy, although quick freeze deep etch revealed a richer ECM environment[92]. Furthermore, the dramatic effect of MMPs on increasing outflow facility[93] supports an important role of ECM in outflow resistance generation.

As for the inner wall of SC, its only potential in generating outflow resistance lies in the presence of pores, since its basement membrane is largely discontinuous. However, calculations showed that pores could only account for 10% of total outflow resistance[61]; moreover, their role in shaping outflow resistance is undermined by studies which measured an increase in pore density with increasing outflow resistance caused by fixation[59,62] or increased IOP[94–97]. Finally, it has been suggested pores could be an artefact from fixation[59], although recent in vitro studies from our laboratory have shown pore density was not affected by fixation modes (immersion vs. perfusion fixation; personal communication, Dr. Pedrigi).

Finally, the post-trabecular pathway was thought to be negligibly involved in outflow resistance generation, ever since Mäepea and Bill measured a very small pressure drop between SC and episcleral veins[75]. Indeed, collector channels and aqueous veins are too large to generate

significant outflow resistance according to Poiseuille's law[98]. However, experimental studies showed that 25% of outflow resistance remained following a trabeculotomy, although these results were measured at relatively high pressures ranging from 15 to 25 mmHg[89]. Nonetheless, this work suggests the role of the post-trabecular pathway in outflow resistance generation might have been underestimated.

Altogether, studies suggest most of the outflow resistance is found in the vicinity of Schlemm's Canal, although it fails to explain all of the measured resistance.

3.4.1.1. Synergistic model of outflow resistance

The observation that the sum of the outflow resistances generated by each region of the trabecular pathway did not equal the total outflow resistance led to a revised synergistic model of outflow resistance generation[39,99]. This approach postulates outflow resistance is defined by interactions between the different layers of the trabecular pathway, rather than by the sum of their individual effects. This further motivated the funnelling theory[99] which hypothesized that effective outflow resistance is increased by the proximity of the JCT to the inner wall of SC. More specifically, pores force flow in the JCT to percolate towards them, which in turn forces flow to use only the regions of the JCT underlying the pores; since pores are found only every other 20-30 µm along SC inner wall on average[39], the area available for AH filtration is therefore reduced, which in turn increases outflow resistance. This synergistic effect was also suggested by studies which showed that pharmacological disruption of the inner wall SC had a drastic effect on outflow resistance although the inner wall alone was supposed to only be able to generate a small part of outflow resistance[100]. Furthermore, the decrease in outflow resistance caused by drugs which specifically targeted the SC inner wall did not correlate with the loss of SC cells[101]. This suggested SC cells alone were not responsible for generating outflow resistance. Thus the evidence points towards a synergistic effect, such as the funnelling model, which however, still forecasted a resistance higher than that found in experimental studies[99]. A revised version of the funnelling theory which includes the effect of the increased area available for filtration provided by the giant vacuoles gave better but still high predictions of outflow resistance; it has been suggested the basement membrane

discontinuity could generate the remaining resistance, although this effect has never been quantified[39].

3.4.1.2. Outflow resistance and AH humour patterns

Finally, outflow resistance has been related to outflow patterns in the TM. Using fluorescent tracers to represent AH outflow, it was shown eyes with artificially high IOP and high outflow resistance showed less fluorescent tracers in their TM[102,103]. More specifically, fluorescent tracers were found only in preferential regions of the TM, which combined together were referred to as the effective filtration area. Interestingly, this area increased in eyes with lower IOPs and lower outflow resistance, such that much more of the TM was actively perfused with tracers, i.e. with AH. Thus, there seems to be a relationship between outflow resistance and effective filtration area, or AH outflow patterns. Similar results were found using a drug which decreased outflow resistance without affecting SC integrity, namely Y-27. Following treatment with Y-27[104], tracers were found much more homogeneously along the inner wall of SC (Fig. 5B) than in the fellow untreated eye (Fig. 5A). Interestingly, this drug also caused a separation between the inner wall SC and the JCT, which supported previous speculations from the funnelling theory regarding the role of their mechanical coupling in generating outflow resistance.

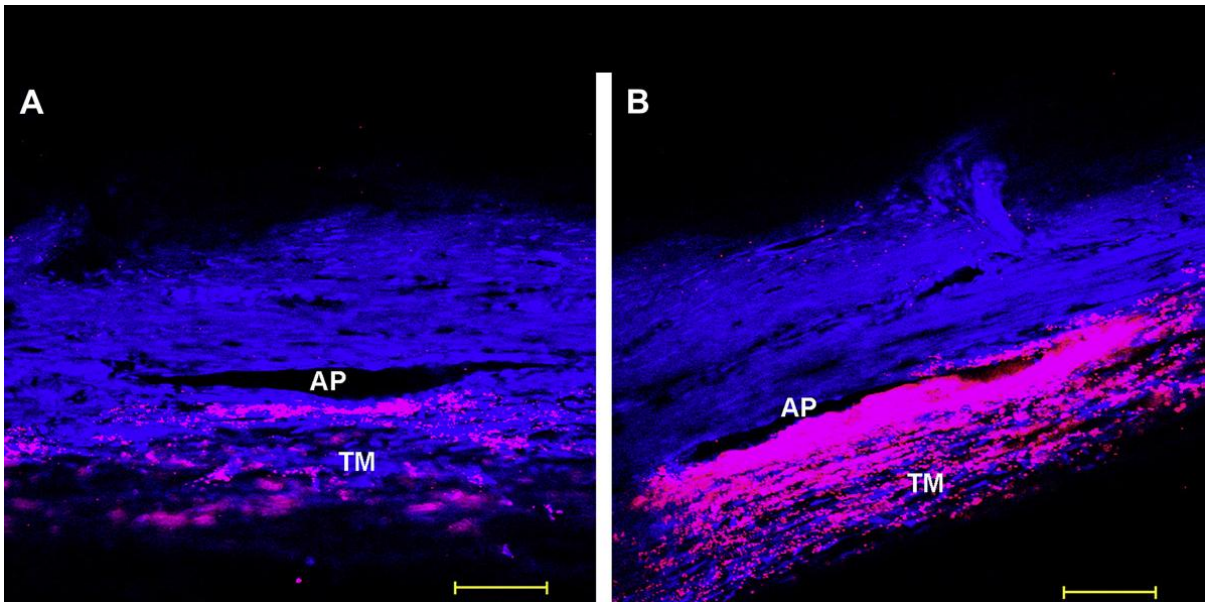

Figure 5:Confocal image of a frontal section of the bovine conventional pathway in a control eye (A) and a Y-27 treated eyes (B).TM: Trabecular Meshwork AP: Aqueous plexus. Note AP is the equivalent of SC in bovine eyes. Scale bar is 100 µm. Reproduced from Lu et al. 2008. Reprinted with permission of Elsevier through the Copyright Clearance Centre (see Appendix 2).

These findings warrant further research into differences between the regions of the TM which are, or are not, actively perfused by AH to further understand outflow resistance generation. Yet, these analyses were only carried out on a limited number of histological sections, representing only a minimal part of the entire TM. Thus, in spite of important advances in understanding outflow resistance generation at the tissue-scale, there is room for deeper understanding of the molecular and physical forces at play. Their unravelling would dramatically help the design of drugs which better target the mechanisms responsible for increased outflow resistance, and thus IOP in glaucoma.

3.5. Glaucoma

3.5.1. The disease

Glaucoma is the second leading cause of blindness worldwide, forecasted to affect 80 million people in 2020[105]. Importantly, half of the people affected by the disease are thought to be undiagnosed[1], amongst other reasons because it is asymptomatic until its later stages. It typically appears in patients older than 40, after which its prevalence increases exponentially with age. It is an important burden to healthcare, which for example drastically affects Europe with a total related annual cost of 2.7€ B[106] yearly, or the United States which spent similarly 2.9 billion $ in 2004[107]. There are several forms of glaucoma which differ in their onset; yet they are all characterized by the death of a substantial number of retinal ganglion cells in the optic nerve in at least one eye, which leads to visual field loss[1]. The most common form of glaucoma is primary-open angle glaucoma (POAG), which is characterized by a slow and asymptomatic progression. The main risk factor for POAG is an increased IOP caused by an impaired aqueous humour outflow within the trabecular pathway. In contrast, the second most common glaucoma is closed-angle glaucoma. Closed-angle glaucoma is caused by the closing of the angle between the iris and the cornea which prevents normal AH outflow, thereby increasing IOP.

Eventually, every form of glaucoma leads to retinal ganglion cell loss resulting into the excavation of the optic disc cup and the thinning of the nerve fibre layer surrounding it, which can be observed with different imaging modes such as Optical Coherence Tomography[1]. Glaucoma is typically associated with an IOP exceeding 21 mmHg, although this is not a definitive criterion. For example,

patients with high IOPs do not necessarily develop the pathology[1], and glaucomatous patients from a Japanese study were shown to have an IOP comparable to that of healthy subjects[108]. However, it is recognized that an increased IOP is a causal risk factor for glaucoma, possibly by conveying stress to the sclera and the optic nerve: a clinical study has shown that patients with ocular hypertension with high IOP were at more risk of developing the disease[109]. It has also been suggested that high-frequency IOP fluctuations (occurring over the time scale of minutes) measured by telemetry could contribute to the onset of the disease, as they might be accentuated in glaucomatous patients because of their stiffer sclera[110]. In addition, large variations in diurnal IOP have been associated with the progression of the disease[111], although other groups failed to find similar results[112]: therefore, is it still not clear whether diurnal variations in IOP are important in glaucoma[113]. Nevertheless, measuring IOP remains one of the only diagnostic tools to detect glaucoma, followed by imaging of the optic nerve head structure, whose thinning and cupping is characteristic of the disease. Thus diagnosis of glaucoma remains poorly developed, and could be dramatically improved thanks to a better understanding of its onset.

3.5.2. Treatments

All current anti-glaucoma therapies aim to lower IOP, which has been shown to be beneficial to glaucomatous patients[1]. In particular, clinical studies have shown that IOP-lowering treatments delay the progression of the disease[114–116], showing that each millimeter of mercury of IOP reduction from baseline decreased the progression risk of the disease by about 10%[116]. The available treatment options to tackle glaucoma consist of using daily eye-drops, laser surgery or conventional surgical procedures. Laser and surgical treatment lower IOP by facilitating AH drainage via the disruption of the TM or the creation of a new drainage route into the sub-conjunctival region of the eye (e.g. trabeculectomy). They are normally effective in lowering IOP but can lead to further complications, e.g. scarring or bacterial infections[1].

Different drugs for increasing outflow facility and thus lowering of IOP have been used, such as muscarinic (pilocarpine), adrenergic (epinephrine) agents or prostaglandins[117]. Although the mechanisms underlying the action of epinephrine are not well understood, it is known that pilocarpine causes contraction of the ciliary muscle and the scleral spur, thereby causing SC to

open[118,119]. Interestingly, pilocarpine was still shown to have an effect on outflow facility after the separation of the ciliary muscle and sclera spur, suggesting it can directly affect TM cells too. This was further supported by studies identifying muscarinic receptors in the TM[120,121], or by showing TM cells have contractile properties[45–47]. In contrast, prostaglandins act by increasing the spaces between the ciliary muscle bundles and reducing the extracellular matrix in such areas, thus increasing uveoscleral outflow[122,123]. Yet, there is still a need for a new generation of drugs which target the root problem in glaucoma located in the trabecular pathway.

3.5.3. Increased outflow resistance in POAG

Although it is known the increased IOP which characterizes glaucoma is associated with an increased outflow resistance in the conventional pathway[2], the underlying reasons remain poorly understood. In essence, the main lines of thoughts revolve around the potential role of increased extracellular matrix deposit in the JCT or changes in SC inner wall conductivity[39].

Indeed, alterations in POAG occurring in other parts of the conventional pathway such as SC and post-trabecular pathway have somewhat been discarded. A trabeculotomy performed by Grant in 1963 on glaucomatous eyes removed all the excessive outflow resistance[89], suggesting it belonged to the excised trabecular pathway rather than the aqueous veins which were left intact. Note however the remaining outflow resistance was still higher in glaucomatous than normal eyes following trabeculotomy (1.60±0.91 vs. 2.97±1.07 µL/min.mmHg). In addition, a recent study has shown morphological changes in CC between glaucomatous and normal samples which suggest their role in POAG might have been underestimated[124]. Although there were no fewer CC in glaucomatous samples, their orifice size and circumference was twice as small as in control eyes. In addition, Johnson and Kamm demonstrated a collapse of SC could not explain the abnormal increase in outflow resistance observed in POAG[125]; however, SC in POAG samples were found to be significantly smaller which undoubtedly worsens the condition[56], although other studies failed to detect a correlation[126].

Differences in the extracellular matrix of the JCT between healthy and POAG donors suggest an accumulation of debris could increase outflow resistance. In particular, an increase in extracellular matrix and the presence of fibrillar elements called “plaque material” was identified in POAG

samples[127,128]. Such plaques were shown to be derived from the elastic fibres in the JCT and correlated with axonal loss in the optic nerve. However, they did not seem to be present in ocular hypertension or early glaucoma, and could therefore just be a symptom rather than a cause of the disease. Similarly, there is an acute interest in the role of TGF-β2 in glaucoma[129] which is found at higher concentrations in AH samples from POAG patients[130]. TGF-β2 is known to participate in fibrosis, and was shown to increase ECM deposition when added to TM cells in culture[131]. Furthermore, anterior segment perfusion with TGF-β2 provoked an accumulation of fibrillar ECM which coincided with a decrease in outflow facility[132].

Finally, changes in pore density could alter outflow resistance in POAG: both Johnson[35] and Allingham[60] measured a decrease in pore density in glaucomatous samples. These observations were also replicated in vitro, wherein pore density was shown to be three fold smaller in glaucomatous SC cells compared to normal SC cells under perfusion at a physiological pressure drop of 6 mmHg[133].

In summary, although progress has been made, there is still no clear insight into the root problem occurring in the conventional pathway during POAG, undermining the design of efficient drugs. Thus, using an experimental model such as the mouse should prove tremendously useful to further investigate such mechanisms and create anti-glaucoma treatments.

3.6. Mouse model for human aqueous dynamics

3.6.1. Why?

The mouse is the animal model used for a great deal of scientific research, primarily because it can be routinely manipulated genetically[4]. In this way, the relevance of specific genes to any pathology can be studied by knocking them out and studying the corresponding phenotypic effects. The mouse genome is the best characterized within mammals except for humans, and shows important conservation with the human genome[4]. Other advantageous features of the mouse include being small and inexpensive, which facilitates their use and housing. Consequently, their tissue is much more readily available than human tissue. Furthermore, their tight genetic and environmental control allows for clearer studies, especially with regard to complex diseases[4]. Importantly, samples can be obtained immediately after death in contrast with long post mortem

times (24-48 hrs) associated with obtaining human tissue. In addition, their smaller tissues facilitate a more comprehensive analysis across the entire organ of interest, yielding a more representative analysis than would be obtained by analysing as much data in larger tissues from other animals. Similarly, their smaller organs can be more easily visualized in their entirety using imaging modes which can typically only capture a minimal field of view at a high resolution. Their relatively quick life cycle and high metabolism permits the faster study of diseases which would otherwise take decades to develop in humans[4]. Last but not least, the development of a wealth of different inbred strains of mice, each characterized by a unique and uniform genome, has made the mouse a unique and powerful research model. Effectively, phenotypic differences amongst inbred strains can be matched to their genomic polymorphisms via Quantitative Trait Loci analysis (QTL), giving insight into the molecular factors and genes responsible for the trait of interest[134].

Nevertheless, care should be taken in drawing parallels between mice and humans in function of the organ and disease of interest. As far as glaucoma is concerned, its study in mice has been commonly performed in the posterior segment[135], but less so in the anterior segment. This was because the murine anterior segment which was originally thought to be too dissimilar to that of humans, and also because techniques to measure aqueous dynamics had not been adapted to the smaller mouse eye. Now that these technical challenges have been met, the question that needs to be addressed is whether the mouse is a suitable model for human aqueous dynamics.

3.6.2. Anatomy of the mouse eye

The mouse anterior chamber presents a general architecture similar to that of humans with respects to the lens, cornea, limbus and iris[136]. Note the lens is rounder and much larger than that of humans, occupying 75% of the intraocular space[137]. Importantly, several differences exist which must be taken into consideration for aqueous humour dynamics. First, the ciliary body in humans is directly attached to the sclera, whereas in mice only the posterior ciliary processes are, thereby bringing closer or almost exposing the external face of the ciliary body to the TM[137]. In mice, the iris often extends processes towards the cornea, which however does not block AH flow towards the irido-corneal angle[136]. Importantly, the mouse does not possess a scleral spur; yet it has muscle fibres departing from the ciliary body towards the posterior part of Schlemm's Canal[137].

Mice have a continuous SC (Fig. 6) which is however often divided by collagen bridges lined with endothelial cells. Interestingly, giant vacuoles have been detected in mouse SC, as observed in humans. Their TM exhibit similar trabeculae as humans, but are composed of only up to half as many beams[137]. Finally, the post-trabecular pathway in mice is simpler since it only possesses aqueous veins which link directly the SC to the episcleral veins[33,138]. Altogether, the evidence suggests the mouse is a suitable anatomical model for anterior segment studies, although further detailed investigation of their aqueous humour physiology and dynamics is required.

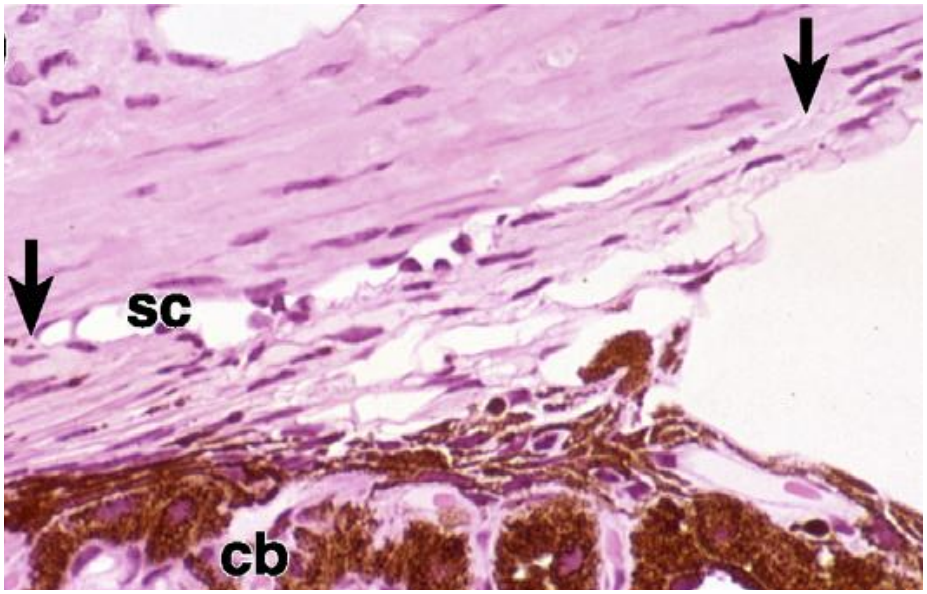

Figure 6: Histological image of the murine conventional pathway from a C57BL/6 mouse aged 2 months. SC: Schlemm's Canal. cb: Ciliary body. Arrowheads demarcate the anterior and posterior ends of the Trabecular meshwork. Reproduced from Smith et al. 2001, *BMC Developmental Biology* (*BioMed Central*). BioMed Central is an open access publisher which does not require permission to reproduce figures.

3.6.3. Physiology and aqueous dynamics

Pioneering studies for aqueous humour outflow have mostly used monkeys which share many similarities with humans. However, primates can be expensive and difficult to maintain. The numerous benefits of mouse models described earlier have prompted the research community to start using mice as a surrogate for human AH studies only in the last decade[5–17]. Perfusion studies have commonly been performed to investigate AH outflow in several species; such work is much more challenging in mouse eyes because of their small size. This results into flow rates as small as 0.1 µL/min during perfusions, or 100 times smaller than that found in human eye perfusions, which therefore requires a much higher precision for measurements. In addition, there is a higher risk of damaging internal structures such as the iris during cannulation, since the anterior chamber is so

small. Finally, such experiments are much more sensitive to leakage issues because of the small volumes and flow rates involved.

Nonetheless, several laboratories[5–17] have successfully measured AH outflow and a host of other related parameters, showing the mouse exhibits many similar characteristics to humans relevant to AH dynamics, as listed in Table 1. Note different strains of mice have been studied, yielding varying aqueous humour dynamics parameters (Table 1 reports the range of parameters measured in different strains such as C57BL/6J, BALB/cJ or NIH Swiss mice); interestingly, strains exhibiting different IOPs also seem to have different facility, although it remains unknown whether changes in IOP directly relate to changes in outflow facility.

	Human	**Mice**
Eye Diameter [mm]	24	3.3[139,140]
AH volume [µL]	200	5.9 [5]
IOP [mmHg]	16.2[20]	10-19[17,141,142]
C [µL/min.mmHg]	0.22[2]	0.0055-0.018[5–17]
F_u [µL/min]	0.28-1.52[72,73]	0.029-0.148[5,6,10,12,13,15]
Fin [µL/min]	2.4[2]	0.06-0.2[5,6,8–10,15]
EVP [mmHg]	7.6-11.4[143]	5.4-10.2[5,6,8,15,144]
F_u contribution [%]	4-54[73,145]	21-82% [5,6,10,12,13,15]
Number of TM trabeculae[-]	12-20	2-4[136]
Number of CC [-]	20-30[33]	8-28[33]

Table 1: Aqueous dynamics characteristics of humans vs. mice.

However, a fundamental unanswered question still revolves around unconventional outflow in mice. Depending on the mouse strain, it has been reported to range from 21-82%[5,6,10,12,13,15] compared to 4-54% in humans[73,145]. It should be noted that F_u is typically measured indirectly, using amongst other parameters values of F_p which can be dramatically affected by anaesthetics[146], which vary between studies. There is therefore a pressing need for direct visualization of tracers to reveal outflow patterns across the entire eye in mice. This would mark a crucial step towards consolidating

the mouse as a model for human AH circulation, as its potentially larger F_u would certainly fail to mimic human eyes' physiology.

3.6.4. Glaucoma in mice

Finally, naturally occurring mouse models of glaucoma exist, but the disease can also be genetically induced. In particular, the DBA/2J mouse strain has been shown to exhibit high intraocular pressures and corresponding lesions in the optic nerve similar to that observed in the human form of the disease[4,147,148]. However, its onset seems to be triggered by an angle-closure form of glaucoma wherein the iris forms synechias at the irido-corneal angle or with the lens, thereby impeding AH flow and increasing IOP[148]. Other murine models rely on altering the expression of genes identified in glaucomatous human patients such as Foxc, whose alterations were shown to replicate key features of the pathology[148]. Thus, the mouse is a promising model for glaucoma research, although its AH physiology still needs to be further investigated to confirm it behaves similarly to humans.

Chapter 2: Characterization of murine outflow facility using an optimized perfusion system

1. Introduction

In the last decade, there has been growing interest in perfusing mouse eyes to measure and study aqueous humour outflow[5–17]. However, mouse eyes are particularly challenging to perfuse because of their small size. Indeed, their diameter is 8-fold smaller than humans, and the volume of their anterior chamber is only 3% that of humans, resulting in perfusion flow rates up to 100 times smaller. Yet several laboratories have successfully measured aqueous humour outflow in vivo, providing promising insight into its fundamental mechanisms[5–17]. Similarly, our laboratory has developed a perfusion system for *enucleated* mouse eyes[12,13] because they present less confounding factors than in vivo experiments. Notably enucleated mouse eyes lack episcleral venous pressure, aqueous humour production and eliminate the need for anaesthetics. In this study, we aimed to better mimic physiological conditions during our ex vivo perfusions, by including control of hydration and temperature. In order to fully characterise our system, their effects on outflow facility were further characterised, as well as the effects of post-mortem times.

The effects of temperature on outflow facility have been previously investigated in enucleated human eyes. Van Buskirk showed the change in outflow facility between eyes perfused at different temperatures could be attributed solely to changes in aqueous humour viscosity[77]. This further suggested there was no metabolic activity that caused aqueous outflow at physiological temperature.

In large enucleated eyes such as humans' or monkeys', hydration is typically maintained during perfusion by immersing the eye in saline up to its limbus and covering it with moist tissue. Yet, owing to their small size, mouse eyes might be more sensitive to hydration effects. For example, a study showed mouse eyes lose up to 13% of their weight within 15 min following enucleation[149]. This effect was reversed following rehydration, which suggests evaporation rates could be non-negligible in mice. Finally, effects of post mortem times on outflow facility have been previously investigated to validate the viability of the tissue as a perfusion model. Results from two studies on

bovine eyes [78,150] revealed changes in outflow facility up to 24 hrs following death, although it is not clear whether they were statistically significant. In addition, the washout rate was more pronounced in eyes stored for 24 hrs in DMEM[150].

Therefore, this study aimed at characterizing the effects of hydration, temperature and post-mortem time on outflow facility measurements in enucleated mouse eyes. More specifically, paired eyes were perfused *(a)* while immersed or not in a saline bath, *(b)* in a saline bath at room or physiological temperature, *(c)* after storage in PBS or DMEM at the following post mortem times: 0, 3 and 24 hrs.

2. Methods

All experiments were performed using ex vivo tissue and were done in compliance with the ARVO Statement for the Use of Animals in Ophthalmic and Vision Research and the Animal Scientific Procedures Act 1986.

2.1. Perfusion

Total outflow, represented by the sum of conventional and unconventional outflow, was measured in mice using a previously validated perfusion system for mouse eyes[12,13]. Following cervical dislocation, eyes were enucleated and stored in PBS at 4°C. Enucleation was performed either by (1) dissecting out the eye and its surrounding muscles with scissors or, (2) pulling out the eye with tweezers wedged behind the eye, in its socket. Paired eyes were perfused sequentially, such that the first eye was perfused within 15 min post mortem, immediately followed by perfusion of its contralateral eye, within 3 hrs post mortem. For perfusion, the eye was placed on a custom-made post filled with gauze using cyano-acrylate glue. A 33G needle (WPI, Stevenage, UK) was held with a special needle holder (MMP Kit, WPI, Stevenage, UK) which was inserted in a micro-manipulator. The needle was inserted into the anterior chamber under a stereoscopic microscope using the micro-manipulator. The needle was connected to a pressure transducer (142PC01G; Honeywell, Fort Washington, PA) which recorded continuously the pressure inside the eye (Fig. 7). In addition, the needle was linked to a syringe (25 or 50 µL; Hamilton GasTight, Reno, NV) placed on a computer-controlled syringe pump (PhD Ultra; Harvard Apparatus, Holliston, MA). A custom

LabView program[151] (National Instruments Corp., Austin, TX) allowed the user to define a pressure which was maintained by the variable flow-rate of perfusate delivered by the syringe-pump. The eye was perfused at 4, 8, 15 and 25 mmHg. Prior to each pressure step, the eye was pre-pressurized for up to 5 minutes with a PBS-filled reservoir connected to the tubing via a three way valve; the three way valve was thereafter closed such that the eye was no longer connected to the PBS-filled reservoir and was pressurized by the syringe pump only. Eyes were perfused for up to 30 min at each pressure step to ensure at least 10 min of stable flow rate data was successfully obtained (Fig. 8A). The perfusion solution was Dulbecco's PBS with cations and 5.5 mM glucose filtered through a 0.22 µm filter, which will be referred to as filtered DBG. DBG was found to mimic more closely the composition of the mock aqueous humour optimized by Bárány [152] for acute perfusions (Table 2). The LabView software recorded the pressure inside the eye every 10 seconds, as well as the flow rate delivered and the cumulative volume injected by the syringe pump.

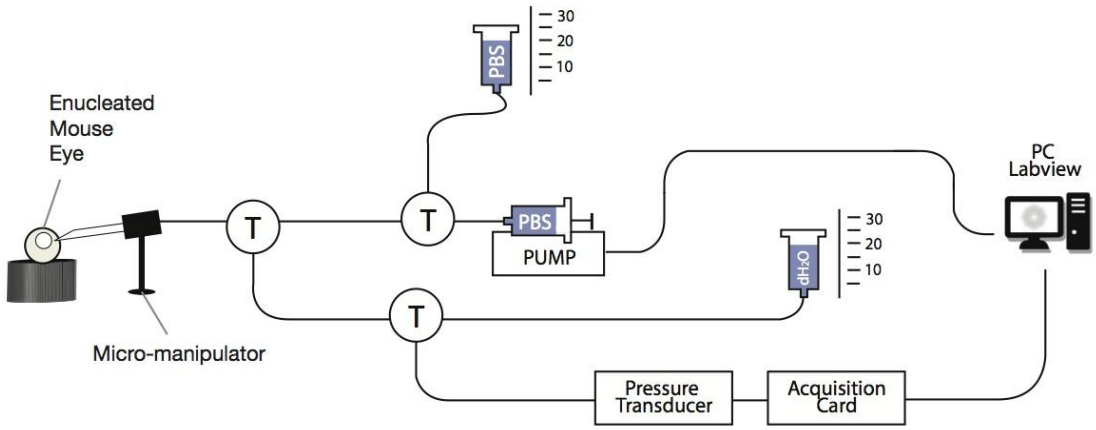

Figure 7: Diagram of the mouse eye perfusion system. The pressure transducer is connected to a water-filled (dH_2O) reservoir for calibration. The PBS-filled reservoir is used to pre-pressurize the eye at each increasing pressure step. Drawing by M. Boussommier-Calleja.

mM	Mock aqueous humour	dPBS+ 5.5 mM glucose	DMEM*
Inorganic Salts			
NaCl	136.89	137.93	110.34
KCL	4.69	2.67	5.33
$CaCl_2$	1.53	0.901	1.8
$MgCl_2$	0.67	0.493	
Na_2HPO_4	0.486	8.06	
NaH_2PO_4	0.114		0.916
KH_2PO_4		1.47	
$Fe(NO_3)_3$			0.000248
$MgSO_4$			0.813
$NaHCO_3$			44.05
Glucose	5.5	5.5	5.5

Table 2: Composition of dPBS and DMEM compared to the mock aqueous humour optimized by Bárány. *In addition, DMEM contains the following compounds: Amino Acids: Glycine L-Arginine hydrochloride, L-Cystine 2HCl, L-Glutamine, L-Histidine hydrochloride-H_2O, L-Isoleucine, L-Leucine, L-Lysine hydrochloride, L-Methionine, L-Phenylalanine, L-Serine, L-Threonine, L-Tryptophan, L-Tyrosine, L-Valine. Vitamins: Choline chloride, D-Calcium pantothenate, Folic Acid, Niacinamide, Pyridoxine hydrochloride, Riboflavin, Thiamine hydrochloride, i-Inositol. Other components: HEPES, Phenol Red, Sodium Pyruvate. Composition of products from LifeTechnology: DMEM (22320-022) and dPBS (14040-091).

2.2. Conventional and unconventional facility measurement

As previously discussed, Goldmann's equation describes the balance of inflow and outflow inside the eye. During the perfusion, an additional source of inflow exists, denoted as *F*. Thus Goldmann's equation becomes:

$$\mathrm{F_p} + \mathrm{F} = \mathrm{C} \times (\mathrm{IOP} - \mathrm{EVP}) + \mathrm{F_u}$$

Equation 7

In enucleated eyes, it is assumed both F_p and *EVP* are zero, thereby simplifying Goldmann's equation as follows:

$$\mathrm{F} = \mathrm{C} \times \mathrm{IOP} + \mathrm{F_u}$$

Equation 8

Thus, conventional (*C*) and unconventional facility (F_u) are calculated by fitting our flow-rate vs. pressure data to the simplified Goldmann's equation (Eq. 8). More specifically, steady flow-rates (red highlights in Fig. 8A) obtained at 4,8,15 and 25 mmHg are averaged and plotted against pressure for each eye (Fig. 8B). Data points at each pressure are averaged between all eyes for a given study, yielding a typical Flow Rate vs. IOP plot shown in Fig. 8C, which is fitted with a best-fit linear regression whose slope and intercept correspond to, respectively, the pressure-dependent or

conventional facility (*C*), and the pressure-independent or unconventional facility (F_u). Note 8 mmHg is considered to represent the physiological pressure drop across the conventional pathway. For example, it was measured to be 6 mmHg in C57BL/6J[15]. Since there is no episcleral venous pressure in enucleated eyes, the pressure drop they experience is solely defined by their IOP. Importantly, Goldmann's equation assumes *F* and *IOP* have reached steady state, and *C* and F_u do not change with *IOP*. A more detailed analysis of some of the latter assumptions can be found in the last chapter of this thesis (Chapter 7).

For each mouse eye the conventional and unconventional facility is calculated as explained (see Fig. 8B-C). An average conventional and unconventional facility is then computed over the entire cohort of mouse. For every cohort, the range of R^2 values of the best fit obtained for each mouse is given as an indication of the accuracy of the linear best-fit to our data.

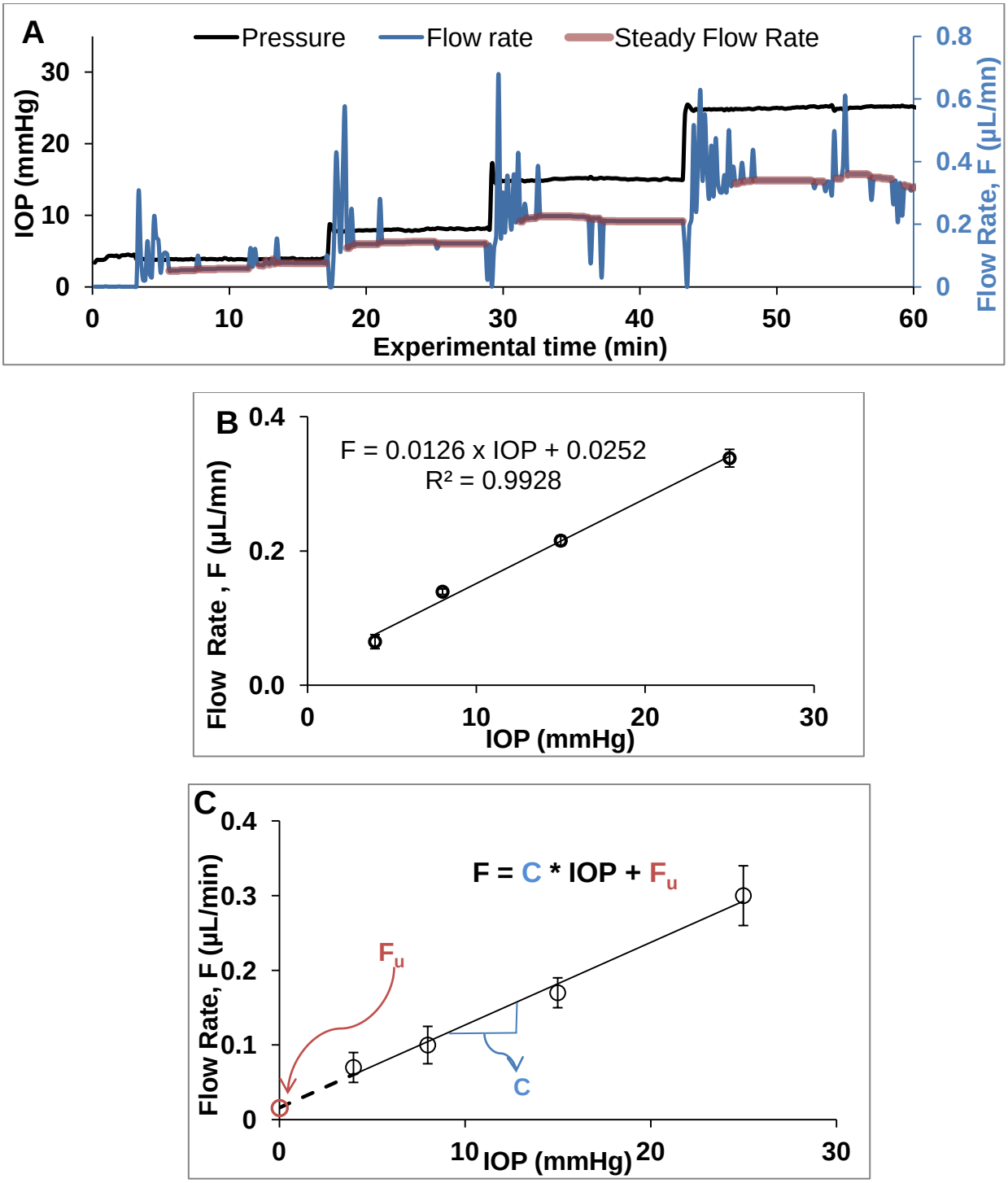

Figure 8: Typical perfusion tracings. A) Example of a perfusion tracing showing the flow rates of the perfusate being delivered by the syringe pump (blue line) to maintain IOP steady at 4, 8, 15 and 25 mmHg (black line). Red highlights show the flow rates deemed steady and averaged at each pressure step. B) Flow rate vs. IOP tracing obtained from the data shown in A, wherein the averages of the steady flow rates are plotted against their pressure level. C) Diagram showing how *C* and F_u are obtained from a typical *F* vs. *IOP* plot. The slope of the best-fit linear equation to the average data is used to estimate conventional facility *C*, whereas its intercept is used to estimate unconventional outflow F_u. Thus, conventional facility in this example (B) was 0.0126 µL/min/mmHg and Fu was 0.0252 µL/min. For each study, we report the range of R^2 values calculated for each individual eye.

2.3. Experimental design

Male and female C57BL/6 mice supplied by Charles Rivers aged 2-24 weeks were used for this study. Mice were fed ad libitum and maintained at 21°C with a 12-hour light (6 AM to 6 PM) and 12-hour dark cycle. Eyes were enucleated 10-15 min following cervical dislocation and placed in PBS at 4 °C. Paired eyes were sequentially perfused in a randomized order, such that one eye acted as the control for its contralateral eye. Table 3 shows the total number of eyes perfused in each cohort, showing most eyes were paired, although data from some unpaired eyes was also used when the perfusion of their contralateral eye failed. Thus, 24 mice were used for this study; 5 out of 48 experiments failed, representing a 90% success rate.

	Total number of eyes	Unpaired eyes	Paired eyes
Cohort 1	7	1	6
Cohort 2	12	4	8
Cohort 3A	10	-	10
Cohort 3B	8	-	8
Cohort 3C	6	-	6

Table 3: Number of mouse eyes perfused in cohorts 1,2 and 3.

Three cohorts of animals were used to investigate the effects of hydration, temperature and post mortem times, as described below. Throughout this report, each cohort will be identified with a unique number, so as to be able to distinguish them.

The first cohort of mice (Cohort 1) was used to investigate the effects of hydration on AH outflow in enucleated mouse eyes. More specifically, during perfusions, eyes were either immersed in a bath of isotonic saline up to their limbus and covered with a tissue paper, or simply covered with a tissue paper moistened every 15 min with a drop of PBS as done previously (Fig. 9 A and B). Eyes perfused in the former and latter configurations will be referred to as “in” or “out” of isotonic saline

bath, respectively. For perfusion, 50 µL of filtered DBG (5.5 mM glucose in DPBS) was backfilled from the needle tip. More specifically, the needle was placed into a 50 µL drop of DBG placed with a pipette on a Petri dish. Once the needle tip was in the drop of DBG, the PBS-filled reservoir connected to the needle was lowered so as to draw the solution into the needle and the tubing. This procedure was used in every study to backfill the needle with the solution of interest. This was typically done to avoid having to fill the entire tubing with the solution of interest. This was particularly important when using expensive or hazardous substances such as pharmacological agents, anti-metabolic agents or fluorescent tracers (cf. Chapter 3, 5, 6).

The effects of temperature on outflow were investigated in a second cohort (Cohort 2) of enucleated mouse eyes. Paired eyes were immersed in isotonic saline and perfused either at room or physiological temperature (i.e. 20 vs. 35 °C; Fig. 9C). A custom-made temperature controller was used to maintain the eye at physiological temperature, which was recorded via a thermocouple placed in the immediate vicinity of the eye. For eyes perfused at room temperature, the temperature controller was not used and a thermometer was generally used to assess temperature at the beginning and end of the perfusion which was approximately 20 °C. 50 µL of filtered DBG was backfilled from the needle tip for perfusion, as previously described.

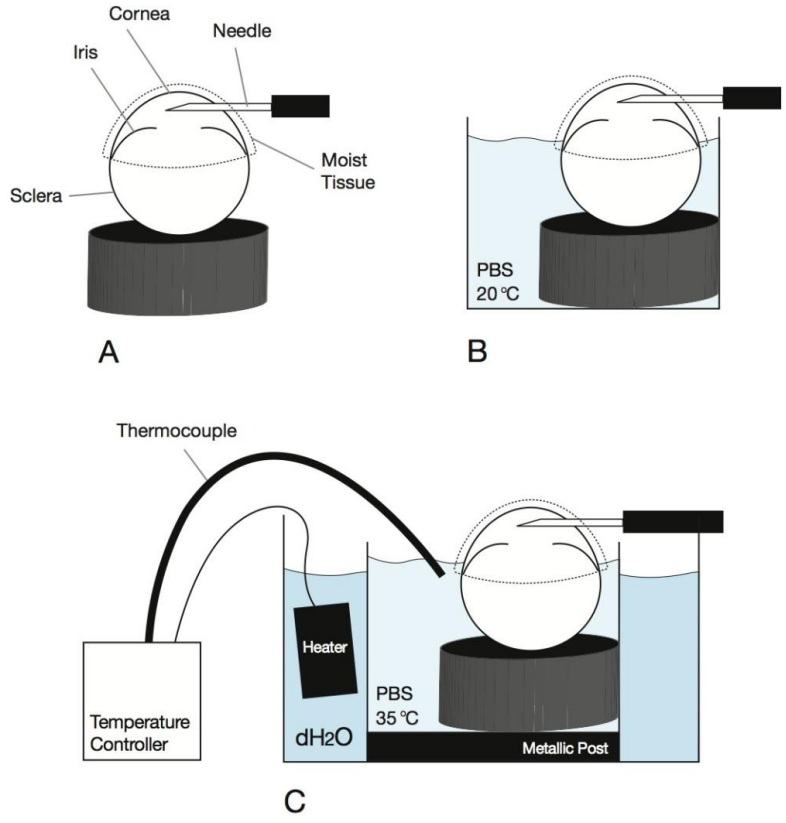

Figure 9: Different configurations for enucleated eyes during perfusions. A) Originally, eyes were covered with a tissue kept moist with PBS drops every 15 min. B) Alternatively, eyes were immersed in an isotonic saline (Dulbecco's PBS) bath up to their limbus as well as covered with a tissue continuously soaked in saline. C) Finally, eyes immersed in the isotonic saline bath were kept at physiological temperature (35 °C) with a customized temperature-controller system which tracked the temperature next to the eye via a thermocouple. After cannulation, the chamber was covered with a lid to help maintain a steady and homogeneous temperature in the bath. Drawing by M. Boussommier-Calleja.

The last cohort (Cohort 3) was used to test the effects of post-mortem times on outflow facility in enucleated mouse eyes. Three sub-groups examined different post mortem times in eyes covered with a tissue paper moistened with saline (Fig. 9A). The first and second sub-group examined outflow facility of eyes stored in PBS at 4°C for 0 vs. 3hrs post mortem (Cohort 3A), or for 0 vs. 24 hrs post mortem (Cohort 3B). The last sub group measured outflow resistance in eyes stored for 0 vs. 24 hrs in DMEM at 4°C (Cohort 3C). 150 µL of filtered DBG was backfilled from the needle tip for perfusion, as previously described. Experiments on Cohorts 3B and 3C were performed by Mr. Jacques Bertrand.

2.4. Statistical analysis

Within each cohort, unpaired two-sided students t-tests were performed to assess whether the difference in conventional and unconventional outflow between eyes perfused under different conditions was statistically significant. A paired t-test was used for groups containing only paired eyes (Cohort C1, C2 and C3). A similar analysis was carried out on the flow rates measured at each pressure step, which represent total facility. A one sided t-test was used to assess whether unconventional outflow was significantly different from 0.

3. Results

3.1. Cohort 1, F_u is negligible in enucleated eyes placed in the isotonic saline bath

Our flow rate vs. pressure data revealed a linear relationship, accurately explained by our best fit linear regressions, whose R^2 values ranges from ($0.783 \leq R^2 \leq 0.997$; Fig. 10). The intercept of the best fit linear regression, or F_u, was -0.0003±0.0041 (N=3) vs. 0.0810±0.0295 (N =4) µL/min in eyes in or out of the isotonic saline bath, respectively. The difference between eyes in or out of the isotonic saline bath was statistically significant (p =0.011; unpaired t-test). Furthermore, F_u was statistically different from 0 in eyes out of the isotonic saline bath (p =0.006; one-sided t-test), but not in eyes placed in the isotonic saline bath (p =0.46; one-sided t-test).

In contrast, the slope of our best fit linear regressions, or C, was unaffected by hydration (0.0056±0.0016 vs. 0.0063±0.0036 µL/min.mmHg in eyes in or out of the isotonic saline bath; p =0.75, unpaired t-test). In addition, flow rates were statistically different at each pressure level (p ≤0.009; unpaired t-test) except at 25 mmHg (p =0.134; unpaired t-test).

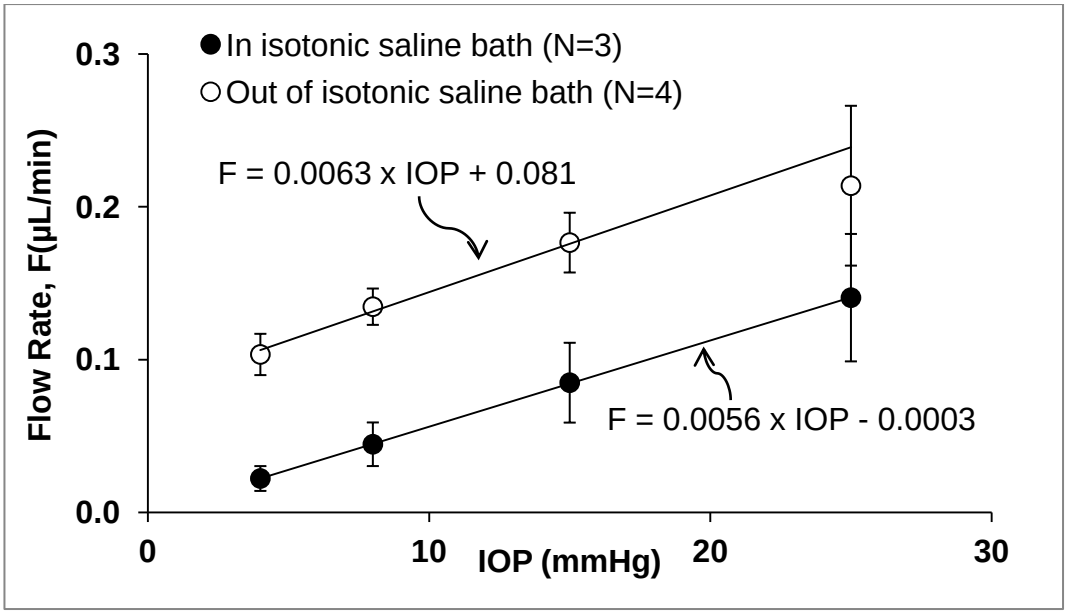

Figure 10: Flow Rate vs. IOP data from Cohort 1. Average flow rate at each IOP level for eyes out of (open circles) or in (filled circles) the isotonic saline bath. The R^2 values of the linear best-fit regression lines computed for each individual mouse ranged between 0.783 and 0.997. Bars are standard deviations and lines represent the best-fit linear regressions to average data.

3.2. Cohort 2, temperature effects on *C* are larger than viscosity effects

The flow-rate vs. pressure data for Cohort 2 was also well explained by our best-fit linear regression, which explained most of the variability of the data for each eye (i.e. $0.949 \leq R^2 \leq 0.999$). The unconventional outflow, or F_u, of eyes placed in the isotonic saline bath perfused at 35 °C or 20°C was -0.0155 ±0.0385 (N =6) and 0.0113±0.0248 (N =6) µL/min (Fig. 11). The difference was not statistically significant (p =0.19; unpaired t-test). In addition, neither F_u were statistically different from 0 ($p \geq 0.16$; one-sided t-test), similarly to eyes in the isotonic saline bath from Cohort 1.

Conventional outflow, or C, was 0.0069±0.0021 (N =6) vs. 0.0172±0.0028 (N =6) µL/min.mmHg in eyes placed in the isotonic saline bath perfused at 20 or 35 °C (Fig. 11). Therefore, the change in temperature caused a 2.5 ±0.86-fold increase in C which was statistically significant ($p = 4 \times 10^{-5}$; unpaired t-test). Importantly, this increase was significantly higher than the 1.4 fold increase predicted by changes in viscosity (p = 0.004; two-sided t-test). This is illustrated in Fig. 11, wherein the conventional facility expected based on the increase in viscosity from 20 to 35°C is shown in green, which is obviously smaller than that measured at 35 °C. The difference in flow rates was statistically significant at 15 and 25 mmHg ($p \leq 0.003$; unpaired t-test), only barely significant at 8 mmHg (p =0.054; unpaired t-test) and not significant at 4 mmHg (p =0.268; unpaired t-test).

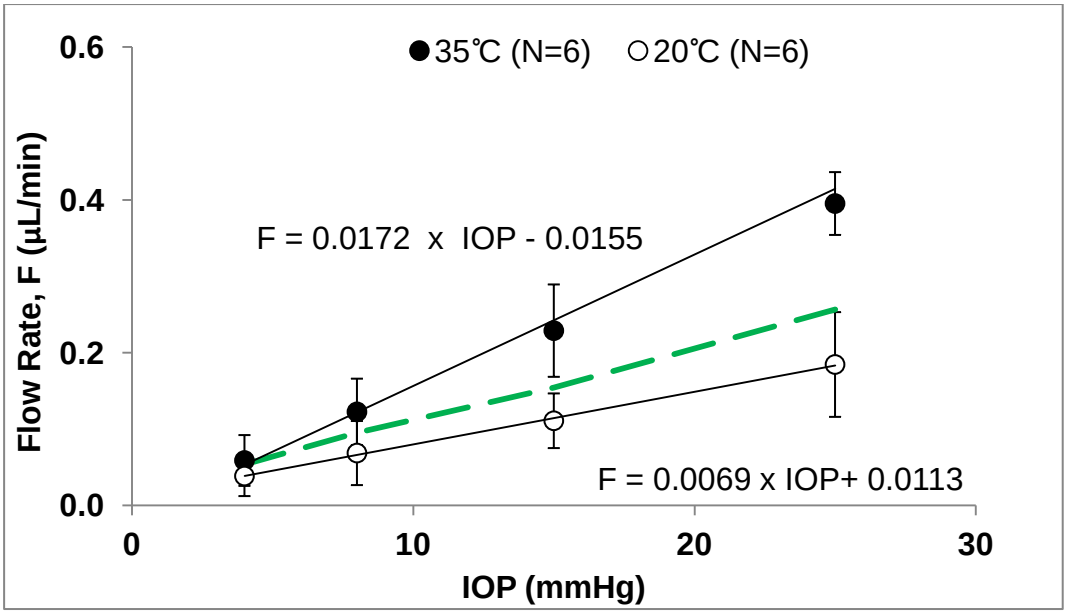

Figure 11: Flow Rate vs. IOP data from Cohort 2. Average flow rate at each IOP level for eyes in isotonic saline bath perfused either at 20°C (open circles) or 35°C (filled circles). The green line shows the increased slope or conventional facility expected based on the decrease in viscosity from 20 to 35 °C. The R^2 values of the linear best-fit regression lines computed for each individual mouse ranged between 0.949 and 0.999. Bars are standard deviations and lines represent the best-fit linear regressions to average data.

3.3. Cohort 3, Post mortem times of 24 hrs affect *C*

Conventional outflow facility in Cohort 3A was 0.0053±0.0025 (*N* =5) in eyes perfused immediately after death and 0.0050±0.0025 (*N* =5) µL/min.mmHg in paired eyes perfused 2-3 hours later. Therefore, post mortem times of 3 hrs did not affect outflow facility (*p* =0.65; paired t-test). More specifically, the normalized difference in conventional facility (C_{diff}; see Eq. 9) between paired eyes was in average 10.2±9.7%. This normalized difference was calculated as the difference in conventional facility measured in the eye perfused immediately after death (C_{t0}) and the eye perfused after longer storage times (C_t), normalized by their sum (Eq. 9).

$$C_{diff} = \frac{C_{t0} - C_t}{(C_{t0} + C_t)}$$

Equation 9

Conventional facility in eyes perfused after death was 0.0064±0.0011 (N =4) µL/min.mmHg and became 0.0055±0.0027(N =4) µL/min.mmHg in their contralateral eyes stored in PBS at 4°C for 24 hrs after death (Cohort 3B). Thus, storage in PBS for 24 hrs post mortem caused a decrease in conventional facility, although it was not statistically different (p =0.55; paired t-test). The average change in conventional facility between contralateral eyes (C_{diff}) caused by storage in PBS for 24

hrs was 22.0±15.3%. Thus the average difference between eyes perfused at 0 vs. 24 hrs after death became two-fold larger than that found between eyes perfused at 0 vs. 3 hrs post mortem.

In Cohort 3C, we investigated whether storing eyes in DMEM rather than PBS helped maintain conventional outflow facility. Conventional outflow facility in eyes stored in DMEM for 24 hrs was 0.0044±0.0013 (*N* =3) µL/min.mmHg, compared to 0.0046±0.0005 (*N* =3) µL/min.mmHg in their contralateral eyes perfused immediately after death (*p* =0.66; paired t-test). Thus storing eyes in DMEM for 24 hrs only caused a 4.7±5.2% change in conventional facility (C_{diff}) compared to their contralateral eyes perfused immediately after death. Note the conventional facility of eyes perfused immediately after death in this cohort was significantly smaller than that of eyes perfused right after death in Cohort 3A or 3B (0.0046 in cohort 3C vs. 0.0053 or 0.0064 in cohorts 3A and 3B respectively). The difference might be attributable to the use of mice with varying age, or of different gender, which we show in the last chapter might have an effect on conventional facility (Chapter 7). Thus conventional facility was unchanged following 3 hrs of storage in PBS, and became much larger following storage in PBS for 24 hrs (10.2 vs. 22.0%; Cohort 3A vs. Cohort 3B). In contrast, eyes stored in DMEM for 24 hrs showed a conventional facility very similar to their paired eyes perfused immediately after death (4.7% difference; Cohort 3C). This is further illustrated in Fig. 12, wherein the conventional facility of eyes perfused immediately after death is plotted against that of their paired eyes perfused either 3 or 24 hrs post mortem, following storage in PBS or DMEM. One data point represents one pair of eyes; the closer the data point is to the unity line, the more similar are the conventional facility of the paired eyes. It is clear the data points from pairs of eyes within Cohort 3B differ the most from the unity line, whereas those from Cohort 3C are found significantly closer to it.

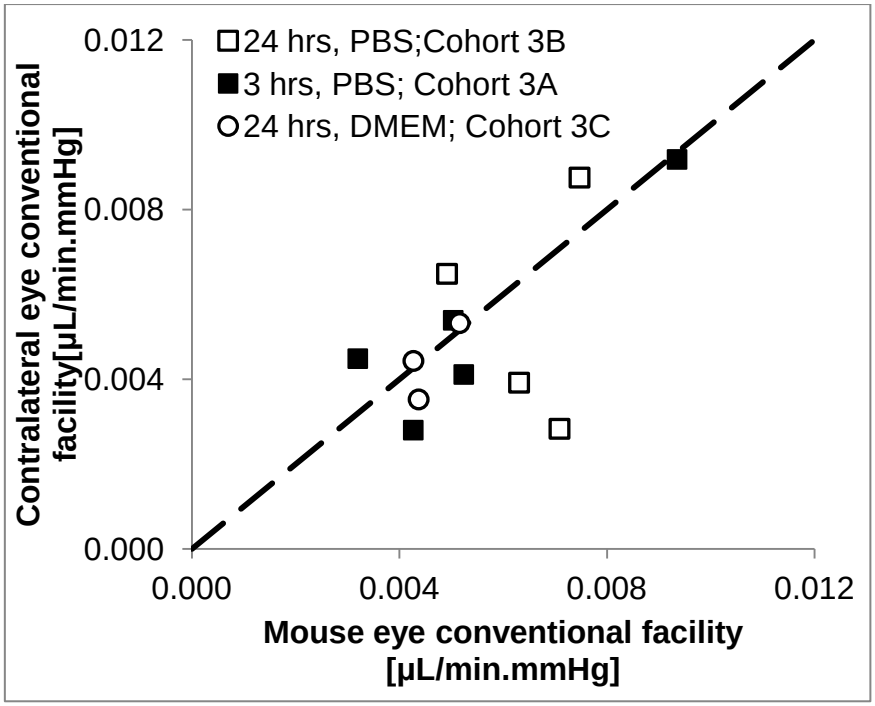

Figure 12: Conventional facility data from cohort 3. Conventional facility of the eye perfused immediately after death (x-axis) plotted against that of its contralateral eye (y-axis) perfused following storage at 4°C in PBS for 3 hrs (filled squares), in PBS for 24 hrs (open squares), or in DMEM for 24 hours (open circles). One data point corresponds to one mouse. The closer data points are to the unity line (dashed line), the more similar are the conventional facilities of the contralateral eyes.

Note unconventional outflow in cohort 3 varied from 0.0093 to 0.0290 µL/min (Table 4) and was only statistically different from 0 in eyes from Cohort 3C perfused following 24 hrs storage in DMEM (p =0.017; one-sided t-test). This variability in unconventional outflow is most likely attributable to the eyes being hydrated variably. Neither post mortem times of 3 or 24 hrs following storage in DMEM or PBS caused a statistically significant change in unconventional outflow (p ≥0.27; paired t-test).

F_u [µL/min]	0 hrs post mortem	3 or 24 hrs post mortem
Cohort 3A	0.0191±0.0169	0.0200±0.0256
Cohort 3B	0.0250±0.0103	0.0178±0.0117
Cohort 3C	0.0093±0.0084	0.0290±0.0094

Table 4: Unconventional outflow in Cohort 3

4- Discussion

We successfully included hydration and temperature-control to mimic physiological conditions in a previously developed perfusion system[12] for enucleated mouse eyes. In vivo, the cornea is hydrated by a tear film and temperature in the eye lies between 35 and 37°C. Both hydration and temperature were shown to have important effects on outflow facility: a thorough hydration eliminated unconventional outflow, while a physiological temperature dramatically increased conventional outflow. Conventional facility measured in enucleated C57BL/6J mouse eyes with our system at 35°C(0.0172±0.0028 µL/min.mmHg, Cohort 2) lay well within the range of outflow facility measured in vivo reported in the literature (0.005-0.018[5–11,14–16] µL/min.mmHg). Thus, we present a technique to measure conventional facility in enucleated mouse eyes in a physiologically-relevant manner so as to investigate its fundamental mechanisms.

An interesting finding was that the magnitude of the increase in conventional facility caused by temperature changes exceeded that expected based on viscosity changes. Indeed, the viscosity of water is known to be highly dependent on temperature, and will therefore intrinsically increase aqueous humour outflow facility at higher temperatures. Accordingly, an increase from 20 to 35°C should only increase viscosity, and thus outflow facility, by a factor of 1.4. However, we observed a much larger increase (2.5±0.86, see Cohort 2) which, importantly, was significantly different from that predicted based on viscosity effects (p= 0.004; two-sided t-test). Therefore, our findings suggest the additional increase in outflow facility that we observed could be attributed to metabolic activity, as opposed to the passive increase caused by changes in physical properties of aqueous humour. This finding is highly interesting as it contradicts previous studies performed in enucleated human eyes, which showed changes in outflow facility with temperature could be entirely explained by changes in viscosity[77]. Studies showing anti-metabolic agents had little or indirect effects on conventional facility reinforced the concept of the trabecular pathway being a passive rather than a metabolic-dependent filter[78,153,154]. However, such studies suffered from limitations such as long post-mortem times or lack of physiological temperature control during perfusions. This prompted us to test the hypothetical metabolic-dependence of outflow facility, as discussed in Chapter 5.

In addition, our results show unconventional outflow in enucleated mouse eyes might have been overestimated in previous studies[12,13] due to incomplete hydration. More specifically, unconventional outflow went from representing 31% of outflow at 8 mmHg in eyes covered with a moist tissue to zero in eyes immersed in an isotonic bath (Cohort 1). This is somewhat similar to the relatively high unconventional outflow (~66%) obtained in previous similar studies where enucleated mouse eyes were only covered with a moist tissue[12,13].The fraction of unconventional outflow (F_u%) at a given pressure (IOP) was calculated according to Eq. 10, where F_u and C are respectively, unconventional and conventional outflow.

$$\mathrm{F_u\%} = \frac{\mathrm{F_u}}{\mathrm{F_u} + \mathrm{C} \times \mathrm{IOP}}$$

Equation 10

It is rather difficult to ascertain the reasons underlying the effects of hydration on unconventional outflow, as the mechanisms of unconventional outflow remain unknown. In our opinion, a lack of hydration could fail to prevent evaporation of perfusion fluid through the cornea. In other words, there could be a constant loss of perfusion fluid during perfusion due to evaporation which is compensated by increased flow rates of perfusate injected by the syringe pump. Thus at every pressure level, the pump has to deliver higher flow rates which shifts the flow rate vs. pressure plot upwards, resulting in a higher intercept or unconventional outflow. Measurements of weight loss in enucleated eyes due to evaporation in another study support this hypothesis[149]. Mouse eyes were weighed repeatedly within 13 min following death and enucleation at room temperature, showing a progressive loss of weight of up to 13%, which corresponds to a rate of perfusion fluid loss of 0.18 µL/min (if perfusion fluid density is equated to that of water). This rate of evaporation is similar, although somewhat larger, than unconventional outflow measurements from the current or previous studies[12,13] (0.09-0.11 µL/min), most likely because eyes in our studies were still partially hydrated with PBS drops every 15 min. In addition, Wisard et al. showed the original weight of the mouse eye was restored following immersion in PBS for 1 hr[149], suggesting these evaporation mechanisms are reversible. This agrees with our hypothesis that hydrating the eyes similarly prevented the loss of

perfusion fluid, thereby eliminating the need for higher flow rates during perfusion, thus eliminating the intercept of the flow rate vs. IOP relationship, or F_u.

Our data showing a negligible unconventional outflow in enucleated mouse eyes could be consistent with stoppage of uveal adsorption of aqueous humour following stoppage of blood perfusion, as shown previously in enucleated porcine eyes[155]. However, unconventional outflow is alternatively thought to rely on trans-scleral passive or bulk flow[66,69], which should not be affected by enucleation and thus still be present in enucleated eyes. Regardless, our results demonstrate hydration is an important physical parameter for perfusions which might have been overlooked in past studies. Indeed, only one study specified they applied drops of PBS on mouse eyes during in vivo perfusions[9], which might be similarly susceptible to evaporation. This in turn could explain the high variability in unconventional outflow reported in the literature ranging from 21 to 82%[5,6,10,12,13,15], although this effect could also be attributed to strain differences. In contrast, conventional facility measured in the current study in enucleated mouse eyes was similar to values reported in vivo[5–11,14–16], suggesting death or enucleation do not affect conventional facility. This is further supported by a previous study which reported similar values for conventional facility in living mouse eyes under anaesthesia and following a lethal dose of anaesthetics[6]. Further, human studies have also reported similar conventional facility values for human eyes in vivo using tonography and shortly after enucleation[156–158].

Another important aspect of this study concerned the changes of conventional facility caused by post-mortem times. This has only been investigated in bovine eyes, first by Bárány in 1954[78] and more recently by Gual[150]. Both studies reported mild changes in AH outflow with post mortem times, without specifying whether the difference was statistically significant. More specifically, data from Gual et al. suggests conventional outflow facility was 30% lower in eyes stored in DMEM at 4 °C for 24 hrs. However, both studies used unpaired eyes, which could have had naturally different facilities regardless of post mortem times. In contrast, our study consisted of using paired eyes which are more likely to have intrinsically similar conventional facilities (see below). In our study, one eye perfused immediately after death was compared to its contralateral eye perfused 3 or 24 hrs later. Our experiments showed the change in conventional facility was 10.2±9.7% within 3hrs post

mortem. In contrast, it was 22.0±15.3% after 24hrs of storage in PBS at 4 °C., although the change was not statistically significant (p =0.55; paired t-test). Finally, we show storing eyes in DMEM minimizes the average difference between paired eyes to 4.7±5.2%, similar to the value obtained for eyes perfused within 3 hrs. Thus, although the effects are not statistically significant, our results show post mortem time can still potentially change outflow facility, and introduce large variability in the results. Indeed, the coefficient of variation for conventional facility was 48% in eyes stored in PBS for 24 hrs as opposed to 17% for eyes perfused immediately after death (Cohort 3B). This can potentially blur results, especially in studies measuring differences following pharmacological treatment, as shown in Chapter 3.

The reasons underlying the change of AH outflow with post mortem times could obviously relate to anatomical changes. Yet Bárány showed total resistance in eyes perfused with hyaluronidase did not change with post mortem times[78]. Thus he proposed post mortem times were promoting the depolymerisation of the hyaluronidase-sensitive outflow resistance, which equates to the resistance generated by the ground substance of the outflow pathway. However, studies showed GAG-profiles of human corneoscleral explants were well maintained within 7 to 14 days post mortem[159]. Interestingly, this study also reported ultra structural changes in the TM of human eyes stored in PBS at 5°C for 48 hrs post mortem[159].

Bárány further proposed post mortem times might cause the loss of carbon dioxide in the aqueous, thereby reducing its acidity and affecting tissue hydration[78]. Note changes of aqueous humour composition cannot explain our results as mouse eyes are always exposed to mock aqueous humour (DBG) during our perfusions since the anterior chamber is typically turned over at least 2-3 times during a perfusion. In light of our previous findings, we hypothesize the decrease in conventional facility we observed could be partially caused by the loss of metabolic activity following death. Interestingly, storing eyes in DMEM minimised the effects of post-mortem times on conventional facility. This agrees with previous studies showing storing TM samples in PBS at 5 °C for up to 2 days caused advanced degradation, which could be reversed following culture in DMEM for a week[159]. This further suggests conventional facility might deteriorate because of lack of metabolic activity, which in turn is somewhat better maintained by DMEM. Altogether, our results

show that eyes should be perfused within 3hrs following death in agreement with previous studies[150], or if otherwise unavoidable, within 24hrs if stored in DMEM at 4 °C. This further emphasises the mouse as a powerful model for eye perfusions as eyes can readily be obtained immediately after death.

Importantly, the natural variability in conventional facility between paired eyes can also be inferred from our post-mortem study. Thus, we show the difference in conventional facility between paired eyes perfused either immediately after death or 3 hrs later is only 10.2%. This corresponded to a coefficient of variation for the change in conventional facility between paired eyes of 31.5% (Cohort 3A). In comparison, the coefficient of variation was 54% between unpaired eyes of different animals from Cohort 3A perfused under identical conditions, immediately after death. This agrees with observations made by Bárány who showed the coefficient of variation between paired cattle eyes was 14% as opposed to 24% for unpaired eyes[78], although he measured total outflow resistance rather than conventional facility. Thus, our results confirm there can be important variations in conventional facilities between different mice which become dramatically reduced between paired eyes. Thus, any difference observed in conventional facility between paired eyes will be much more likely attributable to the treatment of interest than between unpaired eyes which can possess intrinsically different facilities. Consequently, every study described in this thesis has used paired eyes, although a few unpaired eyes were included when their contralateral eye's perfusion failed.

In conclusion, a perfusion system has been designed to measure outflow facility in enucleated mouse eyes in a physiologically relevant manner. Importantly, unconventional outflow was shown to be minimal under efficient hydration conditions, providing a more direct measurement of conventional facility alone. Owing to the sensitivity of unconventional outflow to hydration, most of our subsequent studies mainly focus on conventional facility measurements. This study also demonstrates that eyes should be perfused within few hours following death, or else it could affect results, in particular pharmacological effects as further shown in Chapter 3. Thus we have developed a powerful system to reliably measure conventional facility in mouse eyes, which should prove invaluable to unravelling underlying mechanisms of IOP regulation.

Chapter 3: Pharmacological Manipulation of Conventional Outflow Facility in Ex Vivo Mouse Eyes

This chapter consists of a paper published in IOVS[79], reproduced with permission from Association for Research in Vision and Ophthalmology (ARVO; see Appendix 2).

1- Introduction

Mice provide important models for glaucoma research, due to their genetic malleability and the extensive catalogue of molecular tools that may be exploited to investigate disease mechanisms[4]. While most glaucoma research involving mice has focused on the effect of elevated intraocular pressure (IOP) on the optic nerve, a small but growing community [5–17] has begun using mice to investigate the physiology of aqueous humour outflow, with the aim to better understand the mechanisms of IOP regulation. In fact, recent data show that the morphology and behaviour of the murine conventional outflow pathway is more similar in some ways to humans than are non-human primates (e.g., like humans[160], mice do not appear to exhibit 'washout'[12], while 'washout' is observed in monkeys[160]). Notwithstanding the utility of mouse models, it remains an open question whether mice are appropriate models for IOP regulation at the level of the conventional outflow pathway as occurs within human eyes.

Compounds that affect IOP in humans tend to have similar effects in mice, however the response is not always through the same mechanisms, as noted previously. For example, latanoprost lowers IOP[6,10,144,161,162] and increases conventional outflow facility in mice[6,10] without any detectible effects on unconventional outflow[6,10], unlike the response in human eyes where latanoprost increases both conventional[163] and unconventional outflow[164]. This suggests that the physiology and pharmacology of aqueous humour outflow may differ substantially between mice and humans, and should be carefully examined before accepting the mouse as a reliable model for human IOP regulation.

The goal of this project was to determine whether pharmacological compounds that are known to affect conventional outflow facility in human eyes exert similar effects on conventional outflow facility in C57BL/6 mice. We specifically examined the facility response to two G-protein coupled receptor agonists, sphingosine 1-phosphate (S1P) and the prostanoid EP_4 agonist 3,7-dithia PGE_1, that respectively decrease[80] and increase[86] outflow facility in human eyes. By comparing the facility response measured in enucleated murine eyes against previous reports in enucleated human eyes[80,86], we aimed to determine whether C57BL/6 mice mimic aspects of human conventional outflow pathway pharmacology, which would identify this strain as a promising animal model for S1P and EP4-based regulation of IOP as occurs within human eyes. We also examined whether the pharmacological response is affected by prolonged post-mortem times, which is an important consideration for using the mouse model as a research tool when doing ex vivo perfusions.

2- Methods

All experiments were performed using ex vivo tissue and were done in compliance with the ARVO Statement for the Use of Animals in Ophthalmic and Vision Research and the Animal Scientific Procedures Act 1986.

2.1. Ex Vivo Mouse Eye Perfusion

C57BL/6 mice of either sex, aged 8-15 weeks, were killed by cervical dislocation. Eyes were enucleated within 10 minutes of death and perfused immediately or stored in phosphate buffered saline (PBS) at 4°C for 2-3 hours. For perfusion, each eye was mounted on a single well of a 96-well Stripwell plate (Corning) using cyanoacrylate glue to affix the extra ocular muscles to the plastic sidewalls of a well. Eyes were perfused outside of the isotonic saline bath (Fig. 9A). Special attention was given to maintain hydration throughout the experiment by covering the eye with tissue paper that was kept moist by regular drops of PBS. The perfusion solution was Dulbecco's PBS including divalent cations and 5.5 mM glucose (referred to as "DBG") filtered through a 0.22 µm filter before use. All perfusions were done at room temperature, with a post hoc correction to account for the viscosity difference between room and physiologic temperature[12,77].

Our perfusion method follows previously described techniques[12]. Briefly, a 33-gauge needle was used to cannulate the anterior chamber under a stereomicroscope using a micromanipulator. The needle was connected via rigid pressure tubing to a glass syringe (25 µL, Hamilton GasTight) placed on the rack of a motorized syringe pump (Pump33; Harvard Apparatus) under computer control. A pressure transducer (142PC01G, Honeywell) monitored IOP through a three-way connector placed in the perfusion line. Custom written LabVIEW software[151] was used to automatically vary the flow rate from the syringe pump to maintain the eye at a user-defined IOP. Eyes were perfused at sequential pressure steps of 4, 8, 15, and 25 mmHg; we refer to this as our "standard perfusion regimen." Eyes were typically perfused for 20 minutes at each pressure step to obtain at least 10 minutes of stable perfusion data, and an average stable flow rate was calculated at each pressure step (Fig. 13A). Data were considered acceptable if a stable flow rate was achieved in at least 3 of the 4 pressure steps. Based on this criterion, we rejected 12 eyes out of 88 valid perfusions. Selected eyes were fixed by removing the perfusion needle and immediately immersing the eye in 4% paraformaldehyde (PFA) in isotonic saline for 1 hour, followed by long-term storage in 0.1% PFA. For histology (performed by Lawrence Lorraine), eyes were processed for paraffin embedding, sectioned and stained using hematoxylin and eosin.

2.2. Outflow Facility Analysis

We calculated a pressure-dependent or "conventional outflow facility" (*C*) by fitting our pressure-flow rate data to the modified Goldmann's equation[165]:

$$\mathrm{F} = \mathrm{C} \times (\mathrm{IOP} - \mathrm{EVP}) + \mathrm{F_u}$$

Equation 4

where *F* represents the stable flow rate at each corresponding IOP. F_u in Equation 4 is usually taken as an estimate of the pressure-independent or "unconventional" outflow rate[12]. Equation 4 is valid only when (i) episcleral venous pressure is zero (appropriate for enucleated eyes)*;* (ii) *F* reaches equilibrium at each value of IOP; and (iii) *C* and F_u are independent of IOP. The values of *C* and F_u are defined as the slope and intercept, respectively, of the best-fit linear regression to our measured

F versus IOP data (Fig. 8B-C). In principle, *C* would be consistent with values obtained from a 2-level perfusion[5,8,10,16], except that the additional pressure steps give a much stronger confidence for estimating *C*. In this study eyes were perfused at room temperature, while covered with a tissue paper kept moist with PBS drops during the experiment (Fig. 9A). Thus, both *C* and F_u were multiplied by a factor of 1.38 to account for viscosity differences between physiologic and room temperatures, as previously described[12,77].

2.3. Experimental Design

We conducted three sets of perfusion experiments to measure how conventional outflow facility in the mouse eye responded to receptor-mediated compounds known to affect conventional outflow in human eyes. These were performed in three cohorts of mice, referred to a Cohort 4, 5 and 6, as a continuation of the first three cohorts of mice used in Chapter 2. Most experiments used paired eyes (treated vs. untreated contralateral controls), except for cases where data from one eye were rejected based on the stability criterion described above (Table 5). Paired eyes were perfused sequentially (one eye immediately after enucleation, the contralateral eye 2-3 hrs after enucleation), where we randomised whether the control or experimental eye was perfused first. We also examined whether prolonged post-mortem time (24 hrs storage after enucleation at 4°C) affected the pharmacologic response between paired eyes.

	Total number of eyes	Unpaired eyes	Paired eyes
Cohort 4	14	2	12
Cohort 5A	15	1	14
Cohort 5B	14	2	12
Cohort 5C	10	4	6
Cohort 6A	13	5	8
Cohort 6B	10	2	8

Table 5: Number of mouse eyes perfused in cohorts 4, 5 and 6.

In the first set of experiments (Cohort 4), we examined the effect of sphingosine 1-phosphate (S1P), a bioactive lipid that decreases outflow facility by 31% in porcine eyes[81] and 36% in human eyes[80]. Experimental eyes were perfused with 5 µM S1P in DBG containing fatty acid free bovine serum albumin (FAF-BSA; 2 mg/mL; Sigma-Aldrich A8806) and 17 µM sodium hydroxide (NaOH), while control eyes received DBG and FAF-BSA alone without S1P or NaOH. Independent studies demonstrated that 17 µM NaOH had a negligible effect on the pH of DBG (7.137±0.031 vs. 7.107±0.012 for Dulbecco's PBS with or without 17 µM NaOH, respectively, N = 3 independent trials each, p = 0.23; Student's t-test), and therefore NaOH was not included in the control solution. S1P (CAS 26993-30-6 from Sigma-Aldrich, UK) was dissolved from powder into 10 mM NaOH in water to give a 3 mM S1P stock solution that was stored at -20°C. Prior to cannulation, each needle was backfilled from the tip with 150 µL of the appropriate perfusion solution, a volume sufficient to last several hours even at the highest measured flow rates (~0.3 µL/min). The experimental eye was pre-treated with S1P-containing solution from a reservoir at 8 mmHg for 45 minutes to expose the outflow pathway to the drug prior to the start of the standard perfusion regimen. Control eyes were perfused from a reservoir for the same time with solution without S1P. Data from 14 individual eyes (8 S1P-treated and 6 controls, containing 6 pairs) passed the stability criterion and were included in Cohort 4.

The aim of the second set of experiments (Cohort 5) was to investigate the role of $S1P_1$ and $S1P_2$ receptors in mediating the S1P response. Following a previous study in human eyes[82], we used W146 (Avanti Polar Lipids) or JTE-013 (Cayman Chemical) that are selective antagonists to $S1P_1$ or $S1P_2$ receptors, respectively. W146 was dissolved in water as a 1 mM stock solution containing 10.6 mM cyclodextrin and 100 mM sodium carbonate (Na_2CO_3) as vehicle, and was stored at -20°C. JTE-013 was dissolved in DMSO as a 1 mM stock solution and stored at -20°C. Experimental eyes were pre-treated with antagonist and S1P-containing solution (45 minutes at 8 mmHg from a reservoir) followed by perfusion with the same solution over the standard perfusion regimen. For JTE-treated experimental eyes (Cohort 5A), the perfusion solution contained 5 µM JTE-013 in DBG + 5 µM S1P + 2 mg/mL FAF-BSA + 17 µM NaOH + 70 mM DMSO. For W146-treated experimental

eyes (Cohort 5B), the perfusion solution contained 5 µM W146 in DBG + 5 µM S1P + 2 mg/mL FAF-BSA + 17 µM NaOH + 53 µM cyclodextrin + 500 µM Na_2CO_3.Antagonist concentrations (5 µM) were chosen to be consistent with concentrations used in prior perfusion studies with porcine and human eyes and were several fold larger than reported IC_{50} values (0.83 µM for W146[166] and 1.0 µM for JTE-013[82]). Control eyes were perfused with 5 µM S1P in DBG + 2 mg/mL FAF-BSA + 17 µM NaOH, without antagonist, cyclodextrin, Na_2CO_3 or DMSO vehicle and without pre-treatment. Data from 8 eyes were included in the JTE study (4 JTE-treated and 4 controls, containing 4 pairs), and data from 7 eyes were included in the W146 study (3 W146-treated and 4 controls, containing 3 pairs).

To account for possible vehicle effects caused by cyclodextrin, Na_2CO_3 or DMSO, we repeated the W146 and JTE-013 antagonist studies using the same vehicle formulations in the control eyes. For these studies, the control eyes from the W146 study received 5 µM S1P in DBG + 2 mg/mL FAF-BSA + 17 µM NaOH + 53 µM cyclodextrin + 500 µM Na_2CO_3, while the experimental eyes from the W146 study received the same solution with 5 µM W146. The control eyes from the JTE study received 5 µM S1P in DBG + 2 mg/mL FAF-BSA + 17 µM NaOH + 70 mM DMSO, while the experimental eyes from the JTE study received the same solution with 5 µM JTE-013. Data from 7 eyes were included in the JTE vehicle-controlled study (3 JTE-treated and 4 controls, containing 3 pairs), and data from 7 eyes were included in the W146 vehicle-controlled study (4 W146-treated and 3 controls, containing 3 pairs).

In an additional 10 eyes (3 pairs and 4 unpaired eyes), we examined the influence of JTE antagonist alone on outflow facility (Cohort 5C). For these studies, experimental eyes were perfused with 5 µM JTE-013 + 70 mM DMSO in DBG without FAF-BSA (N = 5 eyes), while the control eyes were perfused with DBG alone without JTE, DMSO, or FAF-BSA (N = 5) using the standard perfusion regimen. Because 70 mM DMSO was found not to affect the facility response in JTE-treated eyes in the presence of S1P (see below), it was not included in the perfusion solution for the control eyes.

In the third set of experiments (Cohort 6A), we examined the influence of prostaglandin EP_4 receptor activation on conventional outflow in the mouse eye by perfusion with 3,7-dithia PGE_1, a highly selective PG-EP_4 receptor agonist[167] that increases conventional outflow facility in human[86] and monkey eyes[87] without affecting unconventional outflow. 3,7-dithia PGE_1 was dissolved in ethanol as a 10 mM stock solution and stored at -20°C. Experimental eyes were pre-treated (45 min at 8 mmHg from a reservoir) and perfused with 10 nM 3,7-dithia PGE_1 in DBG + 17 µM ethanol without FAF-BSA. Control eyes were perfused with DBG alone without ethanol or pre-treatment. Ethanol was not included in the perfusion solution of the control eyes because 17 µM ethanol is approximately 1000-fold smaller than typical millimolar concentrations shown to have minimal effects on cultured cells[168,169]. Data examining the effects of 3,7-dithia PGE_1 included 13 eyes (7 treated and 6 untreated control eyes, containing 4 pairs).

In an additional 10 eyes (including 4 pairs and 2 unpaired eyes), we examined whether the response to 3,7-dithia PGE_1 was affected by post-mortem time (Cohort 6B). For these studies, eyes were enucleated and stored for 24 hrs at 4°C in Dulbecco's modified Eagle's medium (DMEM) and then perfused with 10 nM 3,7-dithia PGE_1 in DBG + 17 µM ethanol (N = 6) or with DBG + 17 µM ethanol (N = 4) using the standard perfusion regimen. We chose to examine the post-mortem facility response to 3,7-dithia PGE_1, rather than to S1P, for two reasons. First, 3,7-dithia PGE_1 causes a larger change in outflow facility compared to S1P (e.g., 69% increase following 3,7-dithia PGE_1[86] versus 36% decrease following S1P in human eyes, respectively), and therefore 3,7-dithia PGE_1 would provide a more conservative test to detect smaller differences in facility that might occur with prolonged post-mortem times. Second, 3,7-dithia PGE_1 is an exogenous compound (unlike S1P) and is therefore more representative of potential candidate drugs that may affect conventional outflow. Therefore, by looking at how the facility response to 3,7-dithia PGE_1 changes with post-mortem time, we can gain some insight into how post-mortem time may affect the interpretation of drug efficacy in perfusion experiments (that often incorporate eyes with post-mortem times up to 24 hours or use transgenic models where eyes are shipped overnight between laboratories).

2.4. Statistical Methods

All experiments included in this study contained some portion of unpaired eyes caused by one eye of a pair failing to pass the stability criterion. To analyze our data, we performed two statistical analyses: (i) a Welch's t-test that included the full set of eyes (accounting for unequal sample sizes); and (ii) a paired, 2-tailed Student's t-test that included only the subset of paired contralateral eyes. Wherever appropriate, we indicate whether a paired Student's t-test or a Welch's t-test was performed. The statistical significance threshold was taken to be a *p*-value of 0.05.

All facility values quoted in the text were temperature-corrected to account for viscosity differences, as described above. Figures showing flow rate data, however, were not corrected and represent the true flow rate output from the syringe pump.

3- Results

3.1. Cohort 4, S1P Decreases Conventional Outflow Facility in Mice

Perfusion with 5 µM S1P caused a reduction in flow rate at each perfusion pressure (Fig. 13A). Compiling data from all eyes revealed a linear relationship between flow rate and IOP (Fig. 13B), consistent with the modified Goldmann equation (Eq. 8). In response to S1P, conventional outflow facility (*C*; slope of the linear regression) decreased by 38.9 ± 24.2% (mean ± SD; $p = 0.029$, paired Student's t-test, $N = 6$ pairs) compared to paired contralateral eyes perfused without S1P. After temperature correction, conventional outflow facility was 0.0125 ± 0.0037 and 0.0073 ± 0.0035 µL/min/mmHg for control and S1P-treated eyes ($p = 0.024$, Welch's t-test, $N = 8$ S1P-treated eyes and 6 controls), respectively. We observed no statistical difference in the intercept of the linear regression in response to S1P in either paired ($p = 0.71$) or unpaired analyses ($p = 0.56$, Welch's t-test). We observed no obvious differences in the morphology of the trabecular meshwork or Schlemm's canal following treatment with S1P (Fig. 14).

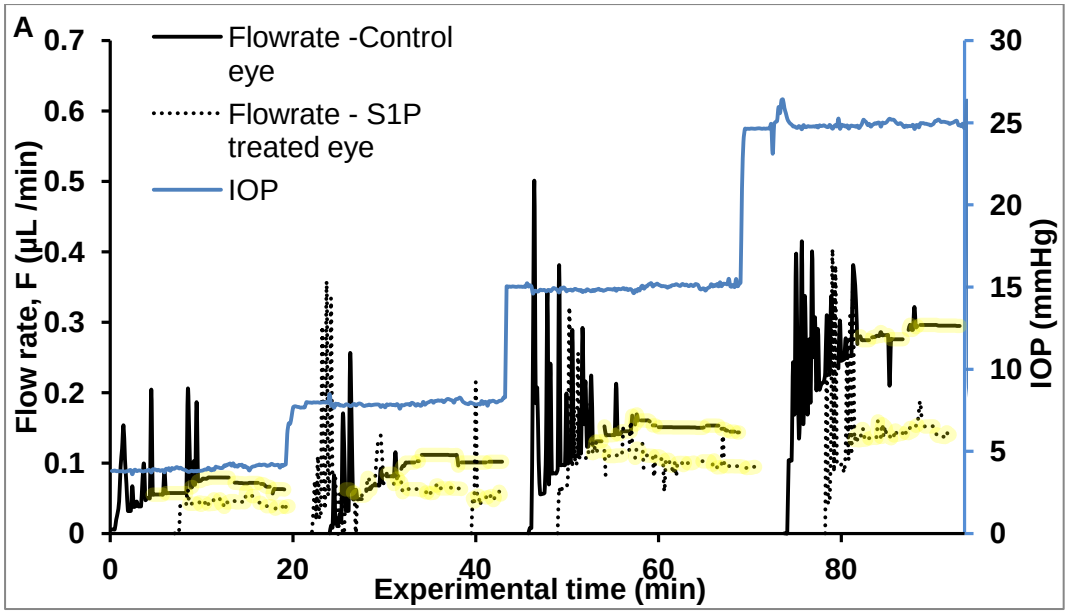

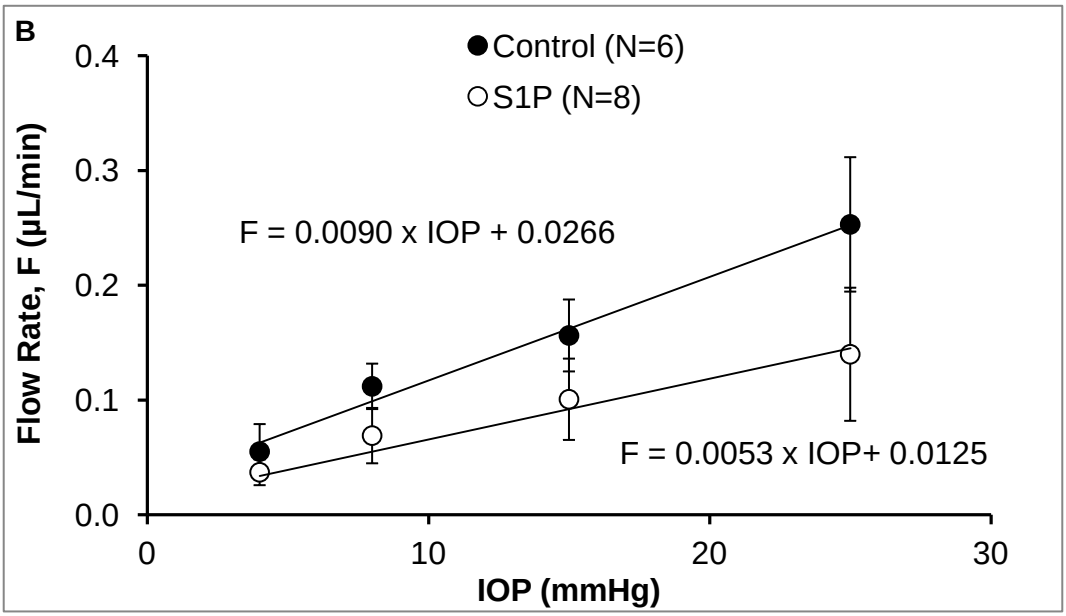

Figure 13: Flow rate vs. IOP data from Cohort 4. Panel A) Typical perfusion tracings showing IOP (blue) and flow rate data for a control (solid black) and an S1P treated (dashed black) eye as a function of time (data taken from unpaired eyes). Yellow highlighted regions represent data used to calculate the average flow rate at each pressure level (4, 8, 15, 25 mmHg). To enable flow traces from both control and experimental eyes to be seen on the same graph, flow rate tracings for the S1P treated eye were shifted by several minutes, and the pressure curve for the S1P-treated eye was omitted. Panel B) the average flow rate at each pressure level for all control (filled circles) and S1P treated eyes (open circles) from Cohort 4. Bars are standard deviations and lines represent the best-fit linear regressions to average data. The R^2 values of the linear best-fit regression lines computed for each individual mouse ranged between 0.846 and 0.990. FAF-BSA was included in the perfusion medium for all eyes represented in Panel B. Flow rate data are not temperature corrected.

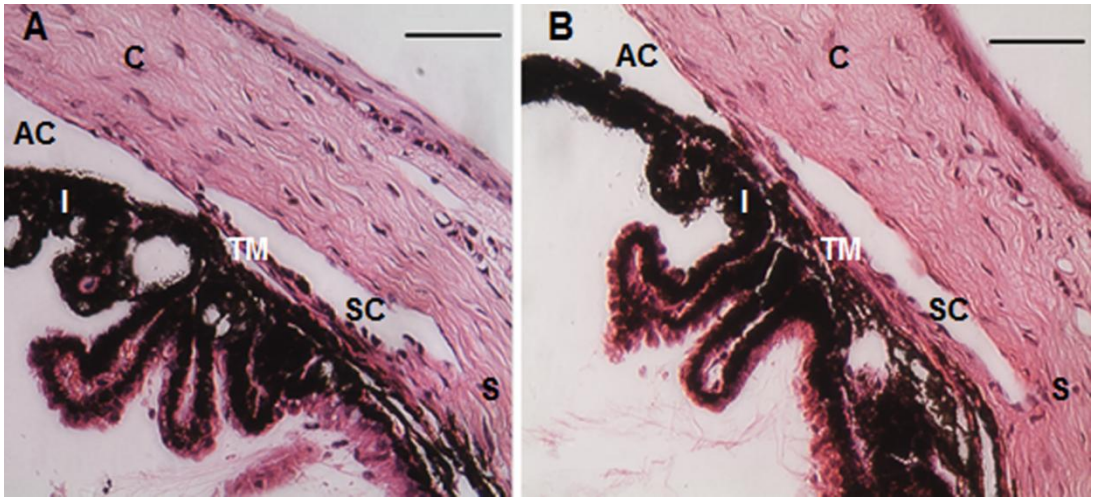

Figure 14: Mouse eye histology for S1P treated or untreated eye. No obvious differences are observed in the histology of the iridocorneal angle from control (A) and S1P-treated (B) mouse eyes. AC, anterior chamber; TM, trabecular meshwork; SC, Schlemm's canal; I, iris; C, cornea; S, sclera. Bars are 50 µm. The absence of giant vacuoles in the inner wall of Schlemm's canal may reflect the fact that the eyes were fixed by immersion.

3.2. Cohort 5, The $S1P_2$ Receptor Mediates the S1P Response

To determine which receptor mediates the S1P response measured in Cohort 4, we perfused contralateral eyes with either S1P or S1P in combination with either an antagonist to the $S1P_2$ receptor (5 µM JTE-013; Fig. 15A) or an antagonist to the $S1P_1$ receptor (5 µM W146; Fig. 15B). In eyes treated with S1P without antagonist, the conventional outflow facility was 0.0074 ± 0.0034 µL/min/mmHg (*N* = 15 control eyes from the JTE and W146 experiments; temperature-corrected), which was similar to the conventional facility measured for S1P-treated eyes in Group A. There was no difference in conventional outflow facility caused by vehicle, either for 70 mM DMSO (0.0072 ± 0.0052 vs. 0.0068 ± 0.0017 µL/min/mmHg in S1P-treated control eyes from the JTE studies with or without DMSO, respectively; temperature-corrected; $p = 0.90$, Welch's t-test, $N = 4$ for each group) or for 53 µM cyclodextrin and 500 µM Na_2CO_3 (0.0078 ± 0.0040 vs. 0.0079 ± 0.0035 µL/min/mmHg in S1P-treated control eyes from the W146 study with or without cyclodextrin + Na_2CO_3, respectively; temperature-corrected; $p = 0.97$, Welch's t-test, $N = 3$ or 4, respectively). For this reason, we compiled all data with and without vehicle control from the W146 or JTE perfusions with S1P. The compiled data shown in Figures 3A and 3B include 15 eyes for the JTE antagonist studies (8 controls + 7 experimentals, including 7 pairs) and 14 eyes for the W146 antagonist studies (7 controls + 7 experimentals, including 6 pairs).

In eyes perfused with both S1P and JTE, the temperature-corrected conventional facility was 0.0133 ± 0.0019 µL/min/mmHg, nearly 2-fold larger than eyes treated with S1P without antagonist (0.0070 ± 0.0036 µL/min/mmHg; p = 0.0012, Welch's t-test , N = 8 S1P vs. 7 S1P + JTE,) and similar to the conventional facility of control eyes from Group A. In contrast, conventional facility was unchanged between eyes perfused with S1P or S1P and W146 (0.0079 ± 0.0034 vs. 0.0094 ± 0.0032 µL/min/mmHg; temperature-corrected; p = 0.41, Welch's t-test, N = 7 S1P vs. 7 S1P + W146; p = 0.145, p = 0.05, assuming the facility values for S1P-treated and untreated eyes from Group A with N = 7 for each group). These data demonstrate that JTE largely blocks the facility-reducing effect of S1P, while W146 has little effect, suggesting that the $S1P_2$ receptor, and not the $S1P_1$ receptor, is principally responsible for mediating the S1P response in C57BL/6 mice. We did not observe significant effects of JTE or W146 in the presence of S1P on the intercept of the pressure-flow relationship ($p \geq 0.27$).

In eyes perfused with 5 µM JTE without S1P, temperature-corrected conventional facility was nearly 2-fold greater than in untreated control eyes (Fig. 15C), increasing from 0.0096 ± 0.0026 to 0.0194 ± 0.0056 µL/min/mmHg (p = 0.017; N = 5 control and N = 5 JTE-treated eyes, Welch's t-test). There was no significant difference in the intercept of the pressure-flow relationship between JTE-treated and untreated eyes (p = 0.19). These data suggest that endogenous S1P signalling may be regulating conventional outflow facility in the mouse trabecular meshwork, which can be blocked by $S1P_2$ receptor antagonist JTE-013.

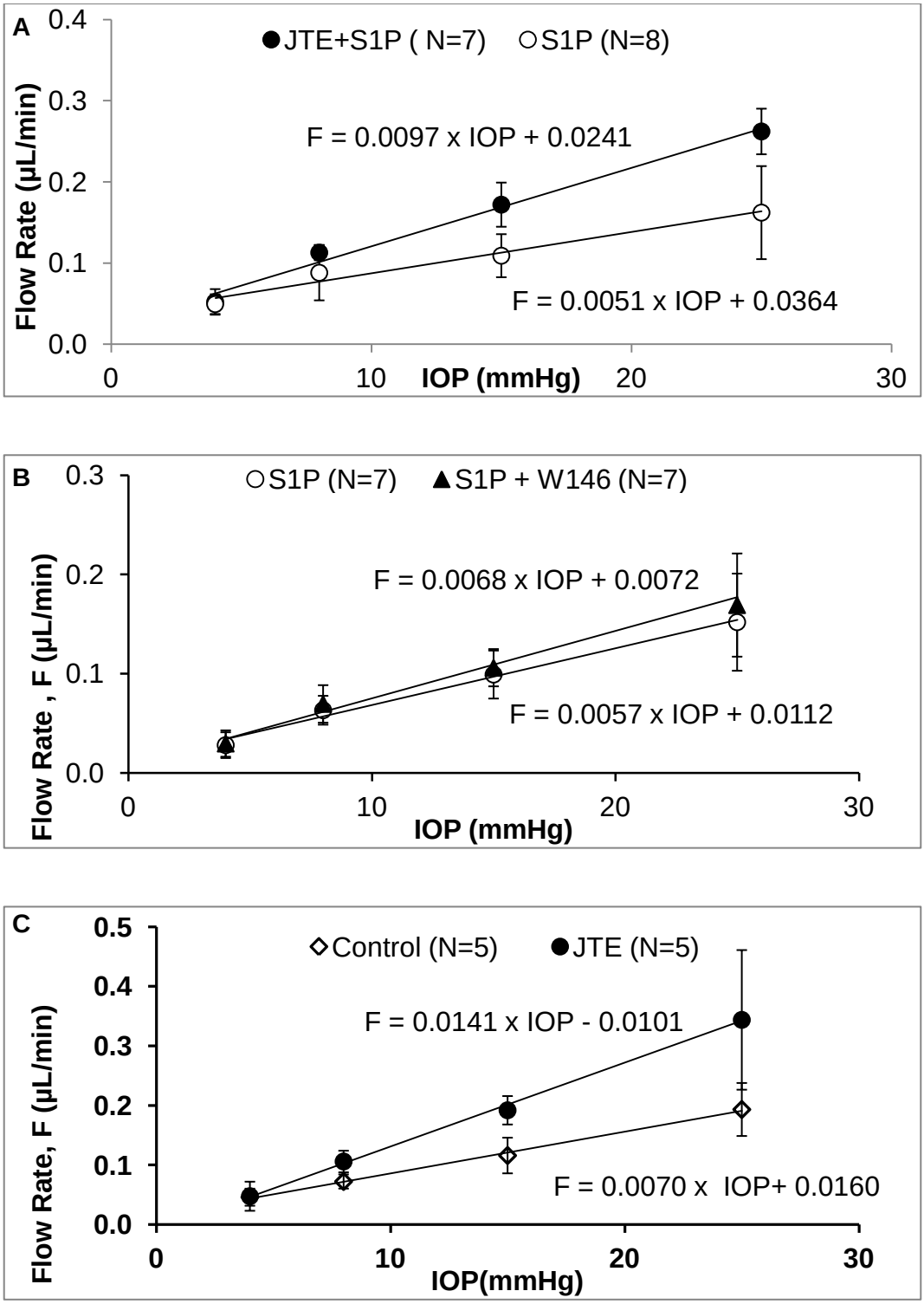

Figure 15: Flow rate vs. IOP data from Cohort 5. Panel A) Average flow rate at each pressure level for S1P (open circles) and S1P+JTE-013-treated eyes (filled circles). Controls for Panels A and B include eyes with and without vehicle formulations, as described in the text. The R^2 values of the linear best-fit regression lines computed for each individual mouse ranged between 0.357 and 0.990. Panel B) Average flow rate at each pressure level for S1P (open circles) and S1P+W146-treated eyes (filled triangles). The R^2 values of the linear best-fit regression lines computed for each individual mouse ranged between 0.842 and 1. Panel C) Average flow rate at each pressure level for control (open diamonds) and JTE-treated eyes without S1P (filled circles). The R^2 values ranged between 0.962 and 1. Bars are standard deviations and lines represent the best-fit linear regression to average data. FAF-BSA was included in the perfusion medium for all eyes represented in Panels A and B, but no FAF-BSA was included in the perfusion medium for Panel C. Flow rate data are not temperature corrected.

3.3. Cohort 6, EP_4 Receptor Agonist Increases Conventional Outflow Facility in Mice

We measured a two-fold increase in conventional outflow facility following perfusion with 10 nM 3,7-dithia PGE_1 (Fig. 16A), with the temperature-corrected facility increasing from 0.0062 ± 0.0005 to 0.0131 ± 0.0024 µL/min/mmHg (p = 0.0003; Welch's t-test; N = 6 or 7 for untreated eyes or eyes treated with 3,7-dithia PGE_1, respectively). Considering only paired eyes, the conventional facility increased by 105.8 ± 48.4% following 3,7-dithia PGE_1 treatment compared to untreated contralateral eyes (p = 0.02; paired Student's t-test, N = 4 pairs). In contrast, 3,7-dithia PGE_1 inconsistently affected the intercept of the pressure-flow relationship. More specifically, while we observed a statistically detectable decrease in the intercept between treated and untreated groups using unpaired analysis (p = 0.04), we observed no difference using paired analysis (p = 0.31).

After 24 hrs post-enucleation and storage at 4°C in DMEM, eyes appeared well preserved with clear corneas and constricted pupils. In contrast, eyes stored for the same period in PBS at 4°C appeared "mushy" with cloudy corneas and dilated pupils. Following 24 hr storage in DMEM, conventional outflow facility in eyes perfused with 3,7-dithia PGE_1 was 0.0128 ± 0.0034 µL/min/mmHg (N = 6 eyes; Fig. 16B), which was significantly larger (p = 0.037, Welch's t-test) than the baseline facility of untreated eyes (0.0087 ± 0.0014 µL/min/mmHg, N = 4 eyes) by unpaired analysis. When considering only paired eyes, the relative facility increase following 3,7-dithia PGE_1 was nearly 3-fold smaller after 24 hrs (38.1 ± 34.5%; N = 4 pairs) versus after 3 hrs (see above) and failed to achieve statistical significance (p = 0.126, paired Student's t-test). Similarly, after 24 hrs for pressures of 8 mmHg and above, there was a tendency for 3,7-dithia PGE_1 to increase the flow rate, but even at 25 mmHg the flow rate increase failed to achieve statistical significance (p = 0.10). This is in contrast to eyes perfused within 3 hrs post-mortem, when 3,7-dithia PGE_1 caused a statistically significant increase in flow rate for all pressures of 8 mmHg or larger (p < 0.05). This suggests that while the facility-increasing effect of 3,7-dithia PGE_1 was present 24 hrs after enucleation, the effect was subtle and detectable only when flow rates were measured over several perfusion pressures and linear regression analysis was used to calculate the slope of the flow rate-pressure relationship.

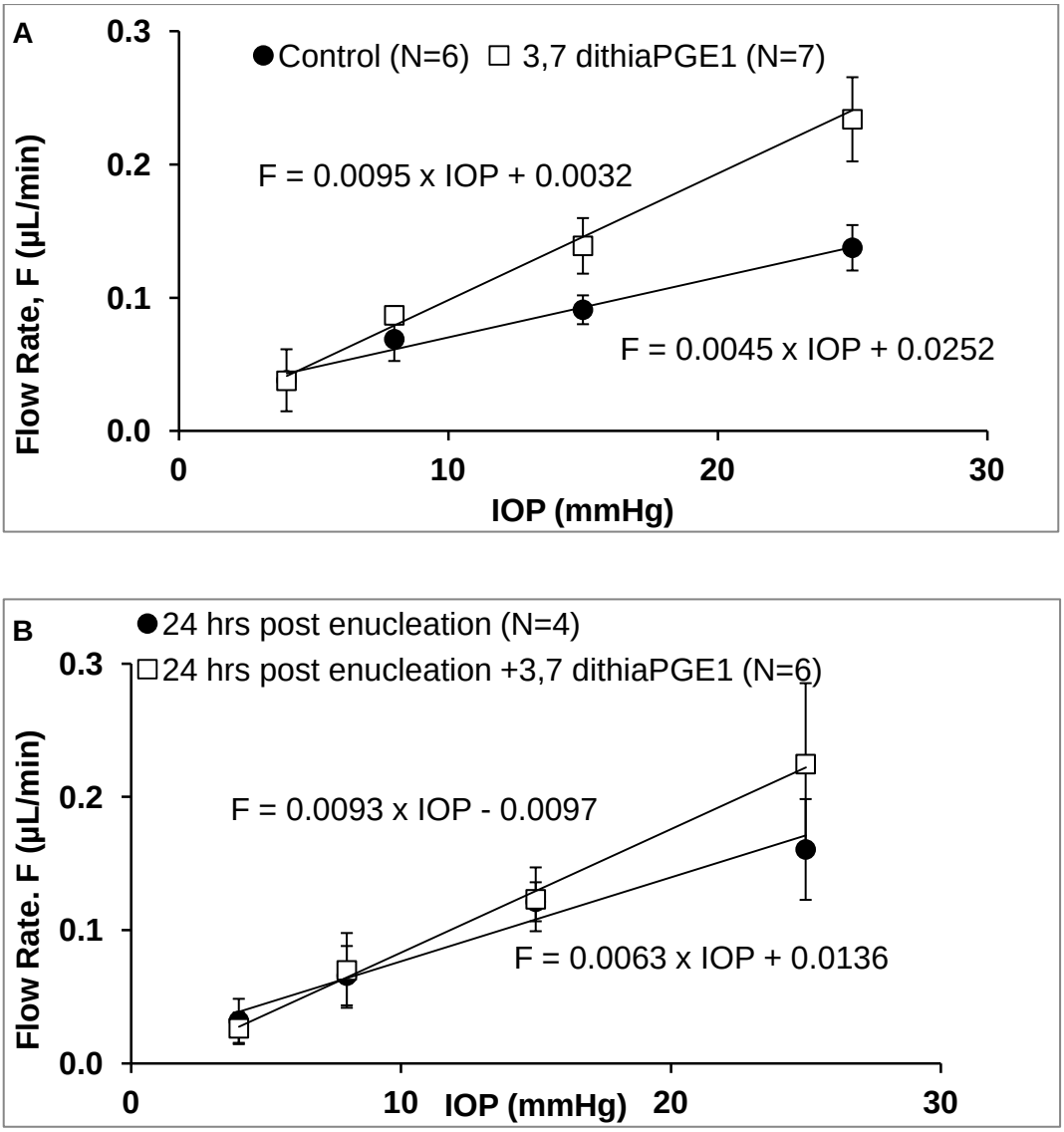

Figure 16: Flow rate vs. IOP data from Cohort 6. Average flow rate at each pressure level for control (filled circles) and 3,7-dithia PGE_1 (open squares) treated eyes, within 3 hrs (Panel A) or after 24 hrs post-mortem storage at 4°C (Panel B). The R^2 values of the linear best-fit regression lines computed for each individual mouse ranged between 0.786 and 1 for Cohort 6A and 0.839-0.997 for cohort 6B. Bars are standard deviations and lines represent the best-fit linear regressions to average data. For Panels A and B, there was no FAF-BSA in the perfusion medium. Flow rate data are not temperature corrected.

4- Discussion

This study demonstrates that C57BL/6 mouse eyes respond to S1P and EP_4 agonist in a similar manner as that previously reported for human eyes. Specifically, S1P decreased murine outflow facility by 39%, which was nearly identical to the 36% decrease previously reported in human eyes[80]. The prostanoid EP_4 agonist, 3,7-dithia PGE_1, caused a facility increase of 106% in mice, which was somewhat larger than the 69% increase observed in human eyes[86]. Quantitative differences aside, the similarity in qualitative response between species suggests that similar

pharmacological signalling mechanisms underlie the facility response to S1P and 3,7-dithia PGE_1 between C57BL/6 mice and human eyes.

S1P is known to bind to one of five G protein-coupled receptors ($S1P_{1-5}$) each of which exhibit different downstream signalling events and are differentially regulated in different tissues[170]. S1P rapidly decreases outflow facility[80,81], and lysophospholipids similar to S1P are found in aqueous humour[171], possibly acting as endogenous regulators of outflow facility[172]. In C57BL/6 mice, we detected expression of $S1P_1$ and negligible levels of $S1P_2$ and $S1P_3$ in Schlemm's canal endothelium by in situ confocal immunofluorescence (Supplemental Figure 1). The relative absence of $S1P_2$ and $S1P_3$ labelling could be attributed to reduced antibody sensitivity compared to prior studies by our group[80] that reported relatively low levels of $S1P_2$ and $S1P_3$ expression, compared to $S1P_1$, by human Schlemm's canal cells in situ. Despite the seemingly low levels of $S1P_2$ expression, the facility-decreasing effect of S1P in mice was almost completely abolished by JTE-013, an antagonist to the $S1P_2$ receptor, but not by W146, an antagonist to the $S1P_1$ receptor. Similar effects were observed in human eyes[82], where JTE-013 blocked facility reduction as well as phosphorylated myosin light chain (pMLC) in response to S1P, while no blocking effect on pMLC was observed in the presence of either W146 or VPC23019 (a dual antagonist to $S1P_1$ and $S1P_3$). Perfusion with JTE-013 alone increased conventional outflow by two-fold in C57BL/6 mice, yielding a conventional outflow facility (0.0194 ± 0.0056 µL/min/mmHg, N = 5) that was larger than that measured in either untreated eyes (0.0125 ± 0.0037 µL/min/mmHg, N = 6, from Cohort 4; p = 0.056, Welch's t-test) or eyes perfused with 3,7-dithia PGE_1 (0.0131 ± 0.0024 µL/min/mmHg, N = 7, from Cohort 6; p = 0.063, Welch's t test). These data strongly implicate the $S1P_2$ receptor as a key mediator of the facility-regulating effect of S1P and suggest an endogenous concentration of S1P within the trabecular meshwork. It should be noted however, that the selectivity of JTE-013 to the $S1P_2$ receptor has been recently called into question based on data reporting an effect of JTE-013 in $S1P_2$ knock-out mice[173,174]. Therefore, future studies should account for potential off-target effects, possibly by incorporating genetically altered mice to better understand the underlying mechanisms by which S1P regulates outflow facility.

3,7-dithia PGE_1 was the first selective agonist developed against the EP_4 receptor[167] and has been shown to lower IOP by nearly 40% in cynomolgus monkeys by increasing trabecular outflow facility without affecting uveoscleral outflow[87]. Other examples of agonists for this receptor include: PGE_2[175], $PGF_{2\alpha}$[176], ONO-4819[177] or carbacyclin[178]. Similarly, 3,7-dithia PGE_1 increases conventional outflow facility in post-mortem human eyes by 69%[86], consistent with the expression of PG-EP_4 in human trabecular meshwork and Schlemm's canal in situ[86,179]. At 10 nM concentration, however, the effect of 3,7-dithia PGE_1 appears to be selective for Schlemm's canal cells, with no observed effect on trabecular meshwork cells, based on cell culture assays of cAMP accumulation following PG-EP_4 receptor activation[86]. Compared to humans, our data show that 3,7-dithia PGE_1 had a nearly two-fold larger effect in C57BL/6 mice (106% vs. 69%[86]), and expression of PG-EP_4 has already been demonstrated within the trabecular meshwork and Schlemm's canal in other strains of mice. The larger facility increase in mice may reflect differences in EP_4 sensitivity between species or with age, or it may be due to improved preservation of mouse tissue due to shorter post-mortem times. Alternatively, because mice have a more prominent Schlemm's canal with only 2-4 trabecular beams compared to 12-20 in humans[40], mice may be predisposed to exhibit a more robust facility response to compounds such as 3,7-dithia PGE_1 that preferentially affect Schlemm's canal (see above), as opposed to trabecular meshwork, cells[86]. Regardless, the robust facility-increasing response following 3,7-dithia PGE_1 strongly suggests that C57BL/6 mice are a good pharmacological model for investigating the contribution of EP_4, and possibly other prostanoid receptors, in the regulation of conventional outflow. This may be particularly interesting given that prostaglandin PGE_2, a natural ligand for EP_4 receptors[180], is present within aqueous humour at reduced concentrations in eyes from patients with primary open-angle and steroid-induced glaucoma[181].

Post hoc comparison of facility data revealed that conventional outflow facility was, rather surprisingly, nearly 60% larger in eyes perfused with 0.2% FAF-BSA in DBG compared to eyes perfused with DBG alone. More specifically, there was a statistical difference ($p = 0.028$, Welsh's t-test) between eyes perfused with 0.2% FAF-BSA from Cohort 4 (0.0125 ± 0.0037 µL/min/mmHg,

N = 6) compared to eyes perfused without FAF-BSA aggregated from Cohorts 5 and 6 (0.0078 ± 0.0025 µL/min/mmHg, *N* = 11). FAF-BSA was included as a carrier for S1P in the perfusion medium, following prior studies in human eyes[80], and therefore FAF-BSA was excluded from experiments that did not contain S1P (i.e., all experiments from Cohort 6 and experiments from Cohort 5 examining JTE alone). We are not certain as to the cause of this difference, nor were there any obvious differences in the gender, age or genetic background of the mice that could explain this difference. Because elevated FAF-BSA would be expected to decrease (due to possible obstruction), rather than increase, outflow facility[182], these data may indicate a potential trace contaminant carried from the FAF-BSA source (e.g., lipoprotein, phospholipid or lipopolysaccharide) that may itself increase facility. We observed that the effect of FAF-BSA on facility persisted through two different batches from the supplier (lot numbers 040M7715V and 108k7425), suggesting a potential widespread, rather than batch-dependent, contaminant. Nevertheless, because our experiments used a paired perfusion approach, in which we compared the relative effects of selective receptor agonists or antagonists diluted in otherwise identical perfusion solutions (both control and experimental), we conclude that the facility effects we observed were in fact due to drug treatment, and not to the presence or absence of FAF-BSA in the perfusion media.

Data from the current study suggest that the fraction of unconventional outflow in mice may be significantly smaller than previously estimated[5,8,10,12]. We calculate the unconventional fraction of total outflow as

$$\frac{F_u}{C \times IOP + F_u}$$

Equation 10

Using the regression parameters from control eyes from Cohort 6 (perfused within 3 hrs post-enucleation without FAF-BSA; Fig. 16A) yields a relative contribution of 37.9 ± 15.6% unconventional to total outflow at 8 mmHg. In contrast, our previous work estimated that unconventional outflow represents 66% of total outflow in C57BL/6 mice[12]. This difference is largely

attributable to the 5-fold difference in F_U between our current study (0.035 ± 0.025 µL/min; temperature-corrected; control eyes of Cohort 6 at 3 hrs) and our previous study (0.157 ± 0.026 µL/min)[12], with a more modest difference observed in conventional outflow facility (0.0062 ± 0.0005 vs. 0.0091 ± 0.0012 µL/min/mmHg[12]). We do not understand the reasons for such a large discrepancy in F_U, but it may be related to differences in experimental techniques, and in particular the hydration of the eye, between the two studies. In the current study, the eye was covered with tissue paper that was kept moist by regular drops of saline, while our previous study[12] used regular drops of saline without tissue paper. It is thus possible that evaporation from the eye contributed to overestimation of F_U, as suggested by our previous study in Chapter 2 (see Fig. 10). Along these lines, a recent study[6] has reported that the fraction of unconventional outflow in BALB/cJ mice (20.5%) is more consistent with the lower range of unconventional outflow estimated in human eyes (4 – 14%[145]), while unconventional outflow may be larger in other strains of mice (e.g., ~80% in NIH Swiss White mice[5,10]) and more consistent with the upper range of unconventional outflow estimated in human eyes (46-54%[73]). This suggests that particular strains of mice (e.g., C57BL/6 or other strains that exhibit similar pharmacological behaviour) may serve as better models for the physiology or pharmacology of IOP regulation as occurs within the conventional outflow pathway of human eyes.

The conventional outflow pathway is sensitive to post-mortem degradation[159], and enucleated whole human globes are routinely accepted for perfusion studies up to 24 hrs or longer after death. After 24 hrs post-enucleation and storage in DMEM at 4°C, the facility-increasing effect of 3,7-dithia PGE_1 remained statistically detectable in C57BL/6 mouse eyes, but only in the larger data set (unpaired set with 10 eyes) when conventional facility was measured as the slope of the flow rate-pressure relationship. When considering only perfusion data at individual pressures, the flow rate increase caused by 3,7-dithia PGE_1 failed to achieve statistical significance at 24 hrs ($p \geq 0.10$). This suggests that a 24 hr post-mortem delay likely represents an upper limit for detection of pharmacological effects in ex vivo mouse eyes. More to this point, post-hoc analysis of conventional facility in DBG-perfused mouse eyes after 24 hrs (0.0087 µL/min/mmHg, temperature-corrected,

from Cohort 6) was approximately 40% greater (p = 0.043; Welch's t-test) than the facility measured in eyes within 3 hrs after enucleation (0.0062 µL/min/mmHg, temperature-corrected, from Cohort 6). This change in baseline facility explains why the relative facility increase following 3,7-dithia PGE_1 after 24 hrs (38%) was nearly 3-fold less than that measured within 3 hrs (106%). Taken together, these data demonstrate that post-mortem changes occurring within 24 hrs can affect both conventional facility and the relative facility response to pharmacological compounds. We are not aware of any studies that have examined outflow facility as a function of post-mortem time in human eyes, but if the post-mortem response of human and mouse eyes are similar, then these data suggest that there may be a considerable loss of sensitivity for detecting pharmacologically-induced changes in outflow facility using human eyes even at 24 hrs post-mortem.

In conclusion, we demonstrate that conventional outflow facility in C57BL/6 mice mimics the pharmacological response of human eyes to PG-EP_4 and S1P receptor agonists that respectively increase and decrease outflow facility. These data strongly support the mouse eye (and possibly C57BL/6 or other strains) as a promising and robust model for the pharmacology of PG-EP_4 and S1P receptor activity on IOP regulation as occurs within the conventional outflow tract of human eyes, as well as for investigating the basic mechanisms of outflow resistance generation as relevant for glaucoma.

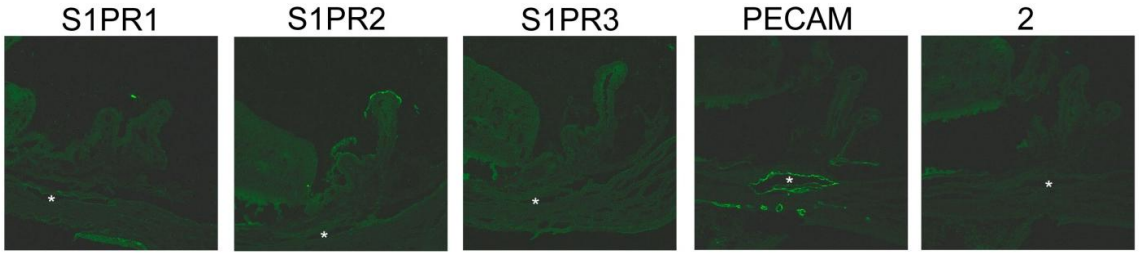

Supplementary figure 1: Confocal immunofluorescence microscopy of S1P receptor expression in angle tissues of the C57BL/6 mouse eye. Slides containing frozen sections of mouse eyes (10 µm; embedded in OCT) were probed with polyclonal antibodies raised against peptides that correspond to carboxyl terminus of *human* S1P receptors 1 (sc-25489), 2 (sc-30024) and 3 (sc-25491), but cross react with mouse. Binding of primary antibodies to mouse tissues was visualized using goat anti-rabbit antibodies conjugated to Dylight that were excited and fluorescence signals digitally captured by a Leica SP5 confocal microscope. Images from all sections were recorded during the same session using identical confocal settings. As a positive control for tissue quality and localization of Schlemm's canal endothelia (asterisks), slides containing mouse eye sections were probed with monoclonal antibodies that specifically recognize PECAM-1, followed by goat anti-mouse secondary antibodies conjugated to Dylight. As a negative control, some slides containing mouse sections were probed only with goat anti-rabbit antibodies conjugated to Dylight (2). This work was performed by Kristin Perkumas, in Prof. Stamer's laboratory.

Chapter 4: The Influence of Genetic Background on Conventional Outflow Facility in Mice

1- Introduction

The facility of aqueous humour drainage through the conventional or trabecular outflow pathway is a major determinant of intraocular pressure (IOP), and decreased conventional facility is the underlying cause of ocular hypertension associated with primary open-angle glaucoma[2]. The physiology of IOP regulation by aqueous humour outflow, however, has remained relatively obscure compared to the significant body of knowledge assembled on inflow (reviewed e.g. by Civan[183]). An improved understanding of aqueous outflow physiology may identify targetable outflow mechanisms that more successfully lower IOP as part of glaucoma therapy.

Because mice exhibit anatomical and functional similarities to humans in regards to aqueous outflow, there is growing interest in using mice as animal models to investigate the physiology of outflow facility regulation. Despite size differences, the murine conventional outflow pathway has a trabecular meshwork and a continuous Schlemm's canal[136] that is lined by endothelial cells containing giant vacuoles and presumably pores. Conventional outflow facility in mice responds to receptor-mediated compounds that affect outflow facility in humans[79], including sphingosine 1-phosphate[80,82] and an EP4 agonist[86]. Like humans, mice do not appear to exhibit a "washout" effect[12], the characteristic increase in conventional outflow facility that occurs during prolonged ocular perfusion[151]. Importantly, washout has been observed in all non-human species examined to date, including even monkeys[160,184], except mice. On the other hand, mice have been described as having a high unconventional fraction (21 – 82%)[5,6,10,12,13,15] representing the proportion of aqueous outflow passing through the pressure-independent or uveoscleral outflow pathway. Whether the bulk of outflow in mice drains through the conventional outflow pathway (like humans) or through a separate unconventional pathway remains unclear, but this is an important issue for establishing whether the mouse accurately represents outflow physiology and IOP regulation as occurs in humans.

In mice, IOP depends strongly on genetic background, with IOP values spanning nearly a 2-fold range between inbred strains (e.g., 11 vs. 19 mmHg between BALB/cJ vs. CBA/CaJ[141,142]). Because phenotypic differences can be linked to genomic polymorphisms[134], there is an opportunity to exploit the natural phenotypic diversity of IOP to gain insight into the genetic basis of IOP regulation. According to Goldmann's equation, differences in IOP could be attributed to differences in any of the four parameters describing aqueous humour dynamics: aqueous humour production rate (F_p), episcleral venous pressure (*EVP*), conventional outflow facility (*C*) and unconventional outflow rate (F_u). While several studies have measured these parameters for a particular strain[5,6,8,10] only one has measured parameters across different strains[9], and post-hoc comparison between studies is complicated by differences in technique or environmental conditions. For example, *C* measured in a single inbred strain (BALB/cJ) varies 3-fold between different reports (0.0055[11] vs. 0.0180[6] µL/min/mmHg). Thus, there is a need for a study that explicitly examines aqueous humour dynamics between different inbred strains of mice.

The aim of this project was to test the hypothesis that differences in IOP between different inbred strains of mice are attributable to differences in *C*. To test this hypothesis, we measured IOP in BALB/cJ, C57BL/6J and CBA/J mice, strains selected based on previous studies[141,142] as exhibiting a low, medium, and high IOP, respectively. We then measured *C* in ex vivo enucleated eyes from the same cohort of animals, and we examined the relationship between *C* and IOP as predicted based on Goldmann's equation.

2- Methods

All experiments were done in compliance with the ARVO Statement for the Use of Animals in Ophthalmic and Vision Research and the Animal Scientific Procedures Act 1986.

2.1. Animal Husbandry

This study used three strains of mice chosen as strains typically exhibiting low, medium and high IOP[141,142]: BALB/cJ (*N* = 13 animals), C57BL/6J (*N* = 13) and CBA/J (*N* = 15), respectively. Preliminary studies used CBA/CaJ (*N* = 10), but this strain did not exhibit as high an IOP as expected based on previous reports[141]; we therefore replaced CBA/CaJ with CBA/J. All mice were

female and were purchased from Jackson Laboratories at 6 weeks of age. Mice were housed in individually ventilated cages, fed ad libitum and maintained at 21°C with a 12-hour light (6 AM to 6 PM) and 12-hour dark cycle. IOP measurements were attempted on 30 mice aged between 3 and 4 months, while facility measurements were attempted on all 41 mice aged between 4 and 7 months. There was a 1-3 month gap between IOP and facility measurement during which the perfusion system was improved as described in Chapter 2. Between IOP and facility measurements, there was an outbreak of pinworm in the room where our mice were housed. There was no evidence as to whether our mice contracted the parasite, and Fenbendazole Prophylaxis was refused to avoid potential effects on facility.

2.2. IOP Measurements

IOP was measured non-invasively using a commercially available rebound tonometer (TonoLab, iCare UK) in conscious or anaesthetized mice. The device measures IOP as a function of the deceleration of a plastic probe propelled against the central cornea. All IOP measurements were performed on the right eye between 12:00 and 16:00 to minimize the influence of diurnal variations[185]. The tonometer was held by hand for consecutive rebound measurements used to calculate a single IOP value, following manufacturer's instructions, and tonometer readings were repeated if there was any sign of error or large variability between consecutive rebound measurements.

The tonometer was calibrated in two eyes of different mice from each strain to validate the tonometer readings and to account for potential inter-strain differences in corneal biomechanics that may affect the rebound measurement. Calibration was performed on cadaveric eyes that were pressurized between 6 and 30 mmHg via a cannula connected to an adjustable height reservoir. The hydrostatic pressure imposed on the eye was estimated as that resulting from the weight of the fluid column extending from the reservoir meniscus to the level of the needle in the limbus. The eyelids were removed and the cannula was inserted into the anterior chamber near the limbus so as to minimize interference with the tonometer probe that rebounds against the central cornea. At each of 10 pressure levels, the eye was hydrated with a drop of PBS and left to equilibrate for at least 3

minutes prior to tonometric measurements. The drop of PBS was removed with tissue paper prior to rebound measurements.

IOP was calculated using two techniques. First, following manufacturer's instructions, a single IOP value was read from the tonometer display following 6 consecutive rebound measurements. We refer to this as the "tonometer-reported IOP". However, the manufacturer provides no information on the algorithm used to calculate the tonometer-reported IOP, and our separate calibration studies suggest that the tonometer-reported IOP is not a simple average of the 6 measurements nor an average after excluding the highest and lowest values as previously suggested[186]. Because of the ambiguity in how the tonometer-reported IOP is calculated, we used a second technique to obtain IOP by manually calculating the average of the 5 initial rebound measurements as presented on the tonometer display after each rebound (the 6th rebound measurement is not actually displayed, but rather is replaced with the tonometer-reported IOP described above). We refer to this as the "manually calculated IOP". A calibration study using one cadaveric mouse eye of each strain suggested that when applied to the same sequence of 6 tonometer rebounds, the manually calculated IOP was slightly more accurate than the tonometer-reported IOP (Supplemental Figure 2). For this reason, we used the manually calculated IOP for all further IOP measurements in this study. No obvious corneal changes appeared during the consecutive measurements taken at each pressure level.

For each strain, the true manometric pressure (IOP_m) was expressed as a linear regression of the tonometric pressure (IOP_t) measured in each of the two eyes according to the following relationship:

$$\mathrm{IOP_m} = \alpha \times \mathrm{IOP_t} + \beta$$

Equation 11

where the slope (α) and intercept (β) values are given in Table 6.

Strain	α	β (mmHg)	R^2
BALB/cJ (*N* = 2)	0.97	1.10	0.984
C57BL/6J (*N* = 2)	0.95	0.47	0.978
CBA/J (*N* = 2)	1.07	-0.57	0.990
All Strains (*N* = 6)	1.00	0.27	0.990

Table 6: Parameters of the linear regression between IOP_m and IOP_t.

In agreement with previous studies[187], there was no statistical difference in the parameters of the linear regression between strains (p = 0.45; one-way ANOVA), and data from all strains were therefore lumped together for a single regression (Figure 17). All IOP values reported in this study were therefore corrected by the following relationship:

$$\mathrm{IOP_m} = 1.00 \times \mathrm{IOP_t} + 0.27$$

Equation 12

where IOP_t is the manually calculated tonometric *IOP*. This amounts to a small correction of 1-2% at physiologic IOP with the tonometer tending to slightly underestimate the true pressure.

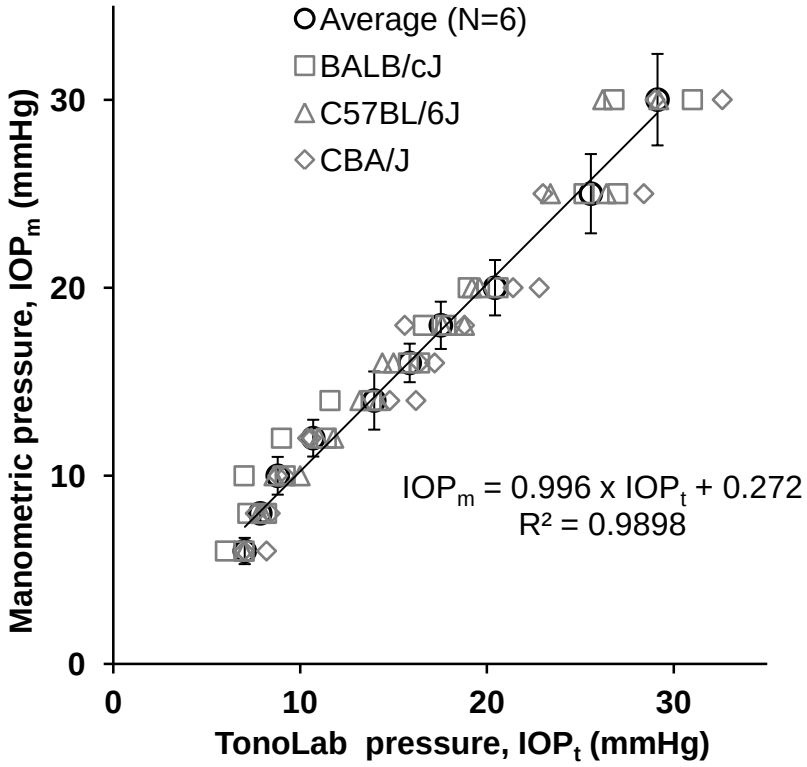

Figure 17: Tonometric pressure (IOP_t) measured in cadaveric mouse eyes pressurized at different manometric pressures (IOP_m). Bars are standard deviation.

To investigate the effects of anaesthesia, IOP measurements were attempted in 10 conscious mice of each strain and again in the same mice under anaesthesia. For conscious measurements, mice were placed in a customized restraining device and allowed to settle for 3 minutes prior to

tonometry. Despite attempts at training, conscious IOP measurements were possible in only 21 mice (6-8 per strain) because either the mice did not remain still or IOP values were unreasonably large (>20 mmHg). For anesthetized measurements, mice were exposed to 4% isoflurane (IsoFlo, Abott Animal Health, Green Oaks, IL, USA) and 2% oxygen for 3 minutes in a sealed box, and then 3.5% isoflurane and 0.7% oxygen via a nose cone for 2 minutes. IOP was measured in the right eye between 5 to 6 minutes after the initial exposure to anaesthesia. Previous studies reveal that anaesthesia lowers IOP in mice[142], and that IOP measurements should be made within minutes following the onset of anaesthesia to minimize the IOP-lowering effect. Animals were then allowed to recover under a steady flow of oxygen without isofluorane.

2.3. Outflow Facility Measurements

Outflow facility was measured in ex vivo mouse eyes using a computer-controlled perfusion system modified from previous studies[12,13,79] to allow the eye to be submerged in a heated bath of isotonic saline (Fig. 9C). On a typical experimental day, one eye was perfused from each strain, with the order of perfusion randomized. Eyes were enucleated within 15 minutes of death by cervical dislocation, and eyes were stored in PBS at 4°C for no longer than 6 hours before perfusion. All 3 strains were euthanized and enucleated at approximately the same time of day, and facility was measured in only one eye per mouse. Typically, the right eye was perfused (*N* = 20 mice), unless failure of the right eye required the left eye to be perfused (*N* = 8). Perfusion was unsuccessful in either eye in 13 mice.

For perfusion, the eye was mounted in a plastic tube trimmed from a 0.2 mL standard centrifuge tube that was filled with gauze, with the extra ocular muscles affixed to the sides of the tube using cyanoacrylate glue. Eyes were immersed to the limbus in a PBS bath and covered with tissue paper to provide thorough hydration (Fig. 9C). The PBS bath was indirectly heated with a custom-built temperature-controller to maintain bath temperature in the physiological range of 35±1ºC. A 33G needle was inserted into the anterior chamber under a stereomicroscope using a micromanipulator. The needle was connected via rigid pressure tubing to a pressure transducer (142PC01G, Honeywell; Columbus, OH) and a 25 µL syringe (Hamilton, Gastight; Reno, NV) placed on a computer-controlled syringe pump (PhD Ultra; Harvard Apparatus; Holliston, MA). Custom-written

software[151] was used to maintain IOP at a user-defined pressure by adjusting the variable flow rate of the syringe-pump. All eyes were perfused with Dulbecco's PBS including divalent cations and 5.5 mM glucose passed through a 0.22 µm filter (referred to as "DBG").

To measure conventional outflow facility (*C*), eyes were perfused at sequential pressure steps of 4, 8, 15 and 25 mmHg, typically 20 minutes at each step to allow at least 10 minutes of steady flow rate data (typical tracing shown in Figure 19). The average flow rate (*F*) at each pressure step was then fit to a simplified version of Goldmann's equation:

$$\mathrm{F} = \mathrm{C} \times \mathrm{IOP} + \mathrm{F_u}$$

Equation 8

where episcleral venous pressure and aqueous humour production are assumed to be zero for an enucleated eye. According to Eq. 8, *C* is equal to the slope of the least-squares linear regression for *F* versus IOP, and F_u is the zero-pressure intercept that is often interpreted as unconventional or pressure-independent outflow. Equation 8 assumes that *C* and F_u are independent of *IOP* and that *F* reaches a steady state at each pressure step. In order for perfusion to be accepted into this study, we required there to be a stable flow rate in at least 3 of the 4 pressure steps. According to these criteria, *C* was successfully measured in 28 of 41 mice (9-10 per strain). Three cohorts of mouse eyes were perfused for outflow facility measurements. In Cohort 7, 10 BALB/cJ mouse eyes were used. In Cohort 8, 9 C57BL/6J mouse eyes were perfused. Cohort 9 consisted of 9 CBA/J mouse eyes. Of the 28 mice where *C* was measured, 14 mice also had measurements of IOP without anaesthesia (3-6 per strain). Of these 14 mice, 11 mice had facility measured in the right eye (the same eye as *IOP* was measured) and 3 mice had facility measured in the contralateral eye.

2.4. Ocular Compliance Measurements

Ocular compliance (*K*) is expressed in units of µL/mmHg and represents the incremental *intraocular* volume necessary to increase IOP by 1 mmHg. *K* was measured immediately after perfusion in 17 mice (4-7 per strain), following previously described techniques[12]. Briefly, with the perfusion needle still in the anterior chamber, pressure was recorded during 6 sequential injections of 1 µL DBG, with one minute between injections. The *total* compliance was then calculated as the change in volume (1 µL) divided by the change in pressure at each injection, averaged over the 6

injections. The total compliance, however, is the sum of the ocular compliance and the *system* compliance arising from the tubing and transducers. The system compliance was measured by repeating the same procedure without an eye using a blocked needle, and system compliance was subtracted from the total compliance to obtain *K*. All compliance measurements were done at 35ºC with the eye immersed in isotonic saline.

2.5. Statistical Analysis

IOP was analyzed using a linear mixed model (LMM) to test for statistical differences between strains with or without anaesthesia. LMM yields three p-values (corresponding to the probability of a type I error) describing the influence of: *(1)* strain, *(2)* anaesthesia and *(3)* any possible interaction on IOP. If a significant influence is detected, SPSS performs a Bonferroni test to evaluate statistical differences between any two strains (SPSS, IBM). To further investigate the interaction effect, i.e. whether anaesthetics had different effects depending on the mouse strain, we performed separate paired t-tests in each strain between IOP data measured with and without anaesthetics on the same eye. The statistical significance threshold was taken as 0.05 divided by the number of comparisons, i.e. 0.016 (Bonferroni correction).

In addition, we analysed IOP data either in conscious or anaesthetized mice separately to assess whether IOP difference was still statistically significant in anaesthetized mice only. Thus, we performed a 1-way ANOVA in two separate cases, in conscious (N =21) or anaesthetized (N =30) animals, followed by a Bonferroni test to indicate which sets of strains had statistically different IOP.

We also carried out statistical tests on quantities other than IOP, namely on C, F_u, α, β and K between strains. Such tests were carried out using a one-way ANOVA, followed by a post-hoc Bonferroni test for detecting pair-wise differences between any two strains.

Data points were considered outliers for the IOP vs. 1/C regression if their Cook's distance was larger than 1, or if the probability of their studentized deleted residual was lower than $0.05/N^{188}$, where N was taken as the number of data points used for the regression (N =14). If one of these criteria was met for any data point, it was removed from the analysis.

3. Results

3.1. IOP Measurements

IOP in conscious mice was significantly different between strains (Fig. 18; $p = 1x10^{-4}$, one-way ANOVA). Consistent with prior reports[141,142], IOP was lowest for BALB/cJ and highest for CBA/J, with an intermediate value of IOP for C57BL/6J (Table 7). According to a post-hoc Bonferroni test, IOP was statistically different between BALB/cJ versus CBA/J and C57BL/6J versus CBA/J, but not between BALB/cJ versus C57BL/6J. Compared to IOP in conscious mice, anaesthesia (i.e. isoflurane) caused a reduction in IOP (Fig. 18 and Table 7; $p = 0.046$, linear mixed analysis) that eliminated any detectable difference between strains ($p = 0.254$; one-way ANOVA). Comparing IOP in individual eyes with and without anaesthesia, the IOP reduction was significant for CBA/J (25.8 ± 18.1%; $p = 0.008$, paired Student's t-test with Bonferroni correction) but smaller or insignificant for C57BL/6J (8.2 ± 11.0%; $p = 0.14$) and BALB/cJ (-0.9 ± 28.8%; $p = 0.86$). These results are consistent with a previous report [11,141,142] which show anaesthesia has an IOP lowering effect that varies between strains.

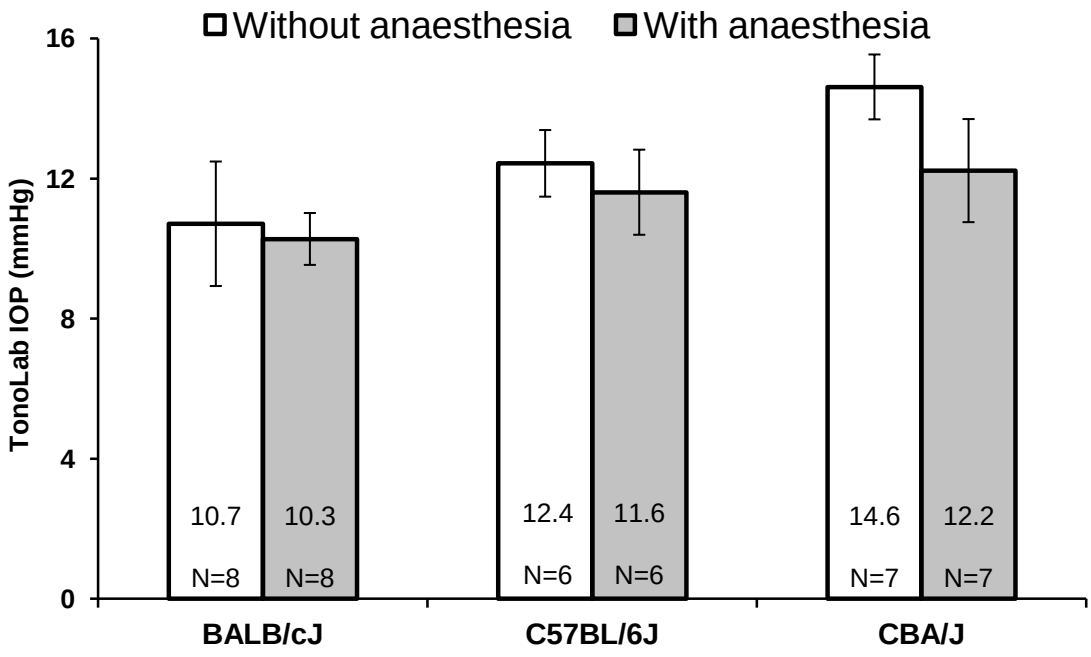

Figure 18: IOP data measured with TonoLab in conscious (white) or anaesthetized (grey) mice. Fewer mice had their IOP measured without anaesthesia because 9 animals were too stressed (see methods)

3.2. Outflow Facility Measurements

Our flow-rate vs. pressure data was well described by the linear best-fit regression (Fig. 20), whose R^2 values ranged from 0.935-1.00 in BALB/cJ, 0.958-1.00 in C57BL/6J and 0.931-1.00 in CBA/J. Conventional outflow facility was significantly different between strains (p = 0.049; one-way ANOVA), as indicated by different slopes of the flow rate versus pressure relationship (Fig. 20). A post-hoc Bonferroni test revealed that C was significantly larger in BALB/cJ compared to CBA/J, with C57BL/6J having an intermediate value of C (Table 7). Importantly, the ranking of C between strains was opposite to the ranking of IOP, suggesting that strains that had a higher conscious IOP also had a lower conventional outflow facility. There was no difference in F_u between strains (p = 0.363; 1-Way ANOVA) and the values measured for F_u were not statistically different from zero in 2 of the 3 strains (p >0.05 for BALB/cJ and CBA/J, p =0.02 for C57BL/6J; one-sided t-test).

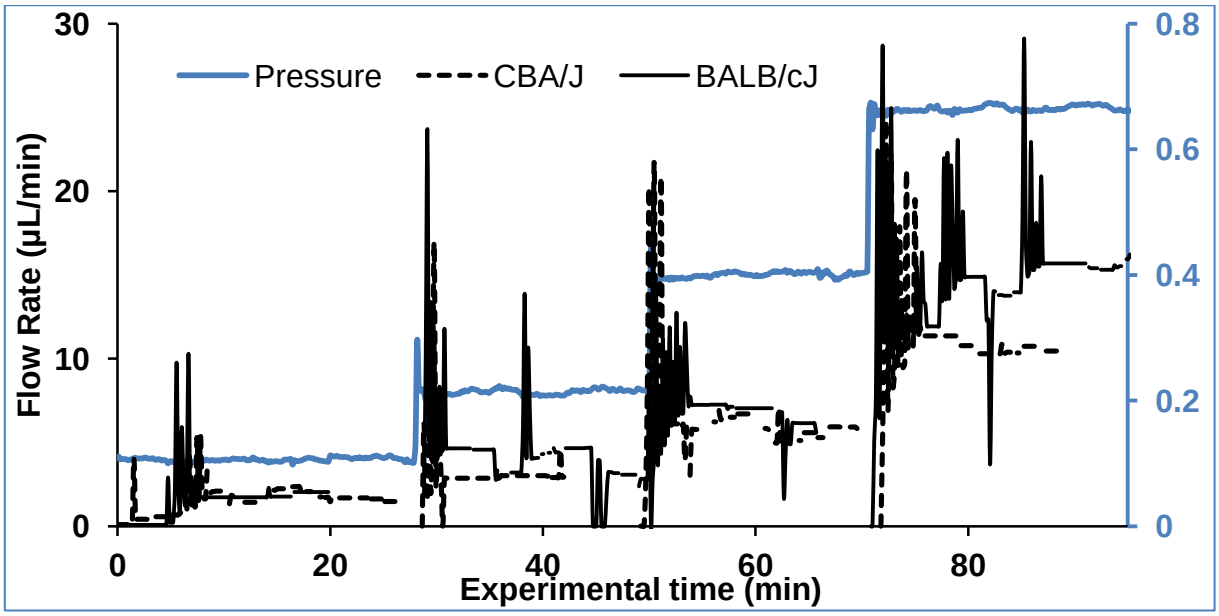

Figure 19: Perfusion tracing showing pressure (blue line) vs. flow rate for an enucleated eye from CBA/J (dashed black line) and BALB/cJ mouse (continuous black line).The flow-rate tracings from the BALB/cJ and CBA/J have been shifted in time such that flow rates overlap at each pressure level. More specifically, the tracing for the CBA/J mouse has been shifted to coincide with the pressure and flow rate tracing from the BALB/cJ tracing.

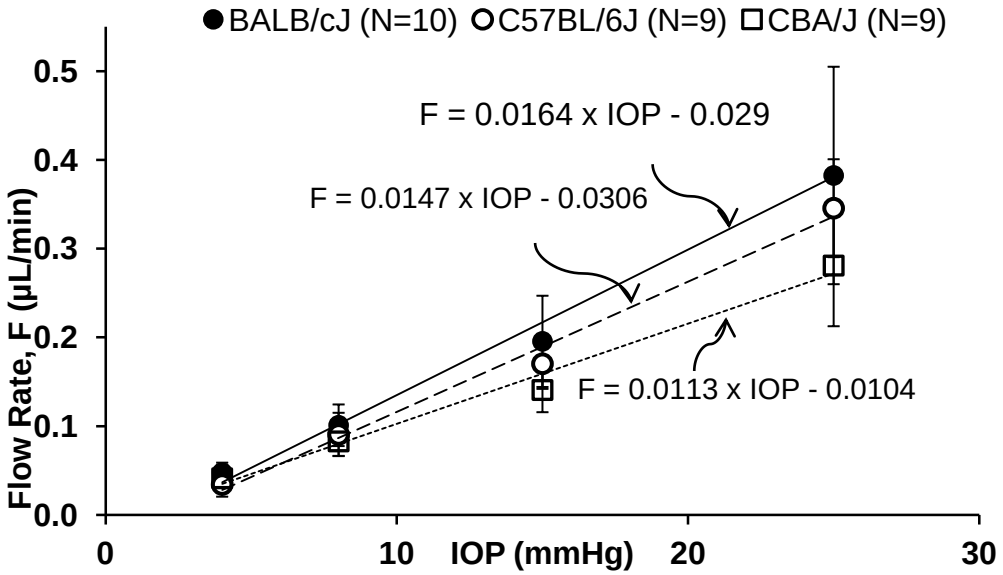

Figure 20: Average flow rate at each pressure step for BALB/cJ (black circles), C57BL/6J (white circles) and CBA/J (white squares). Lines correspond to the best-fit linear regression to the average flow-rate vs. pressure of each strain. The slope and intercept reported in the figure represent the best linear fit to the average flow-rate at each pressure step. R^2 values computed on individual eyes ranged from 0.935-1.00 in BALB/cJ, 0.958-1.00 in C57BL/6J and 0.931-1.00 in CBA/J.

Strain	**IOP** (mmHg)		***C*** (µL/min/mmHg)	F_u (µL/min)	**Ocular Compliance** (µL/mmHg)
	Conscious	**Anesthetized**			
BALB/cJ	10.7 ± 1.8 (*N* = 8)	10.3 ± 2.3 (*N* = 10)	0.0164 ± 0.0059 (*N* = 10)	-0.0290 ± 0.0411 (*N* = 10)	0.028 ± 0.021 (*N* = 4)
C57BL/6J	12.4 ± 1.0 (*N* = 6)	11.6 ± 2.4 (*N* = 10)	0.0147± 0.0029 (*N* = 9)	-0.0306 ± 0.0317 (*N* = 9)	0.022 ± 0.014 (*N* = 7)
CBA/J	14.6 ± 0.9 (*N* = 7)	12.2 ± 3.2 (*N* = 10)	0.0113 ± 0.0031 (*N* = 9)	-0.0104 ± 0.0219 (*N* = 9)	0.029 ± 0.018 (*N* = 6)

Table 7: Measured IOP, conventional outflow facility (C) and ocular compliance (mean ± SD). N refers to the number of eyes the parameters were measured in.

To investigate the relationship between IOP and facility, conscious IOP was plotted against outflow resistance (the mathematical inverse of *C* or 1/*C*) as measured within individual mice (Fig. 21; see Discussion for rationale). The relationship between IOP and 1/*C* was statistically significant ($p = 0.0004$; Welch's t-test), demonstrating that larger conscious IOP was associated with decreased outflow facility in individual mice across all three strains. One data point from a CBA/J

(filled symbol in Fig. 21) was determined to be an outlier (based upon its studentized deleted residual probability) and was not included in the regression, but regardless the regression remained significant even if the outlier was retained (p = 0.007). The R^2 value of the regression in Figure 21 indicates that 70% of the variation in IOP between mice of 3 different strains can be attributed to variation in outflow resistance (excluding the single outlier).

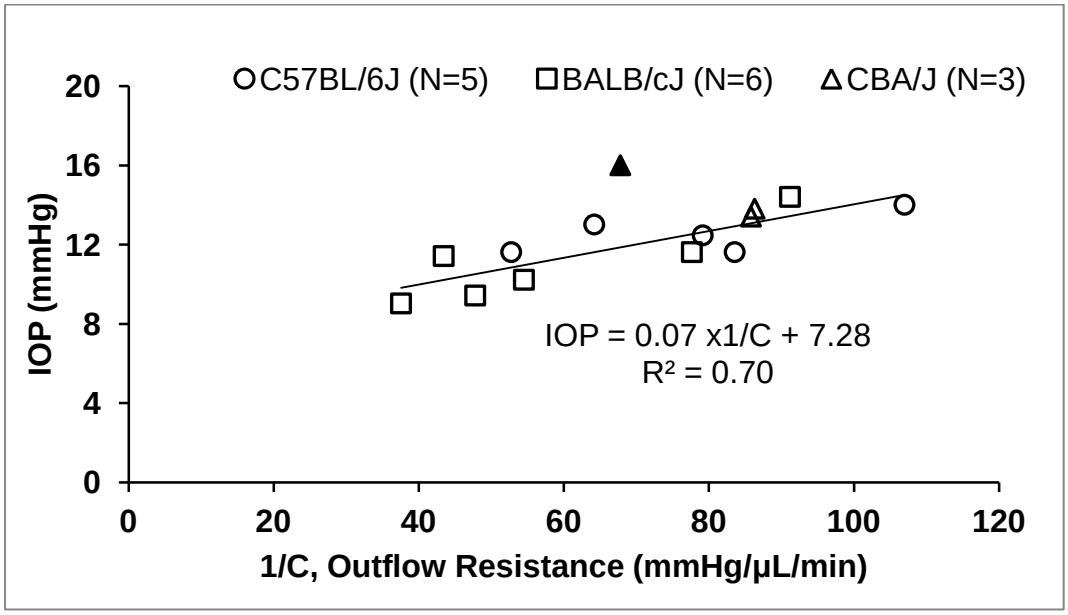

Figure 21: IOP vs. conventional outflow resistance in individual mice. IOP was measured in conscious animals, whereas outflow resistance was measured ex vivo. The filled symbol is an outlier, which was excluded from the best linear fit analysis.

3.3. Ocular Compliance Measurements

Ocular compliance was not significantly different between strains (Table 7, p = 0.796, one-way ANOVA). The system compliance was 0.011 ± 0.007 µL/mmHg. Somewhat strikingly, K measured with the eye in a bath of isotonic saline at physiologic temperature was approximately 3-fold smaller than previously reported by our group[12] with the eye outside of a bath at room temperature (0.086 ± 0.017 µL/mmHg for C57BL/6). This suggests that environmental conditions strongly affect at least some biomechanical measurements in mouse eyes.

4. Discussion

In this study, we provide evidence that differences in IOP between 3 genetically distinct strains of mice are largely attributable to differences in conventional outflow facility. Our data show that the strain having highest IOP (CBA/J) had lowest outflow facility, and conversely the strain having the lowest IOP (BALB/cJ) had the highest outflow facility. The strain having an intermediate value of

IOP (C57BL/6J) had an intermediate value of facility. Regression analysis applied to individual mice from all 3 strains, revealed a highly significant correlation between conscious IOP and conventional outflow resistance (1/*C*), with 70% of the variability in IOP being attributable to differences in conventional outflow resistance as predicted by Goldmann's equation.

4.1. IOP

Our IOP data show clear differences between three inbred strains, in good agreement with prior reports. As described by Savinova et al.[141], IOP for BALB/cJ, C57BL/6J and CBA/J under anaesthesia was approximately 11, 13 and 16 mmHg, respectively (read from Figure 1 of Savinova[141]). Similarly, Wang et al.[142] reported IOP in conscious BALB/c, C57BL/6 and CBA as 10.6, 13.3, and 16.4 mmHg. These values are in good agreement with our conscious IOP measurements reported in Table 7. In regards to anaesthesia, our results suggest that the IOP-lowering effect of isofluorane anaesthesia varies between inbred strains, with a larger IOP reduction observed in strains having a higher baseline IOP, consistent with prior reports[11,142]. Importantly, these data demonstrate that IOP differences between strains can be masked by anaesthesia, and thus the anaesthetic regimen is an important consideration for future studies examining aqueous humour dynamics in mice[11].

Our preliminary studies examined IOP in a fourth strain, CBA/CaJ, chosen based on prior reports[141] suggesting that CBA/CaJ mice exhibit a high baseline IOP (19.3 mmHg). In our hands, however, CBA/CaJ mice exhibited an intermediate IOP of 11.8 ± 1.3 mmHg (*N* =4) that was not dissimilar from IOP in C57BL/6J (12.4 ± 1.0 mmHg), and we therefore replaced CBA/CaJ with CBA/J. It is unclear why our IOP measurements in CBA/CaJ were lower than reported by Savinova [141], but these difference may be attributable to mouse age since that previous study[141] used mice aged between 6-12 months, as compared to our study that used mice between 3-4 months old. In addition, data measured on CBA/CaJ by Savinova et al. also disagreed with results measured telemetrically in the same strain by another group[189]. The latter study [189] measured an IOP of 12.4 ± 2 mmHg averaged over the entire light cycle (6 AM- 6 PM) in adult mice whose age is not specified, which was very similar to our IOP measurements.

4.2. Conventional Outflow Facility in cohorts 7,8,9

Our data raise the interesting question of whether morphological differences in the conventional outflow pathway between strains may underlie the difference in *C* between strains. Savinova[141] examined this question in context of strain-dependent differences in IOP, and found no obvious anatomical or pathological differences in the drainage angle structures between strains, although other studies have shown differences in gross ocular anatomy between strains, including anterior chamber depth, axial length and corneal thickness[140]. It should be noted that our measurements of *C* were done ex vivo using enucleated eyes, while most other studies measured *C* in vivo under anaesthesia. Following enucleation, one may safely assume that aqueous production is eliminated ($F_p = 0$) and EVP = 0 mmHg. Enucleated eyes therefore provide a somewhat more direct means to measure *C* without possible confounding effects of F_p or EVP that may influence in vivo measurements. However, we must assume that *C* measured in enucleated eyes is similar to *C* in vivo. This assumption is often taken for granted in eyes of larger species, such as humans and rabbits[190], where measurements of *C* in enucleated eyes are consistent with in vivo measurements of *C* by tonography or intracameral perfusion under anaesthesia. For mice, however, no studies have yet directly compared *C* between enucleated and in vivo eyes, but Millar and colleagues[6] have shown that *C* is unaffected by euthanization via anaesthetic overdose in BALB/cJ mice.

Somewhat surprisingly, values of *C* measured in this study were significantly larger than previously reported by our own group[12,13,79] for enucleated C57BL/6 eyes (0.0045 - 0.0070 µL/min/mmHg). These differences were likely caused by differences in the temperature and hydration of the eye during perfusion. In the current study, the eye was immersed in a bath of isotonic saline at physiological temperature (Fig. 9C). However, in our previous studies[12,13,79] the eyes were perfused at room temperature without a bath (Fig. 9A), where the facility was corrected for temperature-dependent viscosity[77] and the eyes were kept hydrated by covering with a tissue paper moistened with isotonic saline. Furthermore, the zero-pressure intercept (F_u of Eq. 8) in this study was not significantly different from zero in every strain, in contrast to our previous studies where this intercept was larger than zero (0.0160 – 0.114[12,13,79] µL/min). This intercept is often interpreted as the amount of outflow passing through the unconventional or pressure-independent

pathway (see Introduction, section 3.2.2.2). However, if in fact this intercept is strongly dependent upon temperature and hydration (Fig. 10&11; Chapter 2), the interpretation of the measurement is drawn into question, and the true in vivo value of unconventional outflow becomes ambiguous, at least based on measurements in enucleated eyes. For this reason, we do not analyze it and focus only on conventional facility measurements.

4.3. Relationship between IOP and *C*

Plotting IOP versus 1/*C* as shown in Figure 21 provides a physically meaningful interpretation, as can be seen using Goldmann's equation:

$$\mathrm{F_p} = \mathrm{C} \times (\mathrm{IOP} - \mathrm{EVP}) + \mathrm{F_u}$$

Equation 4

where F_p is the aqueous production rate, EVP is episcleral venous pressure, and F_u is the outflow rate through the unconventional or pressure-independent pathway. All parameters in Eq. 4 apply to conscious mice. Solving Eq. 4 for IOP yields:

$$\mathrm{IOP} = \mathrm{F_c} \times \frac{1}{\mathrm{C}} + \mathrm{EVP}$$

Equation 13

where F_c is the outflow rate through the conventional pathway ($F_c = F_p - F_u$). Assuming that *C* measured in enucleated eyes represents *C* in vivo (see above), Goldmann's equation predicts a linear relationship between IOP and conventional outflow resistance (1/*C*), with the slope of the relationship equal to F_c and the zero-IOP intercept equal to EVP, as previously pointed out[76]. This method therefore allows indirect estimates of F_c and EVP based on measurements of *C* and IOP from a sample population of mice.

If we assume that F_c and EVP are the same between C57BL/6J, BALB/cJ and CBA/J mice, then the regression in Figure 21 predicts (excluding the outlier) that F_c = 0.068 ± 0.013 µL/min and EVP = 7.3 ± 1 mmHg (mean ± stdev). Whether F_c and EVP are truly the same between strains is an open question, however the strong agreement between Eq. 13 and our data (R^2 = 0.70; *N* = 13 mice) suggests that F_c and EVP are reasonably consistent between C57BL/6, BALB/cJ and CBA/J strains or that any variation in F_c and EVP between strains has relatively minor influence (< 30%) on IOP compared to the principal dependence of IOP on *C*. Furthermore, the value of EVP estimated by

linear regression (7.3 mmHg) agrees fairly well, but is slightly higher than published values from the same strains using the blood-reflux technique that requires anaesthesia (where IOP may be artificially depressed[11,142]) (cf. 5.4 mmHg for BALB/cJ[6] and 6.3[15] mmHg for C57BL/6J). The value of F_c estimated by linear regression (0.068 µL/min) also fits within the published range, however the range of published F_c values varies 3-fold between strains (0.032 µL/min in NIH Swiss White[5], 0.062 µL/min for C57BL/6[15], and 0.111 µL/min for BALB/cJ[6]) which may be related to methodological differences between studies or true physiologic differences between strains. It should be pointed out that F_c lumps effects of F_p and F_u such that variations in F_p between strains may be masked by compensatory differences in F_u (or vice versa). We attempted to perform regression analysis on each strain individually, so as to estimate values of F_c and EVP for each strain, but the small numbers of mice (3 - 6 per strain) made this analysis unreliable.

As an alternative to the regression-based approach presented above, one may also examine a population-based approach to investigate whether differences in the mean value of *C* can account for differences in mean conscious IOP between strains. One advantage of the population approach is that it uses all of our data for *C* and conscious IOP (*N* = 32 mice), not just data limited to when *C* and conscious IOP were both measured in the same mouse (*N* = 14 mice). Because Goldmann's equation is essentially a statement of the conservation of mass that is strictly true only for individual eyes (and not populations of eyes), Goldmann's equation must first be expressed in terms of population averages (or expected values). Taking the expected value of Eq. 4 and neglecting the covariance between *C* and IOP or EVP yields:

$$\overline{F_c} = \overline{C}\left(\overline{\mathrm{IOP}} - \overline{\mathrm{EVP}}\right)$$

Equation 14

where the overbars indicate population averages as given in Table 7 for $\overline{C}$ and $\overline{\mathrm{IOP}}$. We did not measure $\overline{F_c}$ or $\overline{\mathrm{EVP}}$, however, let us assume that $\overline{F_c}$ and $\overline{\mathrm{EVP}}$ are the same for all strains. Using the estimated value of EVP from the linear regression analysis above (7.3 mmHg), yields the following values of $\overline{F_c}$ that should be consistent between strains if the assumptions of this scenario hold: 0.056 ± 0.067 µL/min for BALB/cJ, 0.075 ± 0.052 µL/min for C57BL/6J, and 0.083 ± 0.045

µL/min for CBA/J. These values are in reasonably good agreement (within 25% relative to C57BL/6J), consistent with the regression analysis that also assumes consistency of $\overline{F_c}$ and $\overline{EVP}$ between strains. In addition, the differences in $\overline{F_c}$ between strains was not statistically significant ($p>0.38$; unpaired t-test).

In conclusion, our data suggest that differences in IOP between genetically distinct strains of mice are largely attributable to differences in conventional outflow facility, rather than to differences in aqueous inflow, episcleral venous pressure or unconventional outflow. These data motivate further studies to identify the morphological or genetic basis that may underlie the differences in outflow facility between inbred strains, which may provide a promising tool for unravelling the mechanisms of IOP regulation as occurs in the conventional outflow pathway.

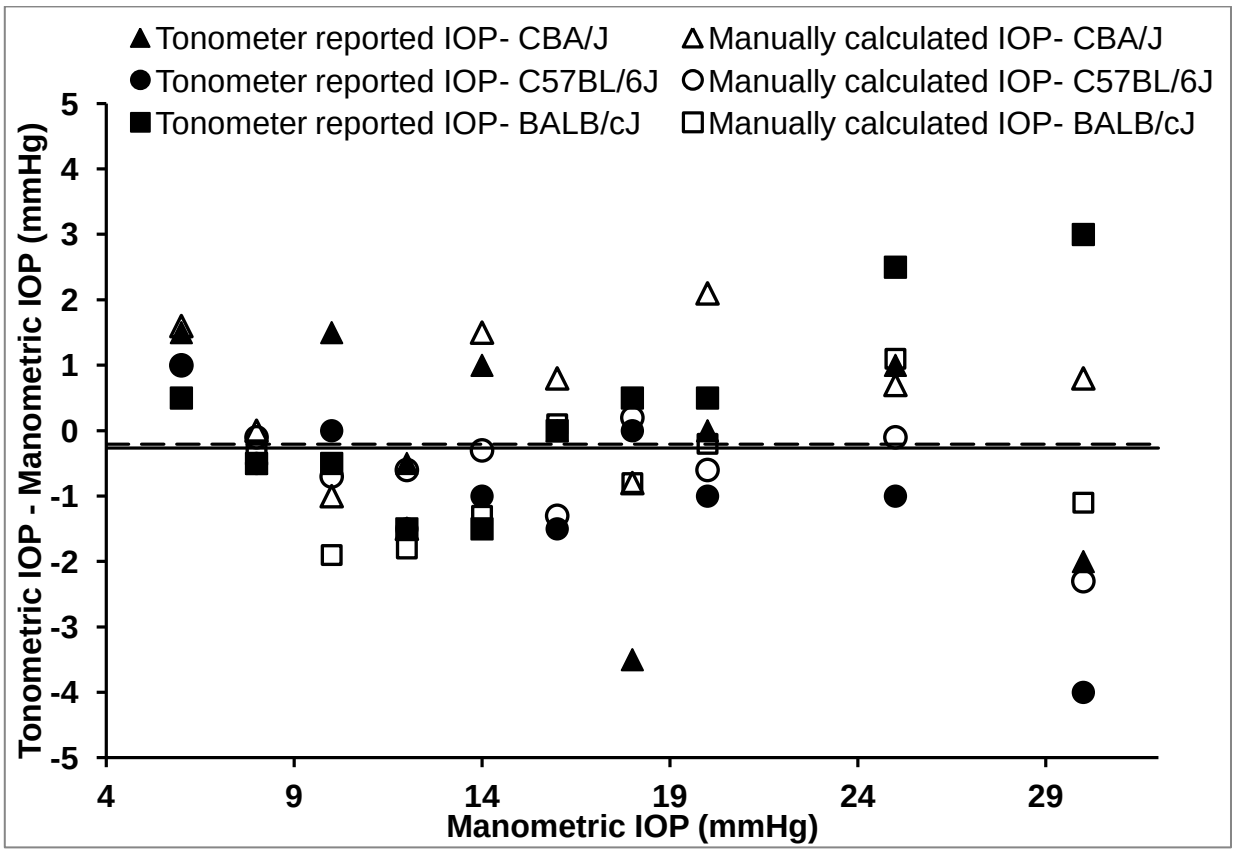

Supplementary figure 2: Bland-Altman plot, showing the difference between tonometric and manometric IOP (y-axis) against the manometric IOP (x-axis). The smaller the difference between tonometric and manometric IOP, the closer the data points are to 0. We show data points corresponding to two tonometric measurements: filled symbols are based on the automatic average tonometric value reported by the tonometer, while empty symbols are based on our manually calculated IOP (corresponding to the average of the first 5 measurements provided by the tonometer). Filled symbols show a larger spread, especially at high manometric pressures. The sold line represents the average difference between tonometer reported and manometric IOP (-0.27). The dashed line represents the average difference between the manually calculated and manometric IOP (-0.21). The dashed line is closer to 0 by 22%, suggesting the manually calculated IOP gives results which are more similar to the manometric pressure than that reported by the tonometer.

Chapter 5: The Role of Cellular Metabolism in Aqueous Humour Outflow in Mice

1- Introduction

Aqueous humour drainage through the trabecular meshwork has long been considered to occur passively, i.e. independently of cellular metabolism. The first evidence on this topic was provided by Bárány, who showed that outflow facility in enucleated cattle eyes was unaffected by several anti-metabolic agents[78]. A subsequent study by Van Buskirk and Grant showed that changes in outflow facility between 4°C and physiological temperature could be fully explained by temperature-dependent changes in the viscosity of aqueous humor[77]. These studies consolidated the concept that aqueous humour outflow was independent of cellular metabolism. As a result, the trabecular meshwork (TM) and Schlemm's canal (SC) have largely been considered to function as passive filter-like tissues without significant active regulation of outflow by the TM or SC cells themselves.

The idea of metabolically-independent outflow de-emphasized the potential role of active cellular processes that may modulate outflow facility. Paradoxically, there has been growing interest in the role of cell contractility [79–84], exocytosis[85], and signal transduction[79,86,87] in conventional outflow regulation, despite the fact that these processes require metabolic energy. Moreover, our data from Chapter 2, in contrast to Van Buskirk's original study[77], reveal that the facility increase between 20°C and physiological temperature was four times greater than expected based on viscosity differences alone, suggesting a significant metabolic contribution to conventional outflow in mice.

In this study, we hypothesize that cellular metabolism contributes to the regulation of conventional aqueous humour outflow in mice. We test this hypothesis by measuring conventional outflow facility in two cohorts of mouse eyes perfused with mock aqueous humour at 20 or 35°C, with or without anti-metabolic agents. The anti-metabolic agents were a cocktail of 2-dideoxy-D-glucose and sodium azide that together inhibit glycolysis and block electron transport to prevent further ATP production. In the first cohort, we examined the effect of temperature in the presence of anti-metabolic agents to determine whether the additional increase in facility beyond that predicted

based on viscosity alone could be eliminated by anti-metabolic agents. In the second cohort, we examined the effect of anti-metabolic agents at physiological temperature, so as to estimate the portion of aqueous humour outflow associated with metabolic activity. Finally, we performed histology to analyze the effects of the anti-metabolic agents on the morphology of the TM and SC.

2- Methods

All experiments were performed using ex vivo tissue and were done in compliance with the ARVO Statement for the Use of Animals in Ophthalmic and Vision Research the Animal Scientific Procedures Act 1986.

2.1. Ex vivo mouse eye perfusion

This study used either C57BL/6 male mice from Charles River or C57BL/6J female mice from Jackson Labs. Mice were aged 9-16 weeks at the time of outflow facility measurement, and were housed at 21°C in individually ventilated cages and fed ad libitum under a 12-hour light (6 AM to 6 PM) and 12-hour dark cycle. Eyes were enucleated within 15 min of death following cervical dislocation, and stored in PBS at 4°C for up to 3 hrs to await perfusion. To mount an eye for perfusion, its posterior pole was set upon a post covered with a minimal amount of cyanoacrylate glue. As previously described (see Chapter 2, Section 2.1), a 33G needle was mounted on a customized holder (MMP Kit, Harvard Apparatus, Holliston, MA, USA) and inserted into the anterior chamber using a micromanipulator while visualized by a microscope. For hydration, the eye was submerged in isotonic saline (PBS) to the limbus and covered with a wet tissue paper. The PBS was contained in a chamber and placed in a custom-made water-bath to maintain the temperature of the eye at 35 °C during the experiment (see Fig. 9C, Chapter 2). Room temperature experiments were done in the same way except the PBS bath was left at room temperature, at 20 ±1°C.

The needle was connected via tubing to a 25 µL syringe placed on a computer-controlled syringe pump (Ultra Pump, Harvard Apparatus, Holliston, MA, USA) and to a pressure transducer (142PC01G, Honeywell, Fort Washington, PA, USA) which continuously read the pressure inside the eye. Customized LabView[151] (National Instruments Corp., Austin, TX) software controlled the flow-rate of the perfusion fluid into the eye such that the intraocular pressure was maintained at a

user-defined level. Eyes were perfused at four increasing pressure steps (4, 8, 15 and 25 mmHg) over 1.5-3 hours. Each pressure step lasted 20-30 min to allow the flow rate to reach steady-state conditions for at least 10 min. The flow rate was subsequently averaged for each pressure, unless it failed to stabilize. Only experiments where a stable flow rate was obtained in at least 3 of the 4 pressure steps were used for outflow facility measurement.

2.2. Outflow Facility Measurement

Conventional, or pressure-dependent, facility (*C)* was calculated as previously described (see Chapter 2, section 2.2). Briefly, the average stable flow-rate (*F*) measured at each pressure step (*IOP*) was fit to the simplified Goldmann's equation (Eq. 4):

$$\mathrm{F} = \mathrm{C} \times \mathrm{IOP} + \mathrm{F_u}$$

Equation 8

where *C* corresponds to the slope of the *F* versus IOP relationship and F_u corresponds to flow rate intercept at zero IOP that represents the unconventional, or pressure-independent, outflow. The simplified Goldmann's equation is valid for enucleated eyes where episcleral venous pressure (*EVP*) and aqueous humour production (F_p) can safely be assumed to equal zero. Importantly, it assumes *C* and F_u do not change with pressure, and *F* and *IOP* have reached steady-state. Thus *C* was calculated as the slope of the best-fit linear regression to our flow-rate (*F*) vs. pressure (*IOP*) data for each individual eye (see Fig. 8, Chapter 2).

2.3. Experimental Design

Two cohorts of mice were perfused under different conditions, referred to as Cohort 10 and 11, as a continuation of the cohort numbering used in the previous studies. Paired eyes were used, such that one eye was perfused within 15 min post mortem while its contralateral eye was kept at 4°C in PBS to await perfusion 2-3 hrs later. Assignment of control or experimental treatment was randomised between paired eyes. Data from unpaired eyes was accepted when the perfusion of their contralateral eyes failed. Overall, data from 12 unpaired eyes out of 36 eyes were accepted because perfusions of their contralateral eyes failed (Table 8).

	Total number of eyes	Unpaired eyes	Paired eyes
Cohort 10	12	6	6
Cohort 11	12	2	10

Table 8: Number of paired or unpaired eyes perfused in cohorts 10 and 11. Eyes were occasionally unpaired because the perfusion of their contralateral eye was unsuccessful. In both cohorts, at least half of the data were based on paired eyes.

The anti-metabolic agents were a cocktail of 10 mM dideoxy-D-glucose (Sigma-Aldrich, D8375) and 2 mM sodium azide (NaN3, Sigma-Aldrich, S8032), as described in previous studies[191]. 2-dideoxy-D-glucose is a glucose-analogue that is phosphorylated by hexokinase but cannot be processed by the next enzyme in the glycolytic pathway, phosphoglucose isomerase, thereby halting glycolytic production of ATP (see supplementary figure 3). Sodium azide blocks the electron transport chain by binding irreversibly to cytochrome oxidase to prevent ATP production in the mitochondria (see supplementary figure 4). Both agents were diluted into Dulbecco's PBS from stock solutions of 20 and 40 mM, respectively. Because sodium azide is light-sensitive, all azide-containing solutions and the MMP Kit were covered with foil. For consistency, the MMP Kit was also covered with foil for perfusion of the untreated contralateral eye. For both cohorts, 150 µL of either anti-metabolic agent or DBG was backfilled from the tip of the needle prior to cannulation.

Eyes were perfused with an open reservoir at 8 mmHg for 1 hr prior to perfusion via the syringe pump. This pre-pressurization aimed at exposing the outflow pathway to the drug prior to the measurement of outflow. For consistency, eyes perfused with DBG were similarly pre-pressurized.

2.4. Histology

Histological analysis was performed on eyes from Cohort 11, perfused at 35 °C either with (N =3) or without (N =4) anti-metabolic agents. Following perfusion, the needle was removed and eyes were immediately immersed either in PFA 4% for fixation or in Karnovsky's solution for 2 hrs prior to changing it to PFA 0.1% for long-term storage. Eyes were shipped to Dr. A. Thomas Read (University of Toronto, Dept. of Ophthalmology) who performed all further histological processing and imaging. The eyes were sectioned near the equator, the lens was removed, and the anterior corneoscleral tissue was cut in quadrants. Tissue was fixed overnight in Sorenson's phosphate

buffer (containing 2.4% glutaraldehyde and 2% formaldehyde) and post-fixed in 4% osmium tetroxide. Quadrants were dehydrated through a graded ethanol series, transferred to propylene oxide, embedded in epon-araldite, and cured for 48 hours at 60°C. The tissue was sectioned radially into semi-thin sections (0.5 µm) using an ultramicrotome (Leica EM UC7, Wetzlar, Germany) and stained with toluidene blue. Sections were affixed to glass slides, examined and photographed at 63x (Zeiss Axioplan, Oberkochen, Germany). One to two quadrants were examined per eye; in each quadrant, approximately 20 sections were cut, and examined under the microscope. Histology was performed by Dr. Thomas Read, at University of Toronto.

2.5. Statistical analysis

Unpaired t-tests were used to assess the statistical significance of differences in conventional facility between eyes perfused under different conditions within cohorts. A two-sided t-test was used to test whether the increase in conventional facility was different from the 1.4 increase expected based on viscosity changes alone.

Outliers within each cohort were identified according to Dixon's test. A linear mixed model (LMM) approach (SPSS, IBM, Armonk, New York, U.S.) was used to analyse the entire dataset combining conventional facility from the two cohorts of mouse eyes perfused in this study as well as that perfused at 20 and 35 °C with DBG, from Chapter 2 (Cohort 2; Fig. 11). This allowed an analysis of all the data to examine the effects of temperature and anti-metabolic agents as well as their interaction, while accounting for the covariance between paired eyes as well as random variations in facility between cohorts and between individual mice. We used a LMM which modelled random effects arising from differences between cohorts and the random nesting of mice within cohorts. The covariance of paired eyes was taken into account by grouping data from paired eyes to their corresponding mouse. The test used a maximum likelihood estimation method to estimate the parameters of the statistical model. The threshold for statistical significance was 0.05.

3- Results

3.1. Cohort 10, anti-metabolic agents reduces temperature-related increase in *C*

All eyes in this cohort were perfused with anti-metabolic agents at room (20°C) or physiological temperature (35°C). At room temperature *C* was 0.0080±0.0021 µL/min/mmHg (mean ± SD; *N* =7), while at physiological temperature *C* increased to 0.0132±0.0046 µL/min/mmHg (*N* =5; Fig. 22B). The difference in *C* was only borderline significant (*p* = 0.063; unpaired t-test) with a relative increase of 1.65±0.72 between room and physiological temperatures. In contrast, earlier studies from Chapter 2 without anti-metabolic agents showed a much larger facility increase between room and physiological temperature (2.50±0.86, Figure 22A), well beyond that expected based on viscosity differences alone (1.4). In the current study, however, the measured facility increase (1.65) was not statistically different from the 1.4-fold increase based on viscosity (p=0.46; two-sided t-test). Taken together, these data suggest that the temperature-associated facility change beyond that caused by viscosity is attributable to active cellular metabolism.

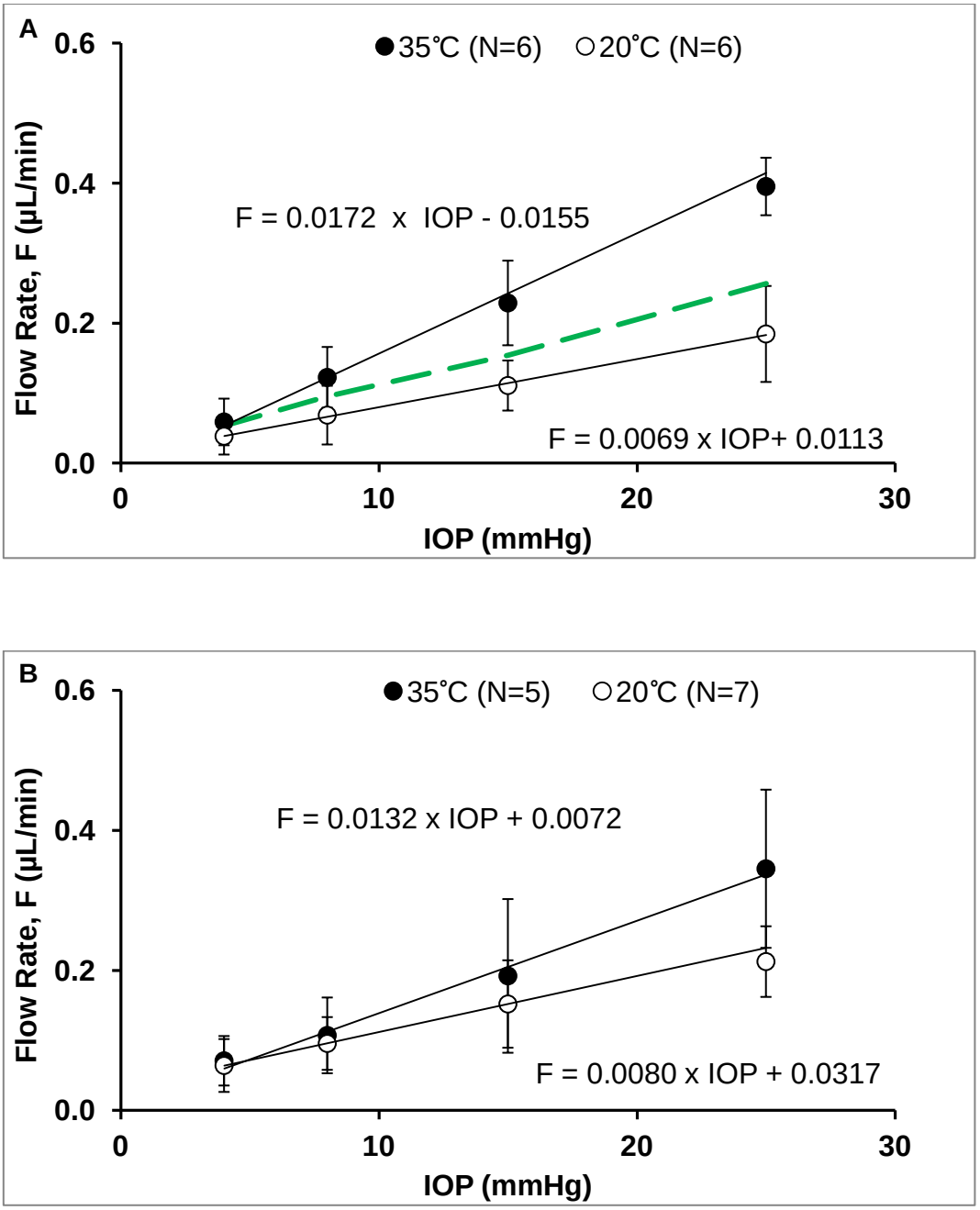

Figure 22: Flow Rate vs. pressure data for eyes from Cohort 2 and 10, perfused at 20 or 35°C with DBG (A) without anti-metabolic agents, (B) with anti-metabolic agents (2 mM dideoxy-D-glucose + 10 mM sodium azide). The green dashed line represents the expected flow-pressure relationship slope, or conventional facility, expected at 35 °C based on the facility measured at 20°C and the decrease in aqueous humour viscosity. Bars are standard deviations. R^2 values ranged from 0.955-0.996 for eyes from Cohort 10 perfused at 20C with anti-metabolic agents and from 0.897-0.999 for eyes perfused at 35C with anti-metabolic agents (Panel B).

3.2. Cohort 11, anti-metabolic agents reduce *C* by 30%

All eyes in this cohort were perfused at physiological temperature (35°C) with or without anti-metabolic agents. At physiological temperature without anti-metabolic agents, *C* was 0.0290±0.0068 µL/min/mmHg (*N* =6), while with anti-metabolic agents C was 0.0203±0.0055 µL/min/mmHg (*N* = 6; Fig. 23). The difference was statistically significant (p = 0.036, unpaired t-test), with anti-metabolic

agents decreasing *C* by 30 %. These data suggest that cellular metabolism contributes to conventional outflow in the mouse eye and inhibiting cellular metabolism decreases outflow facility by 30%.

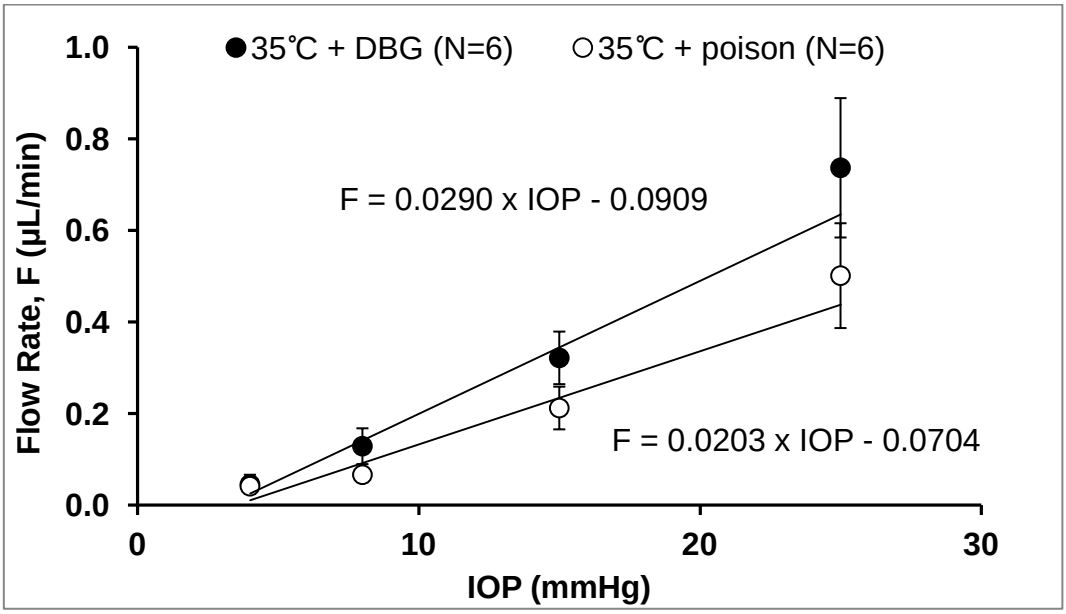

Figure 23: Flow Rate vs. pressure data for eyes from Cohort 11, perfused at 35°C with or without anti-metabolic agents (2 mM dideoxy-D-glucose + 10 mM sodium azide). Bars are standard deviations. R^2 value ranged from 0.900-0.979 for eyes perfused with anti-metabolic agents and 0.969-0.998 for eyes perfused with DBG.

3.3. Pooled statistical analysis

Surprisingly, we found unexpected differences in outflow facility between mice from different cohorts perfused under similar conditions (0.0132±0.0046 vs. 0.0203±0.0055 µL/min/mmHg for eyes perfused at 35 °C with anti-metabolic agents in Cohort 10 and 11; 0.0172±0.0028 vs. 0.0290±0.0068 µL/min/mmHg for eyes perfused at 35 °C with DBG in Cohort 2 vs. Cohort 11). Thus we performed an LMM analysis (see Methods section) on the entire dataset including data from Cohorts 10 and 11 of this study, and data from Cohort 2 of Chapter 2, to determine whether anti-metabolic agents and temperature were consistently affecting outflow facility, regardless of the variability found between cohorts. This analysis upheld the significant effects of temperature (p =1x10^{-6}) and anti-metabolic agents (p =0.018) on *C*, despite the fact that there were fairly large differences in baseline *C* between cohorts. Moreover, the LMM analysis revealed that the effect of anti-metabolic agents was significantly different between 20 and 35°C (p =0.009; interaction effect), consistent with anti-metabolic agents having a greater influence on *C* at physiological versus room

temperature. The dependence of anti-metabolic agents' effect on temperature is attributable to a greater metabolic activity (and hence greater sensitivity to anti-metabolic agents) at physiological versus room temperature because enzymatic reactions are suppressed at lower temperatures according to the Arrhenius equation.

3.4. Histology

The qualitative analysis of histological sections of treated vs. untreated eyes revealed some apparent changes in TM and SC (Fig. 24- 25). In general, there were more giant vacuoles in eyes treated with anti-metabolic agents which extended to the outer wall of SC. Another interesting observation was to find extensive vacuolization of SC in a treated eye (Fig. 25A). Interestingly, the other quadrant of the same eye did not show such an extensive vacuolization but still presented abnormal giant vacuoles, irregularly shaped and almost extending to the outer wall (Fig. 25B). In addition, the TM and SC seemed well-preserved in all eyes; the integrity of the SC endothelium did not seem obviously damaged by the anti-metabolic agents.

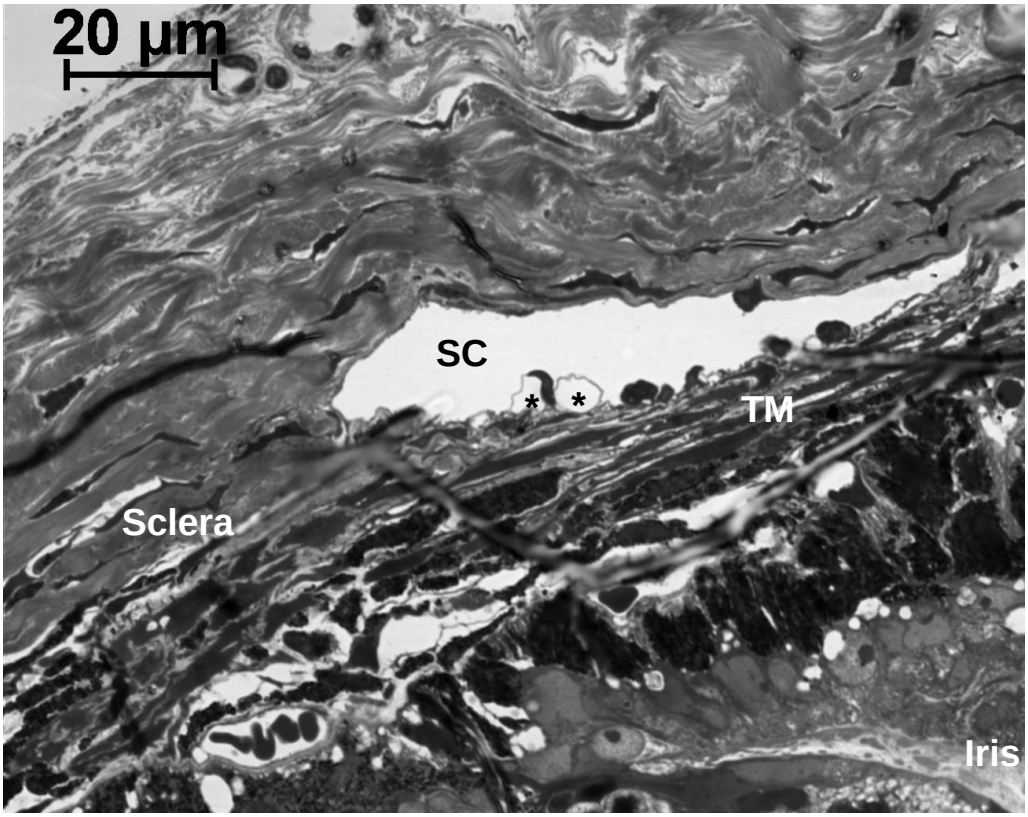

Figure 24: Histological section of SC of a mouse eye perfused with DBG. The eye was immersed in fixative prior to embedding. SC is open and shows a few giant vacuoles. X100 magnification. Asterisks show Giant Vacuoles. TM: Trabecular Meshwork. SC: Schlemm's Canal.

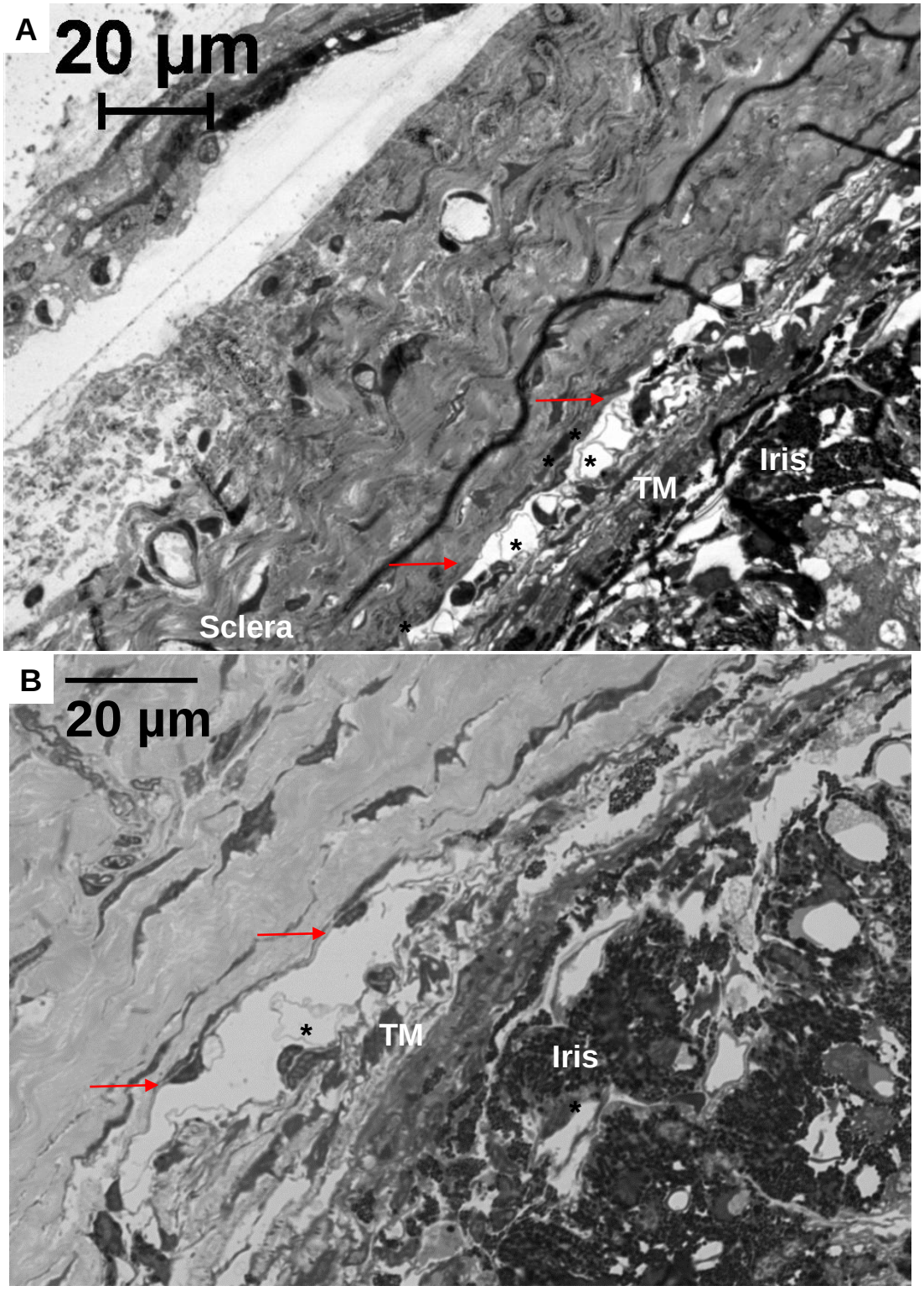

Figure 25: Histological section of SC perfused with anti-metabolic agents from two different quadrants of the same eye (A,B). A) SC is apparently smaller and filled with many more giant vacuoles which extend across the canal, to the outer wall. (x63 magnification), B) SC shows a more open lumen but with an abnormally large giant vacuole, shown by the asterisk(x100 magnification). Red arrows point to the outer wall of SC. Asterisks show selected Giant Vacuoles. TM: Trabecular Meshwork.

4. Discussion

In this study, we present data showing conventional outflow in the mouse eye depends on active cellular metabolism and is reduced by 30% in the presence of anti-metabolic agents. We had originally shown that the increase in conventional facility with temperature in mice was four times larger than that predicted based on viscosity effects alone (see Chapter 2). Our current findings show that anti-metabolic agents eliminate the temperature-related facility change beyond that caused by viscosity. In addition, anti-metabolic agents were shown to decrease conventional facility at physiological temperature by 30%. To the best of our knowledge, this is the first evidence that conventional aqueous humour outflow in mice depends on cellular metabolism, which contradicts findings from previous studies using anti-metabolic agents in bovine eyes[78] or analysing temperature effects on outflow facility in human eyes[77].

One possible explanation for our results being different from previous studies[77,78] could be species-related differences. For example, Bárány[78] tested anti-metabolic agents on bovine eyes which, unlike mice, lack a true SC and possess a disorganized TM. Van Buskirk and Grant[77] used human eyes which, like mice have a true SC, yet differ in the TM which is much thinner in mice[137]. However, we propose the discrepancies with past reports could lie in the different post mortem times of the tissues or in the use of different poisonous substances, as discussed below.

Notably, Van Buskirk and Grant[77] used human eyes up to 48 hrs following death; in contrast, our study used eyes obtained within 3 hrs post mortem. Long post mortem times could have caused reduction of tissue metabolic activity as well as an advanced degradation of the outflow pathway, as previously reported in human eyes stored at 5 °C for 48 hrs[159]. As a result, Van Buskirk and Grant's study might have failed to detect any changes in metabolic activity which had already disappeared or was markedly attenuated. This is further supported by our results showing conventional outflow facility is decreased in mice following long post mortem times (see Chapter 2). Note Grant[158] showed outflow facility was similar in human living and enucleated eyes. Yet he did not specify the post mortem times of the enucleated eyes at the time of facility measurement. In a separate cohort

of enucleated eyes used for a different purpose in that same paper, Grant indicates they were perfused within 24 hrs post mortem. Thus, we can assume the same for the eyes used for facility measurement. The similarity in outflow facility between living and enucleated eyes perfused within 24 hrs post mortem suggests there is no loss of metabolic activity associated with outflow facility with post mortem times < 24 hours. This is different to the situation reported by Van Buskirk[77], who used enucleated human eyes within *48 hrs* post mortem. This suggests that metabolic activity is not dramatically reduced within 24 hrs but might have significantly degraded by 48 hrs in human eyes. This is consistent with our data showing conventional facility in enucleated mouse eyes changed after 24 but not after 3 hrs post mortem (Chapter 2; Cohorts 3A&B).

On the other hand, we propose that Bárány[78] did not detect a similar effect from the multiple anti-metabolic agents he used because they had a limited efficiency at inhibiting production of ATP in the outflow pathway. Metabolic energy (or ATP) is typically produced in cells by glycolysis. One of the end-products of glycolysis is pyruvate, which is used to produce additional ATP through cellular respiration. Per molecule of glucose broken down, glycolysis produces 2 molecules ATP while oxidative phosphorylation produces 34-36 molecules of ATP (see supplementary figures 3-4). Still, the TM has been shown to preferentially harvest most of its energy preferably from glycolysis, while cellular respiration provided only up to 25% of its energetic requirements[192]. Most anti-metabolic agents Bárány used were targeted at either glycolysis or cellular respiration, but not both (see Table 9). Therefore, blocking only one of the metabolic pathways (glycolysis or cellular respiration) could allow the other to compensate for the loss of ATP. This assumes cellular respiration could occur without the simultaneous production of pyruvate by glycolysis, by using the available pool of pyruvate left in the eye. Only one anti-metabolic agent used by Bárány (called Sodium arsenite) is known to affect both pathways, yet it only disturbs glycolysis mildly. Specifically, it does not prevent glycolysis from proceeding, but inhibits the production of some ATP in the process (Supplementary figure 3). Interestingly, the only anti-metabolic agent targeting glycolysis at its early stage (Iodoacetate) had an effect on total resistance. This anti-metabolic agent stops glycolysis after two molecules of ATP have been used, thereby depleting the tissue of the available ATP. Yet the effect

of this anti-metabolic agent on resistance measured by Bárány was later attributed to its ability to affect cellular permeability because it is a sulfhydryl agent, rather than metabolic activity. This was supported by showing other similar sulfhydryl agents also increased outflow facility in spite of not affecting metabolic activity[153,154]. In contrast, we used a anti-metabolic agent that blocks both metabolic pathways in its early stages, thus ensuring total inhibition of ATP production (Supplementary figures 3-4). Altogether, we suggest the anti-metabolic agents used in our study might have been more appropriately targeted at the metabolic activity of the TM than those used by Bárány.

Anti-metabolic agents	Effects on glycolysis	Effects on cellular respiration	Effects on total resistance
Sodium Cyanide (NaCN)	None	Blocks oxidative phosphorylation by acting on cytochrome oxidase.	None
Sodium Azide (NaN_3)	None	Blocks oxidative phosphorylation by acting on cytochrome oxidase.	None
2-4- Dinitrophenol	None	Blocks oxidative phosphorylation by uncoupling it.	None
Sodium Fluoride (NaF)	Interrupts glycoslysis by inhibiting Enolase, resulting in only 1 ATP produced.	None	None
Sodium Arsenite ($NaAsO_2$)	Does not prevent glycolysis to proceed but inhibits the formation of 2 ATP molecules. Causes the production of 1-arseno-3-phosphoglycerate instead of 1,3 biphosphate glycerate, which hydrolyzes directly into 3-phosphoglycerate without forming ATP.[193]	Inhibits the conversion of pyruvate into acetyl-CoA thus blocking Krebs cycle and oxidative phosphorylation.	None
Iodoacetate	Inhibits GPD, by which time one ATP molecule has been already used[194].	None	Decrease by 40%.

Table 9: Effects of anti-metabolic agents used in Bárány's study[78] on metabolic energy production derived either from glycolysis or cellular respiration

Note that previous studies reported the effects of temperature[77] or anti-metabolic agents [78] on *total outflow facility*, while we reported the effects of anti-metabolic agents on *conventional facility*. These metrics are different because total outflow facility takes into account all of the entire aqueous humour outflow, that is, both in the conventional and unconventional pathways. We focused on conventional facility since we have shown the measurement of unconventional outflow in enucleated mouse eyes is strongly influenced by physical parameters such as hydration and temperature (see Chapter 2). Moreover, we assume conventional facility can be directly related to total outflow facility in human eyes, since the majority of aqueous outflow passes through the conventional pathway in the human eye[39,72]. Therefore the changes in conventional facility that we describe should be comparable to changes in total outflow facility reported in previous reports.

On the other hand, our histological analysis suggests anti-metabolic agents might be affecting the morphology of the conventional pathway. We analyzed a total of 12 quadrants from *N* =3 eyes treated with anti-metabolic agents and *N* =4 control eyes from Cohort 11. We noticed there were more giant vacuoles in eyes perfused with anti-metabolic agents, which extended to the outer wall of SC. In particular, one out of five quadrants showed extensive vacuolization (Fig. 25A). Although our analysis is only qualitative, a possible interpretation could consist in AH being retained by GVs, thus increasing outflow resistance and forcing AH to attempt to enter SC via as many GVs as possible. Since it is assumed AH leaves GVs through intracellular pores, their failure to facilitate AH might stem from the absence of intracellular pores caused by anti-metabolic agents. Note anti-metabolic agents could also affect the tone of the ciliary muscle, or TM cell contractility. A more detailed analysis, using EM, will be required to confirm the effects of anti-metabolic agents on outflow facility are not attributable to damage to the TM or SC. On the other hand, our results show giant vacuoles are passive structures, since they were not inhibited by anti-metabolic agents. This is consistent with previous studies showing GVs form even in low temperature

perfusions[77]. Thus, our findings point towards interesting morphological changes caused by anti-metabolic agents which need to be investigated in further detail.

An additional observation arising from this study was the non-negligible variability in conventional facility measured between cohorts of eyes perfused under apparently similar conditions. In particular, the average conventional facility in eyes perfused at 35 °C with DBG in Cohort 2 was markedly different to that measured in eyes similarly perfused Cohort 11 (e.g. 0.0172±0.0028 vs. 0.0290±0.0068 µL/min.mmHg for eyes perfused at 35 °C with DBG in Cohort 2 and 11 respectively). In order to ensure the effects of anti-metabolic agents and temperature were not an artefact from such variability, we used a linear mixed model to analyse their effects statistically while taking into account such random variability. The results confirmed anti-metabolic agents and temperature had a significant effect regardless of the variability between cohorts. In any case, it prompted us to investigate the possible reasons explaining such variability in conventional facility between cohorts, as described in the following and last chapters of this thesis.

In conclusion, we present data which suggests outflow resistance is metabolic-dependent in mouse eyes, thus possibly overturning existing dogma. Our data shows future perfusion studies should be carried out at physiological temperature to take into account metabolic activity. Finally, this study highlights the benefits of using the mouse as a model for studying outflow resistance, notably because of the short post mortem times associated with obtaining tissue.

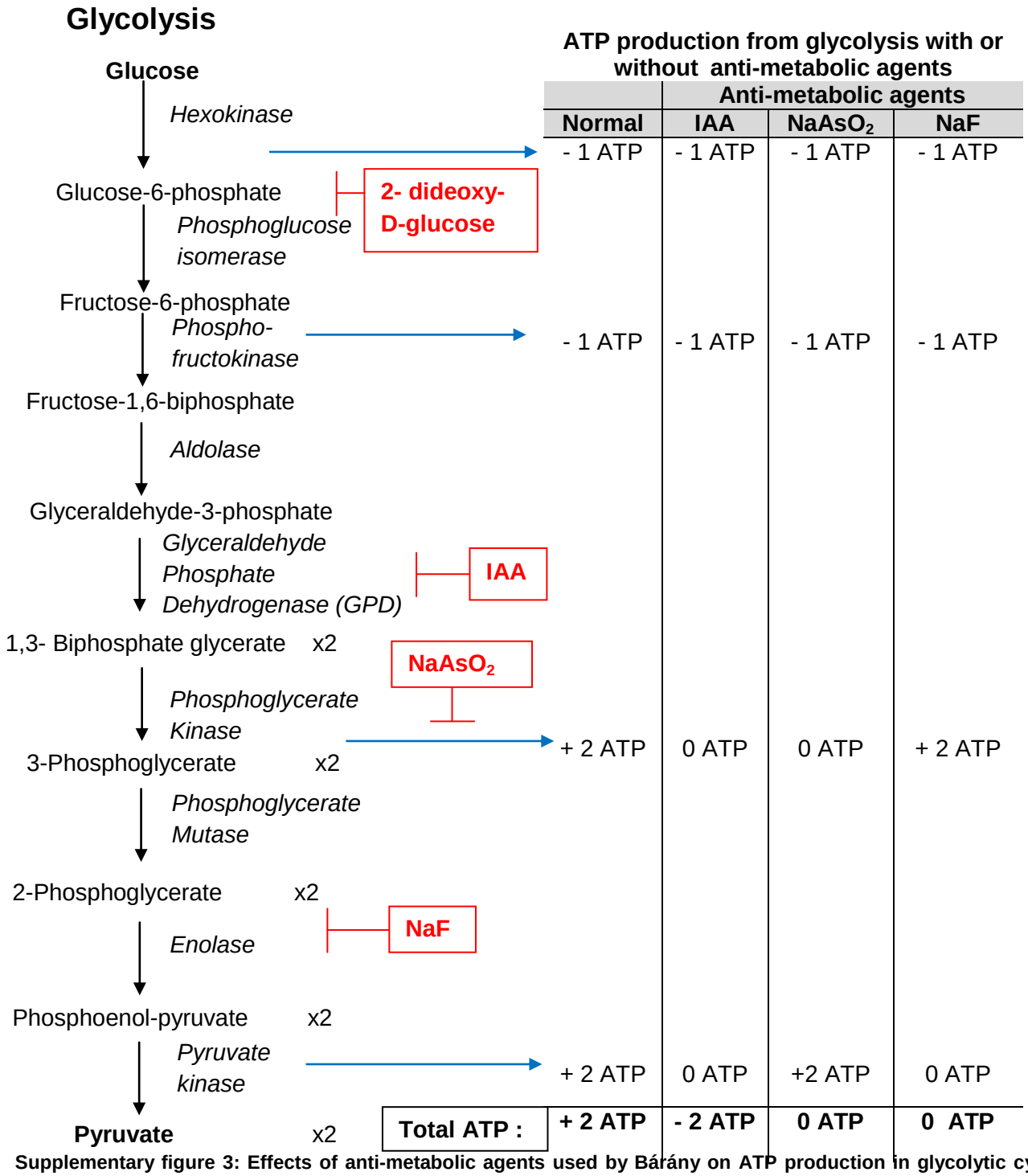

ATP production from glycolysis with or without anti-metabolic agents

	Anti-metabolic agents		
Normal	**IAA**	**$NaAsO_2$**	**NaF**
- 1 ATP	- 1 ATP	- 1 ATP	- 1 ATP
- 1 ATP	- 1 ATP	- 1 ATP	- 1 ATP
+ 2 ATP	0 ATP	0 ATP	+ 2 ATP
+ 2 ATP	0 ATP	+2 ATP	0 ATP
+ 2 ATP	**- 2 ATP**	**0 ATP**	**0 ATP**

Total ATP :

Supplementary figure 3: Effects of anti-metabolic agents used by Bárány on ATP production in glycolytic cycle. On the left hand side, a diagram describes the subsequent products of glycolysis (separated by black arrows), transformed by the enzymes written in italic. Blue arrows show at which stage ATP is normally produced (i.e. + ATP) or used (i.e. – ATP), as indicated by the first column of the table on the right hand side. The remaining columns indicate the amount of ATP produced in presence of either of the anti-glycolytic agent used by Bárány (IAA: Iodoacetate; $NaAsO_2$: Sodium Arsenite; NaF: Sodium Fluoride). Red boxes indicate at which stage of glycolysis the anti-metabolic agents act. x2 indicates the reactions occurs twice.

Normally, a total of 2 molecules of ATP are produced when glucose is transformed into two molecules of pyruvate. IAA inhibits the enzyme GPD, resulting in the final depletion of 2 ATP molecules. $NaAsO_2$ prevents the formation of 2 ATP molecules from the substitution of 1,3-biphosphate glycerate into 3- phosphoglycerate, without preventing glycolysis from proceeding, resulting in 0 ATP produced. NaF inhibits Enolase, resulting in no ATP produced. Therefore, although $NaAsO_2$ and NaF prevent formation of new ATP, they do not deplete the available ATP. In contrast, IAA and our anti-metabolic agent (2-dideoxy-D-glucose) interrupt glycolysis before any ATP has been produced, and after one or two ATP molecules has been used, resulting in ATP depletion.

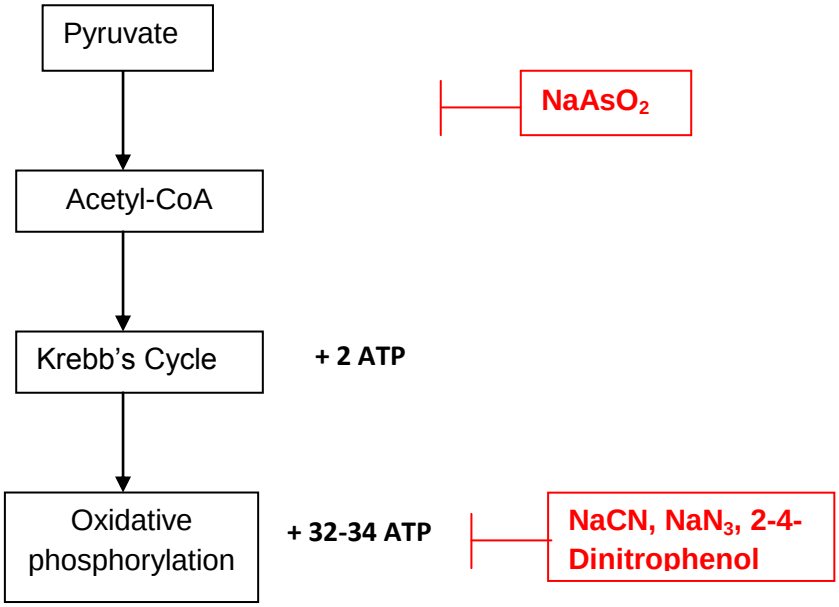

Supplementary figure 4: Effects of anti-metabolic agents used by Bárány on cellular respiration. Pyruvate, produced by glycolysis is first converted in Acetyl-CoA in the mitochondria. Acetyl-CoA is used in the Krebb's cycle to produce 2 molecules of ATP. Subsequently, the oxidative phosphorylation creates 32-34 ATP using a by-product of the Krebb's cycle. The red boxes show where the anti-metabolic agents used by Bárány (and ours, i.e. NaN_3) interrupt cellular respiration. $NaAsO_2$: Sodium Arsenite, NaCN: Sodium cyanide, NaN_3: Sodium Azide.

Chapter 6: Effects of IOP on AH outflow, SC morphology and tracer patterns in enucleated mouse eyes

1- Introduction

In recent studies, conventional facility of enucleated mouse eyes was shown to increase at high pressures [12,13]. Flow-rate vs. IOP data was shown to follow a linear trend line up to 40 mmHg, which represents a constant conventional facility (solid trend line, Fig. 26). Yet, at higher pressures, flow-rates diverged from the linear trend-line, possibly corresponding to an increased conventional facility (red data point, Fig. 26).

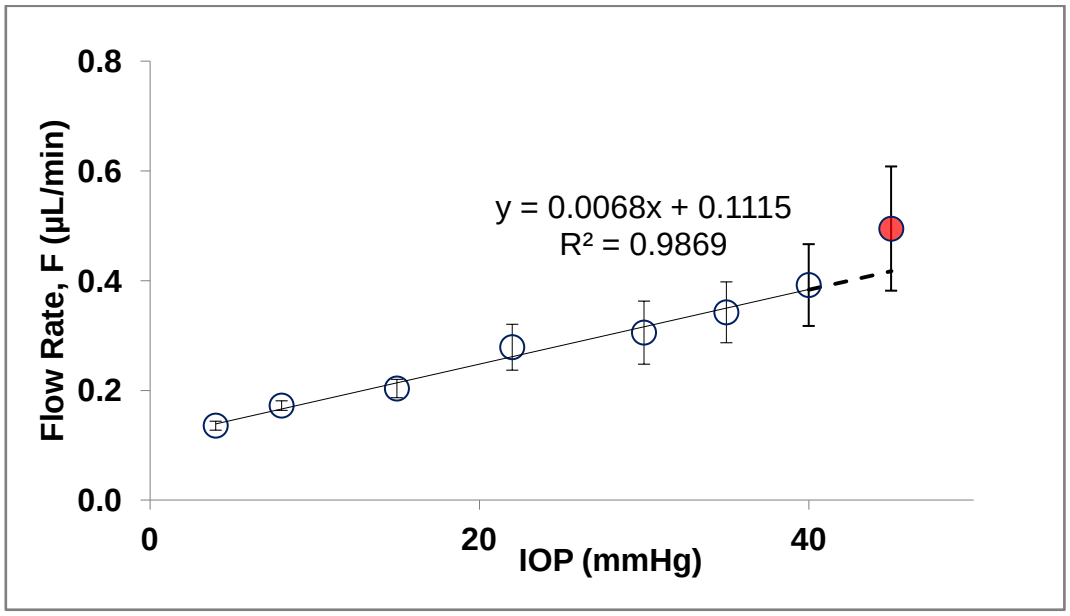

Figure 26: Flow rate vs. IOP data for C57BL/6 enucleated mouse eyes, reproduced from Lei et al. 2010. The solid trend line represents conventional facility from 8 to 40 mmHg, corresponding to 0.0068 µL/min/mmHg. The dashed trend corresponds to the extrapolation of the linear trend line up to 45 mmHg showing that flow rate data at 45 mmHg is not well explained by the linear slope calculated in the pressures ranging from 8 to 40 mmHg. Eyes were perfused at room temperature with the same system described in Chapter 2, Fig. 9A. Bars are standard errors of the means.

Strikingly, this differs from humans and other species which exhibit a *decrease* in conventional facility at high perfusion pressures[76]. This decrease in conventional facility is associated with the collapse of SC[195]. Yet originally, human outflow facility was reported to *increase* at high pressures because of an artefact from the perfusion process[89,195]. More specifically, perfusing fluid directly into the AC pressurized the AC but not the posterior

chamber. This pressure gradient across the iris caused posterior displacement of both the iris and the lens, which applies tension on the TM, thus pulling open SC, resulting in an artificial increase of conventional facility[89,195]. Precautions are commonly taken in human eyes to prevent this effect, called anterior chamber deepening, but never in mouse eyes. Therefore it is possible that mouse eyes suffer from the same artefact, explaining why conventional facility was shown to increase at high pressures in mouse eyes. This needs to be determined for ensuring the viability of the mouse as a model for studying human conventional facility.

In humans or primates eyes where AC deepening is prevented by re-establishing a connection between the posterior and anterior chamber, there is evidence that IOP affects SC morphology. Following iridotomy, Van Buskirk[195] showed SC cross sectional area was significantly decreased at high pressures (20-40 mmHg). On the other hand, studies have shown pressure affects AH outflow patterns in the TM. More specifically, fluorescent tracers were perfused in the eye to reveal outflow patterns. This showed a smaller area of the TM was perfused by tracers, i.e. by flow, at high pressures[102,103]. This prompted us to analyse the effects of IOP on outflow facility, SC morphology and outflow patterns in mouse eyes to investigate whether the effects are similar in mice as in other species. We hypothesize the observed increase in conventional facility in enucleated mouse eyes is caused by AC deepening and correlates with an increase in SC dimensions and a larger TM area perfused by AH.

We performed detailed measurements of AH outflow at increasing pressures in enucleated mouse eyes to confirm that conventional facility increases at high pressures, as suggested by a previous study (Fig. 26[12]). Furthermore, eyes were perfused with fixative at pressures corresponding to high, mid and low outflow facility, and imaged to investigate corresponding changes in the morphology of SC. Specifically, an automated 3D histological device (Histo-Cutter)[196] was used to visualize and reconstruct SC in enucleated mouse eyes. Secondly, fluorescent outflow patterns were visualized in whole mouse eyes by Optical Projection Tomography[197]. Note outflow patterns were not analyzed at different pressures

because we are still in the process of validating this novel protocol. This chapter provides preliminary data acquired with both techniques, which are still the subject of ongoing studies.

2- Methods

All experiments were performed using ex vivo tissue and were done in compliance with the ARVO Statement for the Use of Animals in Ophthalmic and Vision Research the Animal Scientific Procedures Act 1986.

This study includes three cohorts of mice, which are the twelfth, thirteenth and fourteenth cohorts of mice used for this thesis. The first cohort (Cohort 12) was used to investigate changes of AH outflow at increasing pressures. In a second cohort (Cohort 13), we analyzed changes in SC size at different pressures. The last cohort (Cohort 14) was used for analyzing tracer patterns in whole mouse eyes in 3D. In this section, we describe the experimental design for each cohort.

2.1. AH outflow measurements at increasing pressures

In Cohort 12, we measured AH outflow at increasing pressures to identify the pressure levels at which conventional facility started increasing. The aim was to select three pressure levels corresponding to low, mid and high outflow facility which might be associated with morphological changes. A previous study had shown AH outflow increased at pressures above 40 mmHg in enucleated mouse eyes (Fig. 26[12]). We replicated the study using the improved perfusion system described in Ch.2 (see section 2.1; Fig. 9C), with hydration and temperature control. Briefly, a computer-controlled syringe-pump delivered a variable flow rate to the enucleated mouse eye required to maintain the eye at a user-defined pressure. Conventional facility was calculated as the slope of the best-fit linear trend line to our flow rate vs. pressure data (see Eq. 8 and Fig. 9). Our study used numerous pressure steps to more precisely detect changes in outflow resistance. Specifically, flow measurements were performed every 3-4 mmHg, from 8 to 40 mmHg (8,12,15,18,22,25,28,31,34,47,40 mmHg; Fig. 27). 4 unpaired eyes from C57BL/6 mice were used for this study.

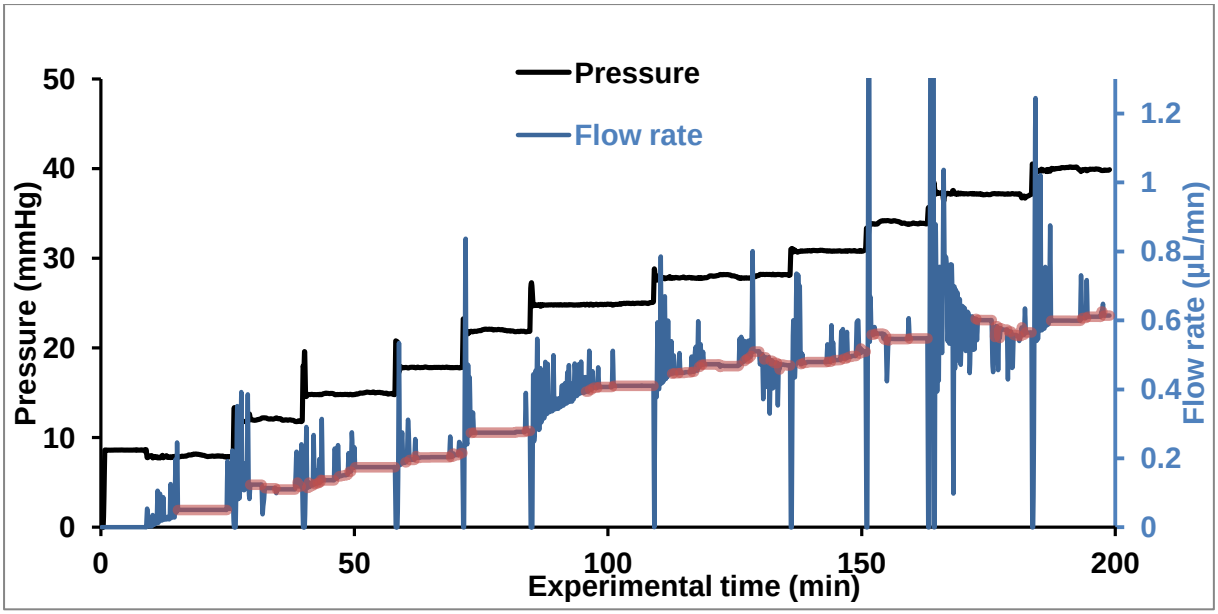

Figure 27: Typical perfusion tracing for experiments performed on mouse eyes from Cohort 12. Pressure is shown in black while flow rate is shown in blue. The red highlights show the regions deemed steady at each pressure level and averaged for the measurement of conventional facility (see Figure 9). In this cohort, we perfused eyes up to 40 mmHg at many more pressure levels than previous cohorts, resulting in longer experiments (200 min vs. approximately 120 for previous cohorts).

2.2. SC imaging at different pressures with the Histo-Cutter

Mouse eyes from Cohort 13 were used for imaging SC in 3D with the Histo-cutter[196]. In particular, we hypothesized changes in AH outflow would be associated with structural changes in SC. Thus, eyes perfusion-fixed at 3 different pressures were imaged to reveal changes in SC dimensions. The pressure levels were chosen according to the results from Cohort 12, as those associated with high, mid and low outflow resistance (or, respectively, 8, 25 and 40 mmHg). Below we describe the functioning of the Histo-Cutter as well as the preparation and imaging of the sample, and the processing of the results.

2.2.1. Perfusion fixation of mouse eyes at different pressures

Eyes were enucleated and placed in PBS at 4 °C until perfusion. Eyes were perfused with the perfusion system previously described (Chapter 2, section 2.1). Briefly, eyes were cannulated with a 33G needle connected to a pressure transducer and a computer controlled syringe pump. The syringe pump delivered variable flow rates required to maintain the pressure inside the eye steady at any user-defined level, thanks to custom LabView software[151]. The eye was perfused at a single pressure level. Eyes were briefly pressurized with a PBS-filled reservoir for than less than a minute prior to the perfusion with the pump.

Eyes were perfused at 35 °C, immersed in isotonic saline as described in Fig. 9C of Chapter 2.

In order to prevent fixation before the eye equilibrates at the desired pressure, the eye was first perfused with a 5 µL bolus of DBG (PBS with 5.5 mM glucose) followed by a bolus of 4% PFA, which allowed the measurement of AH outflow prior to PFA entering the eye. This was done by backfilling 5 µL of DBG from the tip of needle into the tubing filled with 4% PFA. As the fixative is delivered to the outflow pathway it will cross-link the tissue, thus decreasing the flow rates required to maintain the same pressure. Accordingly, the eye was considered fixed when the flow rates required to maintain the eye pressurized had decreased by 40% from the baseline level (Fig. 28). A total of 3 eyes were examined, one eye per pressure level, two of which were paired.

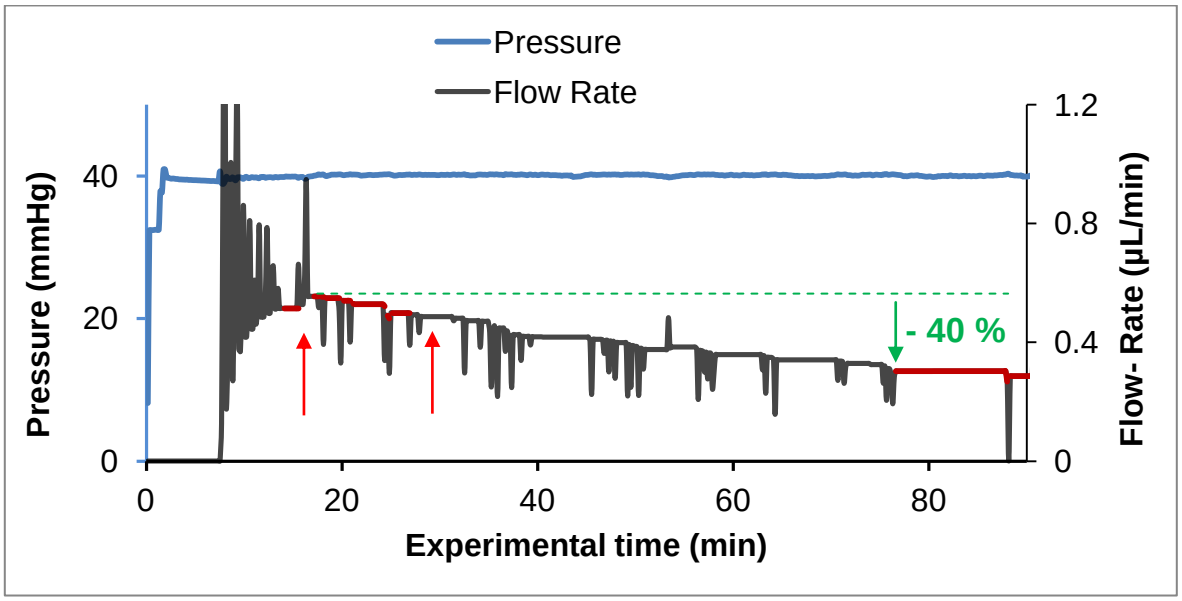

Figure 28: Typical tracing for perfusion-fixation of a mouse eye. The eye was pressurized at a single pressure level (blue tracing) which was maintained steady by the flow rate injected by the syringe pump (black tracing). Red highlights show the steady regions considered to represent the baseline and final flow rate prior to and following fixation. Steady highlighted flow rates were averaged and used as an indication of the drop in flow rate caused by fixation, estimated as 40%. The first red arrow indicates the time by which the 5 µL of DBG had been perfused, and PFA started entering the eye. The second arrow indicates the time point at which 6 µL of PFA had been perfused into the eye, such that the entire AC was filled only with PFA. If no PFA had been perfused, we expect the flow rate to remain steady and not decrease.

2.2.2. Histo-cutter

The Histo-cutter is a 3D histological device that performs automated serial sectioning to image the morphology of tissues embedded within a paraffin block[196]. It relies on fluorescence imaging, and captures the autofluorescence of the tissue typically provided by

chemical groups such as flavins, found in a wide range of tissues[198]. The Histo-cutter automatically images the surface of a block containing a tissue sample as it is progressively sectioned. It is composed of an epifluorescent microscope (Nikon AZ100; Nikon AZ Plan Apo x4 lens, Numerical Aperture 0.4), a mercury lamp, a microtome and a camera (Fig. 29). The sample embedded within the block is sectioned serially by the microtome. Each freshly cut surface is excited at a specific wavelength and imaged through the microscope by the camera. The microscope contains multiple filters such that the same section can be excited and imaged sequentially at different wavelengths.

Importantly, the paraffin block needed to be stained to limit the depth of penetration of the excitation light. This prevents the tissue underneath the surface of the block from being excited, which would otherwise also emit fluorescence. Therefore, a stain is mixed with the paraffin so as to absorb the incoming light and avoid this out-of-focus fluorescence (see following section).

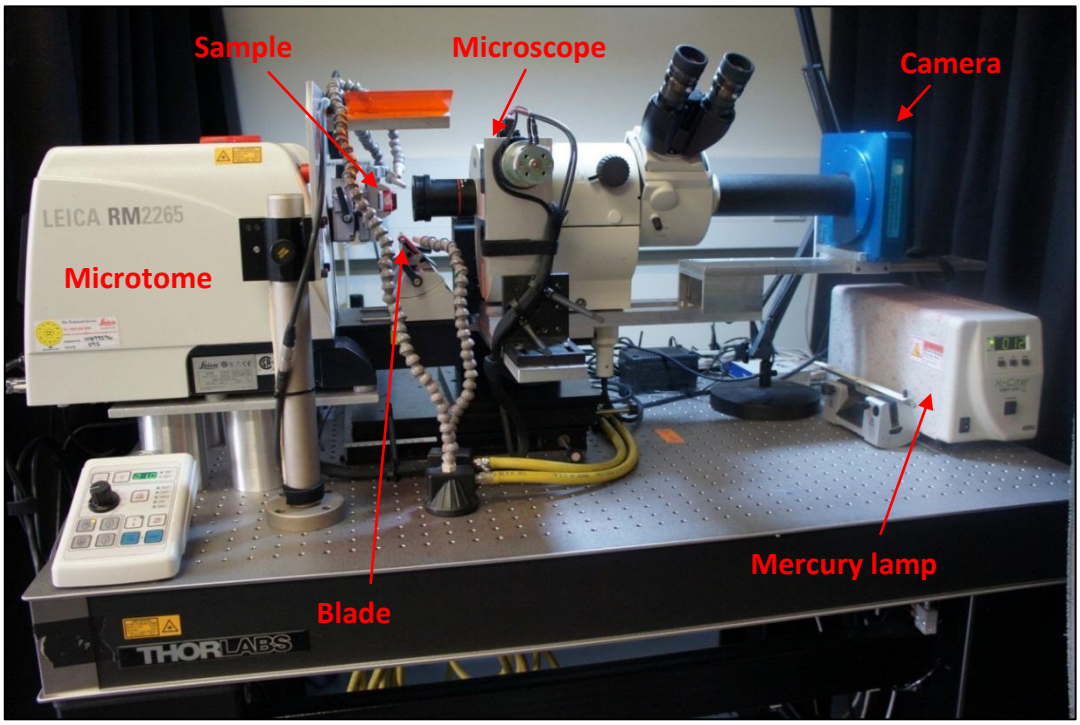

Figure 29: Picture of the Histo-Cutter and its different components, labelled in red. For every section, the sample is automatically lowered towards the blade by the microtome, and brought back up in front of the objective. The mercury lamp is used to excite the tissue at the freshly-cut surface at a specific wavelength, defined by the microscope filters. The image is taken by the camera and recorded on a computer.

The user is required to place the paraffin-embedded tissue onto the sample holder and optimize the focus and brightness of a reference image. The device is thereafter responsible for automatically sectioning the block surface, imaging the freshly cut surface and recording the images. The subsequent images are automatically aligned by the software using a laser position sensor. Images of the freshly cut surface were recorded by a camera resulting in a stack of high-resolution 2-D JPEG images (4096x4096 pixels). The stack of images was then processed with specialized software to yield 3D reconstructions of the tissue.

Sections were cut from the block surface at 1 µm steps. A zoom was chosen such that 1.72 mm x 1.72 mm of the block surface could be imaged, with a digital resolution (i.e. a pixel size) of 420 nm. The theoretical resolution based on light diffraction was 760 nm. Lower zooms captured a larger field of view such that a larger fraction of the eye was imaged but with a decreased resolution, which might have failed to capture small structures of interest such as collector channels. At each zoom, the device was calibrated with a micrometer stage (NT30-592, Edmund Optics, Nether Poppleton, UK).

2.2.3. Tissue autofluorescence

To determine the optimal excitation and emission wavelengths to be used by the Histo-cutter, we first characterized the spectrum of excitation and emission from the tissues comprising the conventional outflow pathway.

A lambda-scan was used to measure the intensity of the fluorescence emitted by the irido-corneal angle after being excited by different lasers (data not shown, studies performed with Tali Ziskind[199]). These studies showed excitation lasers of 561 or 633 nm yielded the autofluorescence with the highest intensities, which was found in the wavelengths ranging from 590 to 680 nm. Therefore, we determined the Texas Red filter had the most optimal wavelengths for excitation/emission, which are 540-580nm for excitation and 600-660 nm for emission.

2.2.4. Tissue embedding

First, eyes had to be embedded in paraffin so as to be able to undergo sectioning. Two MSc students (Ms. Tali Ziskind and Miss Oana Elena) validated a protocol for infiltrating the

eye with paraffin[199,200]. Briefly, the eye was dehydrated in increasing concentrations of ethanol (50, 70, 90 and 100%), prior to several clearing steps with Xylene and infiltration with different solutions containing paraffin at 75 °C. The last step of the embedding protocol consisted of placing the sample in the desired orientation on a thin layer of melted paraffin in the mould. Once the paraffin had solidified, it held the sample in position prior to pouring the remainder of the paraffin to fill the mould entirely.

Importantly, the paraffin had to be stained with a dye to absorb light emitted by deeper layers of the tissue and minimize the depth of penetration of the excitation light into the paraffin block. The optimal stain should absorb both the light exciting the surface of the block and that emitted by the block, which were determined to be 540-580 nm and 600-660 nm, respectively (see previous section, 2.2.3). Thus we searched for a dye which could absorb light in both ranges of wave lengths. Preliminary studies using a spectrophotometer investigated the viability of different dyes such as Sudan II and Sudan IV (Fig. 30). Our results show both Sudan IV and II absorb light within the excitatory light range (540-580 nm), although Sudan IV seems to have higher absorbance rates. However, Sudan IV does not seem to absorb light within the wavelengths where fluorescent light is emitted, between 600-660 nm, whereas Sudan II does.

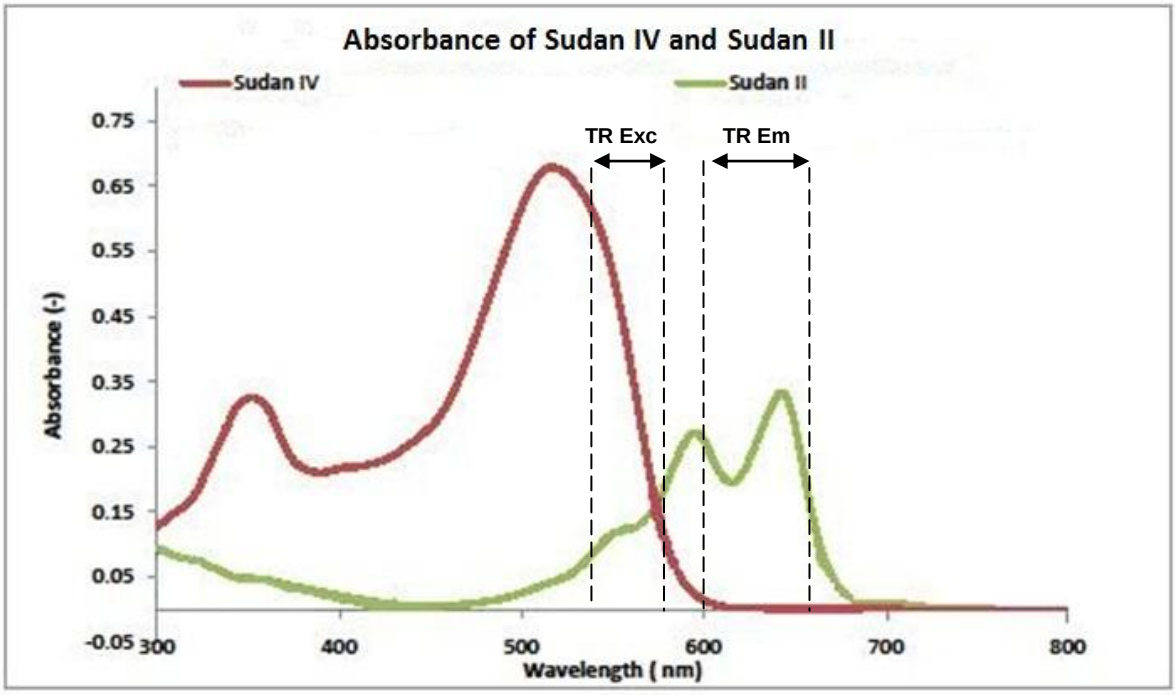

Figure 30: Absorbance spectra of Sudan II (green line) and IV (red line) dyes, measured by a spectrophotometer. Dashed lines represent the wavelengths range of the Texas Red filter excitation (TR Exc) and emission (TR Em) which were found to coincide with the tissue autofluroescence. Sudan IV and II absorb light within the wavelength range of the excitatory light but Sudan IV does not absorb the emitted fluorescence, while Sudan II does. Experiments were done with Barbara Murienne.

Thus we proposed Sudan II might be more efficient at blocking the out-of-focus fluorescent light emitted from the deeper layers of the block. This was further confirmed by Ms. Tali Ziskind and Miss Oana Elena, who showed 4% Sudan II provided the optimal contrast between the SC lumen and the surrounding tissue (Fig. 31).

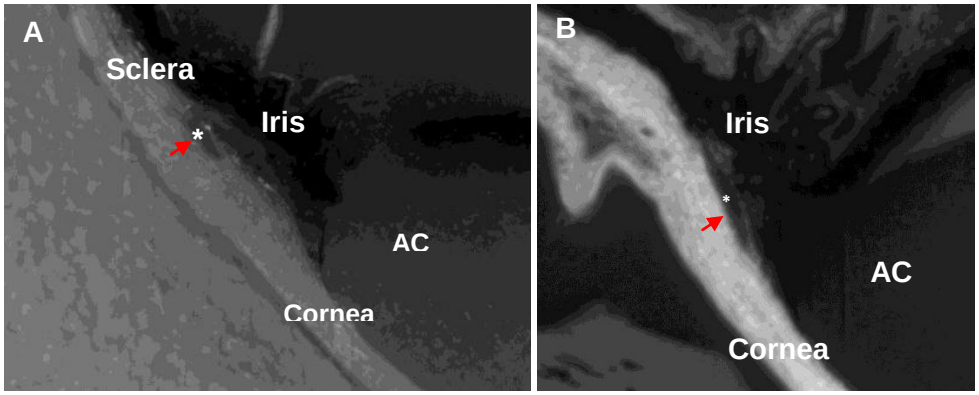

Figure 31: Section of a mouse eye embedded in paraffin stained with Sudan IV 0.5% (A) or Sudan II 0.5% (B). Asterisk shows SC location. Red arrows points to SC outer wall. Other concentrations of dyes were used, but these two are shown to illustrate the difference in contrast between the SC lumen and its surroundings caused by the use of different dyes. SC lumen is hardly detectable with Sudan IV 0.5% (A). In contrast, the cornea contrasts with the dark lumen of SC when using Sudan II 0.5% (B).

The use of the dye introduced an important issue for the tissue embedding: it rendered the tissues opaque, such that they were not visible at the moment of embedding the eye in the wax. This was problematic because the eye needed to be placed in a specific orientation in the paraffin block, so that it was sectioned in the sagittal plane to reveal the cross-section of SC. In order to know the orientation of the eye, the eye was placed in a transparent solution of agarose (Fisher BioReagents, 1.8% agarose in filtered H_20) prior to the start of the embedding protocol. More specifically, the gel was given a particular shape, which was used as an indication of the eye orientation during the embedding protocol, even when the gel became opaque. Typically, the gel was cut such that its largest flat surface was parallel to the sagittal plane of the eye (Fig. 32). The flat surface was easily recognizable at the last stage of embedding, in spite of the gel being opaque. This allowed simply laying the gel on its flat surface in the mould at the last stage of embedding, such that its sagittal plane was parallel to the surface of the block. Thus, when the block was trimmed by the microtome, it would reveal the sagittal plane or the eye, and thus the cross section of SC (Fig. 31B)

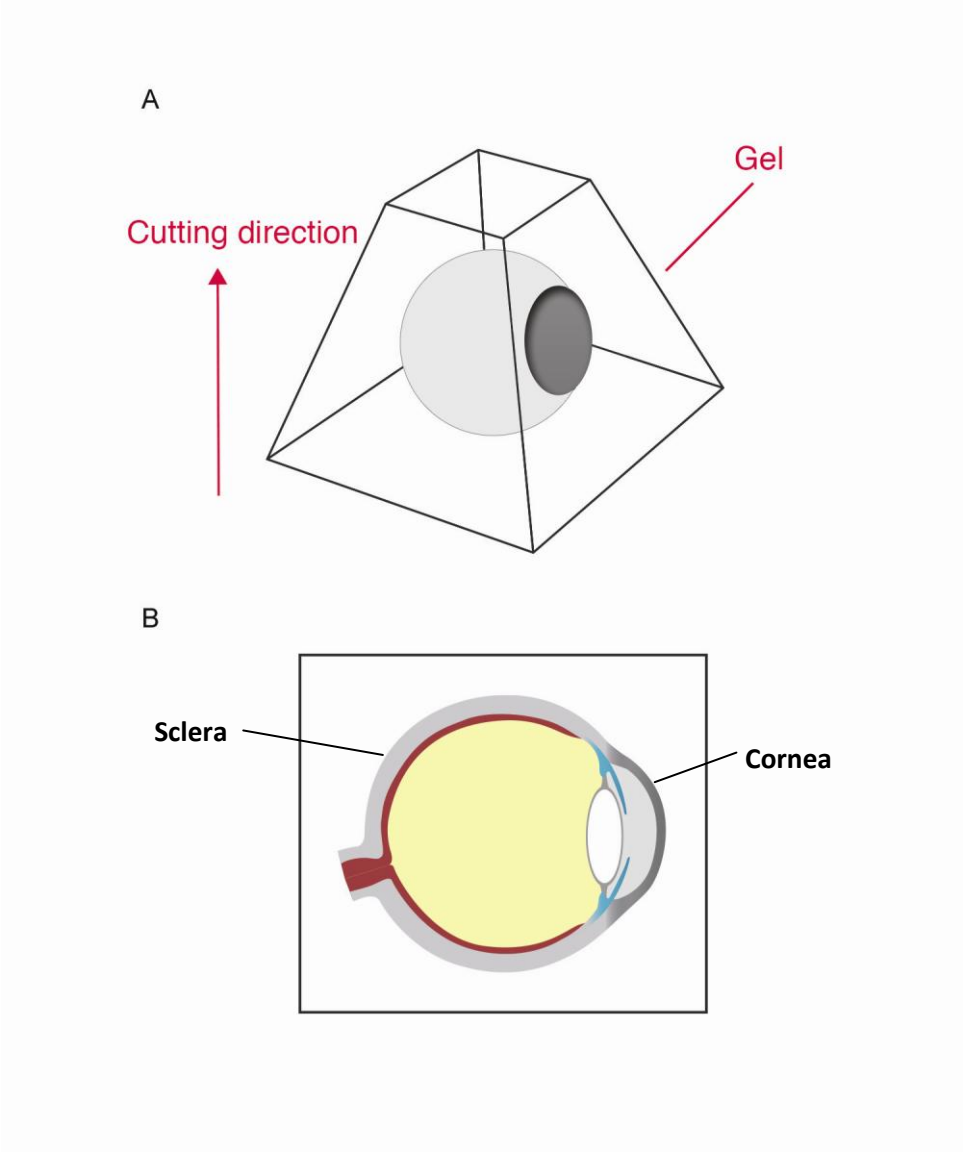

Figure 32: : Schematic diagram of the positioning of the mouse eye in the gel prior to embedding protocol (A), which will be cut such that the cross section drawn in (B) is revealed.

2.2.4. Histo-cutter validation

At first, we aimed to ensure the images acquired with the Histo-cutter compared well with results from conventional histology. Images from the Histo-cutter were compared to images from eyes perfused with DBG that had been prepared by conventional histology in a previous study (Cohort 6, Chapter 3). For conventional histology, eyes were embedded in paraffin, sectioned and stained with hematoxylin and eosin. The sections were imaged under a light microscope. The anterior-posterior length (A-P length) of the SC (see following section, 2.2.5) was measured manually with ImageJ by Tali Ziskind[199] on random sections from one eye provided by conventional histology (*N* =10) and the Histo-cutter (*N* =10).

Images acquired with the Histo-cutter revealed a general limbal architecture similar to that seen by classical histology (Fig. 33). Yet, the images provided different information because the Histo-cutter uses fluorescence, while conventional histology relies on light transmission, and uses stains. Therefore, cell nuclei are visible on the images from conventional histology but not from the Histo-cutter. In any case, the A-P length of SC imaged with the Histo-cutter was similar to that measured from conventional histology sections (129.52 ± 28.66 µm vs. 107.14 ± 34.60 µm, respectively; mean±stdev). The difference was not statistically significant (p = 0.14; unpaired t-test).

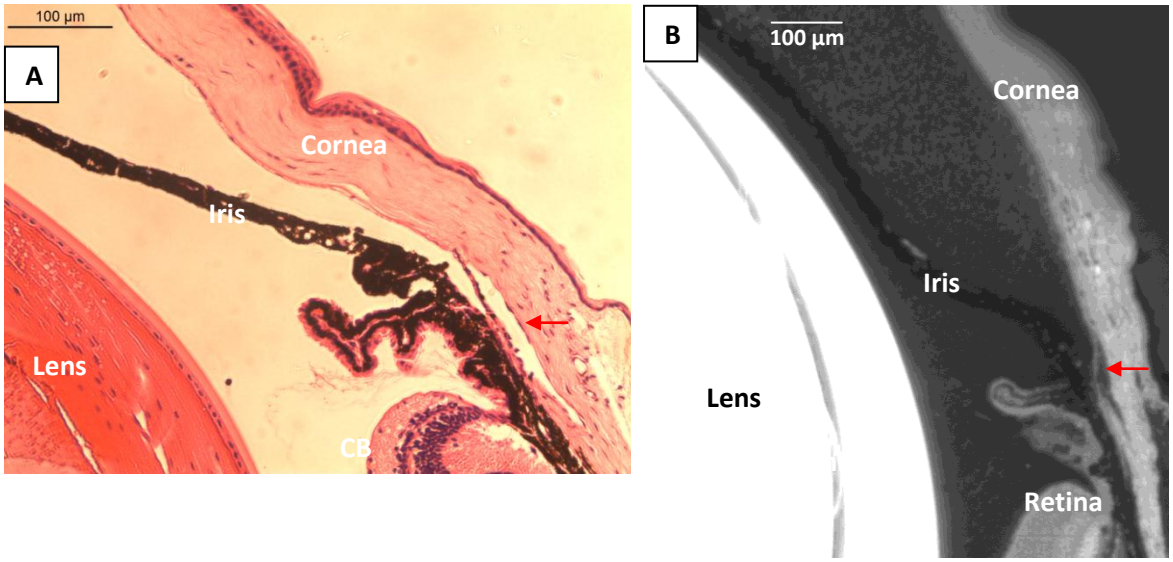

Figure 33: Mouse anterior segment cross section from A) Conventional histology, B) the Histo-cutter. The image acquired with the histo-cutter reveals a limbal organization similar to that shown by classical histology. Legend: CB: Ciliary Body. Red arrows point to SC.

2.2.5. SC or collector channels segmentation

The SC was identified based on the contrast difference between its lumen and the surrounding tissue (i.e. sclera and TM). It was typically composed of one large oval-shaped lumen found at the irido-corneal angle (Fig. 34B). We defined the anterior-posterior length of the SC as the distance from the extremity closest to the cornea to that found most posteriorly in the sclera (Fig. 34B). The SC width was defined as the largest distance between the edge of the SC in contact with the sclera and that in contact with the TM (Fig. 34C). Collector channels were defined as smaller vessels found in the deeper aspects of the sclera. In

addition, they had to depart from SC at some point along their length. This ensured that they were not confused with other intrascleral vessels such as arteries.

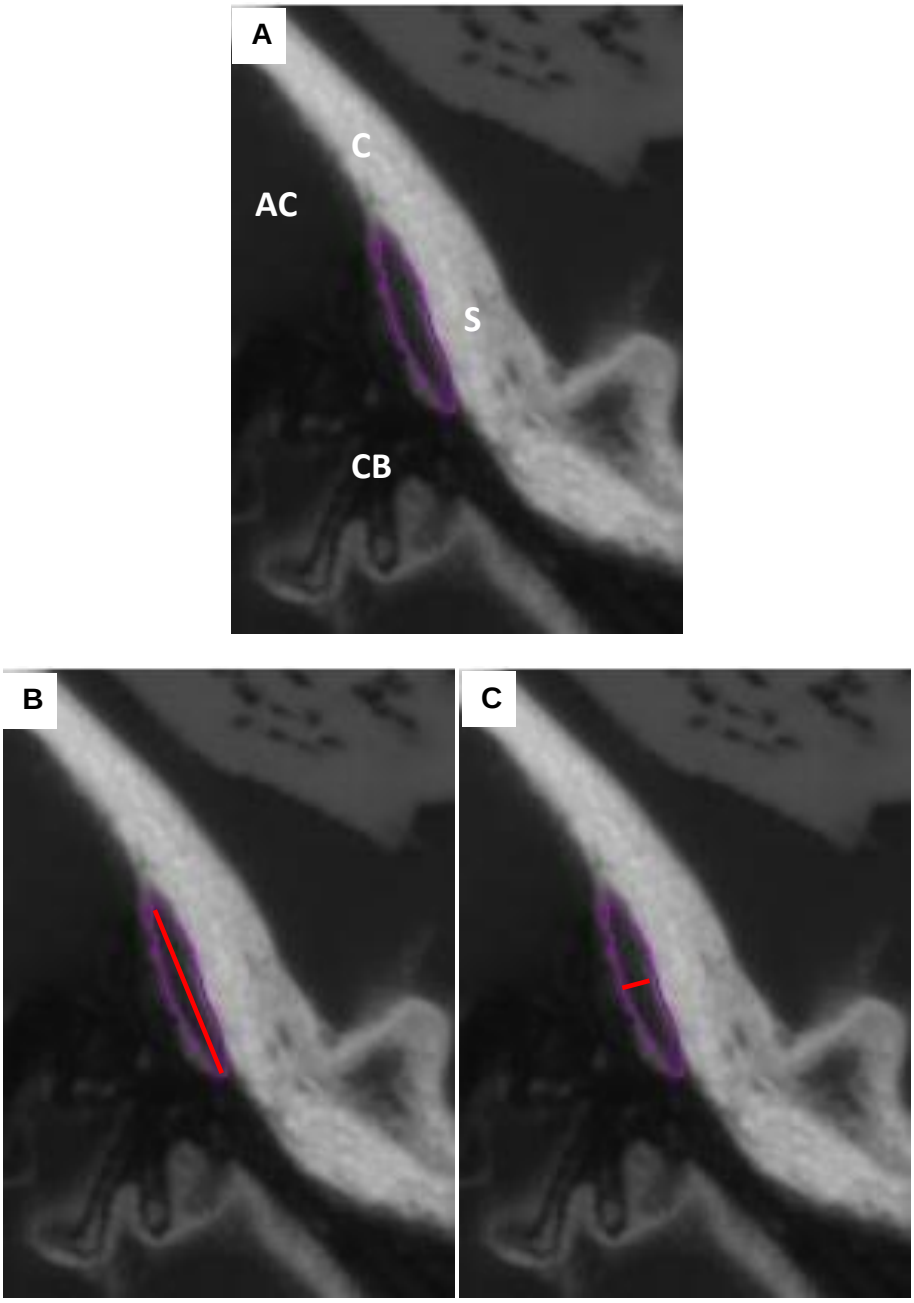

Figure 34: SC segmentation and measurements. A) SC segmented in purple. B) Red line shows A-P length. C) Red line shows SC width. Note measurements were done on the reconstructed 3D representation of SC, rather than the 2D images. Legend: C=Cornea, AC=Anterior Chamber, S= Sclera, CB= Ciliary body.

2.2.8. SC reconstruction

Following the acquisition of stacks of 2D images by the Histo-cutter for each sample, software was used to segment and reconstruct SC in 3D (AMIRA, VSG, Burlington, MA, USA). SC was segmented in a semi-automatic fashion by Ms. Tali Ziskind[199]. First, this

consisted of manually drawing an SC contour with an electronic pen every 5-10 slices. For the remaining sections, the software interpolated SC contours. The sections where SC was interpolated by the software were verified at least twice by the user and modified manually when necessary. A surface was generated by the software along the whole length of SC based on the contours drawn at each section (Fig. 35).

Raw images were imported as stacks and downsized to 1024x1024 pixels from their original size which was 4096x4096 pixels. This caused a 4 fold reduction in the pixel size and thus in resolution. Voxel size was therefore 1.6 μm x 1.6 μm x 1 μm in the x,y,z directions, respectively.

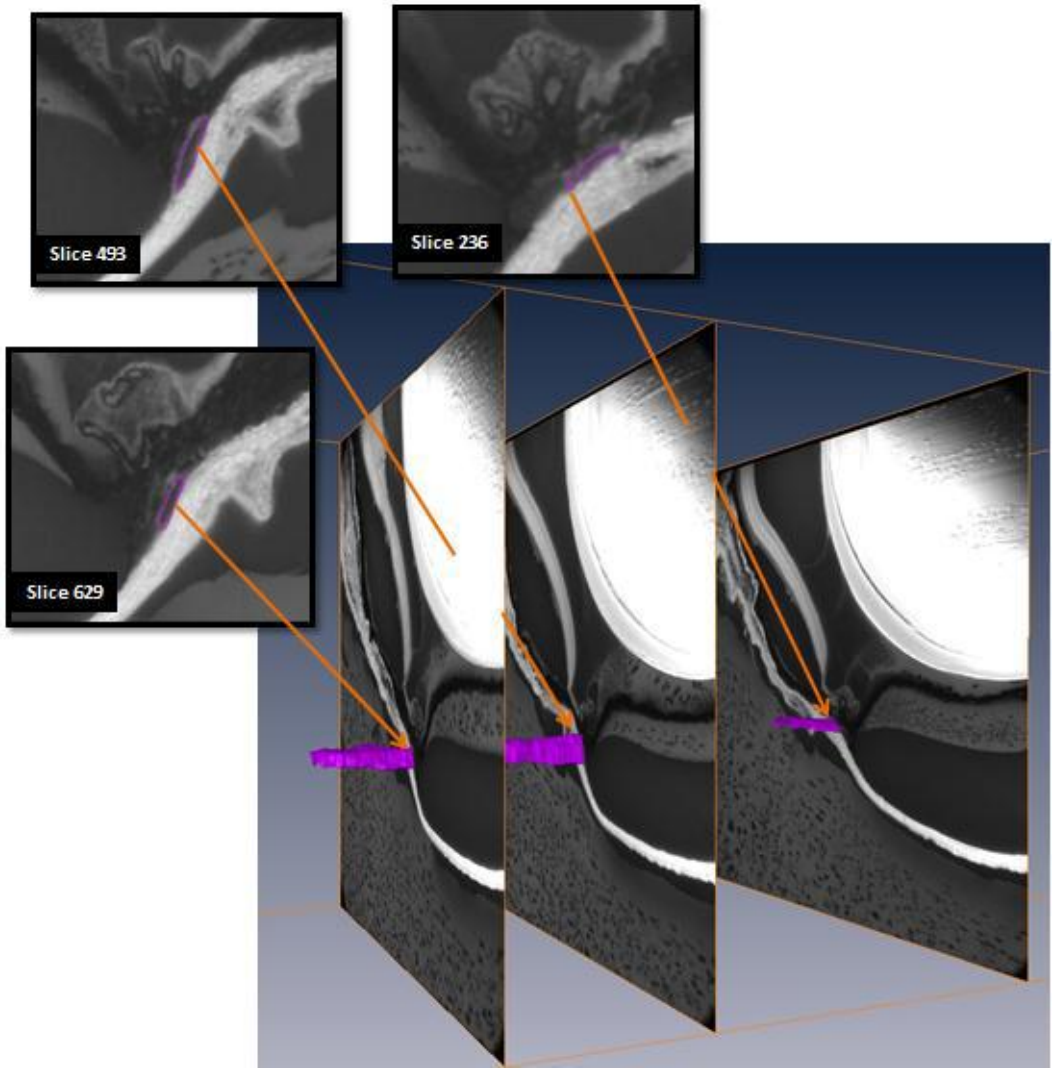

Figure 35: Illustration of SC reconstruction process. SC is manually segmented every 5-10 sections, and automatically segmented in the remaining sections. Amira generates a 3D surface based on the SC segmentations performed in each section, shown in pink. Image taken from MSc dissertation of Miss Tali Ziskind.

2.3. Visualizing outflow patterns across the entire mouse eye: OPT

2.3.1. OPT

Optical Projection Tomography (OPT) is a technique recently developed by Dr. Sharpe et al. to image biological samples in 3D for specimens of size 0.5-10 mm[197]. I was given the opportunity to use the machine in Dr. Sharpe's laboratory in Spain via the Euro-Bioimaging Proof of Concept studies, and later thanks to funding from the Santander Bank. The OPT gives anatomical information about biological samples by mapping the sample's absorption of light. Importantly, the sample had to be optically clarified to maximize light transmission. This allowed taking images through the whole specimen. More specifically, the sample was rotated through 360 degrees in angular steps, such that 400 pictures are taken over one revolution. Projection images taken from each angle are then processed with specialized software to reconstruct the original 3D structure[201].

2.3.2. Tissue preparation

In this study, we used BALB/cJ eyes which lack pigmentation, which facilitates light transmission during the scan. As a preliminary study, eyes were perfused at 8 mmHg with a bolus of 3 μL of 20 nM of quantum dots (Qdots, Q25001MP, Invitrogen, Life Technologies, Carlsbad, CA, USA). Qdots are fluorescent nanocrystals, and the ones that we used were chemically tagged such that they are internalized by cells. Thus, we assumed they represented outflow patterns by entering cells which line the pathways of aqueous humour outflow channels, as in previous studies[202].

Following perfusion, eyes were immersed in fixative. However, they were only placed in 4% paraformaldehyde (PFA) for 20 min as we observed 4% PFA can quench quantum dot fluorescence. Eyes were further immersed in 0.1% PFA for long term storage. Eyes were embedded in an agarose gel to provide mechanical support during scanning. More specifically, the gel containing the eye was glued onto a post which allowed rotating the eye. The gel was filtered to get rid of particles which could refract light during the OPT scan. The gels were then dehydrated with methanol, which was changed three times within 24 hrs. The gels were placed in BABB (2:1 mix of Benzyl Alcohol and Benzyl Benzoate). Because it was

observed BABB quenched the fluorescence of Qdots, we left the samples in BABB as little as possible, typically 1-2 hrs prior to scanning. *N* =2 eyes were successfully imaged for this preliminary study.

2.3.3. OPT scan

Eyes were bathed in BABB during the scan. The filter used for detecting the quantum dots signal (Exc/Em: 405-565/605 nm) was Cy3, with Exc/Em: 530-560/573-637 nm. Autofluorescence was captured with the GFP1, (Exc/Em: 425/475; band pass filter), to provide morphological information about the tissue. 400 images were taken through 360 degrees (0.9° angular steps). Two consecutive scans were performed, each with a separate filter. At each position, the gel was exposed for 0.5-1 sec to the excitation light. Data was reconstructed by Jim Swoger and Laura Quintana Rio in Dr. Sharpe's laboratory with a customized MatLab program.

3- Results

3.1. Cohort 12, AH Outflow changes with pressure

Our flow rate vs. pressure data did not reveal a linear relationship across the pressures ranging from 8 to 40 mmHg (Fig. 36). This was because there was a "break" or transition in the flow vs. pressure data. This transition seemed to occur at 22-25 mmHg, as suggested by the two trend lines drawn below and above 22 mmHg which show very different slopes (0.013±0.005 vs. 0.026±0.014 µL/min.mmHg; *N* =4 eyes). Note however, the difference in conventional facility below and above 22 mmHg was not statistically significant (*p* =0.21; paired t-test). We therefore chose 8, 25 and 40 mmHg as pressure levels corresponding to different outflow facility regimens. 8 and 40 mmHg correspond to the low and high conventional facilities, while 25 mmHg is found at the transition.

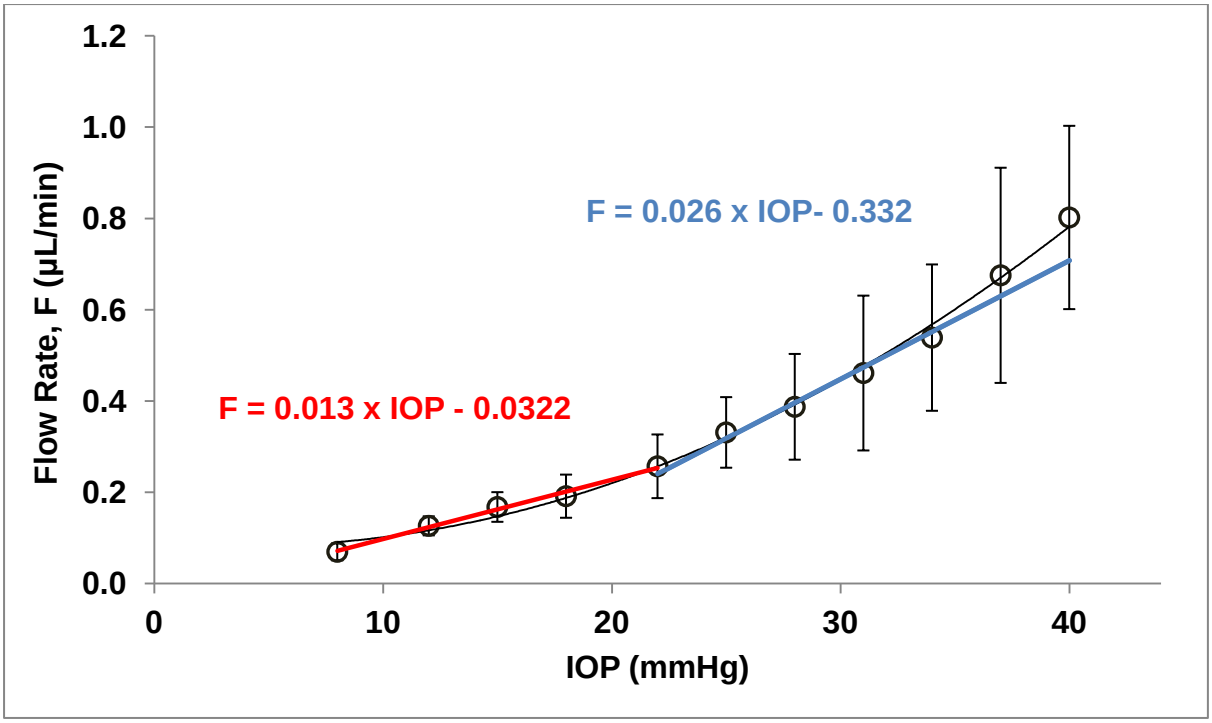

Figure 36: Flow rates measured at pressure steps from 8 to 40 mmHg. The trend line and equation in red correspond to outflow facility across the low range of pressures from 8 to 22 mmHg, whereas the equation and trend line in blue represent outflow facility within the higher pressure range, from 22 to 40 mmHg.

3.2. Cohort 13, SC dimensions change at increasing pressures

3.2.1. SC reconstruction and measurements

SCs from 3 samples, one per pressure level (8, 25 and 40 mmHg), were successfully imaged with the Histo-Cutter, reconstructed and quantified with AMIRA (see Methods and Fig 35). On average, SC was reconstructed for a length of 1062±195 µm (*N*= 3), which represents approximately 11% of the entire circumference (assuming the eye diameter is 3 mm and SC is located at its equator). Fig. 37 shows that SC dimensions vary along its circumference; interestingly, it shows regions where SC is not reconstructed because it was not detected on the 2D images. This could be either because its lumen was collapsed or not detectable in the section. In the eye pressurized at 8 mmHg, SC was not detected in 17.5% of its reconstructed length, as opposed to 5.5% at 25 mmHg and no collapsed regions at 40 mmHg.

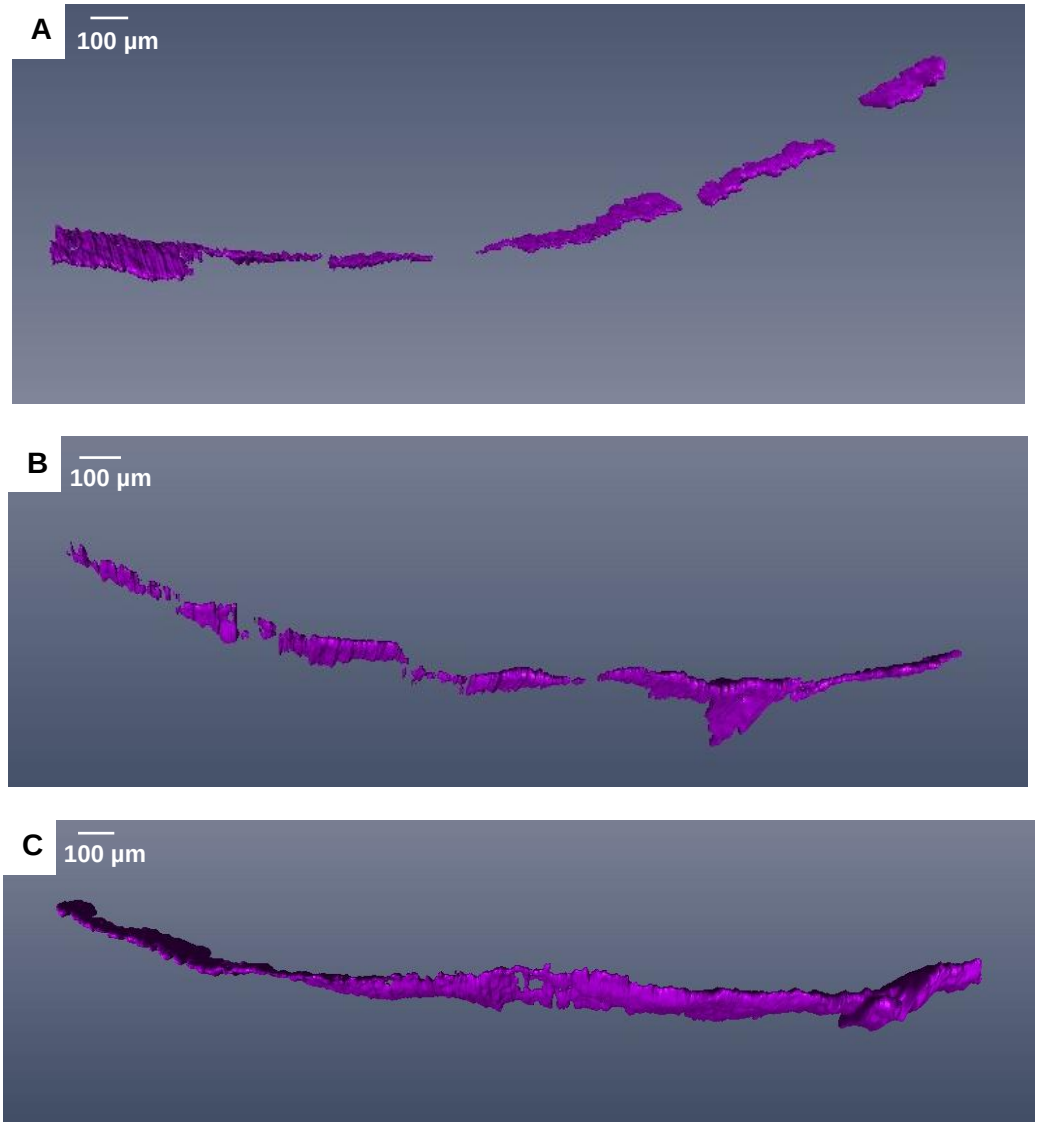

Figure 37: SC reconstructed at: A) 8 mmHg, B) 25 mmHg, C) 40 mmHg. Gaps correspond to regions where the SC lumen was not seen, i.e. it was either collapsed or nonexistent.

3.2.2. AC deepening in the mouse

In order to investigate whether AC deepening occurs in mouse eye perfusions, we analyzed several 2D images from each sample. In particular, we looked at the posterior displacement of the iris at different pressures. Fig. 38 shows a typical example of the general morphology of eyes perfused at 8, 25 and 40 mmHg. The dashed white line represents the iris, which is difficult to distinguish from the opaque background. The images show the iris is dramatically displaced backwards from 8 to 25 or 40 mmHg. This results in the increase of the irido-corneal angle (depicted in blue), which can force the TM and SC to open at higher pressures.

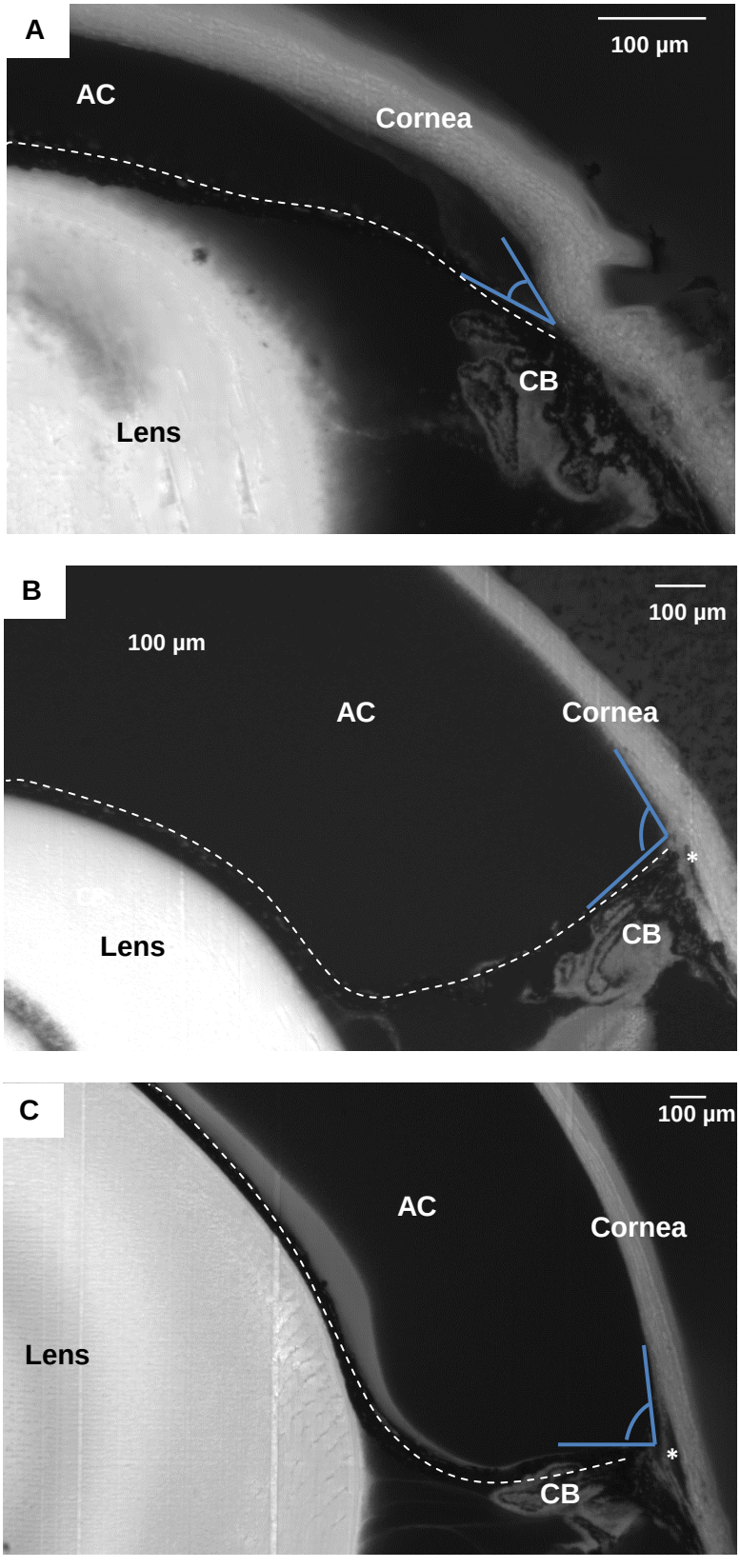

Figure 38: Iris retrograde movement with increasing pressures. 2D images taken with the Histo-cutter of eyes pressurized at A) 8, B) 25, C) 40 mmHg. The white dashed line outlines the iris contour, which forms a larger angle (represented by blue lines) with the cornea at higher pressures (25, 40 mmHg) than at 8 mmHg. Asterisks show the location of SC. Note SC is not visible in Panel A.

3.2.3. Collector channels

Collector channels were also detected, although not often (Fig. 39A-B). Only one CC was reconstructed from a preliminary study (green structure, Fig. 39C).However, CCs seemed to quickly disappear into the sclera, either because they collapsed or became too small to resolve.

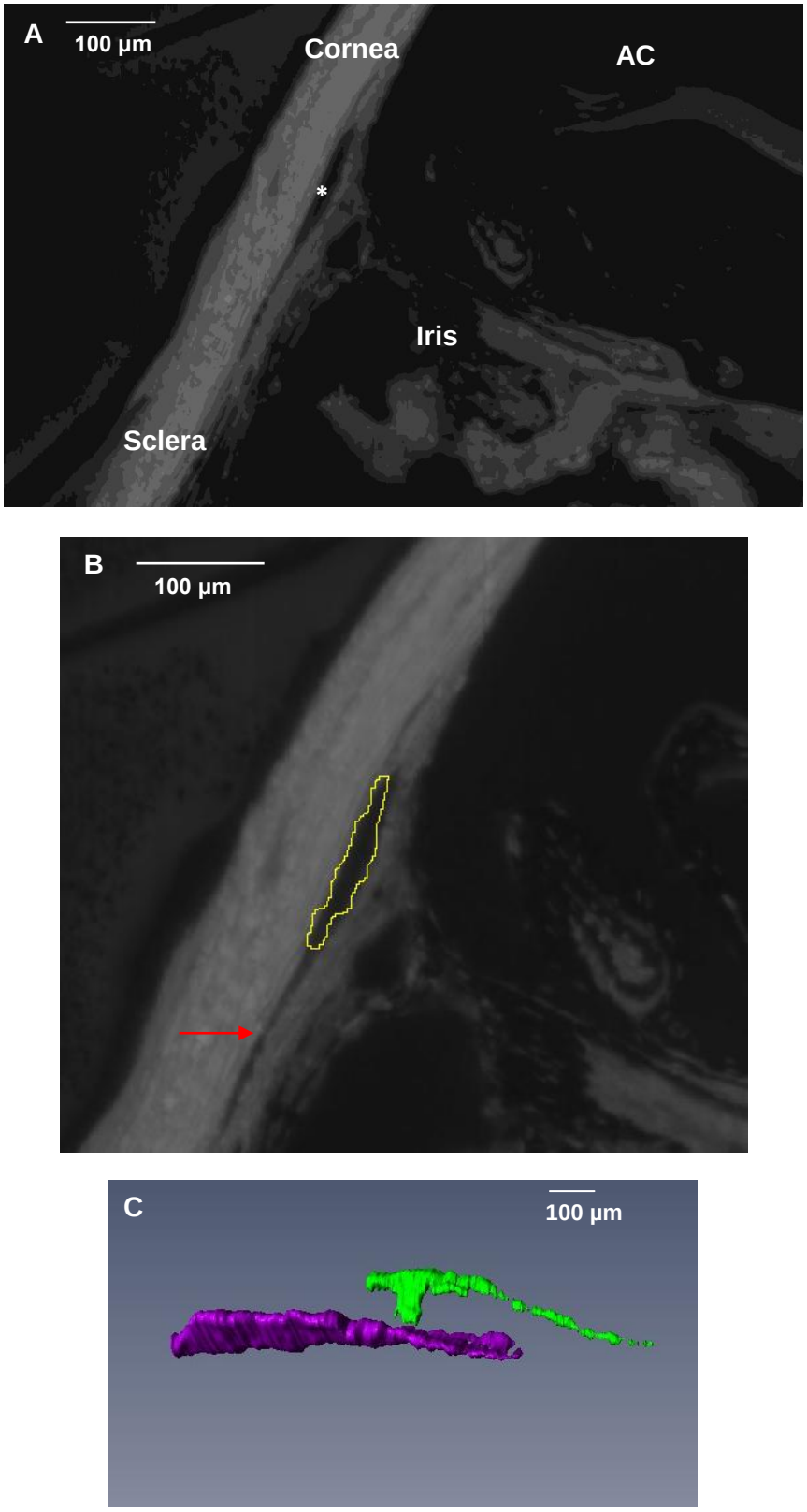

Figure 39: A) Image of the irido-corneal angle of a mouse eye acquired with the Histo-cutter, showing a CC departing from SC. Asterisk shows the SC lumen. B) Close-up of SC from Panel A, which is segmented in yellow. Red arrow points to the CC which in subsequent sections splits from SC. C) 3D reconstruction of a collector channel (in green) departing from SC (in purple).

3.2.4. Link between choroid and SC

We also detected an interesting morphological feature, shown in Fig 40. Images from samples perfused at different pressures showed a possible link between the choroid and SC (red arrow, Fig. 40). The images suggest there might a direct connection, although it is not clear whether it is fibrous or consists of a channel per se. Although further research is needed, this could mean that the conventional pathway could merge directly with choroidal circulation. Yet, this could just be a consequence of pigmentation.

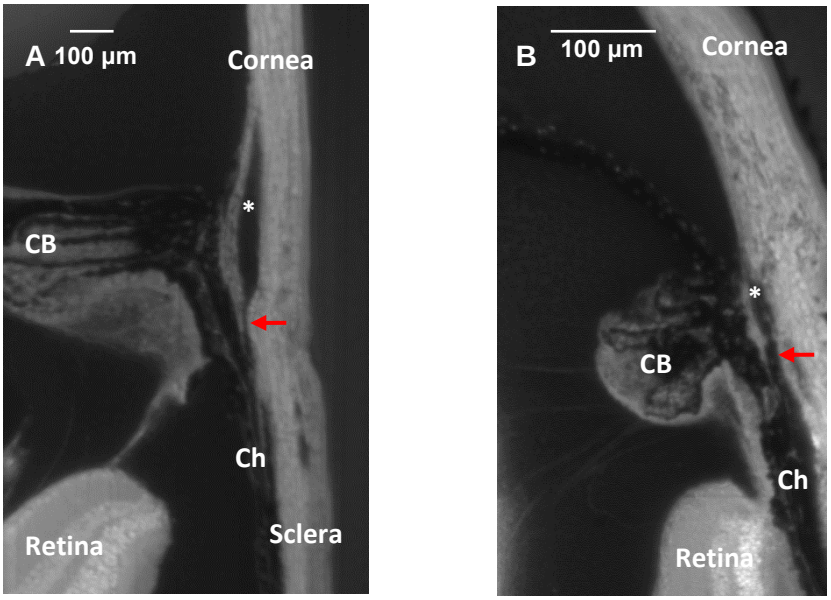

Figure 40: Two examples of fusion of choroid with SC, from two different samples. 2D image taken with the Histo-cutter showing a link (red arrow) between the choroid (Ch) and the SC (star).

3.3. OPT results

Only *N* =2 samples were successfully imaged by OPT. Both were fixed at physiological pressure (i.e. 8 mmHg in enucleated mouse eyes), even though the original aim was to observe changes in outflow patterns in eyes at different pressures. Unfortunately, we have not yet examined eyes at different pressures because we are still in the process of optimizing the protocol. Here, we present preliminary data for validating this novel protocol, which could be later used to examine outflow patterns in eyes fixed at different pressures.

Fig. 41 shows projection images, taken at the same position of the eye. It can be seen that the GFP1 channel captured some autofluorescence from the cornea, but mostly detected signal from the sclera and extra-ocular tissues. The Cy3 channel captured more specifically the fluorescence from the tracers, which were found at the limbus. Interestingly, they were

not found homogeneously around the circumference of the eye, and were highly concentrated only in some regions (Fig. 41C). Due to poor quality of the autofluorescence images, it is not possible to ascertain where the tracers are located in the TM and SC, but it is clear from the major landmarks of the eye (i.e. cornea, lens, sclera) they are in the limbal region.

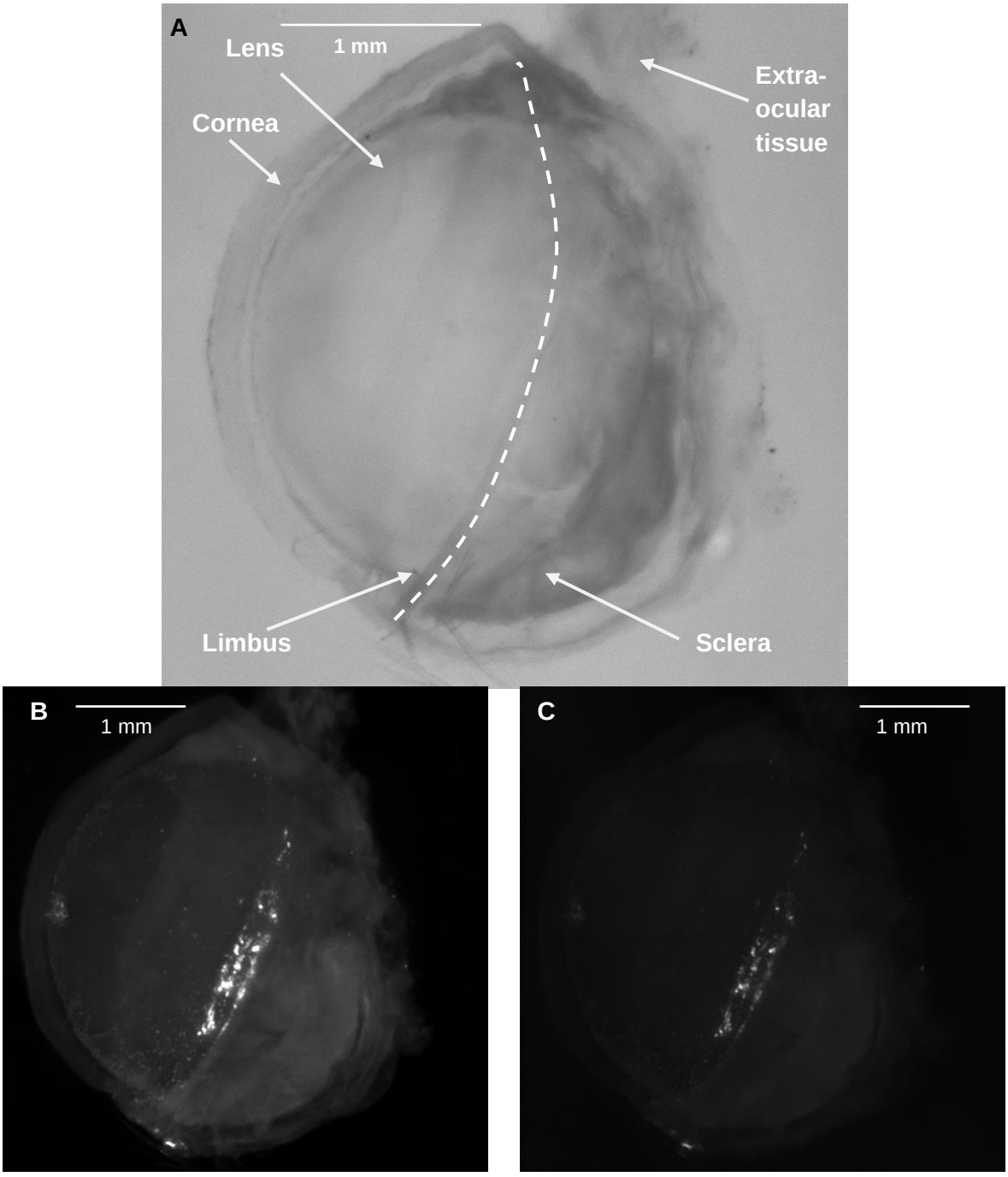

Figure 41: Images obtained with OPT of a BALB/cJ eye perfused with Qdots. Imaged A) in bright field mode, B) with the GFP1 filter, C) with the Cy3 filter. The eye was in the same position for the three images. Fluorescent tracers in B and C are detected as white signal.

A second eye was imaged and reconstructed, as shown in Fig 42. Blue structures represent autofluorescence captured with the GFP1 filter, while Qdots are shown in red. A similar distribution to that observed previously is found, wherein the Qdots are found around the limbus in focal locations only. Note Qdots are also found at the needle insertion site in the cornea. Fig 42B shows the fluorescence from the tracers only (Cy3 filter) from the same eye orientated in a different way, such that the entire circumference of the limbus is in a single plane. Our preliminary images support the findings that AH outflow is segmental in mouse eyes.

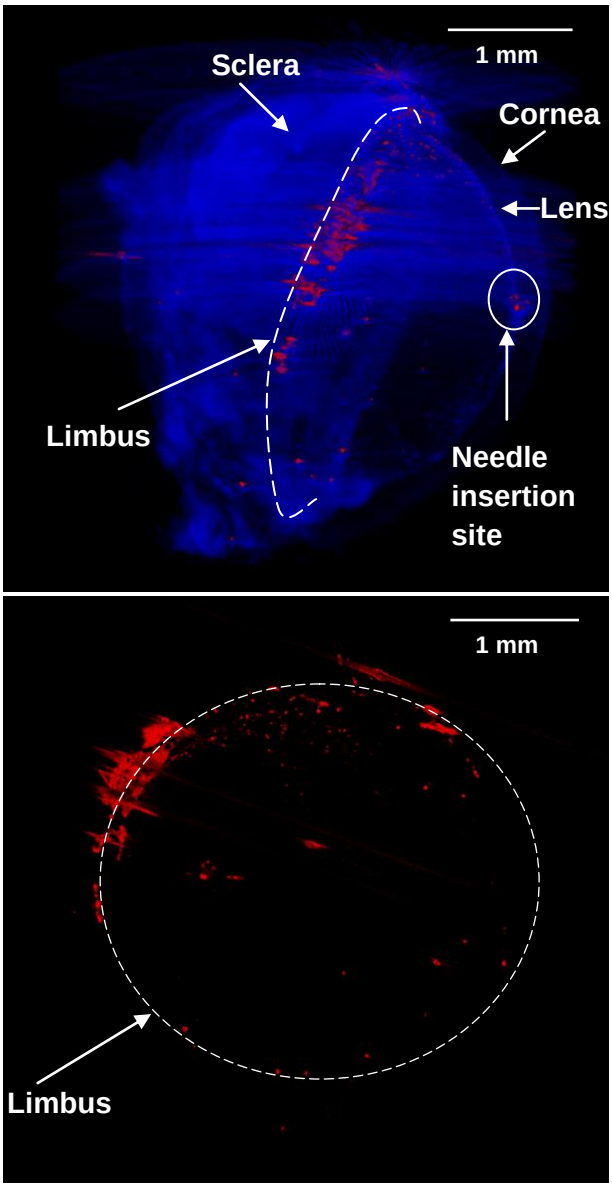

Figure 42: 3D reconstruction of BALB/cJ mouse eye perfused with Qdots. Tissue autofluorescence is shown in blue, whereas the Qdot fluorescence is represented in red. Note images A and B were acquired on the same eye but in different orientations. The autofluorescence in image B is not reported for clarity, but was used to determine the location of the limbus.

4- Discussion

Our results suggest conventional facility in mice is pressure-dependent. This is particularly interesting as it is the opposite of the effect observed in other species, such as humans[76]. Using a 3D automated histological device, we show SC is most open at 40 mmHg, which is consistent with the high conventional facility measured at similar pressures. Importantly, our histological images suggest this effect is likely caused by AC deepening, as previously observed in human studies. This suggests conventional facility in mice might be artificially increased at high pressures. In other words, mouse and human conventional facility may show similar pressure dependence, once AC deepening has been accounted for.

The effects of AC deepening in human eyes were reported in several early studies, amongst others by Grant who reported a two-fold increase in outflow facility in eyes when AC deepening was not prevented at physiological pressure levels[89]. More specifically, he described AC deepening as characterized by the enlargement of the anterior chamber which pushed the lens and the iris backwards, resulting in the iris forming a seal against the lens and closing the posterior chamber. Furthermore, he showed the effect was reversed following the re-establishment of a connection between the anterior and posterior chambers. This suggested that AC deepening was a result of the lack of pressurization of the posterior chamber caused by the direct delivery of perfusate to the anterior chamber. Finally, he showed AC deepening did not affect outflow facility after either the ciliary muscle or the TM was removed. Thus, his data further suggested outflow facility was increased because SC was artificially opened by a tension exerted on the ciliary muscle and TM, caused by the retro-displacement of the iris and the depression of the lens and zonules. This was further supported by studies from Van Buskirk[195], who showed artificially depressing the lens opened SC. Father, he showed SC cross sectional area decreased with pressure in eyes where iridotomy was performed, leading to its collapse at 40 mmHg.

In our study, SC showed no collapsed regions at 40 mmHg, as opposed to the situation in eyes fixed at lower pressures. Our histological images suggest SC opening is likely caused by the deepening of the AC, indicated by the increase in the irido-corneal angle. This agrees

with our morphometric data showing SC was most open at 40 mmHg, as it is pulled open by the retro-displacement of the iris. Unfortunately, due to the small size of the mouse eye, preventing AC deepening in mice will be much more challenging than in humans, resulting in a previously unrealized limitation for mouse eye perfusions. Human or other large eye perfusions have overcome the problem, either by establishing a connection between the posterior and anterior chamber via an iridotomy, or by placing the needle directly in the posterior chamber. Such techniques are much more challenging in mice eyes, and this AC deepening effect might therefore be a fundamental problem for mouse eye perfusions in general. This warrants further research so as to determine whether mouse eye perfusions should only be carried out within a low pressure range that is relatively immune to this effect.

Here we have introduced a novel protocol to image SC morphology in mouse eyes. More specifically, the SC was reconstructed in 3D from a stack of high resolution 2D images of the murine limbal region, acquired with the Histo-Cutter[196]. Our results show SC in mice is mostly continuous, although its lumen was not visible in some regions. It is hard to know how to interpret the zones where SC was not visualized: although the images suggest SC was simply nonexistent, it might have been collapsed and hard to resolve. Apart from classical histology, few techniques to examine SC in mice exist; most recently murine SC was revealed by two-photon microscopy in intact enucleated mouse eyes[203] or by confocal microscopy on PECAM-1 immunostained wholemounts of murine anterior segments[138]. In addition, a goniolens has been developed to monitor the irido-corneal angle in living mice[204], which allows locating SC; yet it provides only a macroscopic view of SC, and worked in albino mice when SC was filled with blood, thus limiting its applications. Currently, a collaborator is imaging the irido-corneal angle in anaesthetized mice, using Optical Coherence Tomography, to confirm our ex vivo data. Using the 3D histological technique, we also detected collector channels, although they were harder to resolve and seemed to disappear quickly in the sclera. In addition to structural information provided by the 3D reconstruction of SC and CC, the high resolution images provided morphological information

about the surrounding structures of the limbus. In particular, an interesting feature was observed at several locations: SC seemed to be linked with the choroid, as shown in Fig. 40. Note however this could be due to pigmentation, and would need to be further investigated.

In addition, a second imaging mode (Optical Projection Tomography[197,201], OPT) was tested to visualize outflow patterns in the whole mouse eye. Eventually, we hope that success with this approach would remove the need for embedding protocols or invasive procedures, such as sectioning, which can potentially damage the tissue and affect results. Note we attempted to combine the morphometric data from the Histo-Cutter with fluorescent outflow patterns, but were unsuccessful due to quenching of the Qdots by the relatively harsh embedding protocol. In contrast, images acquired with OPT successfully captured the fluorescence of the Qdots around the entire eye (Fig. 41, 42). Our results, albeit preliminary, were very encouraging and clearly demonstrated that tracer patterns were segmental around the circumference of the eye, as previously shown[205]. Note Qdots were still shown to be gradually quenched by BABB, a chemical required to clear the samples and maintain a proper refractive index during the OPT scan. Thus, we are currently investigating other potential tracers such as Rhodamine-Dextran which are not sensitive to quenching, and would be therefore more reliable.

Unfortunately, the morphological information provided by OPT was rather poor, thereby limiting our analysis. Indeed, although it is clear from the main landmarks of the eye the tracers are found within the limbal region as expected, no smaller structures such as the SC or CC were resolvable. Thus, it is not possible to infer whether the tracers are solely going through the conventional pathway or whether they are using a different route. The poor morphological rendering might have been caused by short exposure to the fixative (which enhances tissue autofluorescence) or because the structures we aim to observe are close to the resolution limit of the microscope (~ 5 μm). Ongoing studies will refine our protocol in order to obtain more detailed morphology so as to be able to draw more definitive conclusions on the trajectory of the outflow patterns. One possibility is to label the tissue with anti-CD31 antibody so as to stain endothelial cells, which would allow visualization of the

limbal vasculature. Note we assume the tracer distribution represents AH flow patterns, which will also need to be further investigated.

In summary, we have shown encouraging preliminary data on novel protocols to image the detailed morphology and outflow patterns in whole mouse eyes. Importantly, our preliminary morphometric data has already brought insight into the previously unappreciated phenomenon of anterior chamber deepening in the mouse eye. Both techniques (OPT, Histo-Cutter) present major technical challenges, not least because of the small size of mouse eyes. Ongoing studies are aimed at optimizing the relevant protocols, so as to eventually be able to visually assess outflow patterns, their relationship to outflow resistance and their behaviour under pharmacological treatment.

Chapter 7: Generalisation of Goldman's Equation to Account for IOP-Dependent Effects and Wash-Out

1- Introduction

Goldmann's equation (Eq. 5) describes the relationship between parameters that determine *IOP*, including aqueous humour production (F_p), unconventional outflow (F_u), conventional outflow facility (C) and episcleral venous pressure (EVP):

$$\mathrm{IOP} = \frac{\mathrm{F_p} - \mathrm{F_u}}{\mathrm{C}} + \mathrm{EVP}$$

Equation 5

This equation is commonly used to calculate conventional facility as the slope of a line regressed to the flow rate (F_p) vs. pressure (IOP) data (see Chapter 2, section 2.1). However it assumes conventional facility is constant, which is not necessarily true. In particular, conventional facility has been shown to depend on pressure and on the volume of perfusate in some studies on human and other types of eyes [76,206]. More specifically, conventional facility decreases in human eyes at a rate of 1% per mmHg increase in IOP[76], an effect attributed to the collapse of SC at high pressures[195]. Further, outflow facility has been shown to increase with increasing perfused volumes in bovine[206,207] and monkey[208,209] eyes. This phenomenon, termed washout, is possibly caused by a separation of the inner wall of SC from the JCT[151]. In bovine eyes, washout resulted into an increase in outflow facility of up to 81% after 3 hrs of perfusion[184]. Interestingly, washout has been observed in all species studied to date, except for humans[160] and mice[12]. Despite experimental evidence showing that both pressure and washout can affect outflow facility, Goldmann's equation has never been modified to explicitly take these factors into account. Therefore, in this study, we propose a modified Goldmann's equation to include them.

This modification was further motivated by the non-linearity that we sometimes observed in our flow rate vs. pressure data, which is not predicted by Goldmann's equation. Usually,

we obtained a linear flow rate vs. pressure relationship, from which a constant slope could be interpolated to calculate *C* according to Goldmann's equation, see e.g. data from cohorts 2 and 8 in Fig. 43, corresponding to C57BL/6 mouse eyes perfused at 35 °C from studies described in Chapter 2 and 4. However, cohorts of eyes from other studies belonging to the same strain of mouse and perfused under similar conditions behaved differently. For example, flow rates measured in eyes from Cohort 12 increased linearly with pressure until 22 mmHg, after which they increased at a higher rate. This introduced a non-linearity in the flow vs. pressure data curve (dashed curve Fig. 43), not observed in cohorts 2 or 8. In the previous chapter, we showed that this effect might be attributable to AC deepening occurring at high pressures. Interestingly, Cohort 11 also shows a transition in flow rates, but at lower pressures (~ 15 mmHg), resulting in much higher flow rates than any other cohort at 25 mmHg (red data point, Fig. 43).

Since flow rates measured at the same pressure seemed to behave so differently amongst apparently similar cohorts of mice, we investigated whether parameters other than pressure could be playing a role in this process. Interestingly, we found that the volumes of perfusion media delivered to eyes from Cohort 11 were higher than for any other cohort (Table 10). This suggested high volumes could have caused the large outflow facility observed in cohort 11, although the inverse could also be true, i.e. large volumes could have been caused by large outflow facility. This further prompted us to model volume and pressure effects in Goldmann's equation, to test whether they could explain the differences in our flow rate vs. pressure data between cohorts.

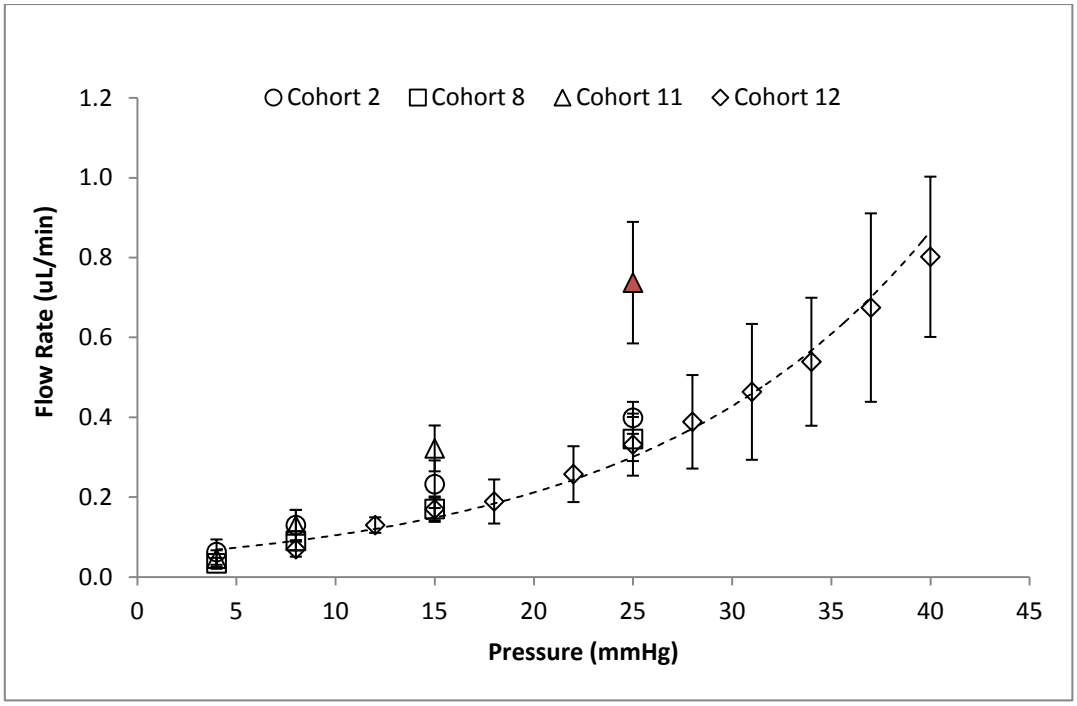

Figure 43: Flow-Rate vs. pressure data for four different cohorts of C57BL/6 mice perfused under ostensibly identical conditions. The dashed curve is a nonlinear trend line fit to the data from Cohort 12, illustrating the nonlinearity observed in the data. The red data point correspond to a particularly high flow rate measured at 25 mmHg in Cohort 11 which differs strikingly from that of the other cohorts. Cohort 2 refers to data from Chapter 2, Cohort 8 to data from Chapter 4, Cohort 11 to data from Chapter 5 and Cohort 12 to data from Chapter 6. All eyes were perfused at 35 °C with DBG while submerged in isotonic saline. Bars are standard deviations.

	C [µL/min.mmHg]	V [µL]
Cohort 2 (*N*= 6)	0.0172± 0.0028	25±16
Cohort 8 (*N* = 9)	0.0147± 0.0029	14±3
Cohort 11 (*N* =6)	0.0290 ± 0.0068	**38±12**
Cohort 12 (*N* =5)	0.0155 ± 0.005	20±5

Table 10: Conventional facility measured in cohorts of C57BL/6 mouse eyes perfused under apparently identical conditions (at 35 °C, submerged in isotonic saline).The highest volume perfused is highlighted in red and pertains to Cohort 11. Data are shown as mean ± standard deviations. *C* is conventional outflow facility, calculated according to the simplified Goldmann's equation, and *V* is the volume perfused into the eye at the end of outflow facility measurement.

Thus, this chapter describes the development and evaluation of a modified Goldmann's equation. We hypothesise pressure and volume affects conventional facility, which could explain its variability between ostensibly similar cohorts of mice. The fit of the proposed modified equation is tested on our data to investigate whether it can better explain our measurements, specifically that of cohort 11. This meta-analysis pools all data reported in this thesis from C57BL/6 mouse eyes submerged in PBS and perfused at 35 °C with DBG. In addition, we analysed possible covariates such as gender, age and supplier that might have explained the variability in flow rate vs. pressure data between cohorts.

2- Methods

2.1. Derivation of modified Goldmann's equation

First, we model the dependence of conventional outflow facility (*C*) on intraocular pressure (*IOP*). Conventional outflow resistance has previously been shown to scale nearly linearly with IOP[76]. Therefore we first express conventional outflow resistance as a linear function of *IOP* in Eq. 15, wherein *β* is a constant describing the proportional increase of R_c with increasing *IOP*, in units of $mmHg^{-1}$:

$$\mathrm{R_c} = \mathrm{R_{p0}} + \mathrm{R_{p0}} * \mathrm{IOP} * \beta = \mathrm{R_{p0}} * (1 + \mathrm{IOP} * \beta)$$

Equation 15

R_{p0} represents the conventional outflow resistance extrapolated to zero pressure. Reported values for *β* in human, rabbit or bovine eyes range from 0.012 to 0.1 $mmHg^{-1}$ [76]. Note a positive value for *β* corresponds to an increase in R_c with IOP, while a negative value would represent a decrease in R_c with IOP. Since conventional outflow resistance corresponds to the inverse of conventional facility (i.e. $\mathrm{R_c} = \frac{1}{\mathrm{C}}$), Eq. 15 can be rewritten as :

$$\mathrm{C} = \frac{\mathrm{C_{p0}}}{1 + \beta * \mathrm{IOP}}$$

Equation 16

Note C_{p0} is the inverse of R_{p0} and represents conventional facility at extrapolated to zero pressure. Thus we obtain the following expression for the relative change of conventional outflow facility:

$$\frac{\mathrm{C}}{\mathrm{C_{p0}}} = \frac{1}{1 + \beta * \mathrm{IOP}}$$

Equation 17

Secondly, we introduce the effects of volume perfused, i.e. washout, on outflow facility. A previous study has demonstrated that outflow facility measured during perfusions scales with volume of the perfusate passing through the conventional outflow pathway (termed V) [206], as modeled by Eq. 18. C_{vo} represents outflow facility measured with minimal or zero volumes

of perfusate (*V*), and *α* is a scalar describing the dependence of *C* upon *V* in units of μL^{-1}. *α* has been reported in bovine eyes to be $0.34*10^{-3}$ μL^{-1} [206].

$$C = C_{v0} + C_{v0} * \alpha * V = C_{v0}(1 + \alpha * V)$$

Equation 18

This corresponds to a relative change in conventional facility described by Eq. 19:

$$\frac{C}{C_{v0}} = 1 + \alpha * V$$

Equation 19

We now combine the effects of washout and of intraocular pressure on outflow facility, such that *C* is a function of the perfused volume *V* and intra-ocular pressure *IOP* (Eq. 20):

$$C = C\ (V, IOP)$$

Equation 20

We assume the effects of pressure and volume on conventional facility are additive, such that

$$C = C_0 \times (1 + f(V) + f(IOP))$$

Equation 21

where f(V) and f(IOP) are equal to zero when V or IOP are zero, and C_0 is outflow facility at zero pressure and volume perfused. Note we assume the effects of perfused volume and IOP on facility are independent of each other. This is supported by a study showing, the washout rate was similar in bovine eyes at 6 and 15 mmHg[206]. No experiment, to our knowledge, has looked at effects of varying perfused volumes on changes in conventional facility with pressure. We assume the assumption of volume and pressure effects being independent holds true for mouse eyes, although this will need to be confirmed.

Thus, if we assume $C_{p0} = C_{v0} = C_{0,}$ for Equation 21 to be consistent with Equation 16 and 18, we have:

$$f(V) = \alpha * V$$

Equation 22

$$f(IOP) = \frac{1}{1+\beta*IOP} - 1$$

Equation 23

Substituting Equation 21 with Equation 22 and 23 yields:

$$C = C_0 \times (1 + \alpha * V + \frac{1}{1 + \beta * IOP} - 1)$$

$$C = C_0 \times (\alpha * V + \frac{1}{1 + \beta * IOP})$$

Equation 24

Finally, we introduce Eq. 24 into Goldmann's equation adapted for enucleated mouse eyes (i.e. F_p=0 and *EVP*=0, cf. Eq. 8)

$$F_p = C_0 * IOP\left(\frac{1}{1 + \beta * IOP} + \alpha * V\right) + F_u$$

Equation 25

Thus our modified Goldmann's equation (Eq. 26) contains four parameters, namely C_o, F_u, β and α as opposed to the two parameters found in the original equation, C and F_u. Note C_o is the reference outflow facility at zero pressure and zero volume perfused and does not equal C at the physiological state. C_o would equal C at the physiological state if $\alpha = \beta = 0$.

2.2. Testing the model viability with our data

In order to test the viability of our new model (Eq. 26), we performed a nonlinear fit of Eq. 26 on our dataset. We also performed a linear fit to obtain the values of C and F_u that would have been obtained with the original Goldmann's equation (Eq. 8). The non-linear fit was done using Matlab's function Nonlinearmodel.fit (described below), while the fitting of the classical Goldmann equation was done using the MatLab function polyfit. Further, the non-linear fit was performed when α and β were either simultaneously, or separately, set to zero. Finally, we tested whether the data were consistent with the predicted relationship of Eq. 26,

with all parameters (C_o, F_u, β and α). For each analysis, we analyzed the values of the optimal values resulting from the fit, and whether they were statistically different from 0.

The function used for fitting our nonlinear model to the data was NonLinearModel.fit in Matlab. The function is asked to fit our *F*, IOP and *V* data (described below) to an equation of the form of Eq. 26, using initial guesses for each parameter. This function searches for values of parameters (in our case C_o, F_u, β and α) that minimize the least square differences between the measured data and the values predicted by the model of interest. NonLinearModel.fit provides p-values to assess whether the estimates of the parameters are statistically significantly different from 0. Nonlinearnodel.fit reports the R^2 coefficient for the best fit, describing the amount of variability in the data which can be described by the fit. However, the R^2 value is known to automatically increase with the addition of parameters in the fit since a better fit can invariably be obtained by using more parameters. Thus, the values we show are the adjusted R^2, which adjusts the fit by accounting for the number of parameters in the fit. In other words, the adjusted R^2 will only increase if the R^2 obtained with the additional parameter is larger than that expected based on the addition of any explanatory variable. Finally, Nonlinearmodel.fit can also provide the confidence interval for each parameter estimated by the best fit. We report the 95% confidence interval, such that there is less than 5% chance that the estimated parameter does not fall within that interval. The greater the variability of the parameter, the larger the confidence interval.

The initial guesses used for the parameters C_o, F_u, β and α are listed in Table 11, which were chosen according to values found in the literature [15,76,206]. Note the initial value for β was set as negative because we have observed an increase in outflow facility with pressure in Cohort 12 (cf. Chapter 6). We also tested positive initial values for β (i.e. either -0.01 or 0.01, table 11). In order to test the robustness of our model, we performed the fit with different initial values, increasing or decreasing each one by a factor of ten (see table 18, results section). No constraints were imposed on the predicted optimal values of the parameters C_o, F_u, β and α.

	Initial values
C_o [µL/min.mmHg]	0.01
F_u[µL/min]	0.01
β [mmHg $^{-1}$]	-0.01 or 0.01
α [µL $^{-1}$]	0.01

Table 11: Initial values used to search the optimal fit to our data with NonLinearModel.fit

All data used for fitting were taken from the custom Labview perfusion software[151]. The *IOP* data corresponds to the pressure level imposed during perfusions (4-40 mmHg). The software calculates the volume perfused, *V,* by numerically integrating the flow rate data over time. We use the average of the flow rate data (*F*) acquired at each steady pressure level (see Fig. 8, Chapter 2), and the *total* volume (*V*) perfused at the end of each pressure level. For Cohort 11, we needed to account for the volume perfused during their pre-pressurization step at 8 mmHg for 60 min with a PBS-filled reservoir before the perfusion. We estimated this volume using the conventional facility measurement performed at 8 mmHg, assuming conventional facility did not change between the start of the pressurization and the flow rate measurement at 8 mmHg. This assumption seems reasonable since the volume perfused between the pre-pressurization step and the measurement of conventional facility at 8 mmHg was small, on average 1.27±0.64 µL.

This analysis considers each pressure measurement of each eye from cohorts 2, 8, 11 and 12 individually. Note data from only one eye per animal was used in this study. This was because they correspond to untreated eyes from different studies, whose contralateral eyes typically received a different solution. Thus, data from their paired eyes were not considered in this meta-analysis, since they were treated differently. A total of 118 data points were used in this analysis, each of which was associated with a pressure level, a flow rate and a volume of perfused solution. In three cohorts of eyes (cohorts 2, 8 and 11), 3-4 data points belonged to the same eye; in cohort 12, 12 data points were measured in the same eye because perfusions were done up to 40 mmHg.

2.3. Analysis of the effects of age, gender and supplier

In order to investigate whether potential difference in age, gender or animal supplier could influence the variability observed in outflow facility between cohorts, we pooled our outflow facility data according to these variables and compared them between groups. The supplier was either Jackson laboratory (UK) or Charles River (UK). Mice were aged from 5 to 29 weeks. Unfortunately, all mice from Jackson's laboratories were female and all mice from Charles River were male, which made it impossible to distinguish between supplier or gender effects. The comparison of outflow facility data between mice of different gender, supplier or age was made with 2-sided unpaired t-tests. In addition, we tested whether the slope of the best-fit linear trend line for the conventional facility vs. age data was significantly different from 0 with a two-sided t-test. For this analysis, data from both males and females was used together.

3- Results

3.1. Non linear vs. linear model

Using the function polyfit, we found the optimal values for the parameters in the classical Goldmann's equation listed in Table 12.

	Optimal values
F_u [µL/min]	-0.0454
C [µL/min.mmHg]	0.0178
R^2	0.753

Table 12: Values for the estimated parameters and R^2 from the linear fit (i.e. Goldmann's equation, Eq. 8) with polyfit.

Using the function Nonlinearmodel.fit, we fit an equation of the form of Eq. 26 with the constraints that α=β=0, thereby reducing it to the classical Goldmann's equation (Eq. 8). In this case, we obtained identical values for C_o, F_u as were obtained for the previous linear fit (Table 13). Note in this case, we report the adjusted R^2, for comparison with the following models with additional parameters (see Methods). In the previous analysis we reported the

R^2, explaining why they are not exactly the same (0.753 vs. 0.751 for the R^2 from the previous analysis and the adjusted R^2 for the current analysis). Both parameters C_o and F_u were statistically different from 0. As previously indicated (Fig. 43), flow rate values from cohort 11 seem to be considerably larger than that of other cohorts, and not particularly well explained by the linear fit (as shown by the arrows in Fig. 44). The linear fit predicts that F_u is negative, suggesting somewhat unrealistically an inward-directed unconventional outflow.

Nonlinear model $\alpha=\beta=0$	Optimal values	P-values	CI
F_u [µL/min]	-0.0454	0.01456	-0.0816 -0.0091
C_o [µL/min.mmHg]	0.0178	$4.58*10^{-37}$	0.0160 0.0197
Adjusted R^2	0.751		

Table 13: Values for the estimated parameters and the adjusted R^2 from the nonlinear fit with α=β=0. P-values lower than 0.05 indicate parameters that are statistically different from 0. CIs are confidence intervals reported for each optimal value.

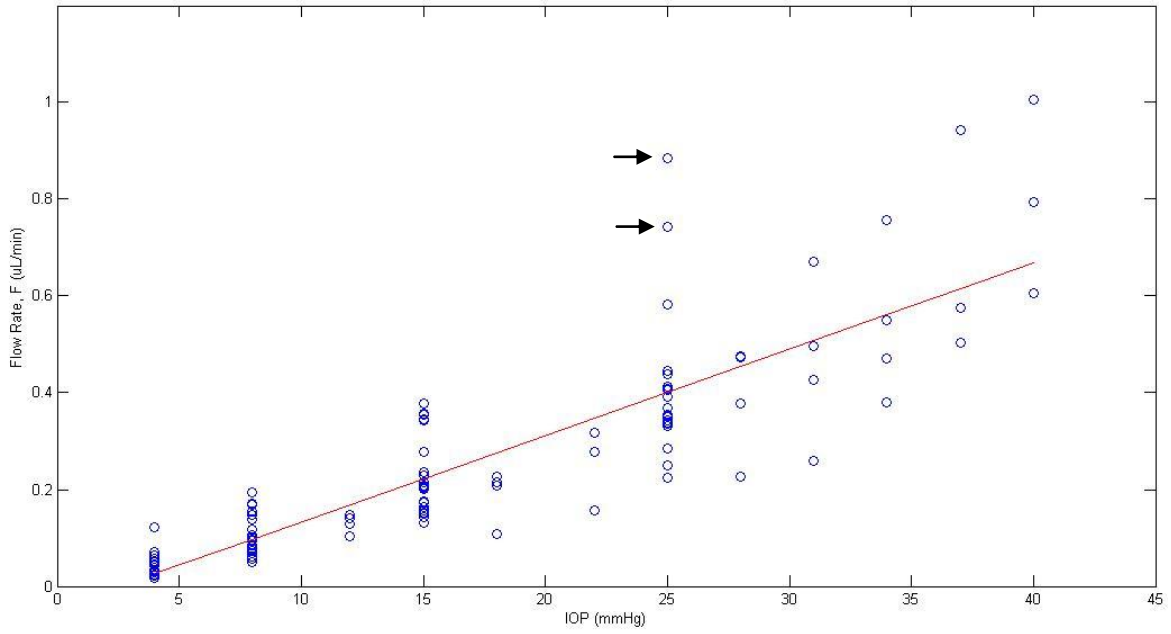

Figure 44: Nonlinear fit to the modified Goldmann's equation, where $\alpha=\beta=0$. The fit was performed on flow rate vs. pressure data comprising data points from cohort 2,8,11 and 12. The red line corresponds to the best fit using the nonlinear model with when $\alpha=\beta=0$ (Eq. 26), and blue points represent the raw data. Note that the non-linear model produces the identical fit as the linear model when $\alpha=\beta=0$. Arrow heads point to data points from cohort 11 at 25 mmHg, which seem to diverge from the prediction shown in red.

We next fit an equation of the form of Eq. 26 with the parameters F_u, C_o and β but with α set to zero (Table 14). This case is motivated by the putative observation that washout does not occur in enucleated mouse eyes, which is consistent with $\alpha = 0$[12]. In this case, we obtain a statistically significant C_o value, which at 8 mmHg corresponds to a facility of 0.0120

µL/min.mmHg (using Eq. 16), which is similar to that obtained with the original Goldmann's equation (0.0178 µL/min.mmHg; tables 12&14) and in the physiological range. The optimal value for β was also significantly different from 0. It was negative, indicating facility increased with pressure, consistent with our previous data indicating AC deepening at high pressures (Chapter 6). In contrast, F_u was not statistically different from 0. The adjusted R^2 value for this model was 0.763, only moderately higher than that of the previous model. Note this increase cannot be attributed to the addition of a parameter in our fit, because that is taken into account by the adjusted R^2 value. Thus, our findings suggest that a model taking into account only pressure effects could explain relatively well our data but caused the intercept (or F_u) to disappear. Yet, it still does not explain the very high flow rates from cohort 11, shown in Fig. 45 by the arrow heads.

Nonlinear model α =0	Optimal values	P-value	CI
F_u [µL/min]	0.0068	0.76	-0.0385 0.0522
C_o [µL/min.mmHg]	0.0110	$5.03*10^{-8}$	0.0073 0.0147
β [mmHg $^{-1}$]	-0.0104	0.0002	-0.0158 -0.0050
Adjusted R^2	0.763		

Table 14: Values for the estimated parameters and the adjusted R^2 from the nonlinear fit with α=0. P-values lower than 0.05 indicate the parameters are statistically different from 0. CIs are confidence intervals reported for each optimal value.

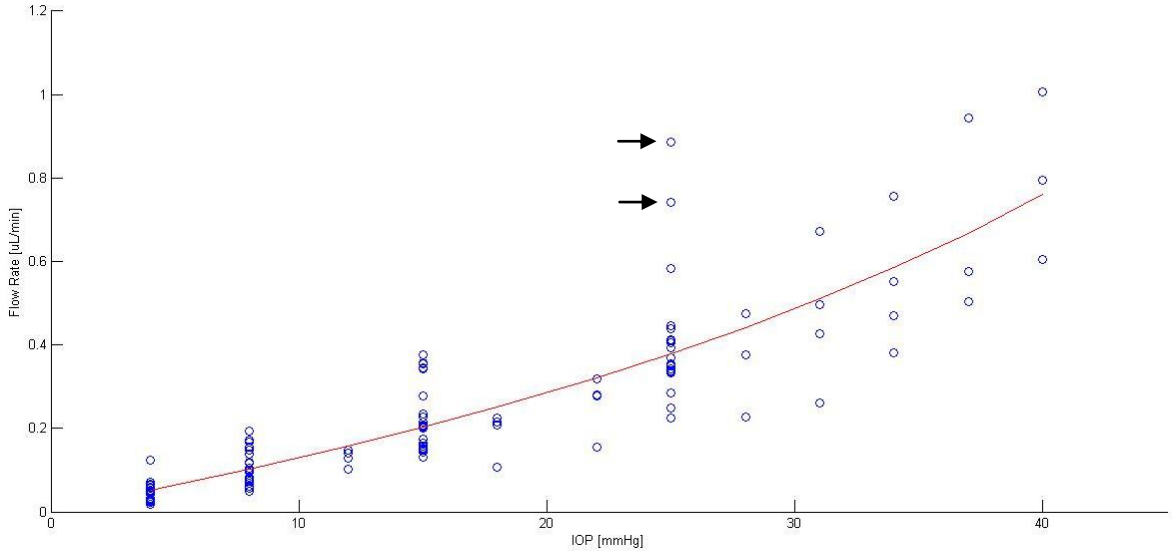

Figure 45: Non linear fit to the modified Goldmann's equation, where α=0. The fit was performed on flow rate vs. pressure data comprising data points from cohorts 2,8,11 and 12. The red curve corresponds to the best fit using the nonlinear model with α=0 (Eq. 26), and blue points represent the raw data. Arrow heads point to data points from cohort 11 at 25 mmHg, which seem to diverge from the fit shown in red.

We further analyzed the fit of Eq. 26 with the parameters F_u, C_o and α, but with β set to zero (Table 15). Similarly to our previous analysis, F_u was not statistically different from 0, but C_o and α were significantly different from zero. C_o is very similar to that found when α was set to zero (0.0104 vs. 0.0110 µL/min.mmHg; tables 14&15). The value of α is larger than values previously reported in the literature (α =0.0003 µL $^{-1}$ [206]), possibly suggesting an unanticipated washout effect in mice[12]. The adjusted R^2 value for this model was 0.82, relatively higher than that obtained by either previous analyses (Table 13&14). Note this increase in R^2 compared to that obtained with only two parameters (Table 12) cannot be attributed to the addition of a parameter in our fit, because that is taken into account by the adjusted R^2 value. Thus, our findings suggest that a model taking into account only volume pressure effects could also explain well our data. However, it still does not explain the very high flow rates from cohort 11, shown in Fig. 46 by the arrow heads.

Nonlinear model β =0	**Optimal values**	**P-value**	**CI**
F_u [µL/min]	0.0214	0.26	-0.0157 0.0586
C_o [µL/min.mmHg]	0.0104	$2.83*10^{-11}$	0.0076 0.0131
α[µL $^{-1}$]	0.0136	0.0004	0.0062 0.0210
Adjusted R^2	0.817		

Table 15: Values for the estimated parameters and the adjusted R^2 from the nonlinear fit with β=0. P values lower than 0.05 indicate the parameters are statistically different from 0. CIs are confidence intervals reported for each optimal value.

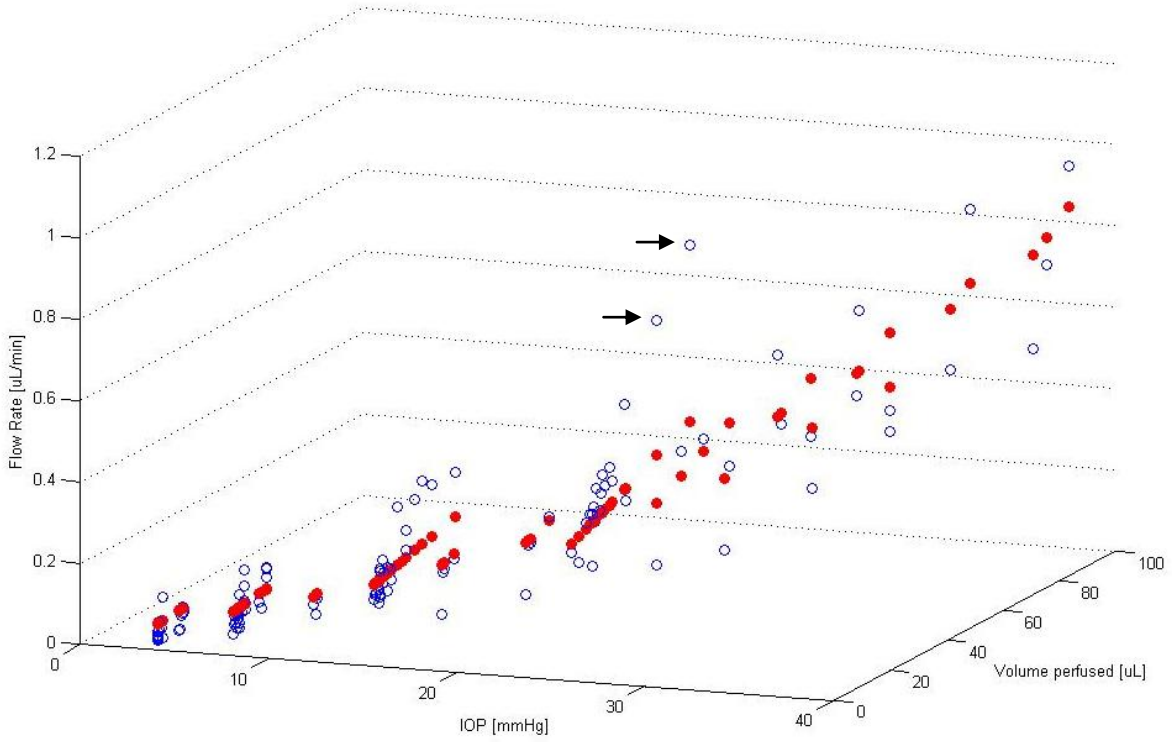

Figure 46: Non linear fit to the modified Goldmann's equation, where β=0. The fit was performed on flow rate vs. pressure data comprising data points from cohorts 2,8,11 and 12. The filled red circles corresponds to the best fit using the non linear model with β=0 (Eq. 26), and blue empty circles represent the raw data. Arrow heads point to data points from cohort 11 at 25 mmHg, which seem to diverge from the fit shown in red

Since both models considering either volume or pressure effect caused the intercept (or F_u) to become not statistically different from 0, we now consider the non linear model with α, β and C_o but where F_u is set to zero. Further, our analysis showed that the optimal value for F_u differed three fold between the analyses considering either volume or pressure alone, while C_o varied only by 10%. This suggests the nonlinear effects of pressure or volume may artificially give rise to the appearance of a non-zero intercept in the *F* vs. *IOP* relationship, which could be wrongly interpreted as F_u. For these reasons, F_u was eliminated from the next analysis by setting it to zero.

When a non linear fit was performed with F_u set to zero, we obtained optimal values for C_o and α which were statistically different from 0, while that of β was not (table 16). The value found for C_o corresponded to a *C* at physiological pressure of 0.0141 µL/min.mmHg. This is consistent with in vivo values reported in the literature[5,6,9,10,14,15,102] and was close to the original value found with Goldmann's equation (0.0178 µL/min.mmHg table 12). The optimal value for α is still somewhat larger than that found in bovine eyes. In this case, the non linear

fit explains 83% of the variation seen in the data, but still fails to predict the high flow rates from cohort 11 (Fig. 47). This adjusted R^2 value was relatively higher than the two first analyses (Table 13&14), but very similar to the model wherein β was set to zero (Table 15). These results suggest our data is consistent with a model where washout causes high flow rates and high C at large perfusion volumes.

Nonlinear model F_u =0	Optimal values	P-value	CI
C_o [µL/min.mmHg]	0.0170	$1.75*10^{-6}$	0.0103 0.0236
β [mmHg $^{-1}$]	0.0257	0.13	-0.0075 0.0589
α[µL $^{-1}$]	0.0104	$6.03*10^{-9}$	0.0071 0.0136
Adjusted R^2	0.828		

Table 16: Values for the estimated parameters and the adjusted R^2 from the nonlinear fit with Fu=0. P values lower than 0.05 indicate the parameters are statistically different from 0. CIs are confidence intervals reported for each optimal value.

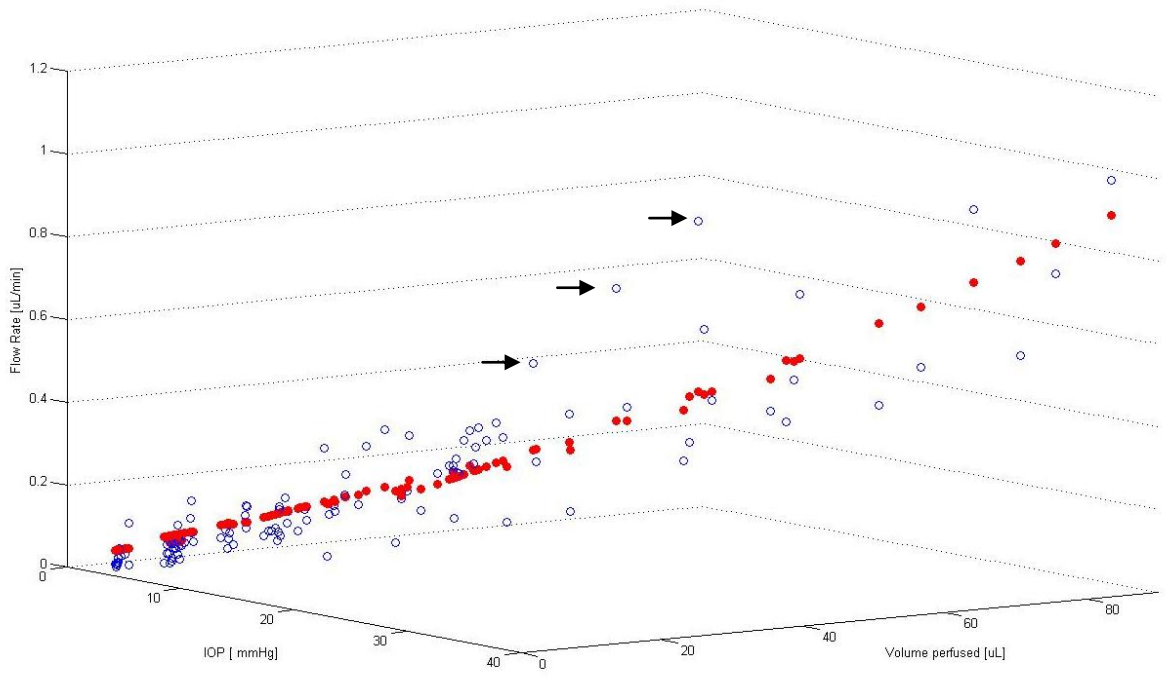

Figure 47: Non linear fit to the modified Goldmann's equation, where F_u=0. The fit was performed on flow rate vs. pressure data comprising data points from cohorts 2,8,11 and 12. The filled red data points corresponds to the best fit using the non linear model with F_u=0, and blue points represent the raw data. Arrow heads point to data points from cohort 11 at 25 mmHg, which seem to diverge from the fit shown in red

Finally, we performed the non linear model with all four parameters (Table 17), i.e. including F_u. In this case, none of the parameters are statistically different from 0. The adjusted R^2 value was relatively higher than the two first analyses (Table 13&14), but very similar to the model wherein β or F_u were set to zero (Table 15&16). More importantly, the

values for C_o and F_u changed significantly from those found in the previous analyses where either α, β or F_u were constrained to equal zero (Tables 14-16). Further, in this case β was positive, indicating a decrease of facility with pressure, which disagrees with what we observed in cohort 12 (Chapter 6). These discrepancies further motivated the use of a model where F_u is not considered.

Nonlinear model	Optimal values	P-value	CI	
F_u [µL/min]	-0.0847	0.30	-0.2448	0.0753
C_o [µL/min.mmHg]	0.0381	0.19	-0.0196	0.0958
β [mmHg $^{-1}$]	0.0718	0.27	-0.0558	0.1995
α[µL $^{-1}$]	0.0048	0.15	-0.0018	0.0115
Adjusted R^2	0.831			

Table 17: Values for the estimated parameters and the adjusted R^2 from the full non-linear fit. P-values lower than 0.05 indicate the parameters are statistically different from 0. CIs are confidence intervals reported for each optimal value.

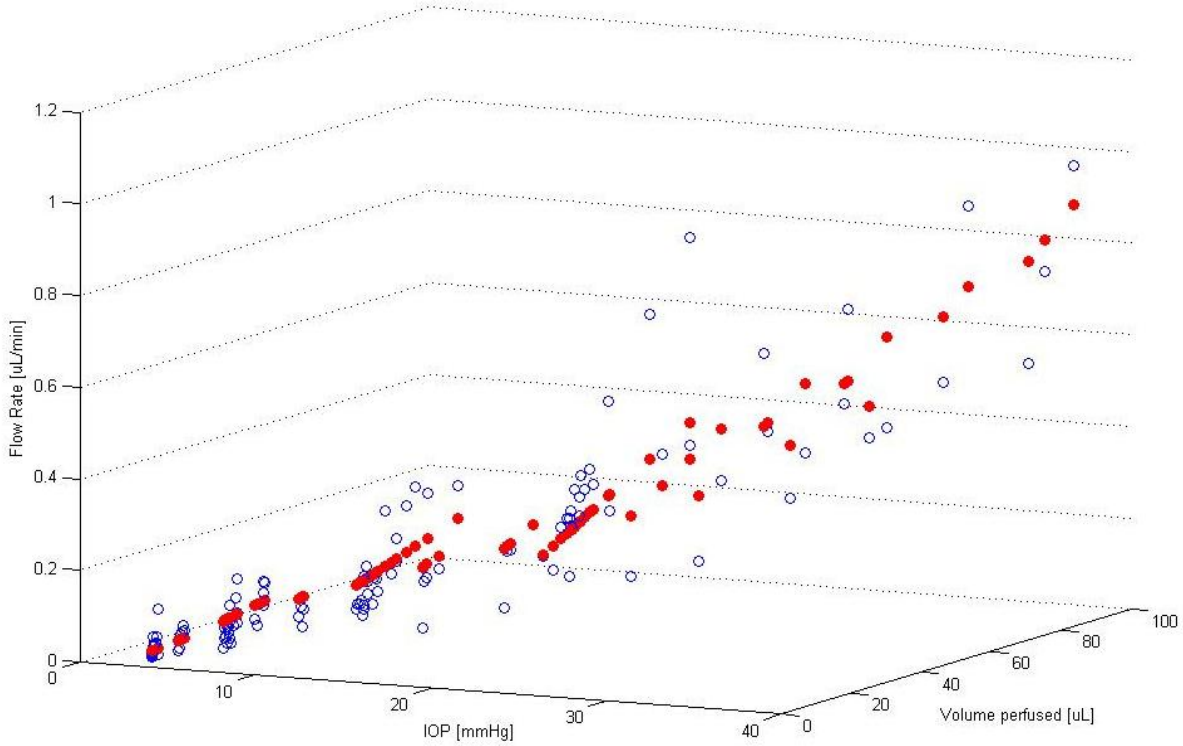

Figure 48: Non linear fit to the modified Goldmann's equation. The fit was performed on flow rate vs. pressure data comprising data points from cohorts 2,8,11 and 12. Red points correspond to the best fit model calculated by NonLinearModel.Fit and blue points represent the raw data. Arrow heads point to three data points from cohort 11 at 25 mmHg, which seem to diverge from the nonlinear fit shown in red.

Taken together, our analyses suggest our data cannot be explained by a combination of both volume and pressure effects, either when F_u is considered or not. We further investigated whether there was any combination of α and β which could explain our data within a domain of varying values of α and β. Thus, we computed the sum of squared differences between the measured and predicted data by plotting the sum of squared differences over a range of values for α and β to *directly* visualize for which parameters of α and β the sum of squared difference was the smallest in the domain of interest. The aim was to investigate whether there were other minima in the vicinity of the optimal values found by our previous analyses, which could have corresponded to values of α, β, C_o *and* F_u wherein both volume and pressure effects where statistically different from 0. This analysis was performed for values of α and β neighbouring the optimal values determined from the two previous analyses, where either α or β was set to zero (see tables 14&15). This was done both with and without considering Fu in the non linear model. The values of C_o and F_u were fixed and chosen according to the optimal values found in the analysis wherein α and β were separately set to 0 (Table 14&15). Interestingly, in both cases, we observed the landscape in the domain was flat (Fig. 49, white region). The flat landscape suggests that there are a wide range of α and β parameters that produce equivalent fits. In other words, with our current data set, it is not possible to distinguish the non-linear effects arising from volume or pressure effects.

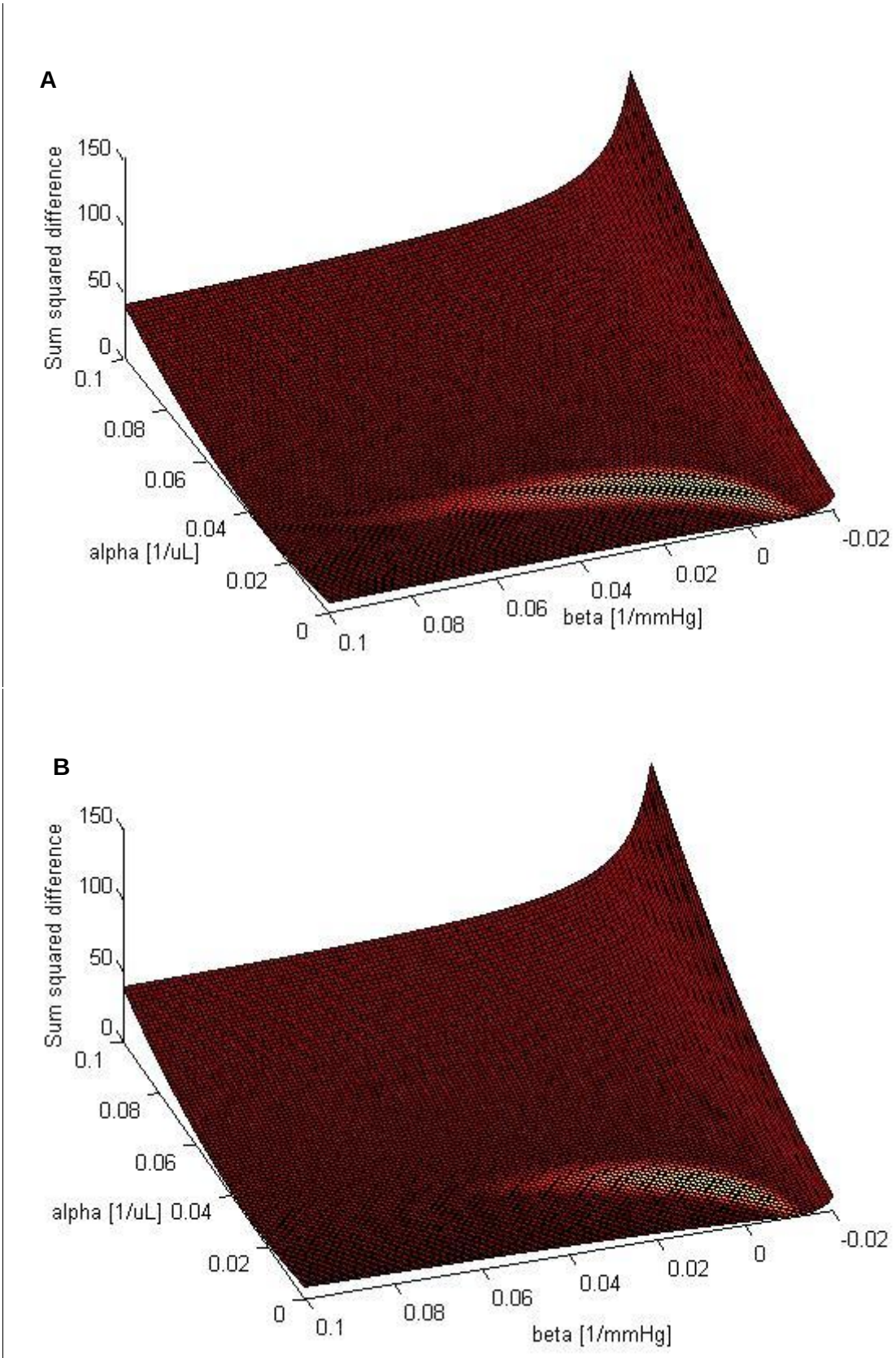

Figure 49: Sum of squared difference between the flow rate data measured and that predicted by our nonlinear model either with (A) or without (B) considering Fu, using a range of α (x-axis) and β (y-axis) parameters. The clear white regions correspond to the lowest sum of squared differences. In panels A and B, the value used for C_o was 0.0104 µL/min.mmHg taken from the analysis where β was set to zero. In A, the value for F_u was 0.0214 µL/min taken from that same analysis (table 15).

In summary, using a linear model (Goldmann's equation), both C and F_u are statistically different from 0. In contrast, F_u was not statistically different from 0 when either only α or β were considered in the nonlinear model (Eq. 26). Thus we performed the analysis setting F_u is equal to zero, in which case only the volume effects were significant. Thus, our current dataset seems to be explained by volume effects rather than pressure effects. Yet, even in that case, there seems to be numerous combinations of α or β which give the same predictions, suggesting our model might not be able to distinguish between the two effects.

Finally, we repeated the nonlinear fit with the model without F_u (i.e. with α, β or C_o) using a range of initial guesses, to investigate how consistent our results were. Table 18 lists the values of the estimated parameters for each analysis where only one initial value has been changed (i.e. either α, β or C_o). Interestingly, the estimated parameters are similar for most of the proposed changes to the initial values. Only the tenfold decrease of the initial guess for β parameter caused a significant change in the estimated parameters as well as a decrease in the adjusted R^2 value (red highlights in Table 18). This repeatability of the results over a range of initial guesses suggests they correspond to the global solution, as suggested by our previous analysis showing only one minimum in the landscape of the sum squared differences in predicted and measured flow rates (Fig. 49).

	Original initial values	Increasing one initial value at a time by tenfold					
Optimal values	**C_o=α =0.01 β =-0.01 F_u=0**	**C_o =0.1**	**β=-0.1**	**α=0.1**	**C_o =0.001**	**β=-0.001**	**α=0.001**
C_o [µL/min.mmHg]	0.0170	0.0170	**-0.004**	0.0170	0.0170	0.0170	0.0170
β [mmHg $^{-1}$]	0.0257	0.0258	**-0.0471**	0.0257	0.0257	0.0257	0.0258
α[µL $^{-1}$]	0.0104	0.0104	**-0.9727**	0.0104	0.0104	0.0104	0.0104
Adjusted R^2	0.828	0.828	**0.44**	0.828	0.828	0.828	0.828

	Original initial values	Increasing one initial value at a time by tenfold					
Optimal values	**C_o=α =0.01 β =0.01 F_u=0**	**C_o =0.1**	**β=0.1**	**α=0.1**	**C_o =0.001**	**β=-0.001**	**α=0.001**
C_o [µL/min.mmHg]	0.0170	0.0170	0.0170	0.0170	0.0170	0.0170	0.0170
β [mmHg $^{-1}$]	0.0258	0.0258	0.0258	0.0258	0.0257	0.0258	0.0258
α[µL $^{-1}$]	0.0104	0.0104	0.0104	0.0104	0.0104	0.0104	0.0104
Adjusted R^2	0.828	0.828	0.828	0.828	0.828	0.828	0.828

Table 18: Values of the optimal values for the parameters from the nonlinear fit (with F_u=0) and adjusted R^2, when the initial value of either C_o, α, or β are increased or decreased10-fold. The first table uses negative values for β while the second table uses positive values. Only the increase in β seems to affect the estimated parameters as well as the adjusted R^2 value (shown in red). Note that in each case, α and C_o were statistically different from 0 but β was not.

3.2. Effects of gender/supplier and age on *C*

We also analysed the possible effects of gender and supplier on outflow facility, which could not be separated because all mice supplied by Jackson Laboratories were female whereas all mice provided by Charles River were male. Fig. 50 shows conventional facility seemed to be lower in female mice provided by Jackson Laboratories compared to males supplied by Charles River. The differences was statistically significant (p= 0.0086; unpaired t-test). Note that this is a meta-analysis pooling data acquired in ostensibly similar animals and experiments, which were however not performed at the same time. This should

therefore be confirmed by perfusing, at the same time, mouse eyes from either female or male C57BL/6 from the same supplier.

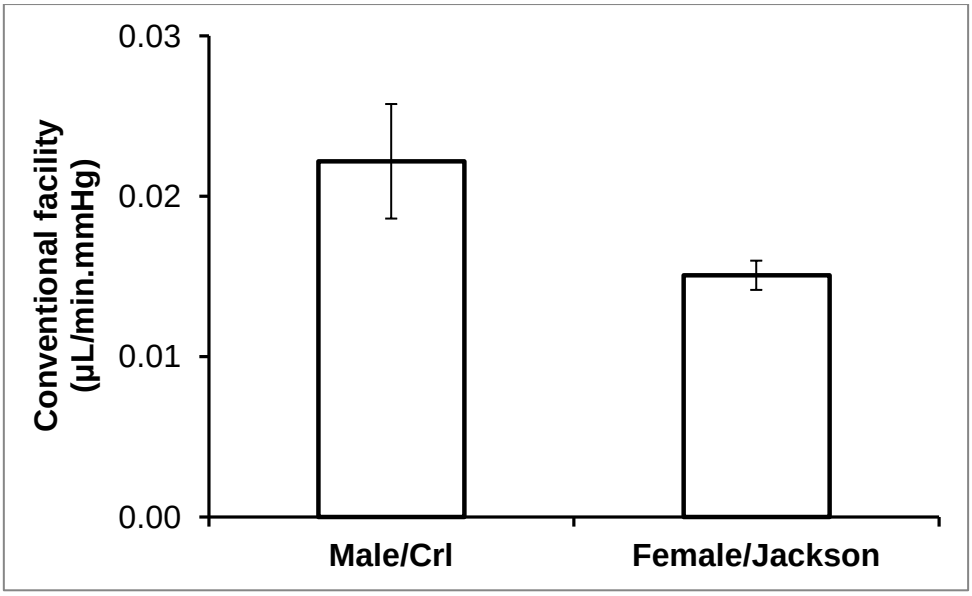

Figure 50: Conventional facility shown by gender or supplier. Bars are SEM. All male mice were supplied by Charles River (Crl) while all female animals were supplied by Jackson's laboratories.

Older animals seemed to show a decreased conventional facility, as shown by Fig. 51. Yet only 11% of the variability of our data could be explained by this correlation, which was not statistically significant (p = 0.14; two-sided t-test). No animals older than 30 weeks were used in any of our studies. Our results suggest facility could decrease by 1.2% per week (assuming the reference facility at birth is the intercept, i.e. 0.0249 µL/min.mmHg). We also show that most data points from young animals also correspond to male animals. Thus, in this study, they would have a higher conventional facility than females as observed previously (Fig. 50) Thus, the difference observed in conventional facility between genders could be attributed mostly to changes in age rather than gender. Inversely, the difference observed in conventional facility with age could be attributed to changes in gender.

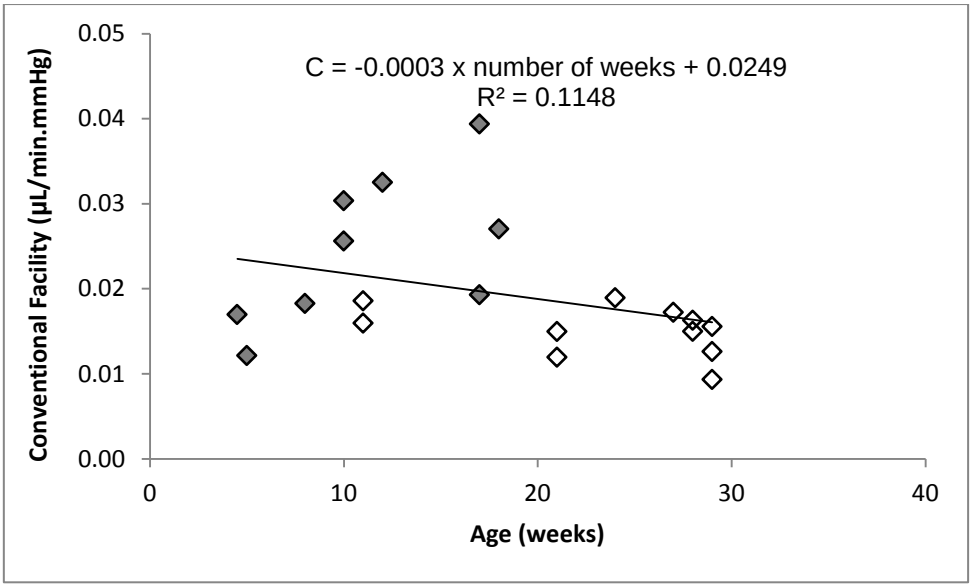

Figure 51: Conventional facility as a function of the age of the animal at the time of enucleation. Each data point represents conventional facility measured ex vivo in one eye of the animal. Data from only one eye per animal was used. Filled data points correspond to males, while empty diamonds belong to females.

4- Discussion

In this chapter, we modify Goldmann's equation to account for both pressure-dependent resistance and perfused volume effects. We show our data in enucleated mouse eyes is most specifically explained by volume rather than pressure effects. This however should be further investigated, as discussed below, especially in light of previous studies showing a lack of washout in mice[12] and the anterior chamber deepening we observed histologically (Chapter 6, Fig. 38). Alternatively, it is possible that our model is unable to distinguish between the two nonlinear effects because of the presence of points with both high IOP and high volumes perfused. Interestingly, our analysis shows the nonlinear effects of pressure or volume might artificially give rise to a non-zero intercept, or F_u. Thus, our findings suggest nonlinear volume effects should be taken into account in future perfusion studies to understand the actual contribution of F_u in mouse eyes. In any case, our work paves the way for a more generalized Goldmann's equation which could be used for perfusion studies in other species too.

In our analysis, we show that when F_u is set to zero, our data is best predicted by volume effects (i.e. only α, and not β, was statistically different from 0). Yet we also show that a range of values for α and β yield similar predictions, suggesting our data set might not be

able to distinguish between the two effects. This is likely caused by our dataset containing few points with either high pressure and low volume perfused, or low pressure and large volume perfused, while containing points having both high IOP and large perfused volumes. Data points with both a high IOP and large perfused volumes could have a high leverage on both estimated parameters α and β, and thus provide leverage on whichever effect is modeled. This is further supported by our separate analyses wherein either α or β were considered. In each case, the best nonlinear fit found that either volume or pressure effects explained our data (i.e. α or β were statistically different from 0). This should be therefore tested by fitting the model to data wherein each effect is represented independently, i.e. in eyes perfused at high pressures with low volumes or eyes at low pressure with large volumes.

Alternatively, perhaps pressure and volume effects on conventional facility interact, i.e. they affect each other. This was not modeled in our equations, and could therefore justify why our model fails to find specific parameters for both α and β that explain our data. Note however, that it was shown the washout rate did not change in bovine eyes at 6 vs. 15 mmHg[206]. This further suggests investigating whether such an interaction occurs in mice, by perfusing eyes at pressures subject to AC deepening or not, with a large volume of perfusate. Further, eyes perfused with small or large volumes at a high pressure prone to AC deepening would be analyzed morphologically as previously shown (Chapter 6) to investigate whether volume affects AC deepening.

The values found for C, β and α from the analyses which considered pressure and volume effect separately, or together when F_u was set to zero (Table 16) agreed well with previous reports from other species (Table 14&15). At 8 mmHg, conventional facility was 0.0141 µL/min.mmHg (calculated using Eq. 16, table 16), which is consistent with published values (0.005-0.018 µL/min.mmHg[5–11,14–16]). The parameter describing the change of conventional facility with pressure, β, was found to be 0.0257 $mmHg^{-1}$, which has the same order of magnitude of previously reported values for bovine or human eyes (0.012-0.1 $mmHg^{-1}$ [76]). Note however it is positive, suggesting a decrease in facility with pressure, unlike what was

observed in Cohort 12 (Chapter 6). Finally the parameter describing the washout rate, α, was found to be 0.0104 μL^{-1} which is larger than that found in bovine eyes (0.0003 μL^{-1} [206]). Assuming a typical perfusion rate of 8 µL/min in bovine eyes[150] at 10.7 mmHg (inferred from data in Gual's paper as the facility measurement, 0.73 uL/min.mmHg, multiplied by the perfusion pressure, 10.7 mmHg), this would correspond to a 14% increase in flow rates after 1 hr of perfusion at 11 mmHg, compared to an 8% increase in mouse eyes after 1 hr of perfusion at a rate physiological inflow rate of 0.13 µL/min at 8 mmHg (see Cohort 2). More specifically, this would represent a 1% increase in conventional facility per µL perfused in mice, or an estimated 26% over a typical perfusion where 25 µL of perfusate is injected. At 8 mmHg, this would result in the increase of flow rate from 0.123 µL/min (measured at 35 °C in eyes immersed in isotonic saline Fig. 11) to 0.155 µL/min after perfusing 25 µL. This increase of 0.032 µL/min could be too low to appreciate since it is in the range of the standard deviation of the flow rates at 8 mmHg which were 0.043 µL/min (Fig. 11). This could explain why no washout has been detected so far in mouse eyes.

It was interesting to observe that the parameters of our model became statistically different from 0 when α or β was set to zero, except for F_u. This suggests enucleated mouse eyes do not demonstrate unconventional outflow, as indicated by our previous findings in Chapter 2, wherein F_u was shown to disappear in eyes immersed in isotonic saline (Fig. 10). This could be consistent with the concept of unconventional outflow relying on uveal reabsorption[34]. More specifically, following enucleation and the stoppage of blood perfusion, there could be an equilibration of osmotic pressure across the uveal capillaries, thus stopping absorption of unconventional outflow into the uveal circulation. Note however F_u has been previously measured in enucleated human, monkey or porcine eyes [65,145,155]. Perhaps F_u still exists immediately after death but disappears as the osmotic pressure gradient across the uveal capillaries equilibrates in the lack of blood perfusion. Further, perhaps this equilibration occurs more quickly in the smaller mouse eye, thus leading to the extinction of F_u. This could possibly be tested by measuring aqueous humour outflow at different pressure levels in enucleated porcine eyes at different time points post mortem for

an extended period of time, in the hope of seeing a decrease in unconventional outflow with time associated with an equilibration of osmotic pressure across the uveal capillaries.

We also considered other effects such as age, supplier and gender in our meta-analysis. We observed a significant effect of gender or supplier on facility, although it is not clear whether they are both affecting outflow facility because all male animals in this study were provided by the same supplier, while all females were obtained from the other supplier. Although no study has examined gender-related differences in outflow facility, it has been shown IOP is higher in female patients[210,211], which could potentially correspond to a lower conventional facility, as observed in this study. Finally, the effects of age on outflow facility have never been measured in mice but it is known that facility decreases with age in humans[73,212,213]. Therefore, our data would agree with such results and further consolidate the mouse as a good model for human AH outflow.

In summary, we propose a novel equation to account for two important phenomena, namely washout and pressure effects on outflow facility. This represents an improvement which could be applied to eye perfusions in general. Yet, it did not seem to be particularly powerful for our data in enucleated mouse eyes. Rather, we found that only volume effects specifically explained our data. This however contradicts a previous study showing there is no washout in mice[12], and our findings about AC deepening occurring in mice at high pressures (Chapter 6). Thus we suggest our model is perhaps not able to differentiate between these effects with the current dataset for reasons described above. In addition, our model did not seem to explain the particularly high flow rates found in cohort 11. This suggests other effects might be at play, or perhaps this cohort of mice presented particular characteristics. Taken together, this suggests important variability in conventional facility can arise between mice either because of intrinsic (e.g. age, gender) or extrinsic (e.g. perfusion system or solution, success of cannulation) factors which are difficult to account for. This highlights the importance of studying conventional facility within cohorts of mice used under the most similar conditions possible, and makes post hoc comparisons between cohorts of mice from different studies more complex and unreliable.

Chapter 8: Conclusions

8.1. Summary

Throughout this project, we have developed the mouse as a valid and useful model for investigating IOP generation and regulation as occurs in the human conventional outflow pathway. Numerous studies were performed to improve our understanding of outflow resistance in the mouse eye, resulting in various interesting contributions described below.

We first presented an **improved perfusion system for measuring conventional outflow facility in enucleated mouse eyes in a physiologically-relevant manner**. More specifically, we included control of hydration and temperature of the tissue during perfusion. Conventional facility was shown to compare well to that previously measured in vivo[5–11,14–16], while unconventional outflow was shown to be highly influenced by hydration. This marked sensitivity of unconventional outflow to hydration prompted us to focus on conventional facility for the rest of the studies. Importantly, we showed that long post mortem times affect conventional facility as shown by a previous study[150], emphasizing the benefits of using mouse eyes which can be obtained immediately after death, as opposed to human eyes which are typically obtained up to 48 hrs post mortem[77]. In addition, we show paired mouse eyes have very similar conventional facility when measured within 3 hrs, so that one eye can be used as a control for its contralateral eye.

We then showed that **two receptor-mediated drugs (S1P, EP4 agonist 3,7-dithisPGE$_1$) either increased or decreased conventional facility in the mouse to a similar extent as the response reported in human eyes**[79,80,86]. This demonstrated the mouse acts as a suitable model for studying the pharmacology of human conventional facility, thereby encouraging its use for testing other drugs for preventing glaucoma. In addition, we show pharmacological effects are reduced by long post mortem times, confirming the importance of using fresh tissues for perfusion studies.

In a third study, we demonstrated that **different strains of mice (BALB/cJ, C57BL/6J, CBA/J) show distinct IOPs because of corresponding differences in conventional**

facility. This suggests conventional facility is an important determinant of IOP in mice, as observed in humans. Importantly, our results warrant further research into the genetic differences between the studied strains which could underlie their different conventional facilities.

In a fourth study, we provided the **first evidence of metabolic activity associated with outflow facility**. More specifically, our results suggested that 30% of conventional facility is dependent on metabolic energy. This represents a novel insight into the process of outflow facility generation, which has commonly been assumed to be passive[77,78].

In a fifth study, we provide data showing **conventional facility *increases* with pressure in mice**, as opposed to what happens in humans. Although initially worrisome for the validity of the mouse model, our histological analysis suggests this effect is probably explained by an artefact previously reported in humans, known as anterior chamber deepening[89,195]. Although this needs to be further investigated, it suggests the fact that conventional facility increases with pressure in mice is an artefact. This further suggests mice do not differ from humans and can continue to be used in perfusion studies. Note however preventing AC deepening in mouse eye perfusions might require non trivial protocol optimization. Lastly, we describe two novel protocols (Histo-Cutter[196] and Optical Projection Tomography[197]) which could pave the way for visualizing morphology and outflow patterns in 3D across the entire intact mouse eye.

Finally, we report a high variability in conventional facility between cohorts of mice, which we hypothesized might be caused by effects of perfusate volume or perfusion pressure. Thus, **we proposed modifications to Goldmann's equation** such that both pressure and volume effects on conventional facility are taken into account. Although the modified equation failed to account for the differences in flow rate between cohorts, it potentially explained better our data in the high pressure range. We show our data in enucleated mouse eyes is most specifically explained by volume rather than pressure effects, although this will require experimental evidence. This prompted us to investigate other effects which might explain the different conventional facility across cohorts, and we concluded that age

and gender may be important factors. Altogether, our data highlights the advantage of performing paired eye studies, wherein each eye is compared to its contralateral eye to minimize variability.

Overall, our findings emphasize the suitability of mice as models for studying the physiology and pharmacology of human conventional facility. We shed light on important phenomenon related to all mouse eye perfusions (both in vivo and ex vivo) which have been so far ignored (e.g. hydration or AC deepening) as well as factors which can influence conventional and unconventional outflow (Table 19). An open question remains about the nature of unconventional outflow in mice, which should be answered to ultimately determine whether it also mimics that of humans. Still, we also present novel tools which could be used to visualize unconventional outflow, so as to answer more fundamental questions related to AH outflow in mice.

	Conventional facility, *C*	**Unconventional outflow, F_u**
Hydration (Ch. 2)		More physiologic hydration decreases F_u
Temperature (Ch. 2)	Increasing temperature increases *C*	
Sphingosine-1-phosphate (Ch. 3)	Decreases *C*	
Dithia-PGE_4 (Ch. 3)	Increases *C*	
Metabolic inhibitors (Ch. 5)	Decrease *C*	
Anterior chamber deepening (Ch. 6)	Increases *C*	
Age (Ch. 7)	*Older mice have decreasing C*	
Gender (Ch. 7)	*Females have lower C*	

Table 19: Factors affecting conventional facility and unconventional outflow in mice. Age and gender effects are in italic because they were only indirectly suggested by our meta-analysis, and would need further testing. Next to each effect is written the chapter where it was reported. In addition, conventional facility was shown to depend on the strain of the mouse (Ch. 4).

8.2. Recommendations for future work

The data acquired during this project raises many interesting questions which could be answered with the technology validated in the present study. In this section, we propose a number of ideas for future work, each motivated by a different chapter.

8.2.1. Unconventional outflow

In Chapter 2, we showed unconventional outflow (F_u) was eliminated in enucleated mouse eyes immersed in isotonic saline. This warrants studies to elucidate the *role of unconventional outflow in mouse eyes*. Importantly, this raises questions both in vivo and ex vivo: first, what is the fraction of unconventional outflow in living mice, and second whether enucleation alters unconventional outflow.

A first interesting study would consist of testing whether hydration affects F_u in living mice, similarly to what we show in enucleated mouse eyes. Our data suggested F_u might have been an artefact from evaporation in enucleated mouse eyes. This could also occur in in vivo perfusion, wherein eyelids are typically maintained open for facilitating cannulation. This exposes a large portion of the cornea, which can potentially suffer from evaporation. Therefore, we suggest in vivo perfusions could be performed with and without PBS dropped onto the cornea to examine resulting changes in F_u.

On the other hand, outflow patterns through the unconventional pathway could be directly visualized by analyzing the trajectory of fluorescent tracers injected into the eye. Tracers could be perfused in eyes from anaesthetized animals, which could be imaged in 3D with OPT following death and enucleation as described in Chapter 6. More specifically, this would allow examining the hypothetical pathway for unconventional outflow through the ciliary muscle into the suprachoroidal space. However, this will require protocol optimization to better visualize the morphology of the limbus, but could eventually shed light into the existence of F_u in mouse eyes. Similarly, eyes perfused with tracers in vivo with and without hydration could confirm whether hydration affects outflow patterns in the unconventional pathway.

In order to understand the effects on F_u of enucleation and halting blood supply to the eye, we propose AH outflow is measured in vivo and compared to that of their contralateral enucleated eyes. Note AH outflow measurement in vivo would require the measurement of *EVP* or F_p, as done in previous studies[5,6].This should reveal whether F_u changes following death and enucleation. A previous study has shown F_u does not change immediately after

death in eyes which were left in the cadaveric mouse[6]. Yet, this does not per se provide information about what happens to of F_u following enucleation. This is important to ultimately validate our ex vivo model for unconventional outflow. Once more, perfusion studies using fluorescent tracers could be performed to reveal different outflow patterns in vivo vs. ex vivo to directly assess changes in unconventional outflow.

8.2.3. Studies on inter-strain differences in conventional facility

The finding that different strains of mice possess different conventional facility raises the possibility of corresponding morphological differences in the outflow pathways. For example, SC in BALB/cJ, C57BL/6J and CBA/J strains could be imaged and analysed so as to reveal whether there exist structural differences that could explain changes in conventional facility. This could be done with the Histo-cutter, as shown in Chapter 6, allowing the analysis of SC in 3D.

Finally, we also report an IOP in CBA/CaJ significantly lower than that reported by Savinova[141], which could stem from our mice being much younger than those used in that study (Chapter 4). Thus, our data motivates research into effects of age on IOP in mice. Similarly, our meta-analysis warrants research into the effects of age on conventional facility (Chapter 7). Our findings suggest conventional facility decreases with age, as observed in humans[73,212,213]. Furthermore, our post hoc analysis suggests conventional facility might be dependent on gender, or on the supplier, which could also be investigated.

8.2.4. Metabolic study

In Chapter 5, we show anti-metabolic agents (2-deoxy-D-glucose and sodium azide) decrease conventional facility. Strikingly, this contradicts a previous study which showed total outflow resistance was unaffected in bovine eyes by several anti-metabolic agents[78], even though one of the anti-metabolic agents was sodium azide, similar to the anti-metabolic agent we used. We propose the reason sodium azide did not affect outflow was because it targets only cellular respiration, which has been shown to provide a minimal amount of the energy requirements in the TM[192]. Similarly, we suggest the rest of the anti-metabolic agents used in that study[78] failed to inhibit ATP production as thoroughly as our anti-metabolic

agents. This could be further confirmed by measuring facility in mouse eyes perfused either with sodium azide alone, or sodium azide and 2-deoxy-D-glucose. We hypothesize sodium alone will not affect conventional facility, because it does not completely inhibit ATP production in the TM, unlike the combination of sodium azide and 2-deoxy-D-glucose. This would further consolidate our findings that conventional facility is indeed dependent on cellular metabolism, and explain the discrepancies with previous pioneering work.

8.2.5. AC deepening in mouse eyes

Perhaps most importantly, future studies will need to address the potential problem associated with AC deepening during perfusions in mice. In Chapter 6 we suggested AC deepening might be occurring in mouse eye perfusions, by showing the iris was pushed backwards at high pressures. This is known to happen when the posterior chamber is not pressurized during perfusions in eyes from other species[89,195]. Therefore, procedures performed in humans to prevent AC deepening could be replicated in mice, such as inserting the needle in the posterior chamber or performing iridotomy. The aim would be to show these procedures have prevented AC deepening by measuring AH outflow and imaging the irido-corneal angle. For example, AH outflow could be measured in an eye cannulated in the posterior chamber and compared to its fellow eye cannulated in the AC. The aim would be to show lower flow rates occur at high pressures in the eye cannulated in the posterior chamber because of a lack of AC deepening. In addition to measuring AH outflow, we could analyse the morphology of the AC of eyes pressurized in the posterior or anterior chamber, as done in Chapter 6. This would confirm whether we have indeed prevented the opening of the irido-corneal angle.

Unfortunately the very small size of mouse eyes will make such procedures extremely challenging. If so, that could mean mouse eyes should only be perfused within the pressure range immune to such artificial AC deepening effects. In other words, this unconsidered phenomenon could pose a major problem for the utility of mouse eye perfusions.

Appendix 1: List of cohorts for each chapter

This table summarizes the effect tested and solutions perfused in either control or experimental enucleated mouse eyes per cohort. DBG stands for PBS with 5.5 mM glucose, BSA for bovine serum albumin and PFA for Paraformaldehyde. The details of each study and compound can be found in the corresponding chapter.

Chapter	Cohort	Effect tested on *C*	Control eye	Experimental eye
2	1	Hydration	DBG	DBG
	2	Temperature	DBG	DBG
	3 A	3 hrs post mortem time in PBS	DBG	DBG
	3 B	24 hrs post mortem time in PBS	DBG	DBG
	3C	24 hrs post mortem time in DMEM	DBG	DBG
3	4	S1P	BSA+DBG+S1P	BSA+S1P
	5A	W146 on S1P	BSA +DBG + S1P	BSA +DBG + S1P+ W146
	5B	JTE-013 on S1P	BSA +DBG + S1P	BSA +DBG + S1P+ JTE-013
	5C	JTE-013 alone	DBG	DBG+JTE-013
	6A	dithia-PGE_1	DBG	DBG+ dithia-PGE_1
	6B	dithia-PGE_1 24 hrs post mortem time	DBG	DBG+ dithia-PGE_1
4	7	Difference between strains of mice (CBA/J, BALB/cJ, C57BL/6J)	DBG	-
	8		DBG	-
	9		DBG	-
5	10	Anti-metabolic agents at 20 vs. 35°C	2-deoxy-D-glucose + sodium azide	2-deoxy-D-glucose + sodium azide
	11	Anti-metabolic agents at 35°C	DBG	2-deoxy-D-glucose + sodium azide
6	12	High pressures	DBG	-

Appendix 2: Permission documents for republishing third party works

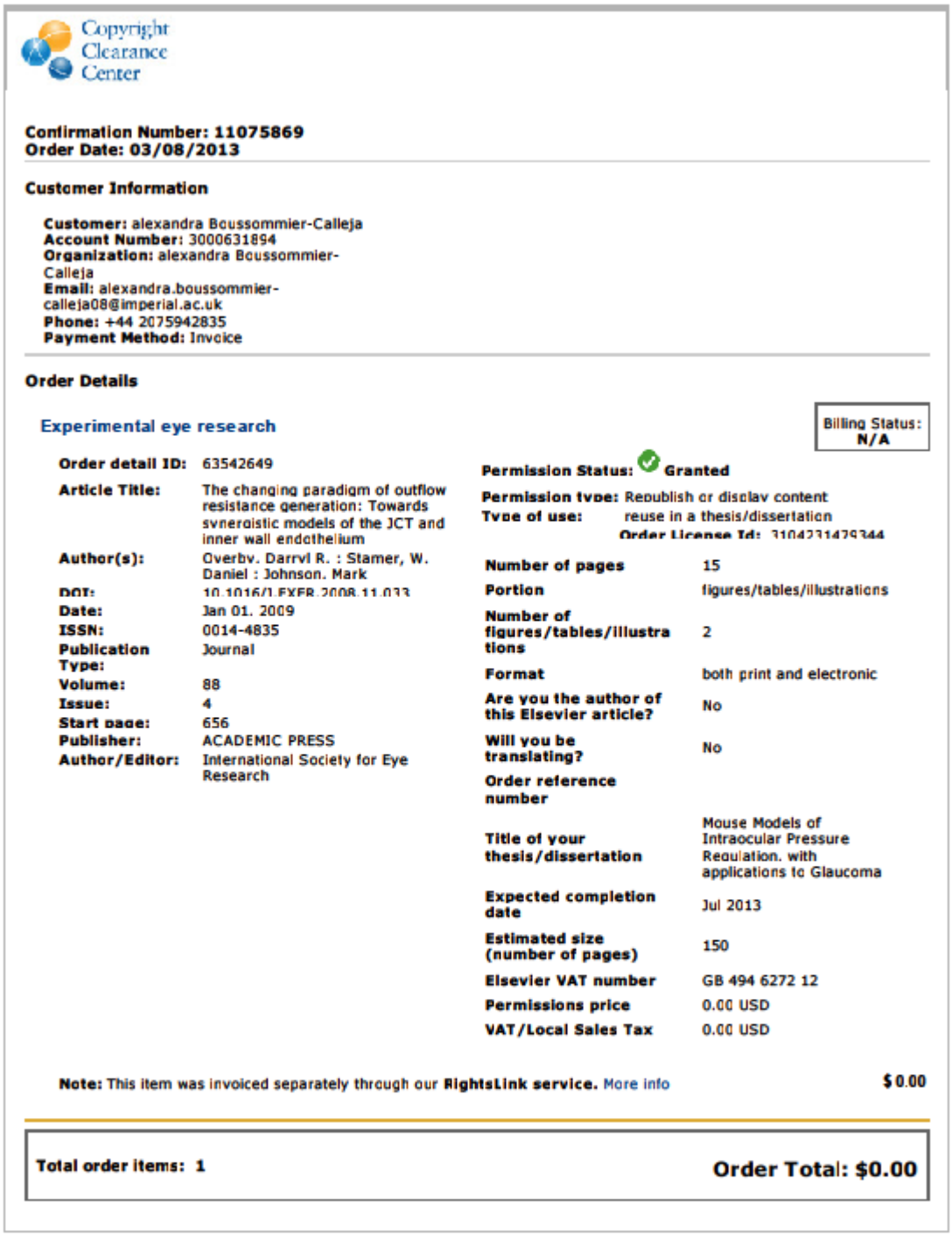

Copyright Clearance Center

Confirmation Number: 11075869
Order Date: 03/08/2013

Customer Information

Customer: alexandra Boussommier-Calleja
Account Number: 3000631894
Organization: alexandra Boussommier-Calleja
Email: alexandra.boussommier-calleja08@imperial.ac.uk
Phone: +44 2075942835
Payment Method: Invoice

Order Details

Experimental eye research

Billing Status: N/A

Order detail ID:	63542649
Article Title:	The changing paradigm of outflow resistance generation: Towards synergistic models of the JCT and inner wall endothelium
Author(s):	Overby, Darryl R. : Stamer, W. Daniel : Johnson, Mark
DOI:	10.1016/J.EXER.2008.11.033
Date:	Jan 01, 2009
ISSN:	0014-4835
Publication Type:	Journal
Volume:	88
Issue:	4
Start page:	656
Publisher:	ACADEMIC PRESS
Author/Editor:	International Society for Eye Research

Permission Status: Granted
Permission type: Republish or display content
Type of use: reuse in a thesis/dissertation
Order License Id: 3104231479344

Number of pages	15
Portion	figures/tables/illustrations
Number of figures/tables/illustrations	2
Format	both print and electronic
Are you the author of this Elsevier article?	No
Will you be translating?	No
Order reference number	
Title of your thesis/dissertation	Mouse Models of Intraocular Pressure Regulation, with applications to Glaucoma
Expected completion date	Jul 2013
Estimated size (number of pages)	150
Elsevier VAT number	GB 494 6272 12
Permissions price	0.00 USD
VAT/Local Sales Tax	0.00 USD

Note: This item was invoiced separately through our **RightsLink service.** More info **$0.00**

Total order items: 1 **Order Total: $0.00**

Get Permission | License Your Content | Products And Solutions | Partners | Education | About Us
Privacy Policy | Terms & Conditions

Copyright Clearance Center

Confirmation Number: 11087694
Order Date: 04/23/2013

Customer Information

Customer: alexandra Boussommier-Calleja
Account Number: 3000631894
Organization: alexandra Boussommier-Calleja
Email: alexandra.boussommier-calleja08@imperial.ac.uk
Phone: +44 2075942835
Payment Method: Invoice

Order Details

Experimental eye research

Billing Status: **N/A**

Order detail ID:	63619947
Article Title:	The trabecular meshwork outflow pathways: Structural and functional aspects
Author(s):	Tamm, Ernst R.
DOI:	10.1016/J.EXER.2009.02.007
Date:	Jan 01, 2009
ISSN:	0014-4835
Publication Type:	Journal
Volume:	88
Issue:	4
Start page:	648
Publisher:	ACADEMIC PRESS
Author/Editor:	International Society for Eye Research

Permission Status: **Granted**
Permission type: Republish or display content
Type of use: reuse in a thesis/dissertation
Order License Id: 3134830952820

Number of pages	8
Portion	figures/tables/illustrations
Number of figures/tables/illustrations	1
Format	both print and electronic
Are you the author of this Elsevier article?	No
Will you be translating?	No
Order reference number	
Title of your thesis/dissertation	Mouse Models of Intraocular Pressure Regulation, with applications to Glaucoma
Expected completion date	Jul 2013
Estimated size (number of pages)	150
Elsevier VAT number	GB 494 6272 12
Permissions price	0.00 USD
VAT/Local Sales Tax	0.00 USD

Note: This item was invoiced separately through our **RightsLink service.** More info **$ 0.00**

Total order items: 1 **Order Total: $0.00**

Copyright Clearance Center

Confirmation Number: 11075871
Order Date: 03/08/2013

Customer Information

Customer: alexandra Boussommier-Calleja
Account Number: 3000631894
Organization: alexandra Boussommier-Calleja
Email: alexandra.boussommier-calleja08@imperial.ac.uk
Phone: +44 2075942835
Payment Method: Invoice

Order Details

Experimental eye research

Billing Status: **N/A**

Order detail ID:	63542657
Article Title:	The mechanism of increasing outflow facility by rho-kinase inhibition with Y-27632 in bovine eyes
Author(s):	Lu, Zhaozeng ; et al
DOI:	10.1016/J.EXER.2007.10.018
Date:	Jan 01, 2008
ISSN:	0014-4835
Publication Type:	Journal
Volume:	86
Issue:	2
Start page:	271
Publisher:	ACADEMIC PRESS
Author/Editor:	International Society for Eye Research

Permission Status: Granted
Permission type: Republish or display content
Type of use: reuse in a thesis/dissertation
Order License Id: 3104240254452

Number of pages	11
Portion	figures/tables/illustrations
Number of figures/tables/illustrations	1
Format	both print and electronic
Are you the author of this Elsevier article?	No
Will you be translating?	No
Order reference number	
Title of your thesis/dissertation	Mouse Models of Intraocular Pressure Regulation, with applications to Glaucoma
Expected completion date	Jul 2013
Estimated size (number of pages)	150
Elsevier VAT number	GB 494 6272 12
Permissions price	0.00 USD
VAT/Local Sales Tax	0.00 USD

Note: This item was invoiced separately through our **RightsLink service.** More info **$0.00**

Total order items: 1 **Order Total: $0.00**

RE: permission for reproducing my paper in my thesis

Debbie Chin [dchin@arvo.org]
Date d'envoi : vendredi 8 mars 2013 16:02
À : Boussommier-Calleja, Alexandra

Dear Dr. Boussommier-Calleja,

Permission is hereby granted to reprint the following article in your thesis for Imperial College London:

Boussommier-Calleja A, Bertrand J, Woodward DF, Ethier CR, Stamer WD, Overby DR. Pharmacologic manipulation of conventional outflow facility in ex vivo mouse eyes. Invest Ophthalmol Vis Sci. 2012;53:5838-5845.

A reprint of this material must include a full article citation and acknowledge ARVO as the copyright holder.

Best regards,
Debbie Chin

Association for Research in Vision and Ophthalmology
1801 Rockville Pike, Suite 400
Rockville MD 20852 USA
Direct: +1.240.221.2926 | Main: +1.240.221.2900 | Fax: +1.240.221.0370
www.arvo.org

From: Boussommier-Calleja, Alexandra [mailto:alexandra.boussommier-calleja08@imperial.ac.uk]
Sent: Friday, March 08, 2013 9:39 AM
To: Debbie Chin
Subject: permission for reproducing my paper in my thesis

Dear Miss Chin,

I am writing my thesis and want to include a paper I have published in IOVS as originally printed. Do I need to ask for the journal's permission? Since I need to submit my thesis in less than a month, can you please let me know what I need to do to obtain it before that?

Bibliography

1. Quigley, H. a Glaucoma. *Lancet* **377**, 1367–77 (2011).

2. Grant, W. M. Clinical measurements of aqueous outflow. *A.M.A. archives of ophthalmology* **46**, 113–31 (1951).

3. Brubaker, R. F. Targeting Outflow Facility in Glaucoma Management. *Survey of Ophthalmology* **48**, S17–S20 (2003).

4. John, S. W., Anderson, M. G. & Smith, R. S. Mouse genetics: a tool to help unlock the mechanisms of glaucoma. *Journal of glaucoma* **8**, 400–12 (1999).

5. Aihara, M. Aqueous Humor Dynamics in Mice. *Investigative Ophthalmology & Visual Science* **44**, 5168–5173 (2003).

6. Millar, J. C., Clark, A. F. & Pang, I.-H. Assessment of aqueous humor dynamics in the mouse by a novel method of constant-flow infusion. *Investigative ophthalmology & visual science* **52**, 685–94 (2011).

7. Saeki, T., Ota, T., Aihara, M. & Araie, M. Effects of prostanoid EP agonists on mouse intraocular pressure. *Investigative ophthalmology & visual science* **50**, 2201–8 (2009).

8. Zhang, Y. *et al.* Enhanced inflow and outflow rates despite lower IOP in bestrophin-2-deficient mice. *Investigative ophthalmology & visual science* **50**, 765–70 (2009).

9. Zhang, D., Vetrivel, L. & Verkman, a S. Aquaporin deletion in mice reduces intraocular pressure and aqueous fluid production. *The Journal of general physiology* **119**, 561–9 (2002).

10. Crowston, J. G. Effect of Latanoprost on Outflow Facility in the Mouse. *Investigative Ophthalmology & Visual Science* **45**, 2240–2245 (2004).

11. Camras, L. J. *et al.* Duration of anesthesia affects intraocular pressure, but not outflow facility in mice. *Current eye research* **35**, 819–27 (2010).

12. Lei, Y., Overby, D. R., Boussommier-Calleja, A., Stamer, W. D. & Ethier, C. R. Outflow physiology of the mouse eye: pressure dependence and washout. *Investigative ophthalmology & visual science* **52**, 1865–71 (2011).

13. Stamer, W. D., Lei, Y., Boussommier-Calleja, A., Overby, D. R. & Ethier, C. R. eNOS, a pressure-dependent regulator of intraocular pressure. *Investigative ophthalmology & visual science* **52**, 9438–44 (2011).

14. Shepard, A. R. *et al.* Adenoviral gene transfer of active human transforming growth factor-{beta}2 elevates intraocular pressure and reduces outflow facility in rodent eyes. *Investigative ophthalmology & visual science* **51**, 2067–76 (2010).

15. Lee, Y. S. *et al.* Regulation of anterior chamber drainage by bicarbonate-sensitive soluble adenylyl cyclase in the ciliary body. *The Journal of biological chemistry* **286**, 41353–8 (2011).

16. Dai, Y. *et al.* Outflow facility in mice with a targeted type I collagen mutation. *Investigative ophthalmology & visual science* **50**, 5749–53 (2009).

17. Kumar, S., Shah, S., Deutsch, E. R., Tang, H. M. & Danias, J. Triamcinolone acetonide decreases outflow facility in C57BL/6 mouse eyes. *Investigative ophthalmology & visual science* **54**, 1280–7 (2013).

18. Gabelt, B. T. & Kaufman, P. L. Aqueous humor hydrodynamics. *Adler's Physiology of the eye. Clinical application.* 237–289 (2003).

19. Alexander, P. & Ramirez-Florez, S. Hypotony and choroidal detachment as a complication of travoprost after trabeculectomy surgery. *Eye (London, England)* **22**, 736–7 (2008).

20. Kerr, J., Nelson, P. & O'Brien, C. Pulsatile ocular blood flow in primary open-angle glaucoma and ocular hypertension. *American Journal of Ophthalmology* **136**, 1106–1113 (2003).

21. Drance, S. M. The significance of the diurnal tension variations in normal and glaucomatous eyes. *Archives of ophthalmology* **64**, 494–501 (1960).

22. Bengtsson, B. & Heijl, A. Diurnal IOP fluctuation: not an independent risk factor for glaucomatous visual field loss in high-risk ocular hypertension. *Graefe's archive for clinical and experimental ophthalmology* **243**, 513–8 (2005).

23. Olsen, T. W., Aaberg, S. Y., Geroski, D. H. & Edelhauser, H. F. Human sclera: thickness and surface area. *American journal of ophthalmology* **125**, 237–41 (1998).

24. Edelhauser, H. F. & Ubels, J. L. The cornea and the sclera. *Adler's Physiology of the eye. Clinical application.* 47–114 (2003).

25. Guyton, A. C. & Hall, J. E. The Eye:I. optics of vision. *Textbook of medical physiology* 566–577 (2000).

26. Khurana, A. K. & Khurana, I. Cornea, Limbus and Sclera. *Anatomy and Physiology of the Eye* 22–42 (2006).

27. Beebe, D. C. The lens. *Adler's Physiology of the eye. Clinical application.* 117–158 (2003).

28. Kardon, R. The pupil. *Adler's Physiology of the eye. Clinical application.* 713–743 (2003).

29. Tamm, E. R. & Lütjen-Drecoll, E. Ciliary body. *Microscopy research and technique* **33**, 390–439 (1996).

30. Glasser, A. & Kaufman, P. L. Accomodation and presbyopia. *Adler's Physiology of the eye. Clinical application.* 197–233 (2003).

31. Lund-andersen, H. & Sander, B. The vitreous. *Adler's Physiology of the eye. Clinical application.* 293–316 (2003).

32. Cioffi, G. A., Granstam, E. & Alm, A. Ocular circulation. *Adler's Physiology of the eye. Clinical application.* 747–784 (2003).

33. Van der Merwe, E. L. & Kidson, S. H. Advances in imaging the blood and aqueous vessels of the ocular limbus. *Experimental eye research* **91**, 118–26 (2010).

34. Pederson, J. E., Gaasterland, D. E. & MacLellan, H. M. Uveoscleral aqueous outflow in the rhesus monkey: importance of uveal reabsorption. *Investigative ophthalmology & visual science* **16**, 1008–7 (1977).

35. Johnson, M. *et al.* The Pore Density in the Inner Wall Endothelium of Schlemm ' s Canal of Glaucomatous Eyes. 2950–2955 (2002).

36. Sultan, M. & Blondeau, P. Episcleral venous pressure in younger and older subjects in the sitting and supine positions. *Journal of glaucoma* **12**, 370–3 (2003).

37. Johnson, D. H. & Johnson, M. How does nonpenetrating glaucoma surgery work? Aqueous outflow resistance and glaucoma surgery. *Journal of Glaucoma* **10**, 67–70 (2002).

38. Johnson, M. "What controls aqueous humour outflow resistance?". *Experimental Eye Research* **82**, 545–557 (2006).

39. Overby, D. R., Stamer, W. D. & Johnson, M. The changing paradigm of outflow resistance generation: towards synergistic models of the JCT and inner wall endothelium. *Experimental Eye Research* **88**, 656–670 (2009).

40. Gong, H., Tripathi, R. C. & Tripathi, B. J. Morphology of the aqueous outflow pathway. *Microscopy research and technique* **33**, 336–67 (1996).

41. Tripathi, R. C. Aqueous outflow pathway in normal and glaucomatous eyes. *British Journal of Ophthalmology* **56**, 157–174 (1972).

42. Tamm, E. R. The trabecular meshwork outflow pathways: structural and functional aspects. *Experimental eye research* **88**, 648–55 (2009).

43. Tripathi, C. R. Comparative physiology and anatomy of the aqueous outflow pathway. *The Eye* 163–356 (1974).

44. Rohen, J. W., Futa, R. & Lutjen-drecoll, E. The fine structure of the cribriform meshwork in normal and glaucomatous eyes as seen in tangential sections. 574–585 (1981).

45. Llobet, A., Gasull, X. & Gual, A. Understanding trabecular meshwork physiology: a key to the control of intraocular pressure? *News in physiological sciences* **18**, 205–9 (2003).

46. Coroneo, M. T. *et al.* Electrical and morphological evidence for heterogeneous populations of cultured bovine trabecular meshwork cells. *Experimental eye research* **52**, 375–88 (1991).

47. Wiederholt, M., Thieme, H. & Stumpff, F. The regulation of trabecular meshwork and ciliary muscle contractility. *Progress in retinal and eye research* **19**, 271–95 (2000).

48. Selbach, J. M., Gottanka, J., Wittmann, M. & Lu, E. Efferent and Afferent Innervation of Primate Trabecular AND. **41**, 2184–2191 (2000).

49. Ruskell, G. L. The source of nerve fibres of the trabeculae and adjacent structures in monkey eyes. *Experimental eye research* **23**, 449–59 (1976).

50. Tamm, E., Flügel, C., Stefani, F. H. & Rohen, J. W. Contractile cells in the human scleral spur. *Experimental eye research* **54**, 531–43 (1992).

51. Tamm, E. R., Koch, T. A., Mayer, B., Stefani, F. H. & Lütjen-Drecoll, E. Innervation of myofibroblast-like scleral spur cells in human monkey eyes. *Investigative ophthalmology & visual science* **36**, 1633–44 (1995).

52. Lütjen-Drecoll, E. Functional morphology of the trabecular meshwork in primate eyes. *Progress in retinal and eye research* **18**, 91–119 (1999).

53. Rohen, J. W. & Van der Zypen, E. The phagocytic activity of the trabecularmeshwork endothelium. An electron-microscopic study of the vervet (Cercopithecus aethiops). *Albrecht von Graefe's archive for clinical and experimental ophthalmology* **175**, 143–60 (1968).

54. Gasiorowski, J. Z. & Russell, P. Biological properties of trabecular meshwork cells. *Experimental Eye Research* **88**, 671–675 (2009).

55. Hann, C. R., Bentley, M. D., Vercnocke, A., Ritman, E. L. & Fautsch, M. P. Imaging the aqueous humor outflow pathway in human eyes by three-dimensional micro-computed tomography (3D micro-CT). *Experimental eye research* **92**, 104–11 (2011).

56. Allingham, R. R., De Kater, A. W. & Ethier, C. R. Schlemm's canal and primary open angle glaucoma: correlation between Schlemm's canal dimensions and outflow facility. *Experimental eye research* **62**, 101–9 (1996).

57. Grierson, I., Lee, W. R., Abraham, S. & Howes, R. C. Associations between the cells of the walls of Schlemm's canal. *Albrecht von Graefe's archive for clinical and experimental ophthalmology* **208**, 33–47 (1978).

58. Johnstone, M. A. Pressure-dependent changes in nuclei and the process origins of the endothelial cells lining Schlemm's canal. 44–51 (1979).

59. Ethier, C. R., Coloma, F. M., Sit, A. J. & Johnson, M. Two pore types in the inner-wall endothelium of Schlemm's canal. *Investigative ophthalmology & visual science* **39**, 2041–8 (1998).

60. Allingham, R. R. *et al.* The relationship between pore density and outflow facility in human eyes. *Investigative ophthalmology & visual science* **33**, 1661–9 (1992).

61. Bill, A. & Svedbergh, B. Scanning electron microscopic studies of the trabecular meshwork and the canal of Schlemm--an attempt to localize the main resistance to outflow of aqueous humor in man. *Acta ophthalmologica* **50**, 295–320 (1972).

62. Sit, A. J., Coloma, F. M., Ethier, C. R. & Johnson, M. Factors Affecting the Pores of the Inner Wall Endothelium of Schlemm ' s Canal. **38**, 1517–1525 (1997).

63. Ashton, N. Anatomical study of Schlemm's canal and aqueous veins by means of neoprene casts. II. Aqueous veins. *The British journal of ophthalmology* **36**, 265–7; contd (1952).

64. Bill, A. The aqueous humor drainage mechanism in the cynomolgus monkey (Macaca irus) with evidence for unconventional routes. *Investigative ophthalmology* **4**, 911–9 (1965).

65. Bill, A. Conventional and uveo-scleral drainage of aqueous humour in the cynomolgus monkey (Macaca irus) at normal and high intraocular pressures. *Experimental eye research* **5**, 45–54 (1966).

66. Inomata, H., Bill, A. & Smelser, G. K. Unconventional routes of aqueous humor outflow in Cynomolgus monkey (Macaca irus). *American journal of ophthalmology* **73**, 893–907 (1972).

67. Inomata, H. & Bill, A. Exit sites of uveoscleral flow of aqueous humor in cynomolgus monkey eyes. *Experimental eye research* **25**, 113–8 (1977).

68. Pederson, J. E. & Toris, C. B. Uveoscleral outflow: diffusion or flow? *Investigative ophthalmology & visual science* **28**, 1022–4 (1987).

69. Alm, A. & Nilsson, S. F. E. Uveoscleral outflow--a review. *Experimental eye research* **88**, 760–8 (2009).

70. Yücel, Y. H. *et al.* Identification of lymphatics in the ciliary body of the human eye: a novel "uveolymphatic" outflow pathway. *Experimental eye research* **89**, 810–9 (2009).

71. Birke, K., Lütjen-Drecoll, E., Kerjaschki, D. & Birke, M. T. Expression of podoplanin and other lymphatic markers in the human anterior eye segment. *Investigative ophthalmology & visual science* **51**, 344–54 (2010).

72. Nilsson, S. F. The uveoscleral outflow routes. *Eye (London, England)* **11 (Pt 2)**, 149–54 (1997).

73. Toris, C. B., Yablonski, M. E., Wang, Y. L. & Camras, C. B. Aqueous humor dynamics in the aging human eye. *American journal of ophthalmology* **127**, 407–12 (1999).

74. Brubaker, R. F. The measurement of pseudofacility and true facility by constant pressure perfusion in the normal rhesus monkey eye. *Investigative ophthalmology* **9**, 42–52 (1970).

75. Mäepea, O. & Bill, a The pressures in the episcleral veins, Schlemm's canal and the trabecular meshwork in monkeys: effects of changes in intraocular pressure. *Experimental eye research* **49**, 645–63 (1989).

76. Brubaker, R. F. The effect of intraocular pressure on conventional outflow resistance in the enucleated human eye. *Investigative ophthalmology* **14**, 286–92 (1975).

77. VanBuskirk, E. M. & Grant, W. M. Influence of temperature and the question of involvement of cellular metabolism in aqueous outflow. *American journal of ophthalmology* **77**, 565–72 (1974).

78. Bárány, E. H. In vitro studies of the resistance to flow through the angle of the anterior chamber. *Acta Societatis Medicorum Upsaliensis* **59**, 260–76 (1954).

79. Boussommier-Calleja, A. *et al.* Pharmacologic manipulation of conventional outflow facility in ex vivo mouse eyes. *Investigative ophthalmology & visual science* **53**, 5838–45 (2012).

80. Stamer, W. D., Read, a T., Sumida, G. M. & Ethier, C. R. Sphingosine-1-phosphate effects on the inner wall of Schlemm's canal and outflow facility in perfused human eyes. *Experimental eye research* **89**, 980–8 (2009).

81. Mettu, P. S. Role of Lysophospholipid Growth Factors in the Modulation of Aqueous Humor Outflow Facility. *Investigative Ophthalmology & Visual Science* **45**, 2263–2271 (2004).

82. Sumida, G. M. & Stamer, W. D. $S1P_2$ receptor regulation of sphingosine-1-phosphate effects on conventional outflow physiology. *American journal of physiology. Cell physiology* **300**, C1164–71 (2011).

83. Sumida, G. M. & Stamer, W. D. Sphingosine-1-phosphate enhances cortical actomyosin organization in cultured human Schlemm ' s canal endothelial cell monolayers. 1–28 (2010).

84. Rao, P. V, Deng, P. F., Kumar, J. & Epstein, D. L. Modulation of aqueous humor outflow facility by the Rho kinase-specific inhibitor Y-27632. *Investigative ophthalmology & visual science* **42**, 1029–37 (2001).

85. Hoffman, E. A., Perkumas, K. M., Highstrom, L. M. & Stamer, W. D. Regulation of myocilin-associated exosome release from human trabecular meshwork cells. *Investigative ophthalmology & visual science* **50**, 1313–8 (2009).

86. Millard, L. H., Woodward, D. F. & Stamer, W. D. The role of the prostaglandin EP4 receptor in the regulation of human outflow facility. *Investigative ophthalmology & visual science* **52**, 3506–13 (2011).

87. Woodward, D. F. *et al.* Prostanoid EP4 receptor stimulation produces ocular hypotension by a mechanism that does not appear to involve uveoscleral outflow. *Investigative ophthalmology & visual science* **50**, 3320–8 (2009).

88. McEwen, W. K. Application of Poiseuille's law to aqueous outflow. *A.M.A. archives of ophthalmology* **60**, 290–4 (1958).

89. Grant, W. M. Experimental aqueous perfusion in enucleated human eyes. *Archives of ophthalmology* **69**, 783–801 (1963).

90. Ethier, C. R., Kamm, R. D., Palaszewski, B. a, Johnson, M. C. & Richardson, T. M. Calculations of flow resistance in the juxtacanalicular meshwork. *Investigative ophthalmology & visual science* **27**, 1741–50 (1986).

91. Keller, K. E., Bradley, J. M., Kelley, M. J. & Acott, T. S. Effects of modifiers of glycosaminoglycan biosynthesis on outflow facility in perfusion culture. *Investigative ophthalmology & visual science* **49**, 2495–505 (2008).

92. Gong, H., Ruberti, J., Overby, D., Johnson, M. & Freddo, T. F. A New View of the Human Trabecular Meshwork Using Quick-freeze, Deep-etch Electron Microscopy. *Experimental Eye Research* **75**, 347–358 (2002).

93. Bradley, J. M. *et al.* Effect of matrix metalloproteinases activity on outflow in perfused human organ culture. *Investigative ophthalmology & visual science* **39**, 2649–58 (1998).

94. Grierson, I. & Lee, W. R. Pressure-induced changes in the ultrastructure of the endothelium lining Schlemm's canal. *American journal of ophthalmology* **80**, 863–84 (1975).

95. Grierson, I. & Lee, W. R. Pressure effects on flow channels in the lining endothelium of Schlemm's canal. A quantitative study by transmission electron microscopy. *Acta ophthalmologica* **56**, 935–52 (1978).

96. Lee, W. R. & Grierson, I. Pressure effects on the endothelium of the trabecular wall of Schlemm's canal: a study by scanning electron microscopy. *Albrecht von Graefe's archive for clinical and experimental ophthalmology* **196**, 255–65 (1975).

97. Svedbergh Bjorn Effects of intraocular pressure on the pores of the inner wall of Schlemm's canal: A scanning electronmicroscopic study. *Japanese Journal of Ophtalmology* **20**, 127 (1976).

98. Rosenquist, R., Epstein, D., Melamed, S., Johnson, M. & Grant, W. M. Outflow resistance of enucleated human eyes at two different perfusion pressures and different extents of trabeculotomy. *Current eye research* **8**, 1233–40 (1989).

99. Johnson, M., Shapiro, a, Ethier, C. R. & Kamm, R. D. Modulation of outflow resistance by the pores of the inner wall endothelium. *Investigative Ophthalmology & Visual Science* **33**, 1670–1675 (1992).

100. Hamanaka, T. & Bill, A. Morphological and functional effects of Na2EDTA on the outflow routes for aqueous humor in monkeys. *Experimental eye research* **44**, 171–90 (1987).

101. Bahler, C. K., Hann, C. R., Fautsch, M. P. & Johnson, D. H. Pharmacologic disruption of Schlemm's canal cells and outflow facility in anterior segments of human eyes. *Investigative Ophthalmology & Visual Science* **45**, 2246–2254 (2004).

102. Zhang, Y., Toris, C. B., Liu, Y., Ye, W. & Gong, H. Morphological and hydrodynamic correlates in monkey eyes with laser induced glaucoma. *Experimental eye research* **89**, 748–56 (2009).

103. Battista, S. a *et al.* Reduction of the available area for aqueous humor outflow and increase in meshwork herniations into collector channels following acute IOP elevation in bovine eyes. *Investigative ophthalmology & visual science* **49**, 5346–52 (2008).

104. Lu, Z., Overby, D. R., Scott, P. a, Freddo, T. F. & Gong, H. The mechanism of increasing outflow facility by rho-kinase inhibition with Y-27632 in bovine eyes. *Experimental eye research* **86**, 271–81 (2008).

105. Quigley, H. a & Broman, a T. The number of people with glaucoma worldwide in 2010 and 2020. *The British journal of ophthalmology* **90**, 262–7 (2006).

106. Poulsen, P. B., Buchholz, P., Walt, J. G., Christensen, T. L. & Thygesen, J. Cost analysis of glaucoma-related-blindness in Europe. *International Congress Series* **1282**, 262–266 (2005).

107. Rein, D. B. *et al.* The economic burden of major adult visual disorders in the United States. *Archives of ophthalmology* **124**, 1754–60 (2006).

108. Suzuki, Y. *et al.* Risk factors for open-angle glaucoma in a Japanese population: the Tajimi Study. *Ophthalmology* **113**, 1613–7 (2006).

109. Bengtsson, B. & Heijl, A. A long-term prospective study of risk factors for glaucomatous visual field loss in patients with ocular hypertension. *Journal of glaucoma* **14**, 135–8 (2005).

110. Downs, J. C. *et al.* 24-hour IOP telemetry in the nonhuman primate: implant system performance and initial characterization of IOP at multiple timescales. *Investigative ophthalmology & visual science* **52**, 7365–75 (2011).

111. Asrani, S. *et al.* Large diurnal fluctuations in intraocular pressure are an independent risk factor in patients with glaucoma. *Journal of glaucoma* **9**, 134–42 (2000).

112. Jonas, J. B., Budde, W. M., Stroux, A., Oberacher-Velten, I. M. & Jünemann, A. Diurnal intraocular pressure profiles and progression of chronic open-angle glaucoma. *Eye (London, England)* **21**, 948–51 (2007).

113. Quaranta, L., Katsanos, A., Russo, A. & Riva, I. 24-Hour Intraocular Pressure and Ocular Perfusion Pressure in Glaucoma. *Survey of ophthalmology* **58**, 26–41 (2013).

114. Kass, M. A. *et al.* The Ocular Hypertension Treatment Study: a randomized trial determines that topical ocular hypotensive medication delays or prevents the onset of primary open-angle glaucoma. *Archives of ophthalmology* **120**, 701–13; discussion 829–30 (2002).

115. Heijl, A. *et al.* Reduction of intraocular pressure and glaucoma progression: results from the Early Manifest Glaucoma Trial. *Archives of ophthalmology* **120**, 1268–79 (2002).

116. Leske, M. C. *et al.* Factors for glaucoma progression and the effect of treatment: the early manifest glaucoma trial. *Archives of ophthalmology* **121**, 48–56 (2003).

117. Johnson, M. & Erickson, K. Mechanisms and routes of aqueous humor drainage. *Principles and Practice of Ophthalmology, Volume I: Basic Sciences* 2577–2595 (2000).

118. Kaufman, P. L. & Bárány, E. H. Loss of acute pilocarpine effect on outflow facility following surgical disinsertion and retrodisplacement of the ciliary muscle from the scleral spur in the cynomolgus monkey. *Investigative ophthalmology* **15**, 793–807 (1976).

119. Grierson, I., Lee, W. R. & Abraham, S. Effects of pilocarpine on the morphology of the human outflow apparatus. *The British journal of ophthalmology* **62**, 302–13 (1978).

120. Gupta, N. *et al.* Localization of M3 muscarinic receptor subtype and mRNA in the human eye. *Ophthalmic research* **26**, 207–13 (1994).

121. Shade, D. L., Clark, A. F. & Pang, I. H. Effects of muscarinic agents on cultured human trabecular meshwork cells. *Experimental eye research* **62**, 201–10 (1996).

122. Lütjen-Drecoll, E. & Tamm, E. Morphological study of the anterior segment of cynomolgus monkey eyes following treatment with prostaglandin F2 alpha. *Experimental eye research* **47**, 761–9 (1988).

123. Gabelt, B. T. & Kaufman, P. L. Prostaglandin F2 alpha increases uveoscleral outflow in the cynomolgus monkey. *Experimental eye research* **49**, 389–402 (1989).

124. Hann, C. R., Vercnocke, A. J., Bentley, M. D., Ritman, E. . & Fautsch, M. P. 3-Dimensional Analysis of Collector Channels in Normal and POAG Eyes. *ARVO abstract* 2735/D724 (2010).

125. Johnson, M. C. & Kamm, R. D. The role of Schlemm's canal in aqueous outflow from the human eye. *Investigative ophthalmology & visual science* **24**, 320–5 (1983).

126. Johnson, D. H. & Matsumoto, Y. Schlemm's canal becomes smaller after successful filtration surgery. *Archives of ophthalmology* **118**, 1251–6 (2000).

127. Lütjen-Drecoll, E., Shimizu, T., Rohrbach, M. & Rohen, J. W. Quantitative analysis of "plaque material" in the inner- and outer wall of Schlemm's canal in normal- and glaucomatous eyes. *Experimental eye research* **42**, 443–55 (1986).

128. Rohen, J. W., Lütjen-Drecoll, E., Flügel, C., Meyer, M. & Grierson, I. Ultrastructure of the trabecular meshwork in untreated cases of primary open-angle glaucoma (POAG). *Experimental eye research* **56**, 683–92 (1993).

129. Lütjen-Drecoll, E. Morphological changes in glaucomatous eyes and the role of TGFbeta2 for the pathogenesis of the disease. *Experimental eye research* **81**, 1–4 (2005).

130. Tamm, E. R. & Fuchshofer, R. What increases outflow resistance in primary open-angle glaucoma? *Survey of Ophthalmology* **52 Suppl 2**, S101–S104 (2007).

131. Li, J., Tripathi, B. J. & Tripathi, R. C. Modulation of pre-mRNA splicing and protein production of fibronectin by TGF-beta2 in porcine trabecular cells. *Investigative ophthalmology & visual science* **41**, 3437–43 (2000).

132. Gottanka, J., Chan, D., Eichhorn, M., Lütjen-Drecoll, E. & Ethier, C. R. Effects of TGF-beta2 in perfused human eyes. *Investigative ophthalmology & visual science* **45**, 153–8 (2004).

133. Pedrigi, R. . *et al.* Pore formation is impaired in glaucomatous SC cells perfused in vitro. *ARVO conference* 3278/A123 (2012).

134. Karp, C. L. *et al.* Identification of complement factor 5 as a susceptibility locus for experimental allergic asthma. *Nature immunology* **1**, 221–6 (2000).

135. Levkovitch-Verbin, H. Animal models of optic nerve diseases. *Eye (London, England)* **18**, 1066–74 (2004).

136. Smith, R. S., Zabaleta, A., Savinova, O. V & Wm, S. The mouse anterior chamber angle and trabecular meshwork develop without cell death. (2001).

137. Smith, S. S., Sundberg, J. P. & John, S. W. M. The anterior segment and ocular adnexae. *Systematic evaluation of the mouse eye* 3–23 (2002).

138. Van Der Merwe, E. L. A Structural and Developmental Study of the Posttrabecular Aqueous Outflow Pathway in the Mouse Eye. (2009).

139. Schmucker, C. & Schaeffel, F. In vivo biometry in the mouse eye with low coherence interferometry. *Vision research* **44**, 2445–56 (2004).

140. Puk, O., Dalke, C., Favor, J., De Angelis, M. H. & Graw, J. Variations of eye size parameters among different strains of mice. *Mammalian genome: official journal of the International Mammalian Genome Society* **17**, 851–7 (2006).

141. Savinova, O. V *et al.* Intraocular pressure in genetically distinct mice: an update and strain survey. *BMC genetics* **2**, 12 (2001).

142. Wang, W.-H., Millar, J. C., Pang, I.-H., Wax, M. B. & Clark, A. F. Noninvasive measurement of rodent intraocular pressure with a rebound tonometer. *Investigative ophthalmology & visual science* **46**, 4617–21 (2005).

143. Sit, A. J. & McLaren, J. W. Measurement of episcleral venous pressure. *Experimental eye research* **93**, 291–8 (2011).

144. Crowston, J. G., Lindsey, J. D., Aihara, M. & Weinreb, R. N. Effect of latanoprost on intraocular pressure in mice lacking the prostaglandin FP receptor. *Investigative ophthalmology & visual science* **45**, 3555–9 (2004).

145. Bill, A. & Phillips, C. I. Uveoscleral drainage of aqueous humour in human eyes. *Experimental eye research* **12**, 275–81 (1971).

146. Toris, C. B., Fan, S., Johnson, T. V. & IshomotoB. Aqueous flow measured by fluorophotometry in the mouse. *Association for ocular pharmacology and therapeutics* 39 (2007).

147. John, S. W. *et al.* Essential iris atrophy, pigment dispersion, and glaucoma in DBA/2J mice. *Investigative ophthalmology & visual science* **39**, 951–62 (1998).

148. Smith, R. S., Sundberg, J. P. & John, S. W. M. Regional ocular pathology: The Anterior segment. *Systematic evaluation of the mouse eye* 111–159 (2002).

149. Wisard, J. *et al.* Non-contact measurement of linear external dimensions of the mouse eye. *Journal of neuroscience methods* **187**, 156–66 (2010).

150. Gual, a *et al.* Effects of time of storage, albumin, and osmolality changes on outflow facility (C) of bovine anterior segment in vitro. *Investigative ophthalmology & visual science* **38**, 2165–71 (1997).

151. Overby, D., Gong, H., Qiu, G., Freddo, T. F. & Johnson, M. The mechanism of increasing outflow facility during washout in the bovine eye. *Investigative Ophthalmology & Visual Science* **43**, 3455–3464 (2002).

152. Barany, E. H. Simultaneous Measurement of Changing Intraocular Pressure and Outflow Facility in the Vervet Monkey By Constant Pressure Infusion. *Investigative ophthalmology* **3**, 135–43 (1964).

153. Epstein, D. L., Hashimoto, J. M., Anderson, P. J. & Grant, W. M. Effect of iodoacetamide perfusion on outflow facility and metabolism of the trabecular meshwork. *Investigative ophthalmology & visual science* **20**, 625–31 (1981).

154. Epstein, D. L., Patterson, M. M., Rivers, S. C. & Anderson, P. J. N-ethylmaleimide increases the facility of aqueous outflow of excised monkey and calf eyes. *Investigative ophthalmology & visual science* **22**, 752–6 (1982).

155. Wagner, J. a, Edwards, A. & Schuman, J. S. Characterization of uveoscleral outflow in enucleated porcine eyes perfused under constant pressure. *Investigative ophthalmology & visual science* **45**, 3203–6 (2004).

156. Becker, B. & Constant, M. A. The facility of aqueous outflow. *Archives of ophthalmology* **55**, 305–312 (1956).

157. Grant, W. M. Tonographic method for measuring the facility and rate of aqueous flow in human eyes. *Archives of ophthalmology* **44**, 204–214 (1950).

158. Grant, W. M. & Trotter, R. R. Tonographic mesurements in enucleated eyes. *Archives of ophthalmology* **53**, 191–200 (1955).

159. Acott, T., Kingsley, P. D., Samples, J. R. & Buskirk, E. M. Van Human Trabecular Mesh work Organ Culture□: Morphology and Glycosaminoglycan Synthesis. **29**, (1988).

160. Erickson-Lamy, K., Schroeder, A. M., Bassett-Chu, S. & Epstein, D. L. Absence of time-dependent facility increase ("washout") in the perfused enucleated human eye. *Investigative ophthalmology & visual science* **31**, 2384–8 (1990).

161. Avila, M. Y., Carré, D. a, Stone, R. a & Civan, M. M. Reliable measurement of mouse intraocular pressure by a servo-null micropipette system. *Investigative ophthalmology & visual science* **42**, 1841–6 (2001).

162. Aihara, M., Lindsey, J. D. & Weinreb, R. N. Reduction of intraocular pressure in mouse eyes treated with latanoprost. *Investigative ophthalmology & visual science* **43**, 146–50 (2002).

163. Bahler, C. K., Howell, K. G., Hann, C. R., Fautsch, M. P. & Johnson, D. H. Prostaglandins increase trabecular meshwork outflow facility in cultured human anterior segments. *American journal of ophthalmology* **145**, 114–9 (2008).

164. Weinreb, R. N., Toris, C. B., Gabelt, B. T., Lindsey, J. D. & Kaufman, P. L. Effects of prostaglandins on the aqueous humor outflow pathways. *Survey of ophthalmology* **47 Suppl 1**, S53–64 (2002).

165. Brubaker, R. F. Goldmann's equation and clinical measures of aqueous dynamics. *Experimental eye research* **78**, 633–7 (2004).

166. Tarrasón, G. *et al.* The sphingosine-1-phosphate receptor-1 antagonist, W146, causes early and short-lasting peripheral blood lymphopenia in mice. *International immunopharmacology* **11**, 1773–9 (2011).

167. Maruyama, T. *et al.* Design and synthesis of a highly selective EP4-receptor agonist. Part 1: 3,7-dithiaPG derivatives with high selectivity. *Bioorganic & medicinal chemistry letters* **11**, 2029–31 (2001).

168. Pignataro, L., Varodayan, F. P., Tannenholz, L. E. & Harrison, N. L. The regulation of neuronal gene expression by alcohol. *Pharmacology & therapeutics* **124**, 324–35 (2009).

169. Toda, N. & Ayajiki, K. Vascular actions of nitric oxide as affected by exposure to alcohol. *Alcohol and alcoholism (Oxford, Oxfordshire)* **45**, 347–55

170. Spiegel, S. & Milstien, S. Sphingosine-1-phosphate: an enigmatic signalling lipid. *Nature reviews. Molecular cell biology* **4**, 397–407 (2003).

171. Liliom, K. *et al.* Growth factor-like phospholipids generated after corneal injury. *The American journal of physiology* **274**, C1065–74 (1998).

172. Wan, Z., Woodward, D. F. & Stamer, W. D. Endogenous Bioactive Lipids and the Regulation of Conventional Outflow Facility. *Expert review of ophthalmology* **3**, 457–470 (2008).

173. Salomone, S. *et al.* Analysis of sphingosine 1-phosphate receptors involved in constriction of isolated cerebral arteries with receptor null mice and pharmacological tools. *British journal of pharmacology* **153**, 140–7 (2008).

174. Pyne, N. J. & Pyne, S. Selectivity and specificity of sphingosine 1-phosphate receptor ligands: "off-targets" or complex pharmacology? *Frontiers in pharmacology* **2**, 26 (2011).

175. Suzawa, T. *et al.* The role of prostaglandin E receptor subtypes (EP1, EP2, EP3, and EP4) in bone resorption: an analysis using specific agonists for the respective EPs. *Endocrinology* **141**, 1554–9 (2000).

176. Davis, T. L. & Sharif, N. A. Pharmacological characterization of [(3)H]-prostaglandin E(2) binding to the cloned human EP(4) prostanoid receptor. *British journal of pharmacology* **130**, 1919–26 (2000).

177. Yoshida, K. *et al.* Stimulation of bone formation and prevention of bone loss by prostaglandin E EP4 receptor activation. *Proceedings of the National Academy of Sciences of the United States of America* **99**, 4580–5 (2002).

178. Abramovitz, M. *et al.* The utilization of recombinant prostanoid receptors to determine the affinities and selectivities of prostaglandins and related analogs. *Biochimica et biophysica acta* **1483**, 285–93 (2000).

179. Schlötzer-Schrehardt, U., Zenkel, M. & Nüsing, R. M. Expression and localization of FP and EP prostanoid receptor subtypes in human ocular tissues. *Investigative ophthalmology & visual science* **43**, 1475–87 (2002).

180. Woodward, D. F., Jones, R. L. & Narumiya, S. International Union of Basic and Clinical Pharmacology. LXXXIII: classification of prostanoid receptors, updating 15 years of progress. *Pharmacological reviews* **63**, 471–538 (2011).

181. Maihöfner, C. *et al.* Expression of cyclooxygenase-1 and -2 in normal and glaucomatous human eyes. *Investigative ophthalmology & visual science* **42**, 2616–24 (2001).

182. Johnson, M., Gong, H., Freddo, T. F., Ritter, N. & Kamm, R. Serum proteins and aqueous outflow resistance in bovine eyes. *Investigative ophthalmology & visual science* **34**, 3549–57 (1993).

183. Civan, M. M. & Macknight, A. D. C. The ins and outs of aqueous humour secretion. *Experimental eye research* **78**, 625–31 (2004).

184. Scott, P. a, Overby, D. R., Freddo, T. F. & Gong, H. Comparative studies between species that do and do not exhibit the washout effect. *Experimental eye research* **84**, 435–43 (2007).

185. Aihara, M., Lindsey, J. D. & Weinreb, R. N. Twenty-four-hour pattern of mouse intraocular pressure. *Experimental Eye Research* **77**, 681–686 (2003).

186. Pease, M. E., Hammond, J. C. & Quigley, H. a Manometric calibration and comparison of TonoLab and TonoPen tonometers in rats with experimental glaucoma and in normal mice. *Journal of glaucoma* **15**, 512–9 (2006).

187. Pease, M. E., Cone, F. E., Gelman, S., Son, J. L. & Quigley, H. a Calibration of the TonoLab tonometer in mice with spontaneous or experimental glaucoma. *Investigative ophthalmology & visual science* **52**, 858–64 (2011).

188. Weisberg, S. *Applied Linear Regression*. (1985).

189. Li, R. & Liu, J. H. K. Telemetric monitoring of 24 h intraocular pressure in conscious and freely moving C57BL/6J and CBA/CaJ mice. *Molecular vision* **14**, 745–9 (2008).

190. Becker, B. & Constant, M. A. The facility of aqueous outflow; a comparison of tonography and perfusion measurements in vivo and in vitro. *A.M.A. archives of ophthalmology* **55**, 305–12 (1956).

191. Charras, G. T., Coughlin, M., Mitchison, T. J. & Mahadevan, L. Life and times of a cellular bleb. *Biophysical journal* **94**, 1836–53 (2008).

192. Anderson, P. J., Wang, J. & Epstein, D. L. Metabolism of calf trabecular (reticular) meshwork. *Investigative ophthalmology & visual science* **19**, 13–20 (1980).

193. Ayi, K., Liles, W. C., Gros, P. & Kain, K. C. Adenosine triphosphate depletion of erythrocytes simulates the phenotype associated with pyruvate kinase deficiency and confers protection against Plasmodium falciparum in vitro. *The Journal of infectious diseases* **200**, 1289–99 (2009).

194. Rego, A. C., Areias, F. M., Santos, M. S. & Oliveira, C. R. Distinct glycolysis inhibitors determine retinal cell sensitivity to glutamate-mediated injury. *Neurochemical research* **24**, 351–8 (1999).

195. Van Buskirk, E. M. Anatomic correlates of changing aqueous outflow facility in excised human eyes. *Investigative ophthalmology & visual science* **22**, 625–32 (1982).

196. Burgoyne, C. F., Downs, J. C., Bellezza, A. J. & Hart, R. T. Three-dimensional reconstruction of normal and early glaucoma monkey optic nerve head connective tissues. *Investigative ophthalmology & visual science* **45**, 4388–99 (2004).

197. Sharpe, J. *et al.* Optical projection tomography as a tool for 3D microscopy and gene expression studies. *Science* **296**, 541–5 (2002).

198. Billinton, N. & Knight, a W. Seeing the wood through the trees: a review of techniques for distinguishing green fluorescent protein from endogenous autofluorescence. *Analytical biochemistry* **291**, 175–97 (2001).

199. Ziskind, T. Schlemm's canal morphology of mouse eye: examination under different Intraocular Pressures using a 3D automated histology system. (2012).

200. Scinteie, E. O. Imaging post trabecular pathway in human glaucomatous versus normal eye using a 3D automated histological technique Master Project Final Report. (2012).

201. Sharpe, J. Optical projection tomography as a new tool for studying embryo anatomy. *Journal of anatomy* **202**, 175–81 (2003).

202. Keller, K. E., Bradley, J. M., Vranka, J. a & Acott, T. S. Segmental versican expression in the trabecular meshwork and involvement in outflow facility. *Investigative ophthalmology & visual science* **52**, 5049–57 (2011).

203. Johnson, A. W., Ammar, D. a & Kahook, M. Y. Two-photon imaging of the mouse eye. *Investigative ophthalmology & visual science* **52**, 4098–105 (2011).

204. Smith, R. S., Korb, D. & John, S. W. M. Technical Brief A goniolens for clinical monitoring of the mouse iridocorneal angle and optic nerve. 26–31 (2002).

205. Swaminathan, S. S. *et al.* Secreted Protein, Acidic and Rich in Cysteine (SPARC)-Null Mice Exhibit More Uniform Outflow. *Investigative ophthalmology & visual science* (2013).doi:10.1167/iovs.12-10950

206. Johnson, M., Chen, A., Epstein, D. L. & Kamm, R. D. The pressure and volume dependence of the rate of wash-out in the bovine eye. *Current eye research* **10**, 373–5 (1991).

207. Bárány, E. H. & Scotchbrook, S. Influence of testicular hyaluronidase on the resistance to flow through the angle of the anterior chamber. *Acta physiologica Scandinavica* **30**, 240–8 (1954).

208. Gaasterland, D. E., Pederson, J. E. & MacLellan, H. M. Perfusate effects upon resistance to aqueous humor outflow in the rhesus monkey eye. A comparison of glutathione-bicarbonate Ringer's solution to pooled aqueous humor as perfusate. *Investigative ophthalmology & visual science* **17**, 391–7 (1978).

209. Kaufman, P. L., True-Gabelt, B. & Erickson-Lamy, K. A. Time-dependence of perfusion outflow facility in the cynomolgus monkey. *Current eye research* **7**, 721–6 (1988).

210. Dane, S., Aslankurt, M., Yazici, A. T. & Gümüştekin, K. Sex-related difference in intraocular pressure in healthy young subjects. *Perceptual and motor skills* **96**, 1314–6 (2003).

211. Pointer, J. S. Evidence that a gender difference in intraocular pressure is present from childhood. *Ophthalmic & physiological optics : the journal of the British College of Ophthalmic Opticians (Optometrists)* **20**, 131–6 (2000).

212. Gaasterland, D. *et al.* Studies of aqueous humour dynamics in man. VI. Effect of age upon parameters of intraocular pressure in normal human eyes. *Experimental eye research* **26**, 651–6 (1978).

213. Becker, B. The decline in aqueous secretion and outflow facility with age. *American journal of ophthalmology* **46**, 731–6 (1958).